The Jerzy Haber Institute of Catalysis and Surface Chemistry
Polish Academy of Sciences

SURFACTANTS, POLYELECTROLYTES AND NANOPARTICLES AS BUILDING BLOCKS FOR NANOCARRIERS

Małgorzata Adamczak

PhD Thesis

Supervised by Professor Piotr Warszyński

Kraków, 2013

Acknowledgments

First, I would like to thank my supervisor Professor Piotr Warszyński for mentoring me during this project. I am very grateful for giving me room to grow and come up with my own ideas, as well as allowing me to learn on my mistakes, while he was always there with valuable suggestions when needed.

I would also like to express my gratitude to Dr. Christian Simon from Sintef Materials and Chemistry, who was our foreign partner in the project. Off and on, I've spent twenty months in Oslo, Norway, which eventually became my second home. My special thanks go to Christelle Denonville, Bente Gilbu Tilset, Isabelle Marthinsen, Marit Stange, Juan Yang, Henrik Raeder, Mathieu Grandcolas and Per Martin Rorvik. Tusen takk til alle sammen!

I would like to acknowledge two amazing teams, which performed the biological tests of my capsules: Hanna Julie Hoel and Professor Gustav Gaudernack from Institute for Cancer Research at the Norwegian Radium Hospital in Oslo, Norway, and Dr. hab. Elżbieta Pamuła, Małgorzata Krok and Urszula Posadowska from Faculty of Materials Science and Ceramics, AGH University of Science and Technology in Kraków, Poland.

I would like to thank all the members of two groups, Colloids and Nanostructures of Soft Matter, for a friendly atmosphere in the laboratories, support and scientific discussions. Special acknowledgments need to be given to Dr. Grażyna Para, Dr. Ewelina Jarek, Dr. Aneta Michna, Dr. Małgorzata Nattich-Rak, Marzena Noworyta, Joanna Piekoszewska and Karolina Podgórna.

It is hard to fully express gratitude to my friends, Maria Dąbkowska (Zaucha:), Monika Stefańska, Jakub Barbasz and Krzysztof Szczepanowicz, for what they have done for me during all these years. You made it all worthwhile. Thanks.

I also would like to thank my partner, Carlos Grande, for his love and support, together with ability to distinguish when it was better to let me stay home writing and eating ice cream, and when it was a good time to take me for a run. You are the only exception.

Most importantly, this thesis would not have been possible without my family. I would especially like to thank my parents and both brothers for their love, understanding, encouragement and endless support.

Contents

CONTENTS

CONTENTS

Chapter 1

LITERATURE REVIEW

1 Introduction

Once described as "pseudosolutions" or "world of neglected dimensions", colloids have come a long way from their use in the enhancement of solubility of substances to the minimization of toxicity and degradation of the drugs. A colloidal suspension consists of two separate phases; one phase finely dispersed in the second continuous phase. Size of dispersed particles ranges from a few to a few thousands nanometers, which gives a rise to a large interfacial area, and various phenomena dominated by surface interactions. Colloids have been in use for centuries in different areas, including additives and pigments for inks, paints, food and cosmetics. However, only last few decades have brought the enormous development in colloid science and technology, related with expanding fields of nanotechnology and nanomedicine.

Size has a significant importance in drug delivery and imaging applications. Control on the cellular level can be achieved only with structures of size similar to biological components of interest. An efficient uptake of drug carriers by endocytosis restricts its maximum size to 200 nm, as most cells cannot effectively internalize microobjects with a bigger diameter. Microvehicles cannot traverse through tumor cells with pore sizes as big as 380–780 nm. Nano-sized drug carriers are more favorable compared to macrocontainers, as their small size facilitates drug targeting. Moreover, the control of the drug release by engineered carrier shells reduces side effects of the treatment.

Surfactants, i.e., amphiphilic compounds possessing surface active properties, poly-

1. LITERATURE REVIEW

electrolytes, i.e., water-soluble polymers with ionizable groups, and nanoparticles are three substance classes of growing interest. They have become a versatile tool for formation of soft nanostructures, which can find application in targeted delivery systems. Quantum dots are nanocrystals of semiconductors characterized with size-dependent intensive fluorescence and excellent stability. Because of these properties, quantum dots are widely used as fluorescent probes in biological staining and diagnostics, e.g., in nucleic acid/antibodies/antigens assays, cancer imaging and detection or in the single quantum dot studies of membrane dynamics and organization. Since the most frequently used cadmium-based quantum dots release highly toxic Cd ions, which results in their *in vitro* and *in vivo* toxicity, embedding them in a stable polymer coating should hinder their corrosion and, therefore, avoid the cytotoxicity of such prepared nanostructures. Polyelectrolyte complexes, often described as symplexes, are another important class of polymeric materials as they combine physicochemical properties of two different polyelectrolytes. Emulsion, defined as a dispersion of two immiscible liquids, has several advantages in drug delivery systems. Oil-in-water emulsions have been widely used as drug carriers since they have the ability to solubilize hydrophobic active ingredients. This feature is of significant importance, since the most of recently explored, highly active drugs are poorly soluble in water. The necessary prerequisite for application of emulsions in pharmaceutical formulations is lack of their cytotoxicity. Therefore, all the compounds used to form an emulsion should be non-toxic. Use of vegetable oils, composed predominantly of medium-chain or long-chain triglycerides, as well as surfactants of biological origin helps to meet that requirement.

Nanocapsules are a particular type of containers composed of a core surrounded by a shell formed from various materials. Usually soft shells are build with polymers (e.g. by surface polymerization of the core material or polymerizable surfactants), while hard inorganic shells can be formed by e.g. hydrolysis and polycondensation of silane derivatives. One of the most convenient methods of polymer shell formation with tailored properties is the layer-by-layer adsorption of polyelectrolytes. Encapsulation of active agents, drugs or biomolecules within the capsule cavity protects the load from the biological environment. Semi-permeable polyelectrolyte membrane can also be used to regulate the release rate of encapsulated active component. Moreover, that type of shell can be easily functionalized to reduce toxicity, to minimize the interactions between the capsules and the immune

system ("stealth effect") and to immobilize target specific ligands for intelligent delivery systems. As a core template for formation of nanocapsules, colloidal particles, emulsion droplets as well as nanoparticles can be used. Liquid cores, although more difficult to handle than the solid cores, have many advantages in use, e.g., lack of core dissolution step at the end of layer-by-layer adsorption process, as well as higher drug loading capacity. When the solid core does not contain active agent, it needs to be dissolved without loosing the integrity of the remaining empty shell, which subsequently needs to be refilled. This process usually has low efficiency and the traces of the core can remain. In the case of encapsulation of the hydrophilic nanoobjects, their complexes with the oppositely charged polyelectrolyte can be used as cores for further encapsulation.

The aim of this thesis is to develop the methods of formation and to characterize various nanostructures obtained for biomedical applications, prepared by polyelectrolyte/nanoparticle complex formation, emulsification and layer-by-layer adsorption of polyelectrolytes. Controlling parameters such as type and composition of suspensions, electric charge, size and stability of complexes, polyelectrolyte-modified nanoparticles, emulsions and capsules enables to prepare systems with desired properties and functionalities.

2   Surfactants and micelles

2.1   Surfactants

2.1.1   General properties and classification of surfactants

Surface active agents, usually referred to as surfactants, are amphiphilic molecules with unique tendency to adsorb at various interfaces, resulting from their chemical structure [1]. The term "amphiphile" indicates that surfactant's molecule consists of two groups behav-
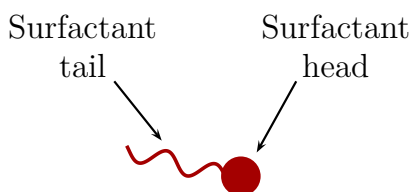
Figure 1.1: The basic structure of a surfactant.

ing differently in the solvents (see Fig. 1.1). The lyophilic part of surfactant, also called "the head", has affinity to a polar solvent, while the lyophobic part (the "tail") has little or no attraction to that phase. Usually the solvent is water and then water-soluble part is called hydrophilic. Water-insoluble group having affinity to nonpolar solvents, such as oils, is described as hydrophobic. The polar head groups content heteroatoms, such as oxygen, sulfur, phosphorus or nitrogen, included in functional groups of alcohols, esters, sulfates, amines etc. Nonpolar, hydrophobic tail consist of a hydrocarbon or fluorocarbon chain, linear or branched, containing usually 8–20 carbon atoms. The length of the chain and its degree of branching, together with position and character of polar head (ionic or nonionic) determine the properties and application of surfactants.

Surfactants can be categorized in several ways. From the commercial point of view, they are often ranked according to their use as emulsifiers, foaming or wetting agents, dispersants, etc. [2]. A weakness of this categorization lies in multiple use of many surfactants. The most useful and accepted classification is based on the ionic character of the head, with subgroups based on the nature of the tail. The four basic groups of surfactants, schematically shown in Fig. 1.2, are then defined as follows:
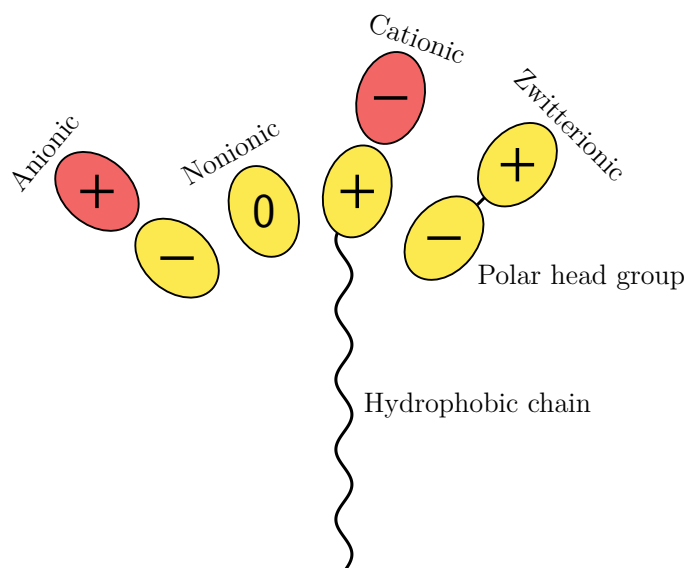
Figure 1.2: Classification of surfactants based on the ionic character of the head [3].

Anionic surfactants The polar head group of anionic surfactant carries a negative charge. Typical classes are as follows: carboxylates, sulfates, sulfonates and phosphates. They are used in the majority of industrial applications, including pharma-

ceutical formulations (sulfosuccinates), soaps (carboxylates), and detergents (alkyl–benzene sulfonates). An important, widely used surfactant belonging to this category is sodium dodecyl sulfate $C_{12}H_{25}OSO_3Na$ (SDS), which belongs to the class of sodium alkylsulfates. In water the alkali metal dissociates as a cation, such that molecule becomes negatively charged. SDS is extensively used both for fundamental studies as well as in many practical applications.

Cationic surfactants This category includes surfactants, which have positively charged, mostly amine–containing head group. The quaternary ammonium compounds are not pH sensitive, while the amines turn into nonionic in the region of high pH values. Due to the high pressure hydrogenation reaction carried out during synthesis, quaternary ammoniums are more expensive than anionic surfactants. They are also known to be less biodegradable and more toxic than other groups of surfactants. As a consequence, they are used mainly in two cases, i.e., as antiseptic agents against bacteria and fungi or, due to their tendency to adsorb at negatively charged surfaces, as corrosion inhibitors. Examples are dodecyl trimethylammonium bromide, $C_{12}H_{25}N(CH_3)_3Br$ (DTABr), and cetyl trimethylammonium bromide $C_{16}H_{33}N(CH_3)_3Br$ (CTABr).

Zwitterionic surfactants These contain both positively (e.g., amine groups) and negatively charged (e.g., carboxyl) head groups, such that the net charge is equal to zero. However, the charge of amphoteric surfactants is strictly dependent on the pH of the surrounding medium. Examples are betaines, sulfobetaines and substances of biological origin, such as aminoacids and phospholipids. Lecithin, a mixture of phospholipids with phosphatidylcholine as main component, is the integral part of cell membranes. Due to its zwitterionic structure, lecithin tends to form aggregates in solutions. These structures, so called liposomes, have been extensively explored as drug delivery systems. Because of the low potential for irritation and their biocompatibility, zwitterionic surfactants are widely used as emulsifiers for food, dermatological products and in many pharmaceutical applications.

Nonionic surfactants The polar head group of nonionic surfactant is not charged. They derive the water solubility from the presence of highly hydrophilic polar groups, such as polyethylene oxide ($-OCH_2CH_2O-$), fatty acid ethoxylates, sorbitan ester

ethoxylates or sugars. Compared to other groups, nonionic surfactants are not sensitive to salts, but often sensitive to the temperature. As more biocompatible than ionic surfactants, they found the most widespread use in pharmaceutical applications. Examples of surfactants used in cosmetics and drug delivery formulations are sorbitan esters and their ethoxylated derivatives (Spans, Tweens).

The chemical structures of most common ionic and nonionic surfactants are shown in Fig. 1.3. Beside the conventional surfactants described above, there are speciality surfactants attracting considerable interest in industrial applications. These include fluorocarbon and silicone surfactants [4]. In fluorosurfactants, some of the hydrogen atoms from the hydrophobic tail are replaced by fluorine. Silicosurfactants are derived from polydimethylsiloxanes by partially replacing methyl groups with polyalkylenoxy or pyrrolidone groups. These surfactants are known for their excellent wetting properties, as well as good thermal and chemical stability. However, due to the high cost of production they are only used for specific applications, such as oil-resistant finishing in textile industry and fire-extinguishing agents. Dimeric surfactants are structures consisting of two amphiphilic molecules connected through a spacer group, which can be located right between two head groups (Gemini surfactants), in the middle or close to the end of alkyl chains (Bolaform surfactants). If more than two surfactants are connected together, they can form tri-, tetra- or polymeric surfactants with interesting properties, often superior compared to monomeric surfactants [1, 5]. Homopolymers are the simplest type of polymeric surfactants, containing only one type of repeating unit, while block copolymers consists of at least two parts - one made of monomer A and the other made of monomer B. Polymeric surfactants are widely applied as stabilizers for suspensions and emulsions. In some cases, the presence of surfactant is needed only in the first stage of procedure and afterwards becomes undesirable, impairing the product's properties. For example, a residual surfactant used as emulsifier in paints will tend to migrate to the film-air interface, causing formation of defects such as lumps and cavities. It is possible to overcome that problem by use of polymerizable surfactants, also referred to as surfmers. Strong chemical bounding of surfmers to the particles and polymerization process will constrain the presence of unbounded surfactant in the final product [6]. Different types of special surfactant molecules are shown in Fig. 1.4.

In addition to synthetic surfactants produced on a large scale, a number of natu-

Anionic

Sodium alkylsulfate
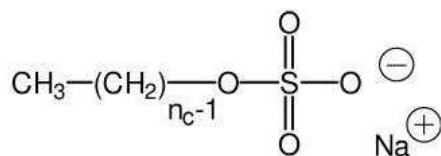
Sodium alkylbenzenesulfonate
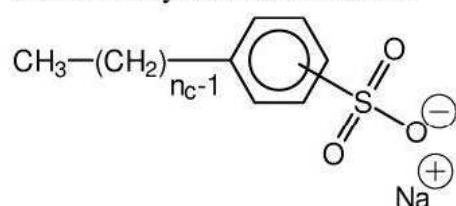
Sodium alkylcarboxylate
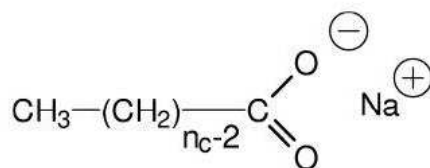
Zwitterionic

Alkyldimethylpropanesultaine
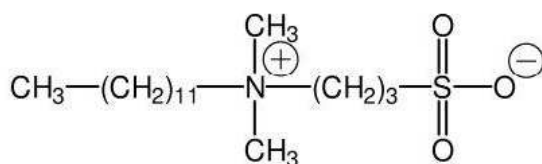
Dipalmitoylphosphatidylcholine
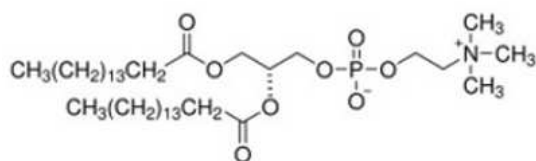
Cationic

Alkyltrimethylammonium bromide
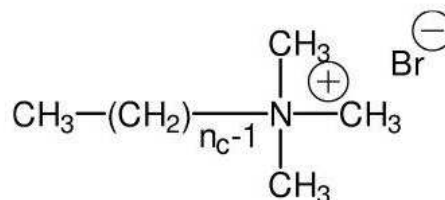
Cetylpyridinium chloride
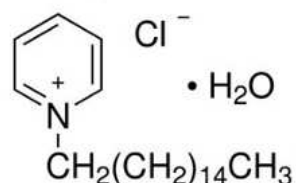
Dialkyldimethylammonium bromide
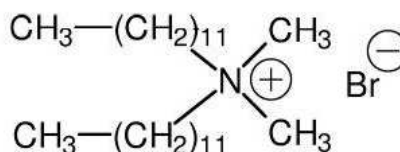
Nonionic

Alkylglucosides
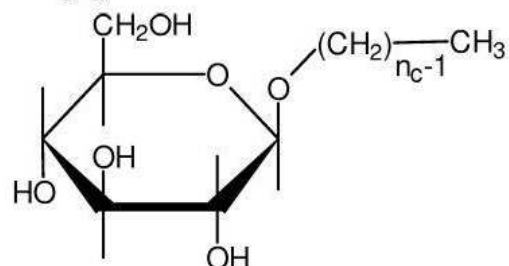
Poly(ethylene oxide)
iso-octylphenyl ether
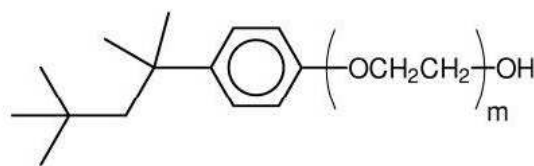
Figure 1.3: Chemical structures of common ionic and nonionic surfactants [1].
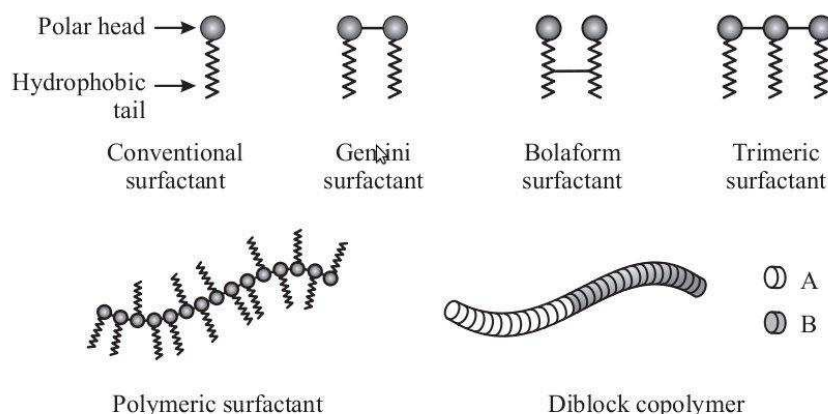
Figure 1.4: Different types of speciality surfactants [1].

rally occurring substances demonstrate surface-active properties [7]. They are involved in essential processes ongoing in the living tissues and cells, just as previously mentioned phosphatidylcholine. As another example, bile salts produced by a pancrease are natural emulsifiers dispersing fat into droplets, which can be then utilized by the body. Pulmonary surfactant present in the lungs is a complex mixture of multiple lipids and four surfactant proteins [8]. It is crucial for the respiration process and the transfer of gases between the atmosphere and the blood. A deficiency of pulmonary surfactant in premature infants causes the respiratory distress syndrome. The treatment is based on administering synthetic or animal derived pulmonary surfactant to the patients [9]. Lipopeptides, molecules consisting of a lipid connected to the peptide, can be used as antibiotics in the treatment of infections caused by certain bacteria. Saponins are glucosides with foaming characteristics, which can be found in various plant species. They are often used in personal care products and as detergents. Saponins are also known to reduce blood cholesterol level. Because of the recent focus on the environmental impact and possible toxic effects caused by synthetic surfactants, it becomes a popular strategy to replace them with bio-based, environmentally friendly surfactants [10–12].

Surfactants are ubiquitous [13]. They find vast application in many branches of chemical industry, including detergents and cleaners, paints, lacquers, cosmetics and personal care products, pharmaceuticals, food and food packaging, paper and cellulose products, mining and flotation, petroleum production, agrochemicals, textiles and fibres, plastics and composite materials. The traditional application of surfactants was their use as soaps and detergents in cleaning operations. Personal care products solely make up a

multi-billion-dollar market worldwide, growing every year as a result of improved living standards [14]. Nowadays, the demands of other technological areas caused the enormous increase in surfactant market [15, 16].

It is important to keep in mind that each application has specific requirements that determine the suitability of selected surfactant. Characteristics such as solubility, surface activity, foaming and wetting properties, detergency power, salt and pH stability can make a given surfactant perform well in some applications and less in the others. The economy is another important aspect concerning the choice of material for specific purpose; preferably the cheapest surfactant producing the desired effect will be chosen. However, there is an increasing demand for nontoxic, biocompatible and biodegradable materials. The proper surfactant disposal is of crucial importance because of the effects of surfactants on groundwater and water treatment operations. The ability of ecosystem to degrade waste products can greatly affect the potential usefulness of a given material [17].

2.1.2   Interfacial tension

An interface is the region, which separates two different phases from each other [1, 18]. Within this region, the properties of the system change from those in one phase to those in the second one. The interfaces between solid-liquid, solid-gas, and the liquid-gas are also called surfaces. There also exist interfaces separating two immiscible liquids, such as oil and water, and solid-solid interfaces separating two solid phases. In the case of solid-gas interface, the transition region resembles a sharp boundary, having essentially a thickness of single molecule. The liquid-gas interface, however, is much less abrupt since molecules can diffuse into the bulk phase, to the surface and evaporate from the liquid into the gaseous phase. A similar situation happens for the interface between two liquid phases with some mutual solubility; the transition region becomes less distinct as the physical differences between phases decrease, until a single phase is obtained.

A unique character of interfaces is resulting from the specific state of the atoms and molecules occurring in the transition region, as shown in Fig. 1.5. It is energetically favorable for molecules to be surrounded by other molecules; a unit of a substance in the bulk phase is exposed to the zero net force due to the balance of interactions with the neighbors. In the interfacial region the number of adjacent molecules is smaller than in the bulk. Because of force asymmetry, interfacial molecules are pulled towards the interior
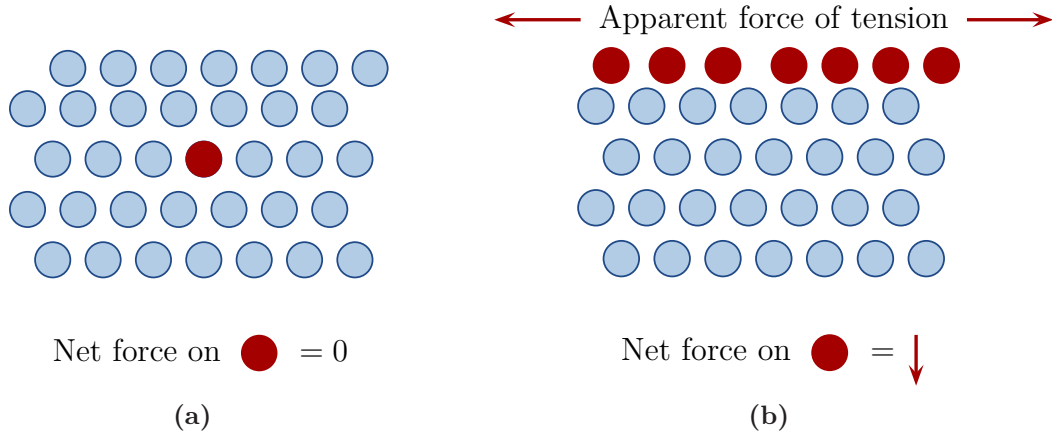
Figure 1.5: Forces acting on the atoms or molecules present in the bulk (a) or at the interfaces (b) according to Ref. [17].

of the bulk. The counteracting force at the surface is known as the interfacial tension. It can be interpreted also in terms of the work $\mathrm{d}w$ required to bring molecules from the bulk to the surface to create new surface area $\mathrm{d}A$:

$$\mathrm{d}w = \gamma\,\mathrm{d}A\,, \tag{1.1}$$

where γ is the interfacial tension. It can also be defined as enthalpy associated with the expansion of a surface at constant pressure p, temperature T and composition i:

$$\gamma = \frac{\mathrm{d}G}{\mathrm{d}A}(p, T, i = \mathrm{const})\,, \tag{1.2}$$

where G is the Gibbs free energy and i represents components forming the interface. There are two equivalent units of interfacial tension: $\mathrm{J/m^2}$ (useful when thinking of the surface tension as of the free energy), and $\mathrm{N/m}$ (reflecting interfacial tension as a contracting force around the perimeter of a surface). Surface tensions of liquids are typically within the range of 20–80 mN/m. In aqueous solutions, there is a large imbalance of forces acting on the surface molecules — on one side, interactions between densely packed, polar water molecules, and on the other side fewer nonpolar gases or water vapor. As a consequence, surface tension of water is quite high (72.8 mN/m at 25°C).

The existence of interfacial tension gives a rise to diverse phenomena encountered in everyday's life. Droplets of liquids, such as rain on waxy leaves or water dribbling from the tap, tend to adopt a spherical shape in order to reduce their surface area. Water

striders can walk on the surface of a pond and do not sink, unless they are heavy enough to counteract the force of surface tension. Most liquids can be poured to a glass until the surface forms a convex meniscus above the edge because of contractile force shrinking the surface [19]. The interfacial tension plays a major role in colloidal dispersions, which is a direct consequence of their enormously developed interfacial area. Colloids are dominated rather by interfacial phenomena than the bulk properties, as long as the gravity is negligible. Surfactants, with their tendency to adsorb at interfaces and to lower the interfacial tension, are therefore extremely important modifiers in colloidal systems [2, 15].

2.1.3 Adsorption of surfactants at an interface

When surfactant is present in a solvent, the lyophobic groups distort the structure of the bulk. Surfactant dissolved in aqueous phase breaks hydrogen bonds between water molecules and structures them in the vicinity of the hydrophobic tails [2]. As the result, the free energy of the system increases. In order to minimize this unfavorable effect, molecules of amphiphile have to rearrange. Surfactant will diffuse and adsorb at the surface with its hydrocarbon tail oriented out of the water (see Fig. 1.6). The presence
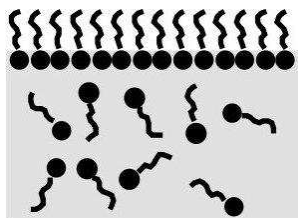
Figure 1.6: Adsorption of surfactants at the air–water interface [2].

of hydrophilic groups prevents the surfactant from being completely expelled from the solvent.

Adsorption of surfactant molecules lowers the interfacial tension and alters other properties of the interface, such as its charge and composition [17]. The denser is the layer of surfactant on the surface, the larger is the reduction of surface free energy. The amount of surfactants adsorption at interface, as well as their efficiency in lowering the interfacial tension depends on their structure, concentration, conditions and the nature of phases forming the interface. For example, more surface active surfactants modify interfacial properties at lower concentrations. For nonionic surfactants repulsion between the head groups is small; therefore, they are usually strongly adsorbed at the surface from

very dilute solutions and lower surface tension much more than ionic surfactants with the same alkyl chain length. Moreover, the adsorption of nonionic surfactants is only
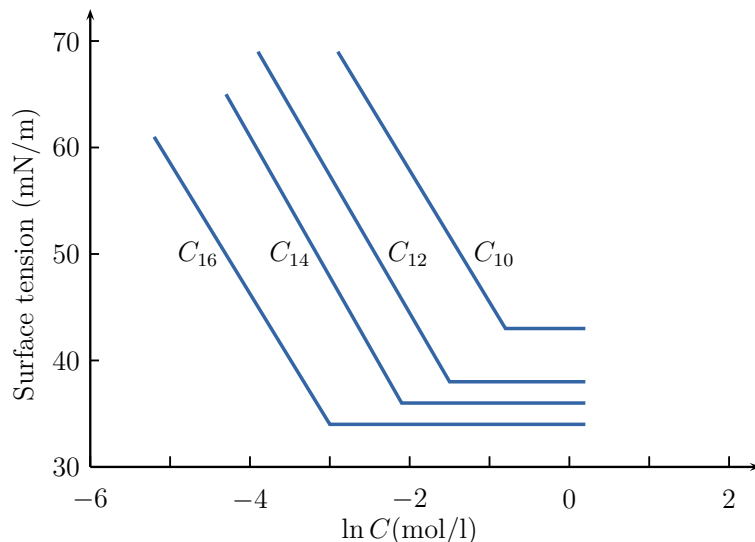
Figure 1.7: Effect of hydrophobic chain length on the surface tension [17].

slightly affected by addition of electrolytes or pH changes. For a given homologous series of straight-chain surfactants in water, efficiency of adsorption is directly related to the length of the hydrophobic chain, as shown in Fig. 1.7. If the temperature or composition of the solvent is changed, the effectiveness of surfactant may be significantly altered. That leads to a conclusion that amphiphile must posses desired properties in a certain solvent, and for the proposed conditions of use. An understanding of the surfactant science is necessary for choosing the best amphiphile for use in a particular system [20].

2.1.4 Thermodynamics of adsorption at interfaces

The presence of an interface influences all thermodynamic parameters of a system. One
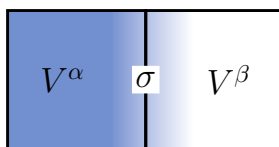
Figure 1.8: The Gibbs dividing plane [1].

of the fundamental concepts of thermodynamics of interfaces is the dividing surface introduced by Gibbs [1, 21]. In his approach, two bulk phases with volumes V^α and V^β are separated by an ideally thin ($V^\sigma = 0$) interfacial layer, called the Gibbs dividing plane

(see Fig. 1.8). All three phases are contributing to extensive quantities of the system such as, for example, the internal energy U:

$$U = U^{\alpha} + U^{\beta} + U^{\sigma} \tag{1.3}$$

and the entropy S:

$$S = S^{\alpha} + S^{\beta} + S^{\sigma} . \tag{1.4}$$

The internal energy U^{σ} of the interface is an excess quantity and can be defined as follows:

$$U^{\sigma} = U - u^{\alpha}V^{\alpha} - u^{\beta}V^{\beta} , \tag{1.5}$$

where u^{α} and u^{β} are the internal energies per unit volume, which are defined in the homogeneous bulk region of the two phases. Similar definitions can be used for other thermodynamic extensive parameters.

The molecular constitution also changes at an interface. The additional quantity present in the system due to existence of the interface is:

$$N_i^{\sigma} = N_i - c_i^{\alpha}V^{\alpha} - c_i^{\beta}V^{\beta} , \tag{1.6}$$

where c_i^{α} and c_i^{β} are the concentrations (numbers of molecules per unit volume) of the ith material in the respective bulk phases. Using the last equation it is possible to define the interfacial excess Γ_i^{σ}:

$$\Gamma_i^{\sigma} = \frac{N_i^{\sigma}}{A} , \tag{1.7}$$

where A is the interfacial area. If we turn to the interfacial excess quantities, the internal surface energy dU^{σ} can be given as follows:

$$dU^{\sigma} = TdS^{\sigma} - p\,dV^{\sigma} + \gamma\,dA + \sum_i \mu_i\,dN_i^{\sigma} , \tag{1.8}$$

where μ_i is the chemical potential of the ith material, respectively. The term pV^{σ} disappears, because in the Gibbs approach interface has no volume, and therefore

$$dU^{\sigma} = T\,dS^{\sigma} + \gamma\,dA + \sum_i \mu_i\,dN_i^{\sigma} . \tag{1.9}$$

Then, one can use thermodynamic relationship for the surface internal energy:

$$U^\sigma = TS^\sigma + \gamma A + \sum_i \mu_i N_i^\sigma \,.$$ (1.10)

Differentiation of the above equation leads to

$$dU^\sigma = T\,dS^\sigma + S^\sigma\,dT + \gamma\,dA + A\,d\gamma + \sum_i \mu_i\,dN_i^\sigma + \sum_i N_i^\sigma d\mu_i \,.$$ (1.11)

A comparison of Eqs. (1.9) and (1.11) results in the following relation

$$0 = S^\sigma\,dT + A\,d\gamma + \sum_i N_i\,d\mu_i \,.$$ (1.12)

At a constant temperature, the above relation can be simplified to

$$d\gamma = -\sum_i \frac{N_i^\sigma}{A}\,d\mu_i = -\sum_i \Gamma_i^\sigma\,d\mu_i \,,$$ (1.13)

upon dividing by A. Equation (1.13) represents the most general form of the Gibbs adsorption equation. It relates change of the interfacial tension γ to the number of moles and changes in the chemical potentials of the components in the system. For example, in a two-component system with surfactant (s) adsorbed at the surface of a liquid (l)

$$-d\gamma = \Gamma_s^\sigma\,d\mu_s + \Gamma_l^\sigma\,d\mu_l \,.$$ (1.14)

If the Gibbs dividing surface is positioned such that $\Gamma_l^\sigma = 0$, the interfacial tension will be the function of relative surface excess concentration $\Gamma_{s,l}^\sigma$

$$-d\gamma = \Gamma_{s,l}^\sigma\,d\mu_s \,.$$ (1.15)

The chemical potential of surfactant is given by the expression

$$\mu_s = \mu^0 + RT\ln(a_s)\,,$$ (1.16)

where R is the gas constant and a_s is the activity of a surfactant, dependent on its concentration c and the activity coefficient $f(c)$. For dilute solutions, $f(c) \sim 1$ and the

activity is equal to concentration. By differentiating the last equation and combining it with Eq. (1.15), one can obtain the Gibbs adsorption equation for a two-component system

$$\Gamma_{s,l}^{\sigma} = -\frac{1}{RT}\frac{d\gamma}{d\ln(c_s)}.$$
(1.17)

This equation directly tells us that when a solute adsorbs at the interface ($\Gamma_{s,l}^{\sigma} > 0$), the surface tension decreases with the increase of solution concentration. This phenomena is also known as positive adsorption. Such a behavior is typical for some organic compounds (e.g., alkyl carboxylic acids) and surfactants, as shown in Fig. 1.9 (curves 1 and 3). When
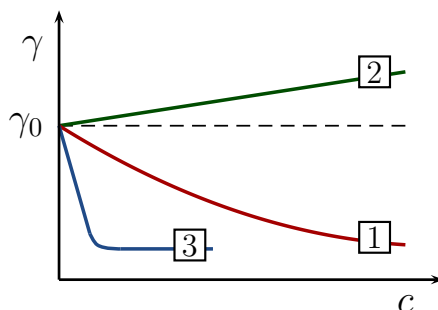
Figure 1.9: Surface tension γ as a function of concentration c for: (1) simple organic solutes, (2) simple electrolytes, and (3) surface active solutes [19].

a solute avoids the interface ($\Gamma_{s,l}^{\sigma} < 0$), the surface tension increases with the increase of the component concentration. The positive slope of the curve $d\gamma/d\ln(c_s)$ (curve 2) indicates a negative adsorption of the solute, which is typical for the inorganic electrolytes and highly hydrated organic compounds.

2.2   Micelles

2.2.1   The critical micelle concentration

When surfactant is present in a solution at low concentration, its molecules are dissolved as individual species. As mentioned before, due to their amphiphilic structure they tend to adsorb at the interfaces and reduce the surface free energy of a system. Figure 1.10 shows that the surface tension decreases strongly with increasing concentration of surfactant molecules in the solution. However, at a certain concentration the decline of surface tension is stopped and its value remains almost constant. This indicates that the surface is saturated by a monolayer of surfactants and no more adsorption sites are available.
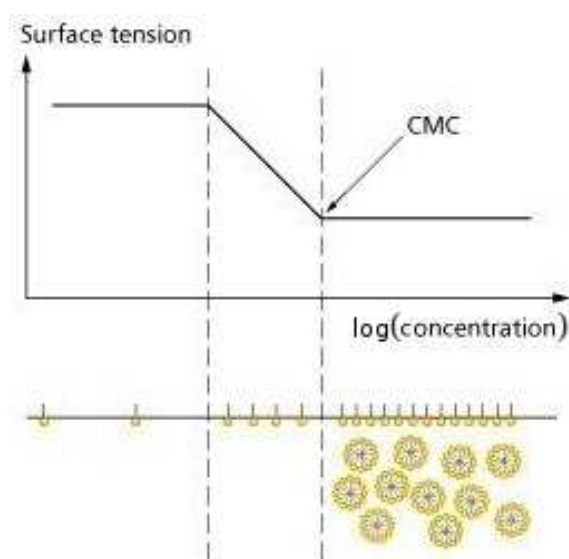
Figure 1.10: Changes in surface tension and organization of amphiphilic molecules with increasing surfactant concentration.

Above that concentration the molecules of surfactant present in the bulk will undergo self-assembly and form well defined aggregates, called micelles [1, 15]. The concentration at which micellization begins is known as the critical micelle concentration (CMC). Below CMC, the most surfactants are unassociated, while above the threshold, micelles and surfactant molecules coexist.

Most micelles just above CMC are usually regarded as a spherical association of 50–100 surfactant molecules. The hydrocarbon chains gather inside to form the core of a micelle, while the shell of ionic or nonionic polar head groups is oriented towards the aqueous phase, as shown in Fig. 1.11 (left). As demonstrated by the nuclear magnetic
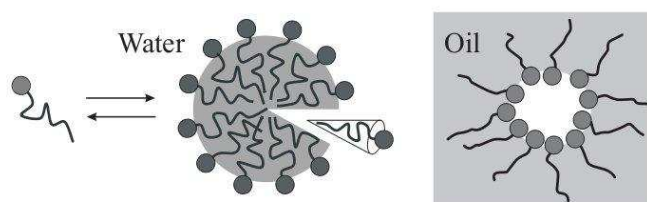
Figure 1.11: The structure of a micelle (left) and reversed micelle (right) [1].

resonance (NMR) the interior of a micelle shows liquid phase properties, such as high mobility of alkyl chains and ability to solubilize water-insoluble molecules. The outer layer also contains associated counterions (for ionic surfactants) or hydrogen bonded solvent molecules (for nonionic surfactants); this region of a micelle is described as the palisade layer. Typically radius of a micelle is equal to the length of the hydrocarbon chain,

and the outer diameter determined by the light scattering and small-angle X-ray scattering (SAXS) is within the range of 3–6 nm. The formation of micelle-like aggregates in nonpolar solvents is also possible, although the changes involved in association process must be considerably different from those in aqueous systems. The orientation of the surfactant in the solvent is opposite to that in water, with hydrophobic chains oriented to the bulk and polar heads inside the core. Such a structure is often described as reversed micelle, and is presented in Fig. 1.11 (right).

Surface tension is by no means the only property of the solution that changes with increasing concentration of a surfactant [22, 23]. There is a number of other physical characteristics, which undergo an alteration at the critical micelle concentration (see Fig. 1.12). For example, the increase in osmotic pressure is abruptly stopped as it
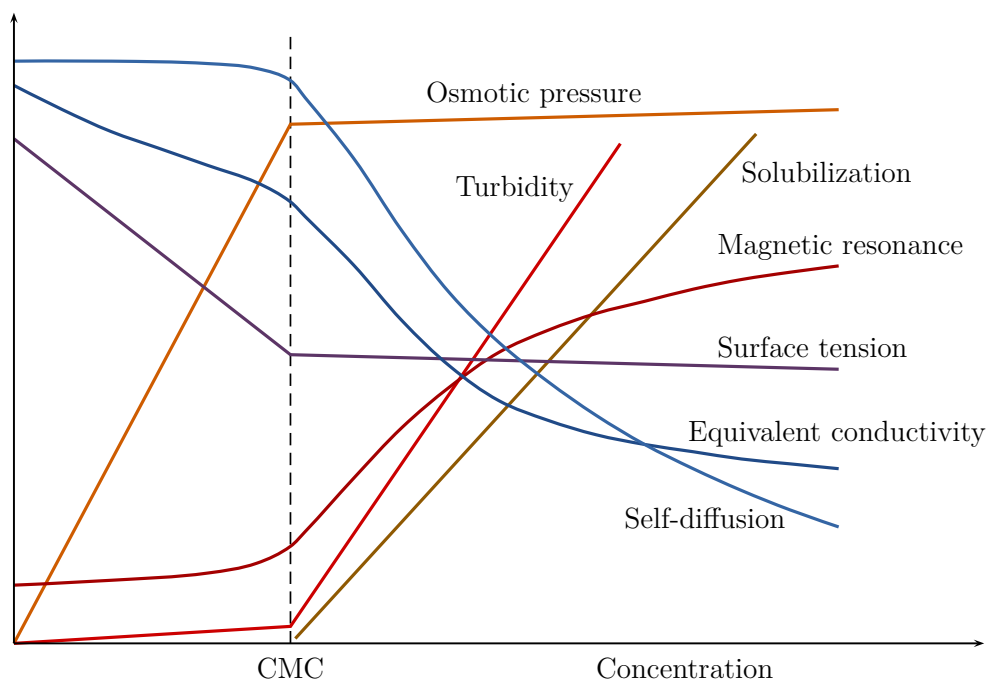
Figure 1.12: Changes in physical properties of the solution around the critical micelle concentration according to Ref. [24].

gains approximately constant value. The slope of electrical conductivity of the solution decreases indicating that there remains less individual charged units compared to associated molecules. The optical turbidity of the solution increases and it may appear opaque. Light scattering experiment indicates the presence of scattering objects with size bigger than individual monomers of surfactant. These observations serve as an evidence of significant change in the arrangement of molecules, which is formation of micelles.

17

Critical micelle concentration has a characteristic value for each surfactant molecules. It is dependent on several parameters including chemical structure of surfactant and external conditions, such as temperature or addition of electrolytes. The CMC of both the ionic and nonionic micelles decreases with increasing length of the hydrophobic chain. Nonionic surfactants have much lower CMC than ionic ones due to the lack of electrical repulsion between hydrophilic heads. Therefore, the greater is the number of ionized groups, the higher is the CMC. The addition of salt to the solution of ionics dramatically lowers the CMC up to an order of magnitude. That effect is moderate for short-chain surfactants and much more distinct for the ones with long hydrophobic group. For nonionic surfactants, electrolyte addition produces only small variations in the CMC. The addition of non-electrolytes, such as alcohols, can also decrease value of the CMC due to their stabilization effect on the micelles [17, 19].The valency of the counterion also matters. Simple monovalent counterions give similar CMC, while increasing the valency to 2 decreases the CMC approximately four times. Micellization process of ionic surfactants is only slightly affected by the temperature, while nonionic surfactants show typically monotonic decrease in CMC with increasing temperature.

2.2.2 Thermodynamics of micellization

Micellization of surfactants is regarded as spontaneous and thermodynamically favorable process [24]. An increase ΔS of entropy in a self-assembly organization of surfactants may seem a bit awkward, because micelles are certainly more ordered than individual surfactant molecules dissolved in a bulk phase. Therefore, aggregation process should result in a negative value of ΔS. However, this effect is negligible compared to the gain in
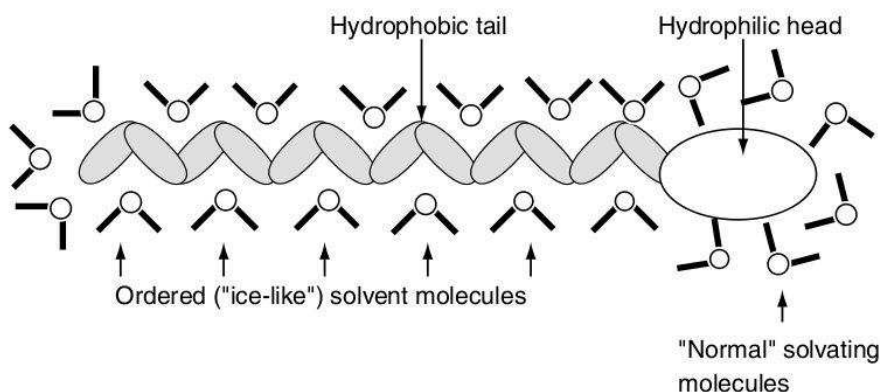
Figure 1.13: Ordering of water molecules around the hydrophobic tail of a surfactant [2].

entropy coming from two other sources. The first one is related to the hydrogen bonding that occurs in the water. When a surfactant is dissolved in the water, hydrocarbon groups occupy a cavity in the bulk structure. Water molecules around alkyl chain are highly ordered and form clusters, also called "icebergs", which is shown in Fig. 1.13. This accounts for decrease in the entropy of a system. When hydrocarbon group is transferred from water to a liquid core of a micelle, water molecules are released and regain their primary structure. A drastic increase of water entropy compensates for negative entropy of surfactant aggregation. This phenomena is described as the "hydrophobic effect". The hydrophobic effect also explains why the CMC decreases with increasing alkyl chain length. Additionally, the entropy growth is a result of increased flexibility of hydrocarbon chains, shielded from water inside oil-like core of a micelle.

There are two main approaches describing thermodynamics of micellization [3, 24]. In the simplest approach, called phase separation model, micelles are considered as a separate phase and CMC as saturation concentration of surfactant in the monomeric state. Increase in surfactant concentration above the CMC is regarded as to affect only the micelle concentration. This is not consistent with the experimental observations, where activity of the monomers is variable also above CMC. Moreover, micelles cannot be regarded as a single phase because of their nonuniform state. The higher is the aggregation number, i.e., the number of surfactant monomers building a micelle, the better approximation phase separation model becomes. In the second approach, the mass action model, micelles and surfactant monomers are considered to be in the association-dissociation equilibrium. This model is more realistic and describes changes in monomer concentration above CMC.

In the phase separation model the chemical potential of surfactant dissolved at low concentration can be described as

$$\mu_{\mathrm{sur}}(\mathrm{solvent}) = \mu_{\mathrm{sur}}^0 + RT \ln [\mathrm{S}] , \tag{1.18}$$

where μ_{sur}^0 is the effective standard chemical potential and $[\mathrm{S}]$ is the concentration of surfactant. When surfactant concentration reaches CMC, the chemical potential of an unassociated surfactant is equal to the chemical potential of a surfactant in a micelle $\mu_{\mathrm{sur}}(\mathrm{micelle})$

$$\mu_{\mathrm{sur}}(\mathrm{micelle}) = \mu_{\mathrm{sur}}^0 + RT \ln [\mathrm{CMC}] . \tag{1.19}$$

The Gibbs free energy of micellization can be then expressed as

$$\Delta G_{\mathrm{mic}} = \mu_{\mathrm{sur}}(\mathrm{micelle}) - \mu_{\mathrm{sur}}^{0} = RT \ln\left[\mathrm{CMC}\right]. \tag{1.20}$$

The last equation can be applied without modifications for nonionic surfactants. In the case of ionic and zwitterionic surfactants, one has to take into account the change in dissociation of the charges from the head groups.

2.2.3 Micelle dynamics

By no means micelles can be regarded as static structures [16, 20]. The hydrophobic chains and heads of surfactant units building a micelle are mobile. Counterions originating from ionic groups are not bounded to the heads, but moving across the surface. There is a constant interchange of the surfactant molecules between the micelles and solution, as shown in Fig. 1.14. Not all the micelles are constituted with the same number of surfactants. Experimental investigations including use of fast kinetic measurements allowed to
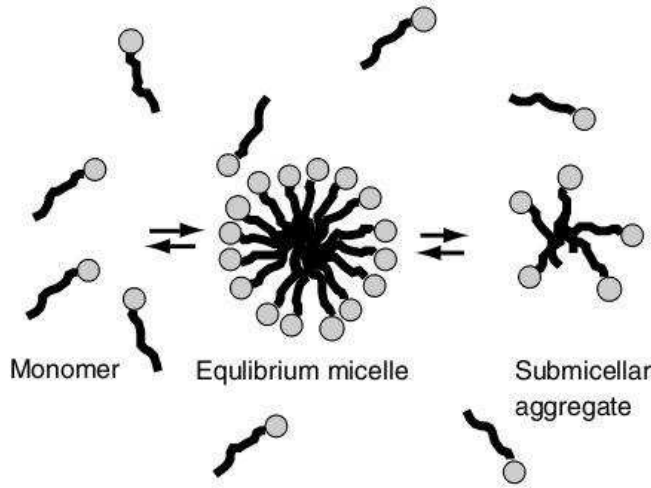
Figure 1.14: Exchange processes in micelles [2].

establish that there are two relaxation times characteristic for micellization process. The faster relaxation time τ_1 is attributed to the exchange of surfactant molecules between micelles and the solution. The slower relaxation time τ_2 represents the rate at which micelles form and disintegrate. The residence time of surfactant molecule in a micelle is within the range of 10^{-8}–10^{-3} s, while the life time of a micelle is usually on the order of miliseconds (10^{-3}–1 s). These timescales depend on different factors such as temperature, surfactant

concentration and, particularly, on the hydrocarbon chain length. The residence time grows significantly with increasing chain length. The phenomenon of solubilization is also able to extend the lifetime of a micelle. Taking into account the above considerations, it is more accurate to think of a micelle as a dynamic unit with a lifetime of approximately 1 ms [24].

2.2.4 Structure of surfactant aggregates

Close to the CMC majority of micelles are believed to have spherical shape. At higher concentrations of surfactant they can form other, more complex phase structures, such as cylinders, vesicles or bilayers [17, 19]. The shapes of the association colloids depend on many factors, such as concentration and geometry of the surfactant, presence of cosurfactants, pH and salt concentration of the solution, temperature. The geometry of surfactant molecule in micelle can be described in terms of three parameters, i.e., the head group area A_h, the volume of the tail V_t, and the length of the tail L_c. Using these parameters, it is possible to express an important factor called packing parameter N_S

$$N_\mathrm{S} = \frac{V_\mathrm{t}}{L_\mathrm{c}\,A_\mathrm{h}}\,. \tag{1.21}$$

This parameter relates the geometry of the molecule to the preferred shape of aggregate formed, as presented in Fig. 1.15. For example, small values of N_S are characteristic for surfactants forming highly curved structures. If $N_\mathrm{S} < 1/3$, the critical packing shape is a cone and a preferred structure of the aggregate is a spherical micelle. This shape is characteristic for single-chained surfactants with large head group areas. When $1/3 < N_\mathrm{S} < 1/2$, the cylindrical micelles are formed. Surfactants in this category are single-chained with charged small head group areas at high salt concentration, such as SDS and CTABr. The rod-like micelles are also formed by nonionic or zwitterionic surfactants. The bilayers – flexible or planar are preferentially formed for $N_\mathrm{S} = 0.5$–1. If $N_\mathrm{S} = 1$, the critical packing shape is a cylinder and the self-assembly of surfactants will lead to a formation of planar bilayers. Such behavior is characteristic for double-chained lipids, such as phosphatidyl ethanolamine. They cannot pack into micellar or cylindrical structures because of small head group area and too bulky hydrophobic chains. At high lipid concentrations, these lipids form lamellar phase consisting of roughly parallel planar
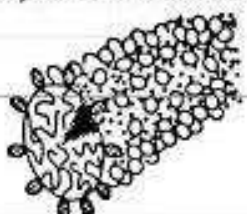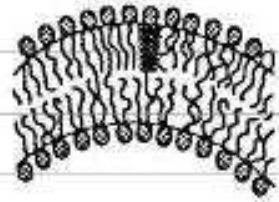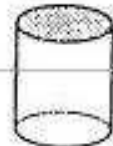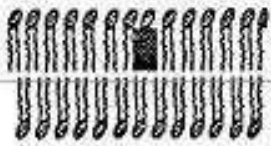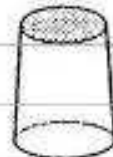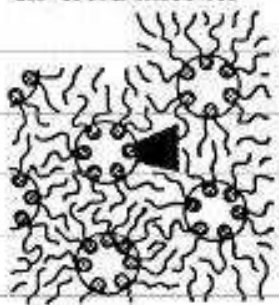
Packing parameter	Critical packing shape	Structures formed
< 1/3	Cone	Spherical micelles
1/3–1/2	Truncated cone	Cylindrical micelles
1/2–1	Truncated cone	Flexible bilayers, vesicles
~1	Cylinder	Planar bilayers
>1	Inverted truncated cone or wedge	Inverted micelles

Figure 1.15: The packing parameter and its relation to the preferred shape of formed aggregate [19].

bilayers, or bicontinuous structures consisting of two continuous phases.

Lipid bilayers are the structures of fundamental importance for living organisms. All biological membranes are composed of bilayers of phospholipids with associated membrane proteins, as shown in Fig. 1.16. The cell membrane surrounds the interior of the cell
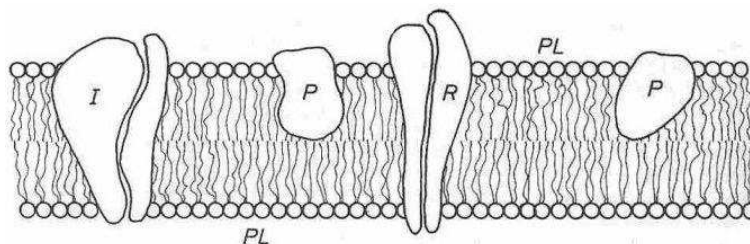
Figure 1.16: The membrane structure — a bilayer of phospholipids (PL) with embedded proteins (P), integrins (I) and receptors (R) [25].

and separates it from the environment. The current model of the membrane structure postulates a fluid mosaic, in which proteins are embedded into a lipid layer [25].

2.2.5   Micellar solubilization

Solubilization is the second most important phenomenon, next to adsorption of surfactants at interfaces, occurring in the solutions of amphiphiles [24, 26]. Typically a hydrophobic substance, which is insoluble in water below CMC will become soluble after exceeding this threshold concentration. This effect is resulting from the presence of the micelles. The higher is the concentration of surfactant (solubilizer), the more solubilizate can be dissolved in the solution. The large solubilization capacity of the micelles towards nonpolar substances is caused by similarity of the micellar core to the corresponding alkane in a pure liquid oil. There is, of course, an upper limit of solubilization for a given component; beyond that concentration solubilizate exhibit properties of separate phase.

The accommodation of solubilizate within a micelle is dependent on its polarity (see Fig. 1.17). The nonpolar solubilizates are present in the hydrocarbon core, while slightly polar and polar solubilizates are positioned in the palisade layer [2, 3]. The solubilization capacity is dependent on several factors, such as surfactant and solubilizate structure or temperature. An increase of surfactant hydrophobic tail length enhances solubilization capacity of nonpolar compounds. The solubilization capability of surfactants with the same alkyl chain increases in the order: anionics < cationics < nonionics. This effect is
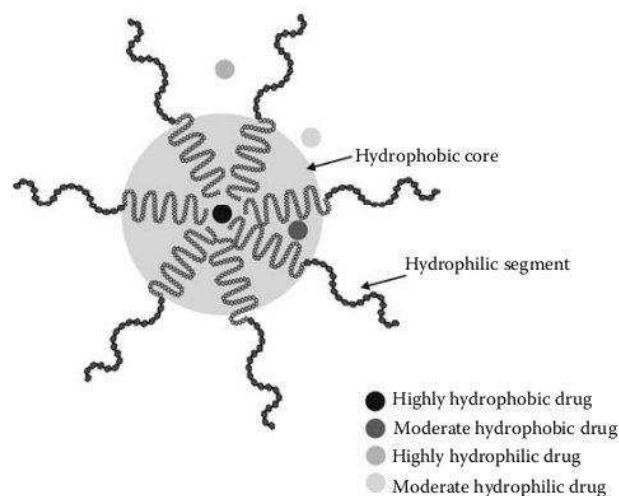
Figure 1.17: Possible accommodations of solubilizate within a micelle [3].

due to an increase of head group area and therefore, formation of looser micelles leaving more space for the solubilizate. The longer the chain of solubilizate, the smaller is its solubility in a core of a micelle. Temperature tends to improve solubilization process. Addition of electrolyte to the solution will increase the solubility of nonpolar compound but can also decrease the solubility of a substance placed in the palisade layer.

Solubilization has been in use for many years and in different applications, such as detergency, pharmaceuticals formulation, or separation processes based on micellar encapsulation [3, 16, 19]. The latter has a great importance in the removal of contaminants
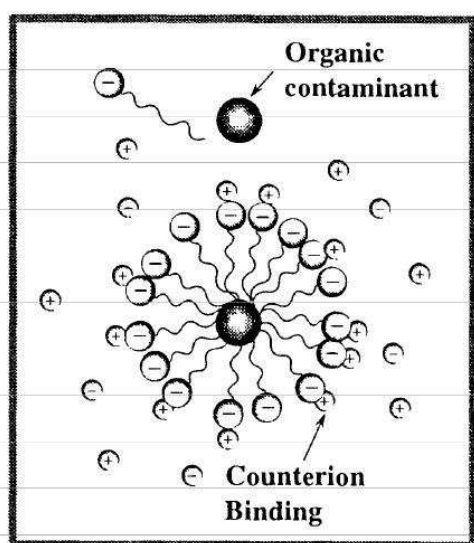
Figure 1.18: Use of micelles to trap hydrocarbon and ionic wastes [19].

from groundwater and industrial wastewater. Bio-based ionic surfactants are added to

contaminated reservoirs at concentrations above CMC. The interior of a micelle will trap hydrocarbon wastes, while ionic contaminants can adsorb to the polar heads of the palisade layer, as shown in Fig. 1.18. Later on, micelles can be removed using ultrafiltration methods. Such a process is both cost effective and environmentally friendly. The ability of micelles to solubilize and deliver promising, but water-insoluble drugs to the required site cannot be overrated as well.

3 Emulsions

3.1 General properties

Oil and water do not mix. This is caused by nonpolar nature of hydrocarbon molecules, which can not strongly interact with water [27]. On many occasions, however, the mixing of such incompatible liquids will help to overcome everyday problems [16]. When vigorously shaken or agitated, oil and water can form a two phase mixture – an emulsion, which can be defined as a heterogeneous dispersion of two immiscible liquids. One phase is the dispersing medium, also called external or continuous phase. The dispersed (internal) phase is finely distributed in the form of small droplets, usually with a diameter smaller than 100 μm [28].

Several classes of emulsions can be distinguished: oil-in-water (O/W), water-in-oil (W/O), and oil-in-oil (O/O). It is worth to mention that oil designates here any liquid
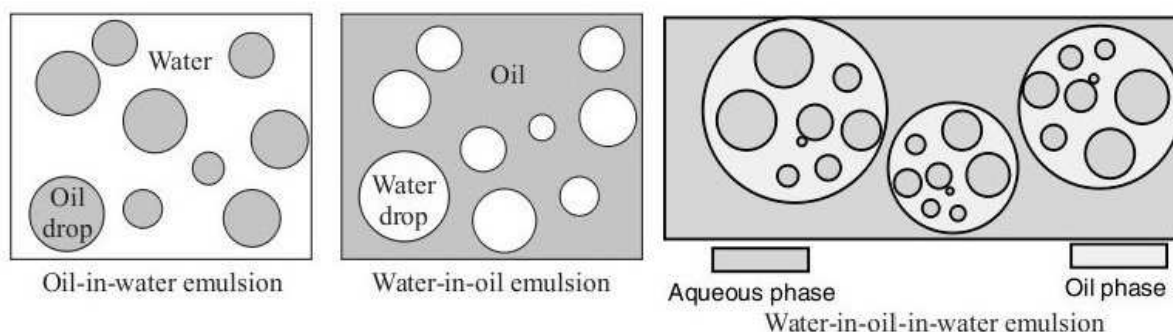
Figure 1.19: Schematic representation of the O/W, W/O and W/O/W emulsions [1, 2].

not soluble in water. The most important emulsions are oil-in-water, where oil droplets are dispersed in aqueous phase, and water-in-oil, consisting of water droplets in oil phase [29].

The O/O emulsions are consisting of a polar oil (e.g., propylene glycol) dispersed in a nonpolar oil (paraffinic oil), or vice versa. Such emulsions are rather seldom, due to high miscibility of most organic liquids. There are also polydispersed systems, referred to as multiple emulsions, in which the dispersed particles are emulsions themselves [30, 31]. The two commonly used emulsions are the oil-in-water-in oil (O/W/O), where emulsion of oil droplets dispersed in water is in turn dispersed in a continuous oil phase, and the water-in-oil-in-water (W/O/W), where W/O emulsion is dispersed in aqueous phase. W/O/W emulsions are widely used in pharmaceutical applications, as well as in the separation process, cosmetics or food industry. Different types of emulsion are schematically shown in Fig. 1.19.

Emulsions are of the great importance in almost every aspect of our lives [15]. Food production and storage benefit a great deal from the colloid chemistry, because an organic nutrient compound must be dispersed in water and stable over a long period of time. The texture and the taste of a product strongly depends on the colloidal size distribution [27]. Lecithin is often used to stabilize the O/W and W/O emulsions and to prevent their phases from separation. Examples of food emulsions involve mayonnaise, milk, butter, dairy products, ice creams, chocolate, sauces, etc. Emulsions are also present in personal care products, such as lotions, hand creams, shampoos and sunscreens, and in cleaning formulations (dry-cleaning fluids, car waxes). Properties of emulsions are widely used in the pharmaceutical field, where they find application as drug delivery systems for oral, dermal or parenteral administration [9]. Application of emulsions in medicine will be discussed in details in Section 5. The latex paints and photographical emulsions (AgBr crystals in a gel of gelatin and water) are the other important applications. Emulsions are also used in the flotation process and oil industry. Crude oils often contain water droplets, which has to be removed by coalescence, followed by the separation process. Oil spilled from tankers to the water must be emulsified and separated [24]. The importance of emulsions in various fields justifies all the efforts put into the research on their properties and stability.

3.2 Thermodynamics of emulsification

During the emulsification one of the two immiscible liquids will break up into small droplets dispersed in the continuous phase. Such a process requires the great amount

of work to increase the area of interface between the two phases. The work required to generate new interface is given by

$$W = \gamma \Delta A \,, \tag{1.22}$$

where γ is the interfacial tension between the two liquid phases and ΔA is the change in interfacial area.

Since the interfacial tension between two immiscible liquids is greater than zero, the Gibbs free energy of a system significantly increases during the emulsification process. At the same time, a positive entropy change accompanying the emulsification can be expressed as

$$\Delta G_{\text{formation}} = \gamma \Delta A - T \Delta S \,. \tag{1.23}$$

The droplets formed within the process are not very small ($\gamma \Delta A \gg T \Delta S$), and therefore the entropy change is negligible [15]. That means that emulsion formation is non-spontaneous process and emulsions are thermodynamically unstable. Two bulk phases are separated by the minimum area interface; therefore, the system tends to undergo phase separation in order to minimize the potential energy. The breakdown of emulsions starts right after the mechanical agitation is stopped. For that reason two pure, immiscible liquids cannot form an emulsion stable over a long period of time. The presence of so called emulsifying agents (e.g., surfactants or polymers) will create an energy barrier between the droplets and the system becomes kinetically stable. Emulsifiers stabilize the system by decreasing the interfacial tension between two phases. As the result, lower amount of mechanical work is required to generate emulsion droplets. Moreover, the rate of coalescence of the droplets is decreased due to formation of mechanical, steric and/or electrical barriers around them. Electrostatic and steric repulsion will be discussed in details in Sec 3.6, together with other aspects of emulsion stabilization.

3.3   Classification of emulsions

Emulsions can be classified according to their stability. From the thermodynamic point of view, two types of emulsions can be distinguished. Unstable or metastable systems are called macroemulsions. Addition of emulsifiers reduces sufficiently the interfacial tension to obtain droplets of the internal phase dispersed in the continuous phase. However, the value of interfacial tension between these two phases is higher than zero and therefore,

macroemulsions tend to separate into two phases. The process of separation, known as demulsification, is often so slow that macroemulsions seem to be stable (kinetic stabilization). Typically, a droplet of macroemulsion has diameter within the range of 0.5–10 μm, which is large enough to scatter the light. Because of that macroemulsions (e.g., milk, being emulsion of fat droplets dispersed in water and stabilized by milk protein — casein) often appear opaque or non-transparent [20]. If the interfacial tension value approaches zero, emulsification can occur spontaneously. The process requires little or no input of mechanical energy beside gentle stirring of components. The dispersions obtained, called microemulsions, are thermodynamically stable. First introduced by Hoar and Schulman in 1943, they were a subject of intensive research for more than six decades [32–36]. Homogeneous on a macroscopic level, they are heterogeneous on a microscopic level as they consist of different microdomains. A typical droplet size of microemulsion is smaller than 500 nm. Among the thermodynamically stable systems one can also distinguish so called nanoemulsions, consisting of fine droplets with the narrow size distribution [37, 38]. In the literature, they are often described as miniemulsions or ultrafine emulsions [39–41]. Nanoemulsions are optically transparent or translucent; therefore, it is easy to observe any symptoms of their destabilization. Due to their small droplet size (typically in the range of 50–200 nm) a large reduction in gravity force is accomplished, preventing their sedimentation or creaming [42]. Therefore, a high stability of such systems can be obtained.

3.4 Methods of emulsification

There are four main methods of emulsion preparation, i.e., the mechanical emulsification, membrane emulsification, phase inversion emulsification and spontaneous emulsification. Two latter methods are often described as low energy techniques, or chemically based processes, since the properties of final emulsion depend mainly on chemical nature of additives, ratio between two phases and temperature [2]. Mechanical emulsification techniques, also known as physical emulsification or high energy techniques, require a large energy input. Here, the nature of obtained product results from rheological and chemical properties of two phases, as well as the amount and form of energy used in the emulsification process [43]. As mentioned before, in almost all cases addition of emulsifier is required to facilitate the formation of droplets.

3.4.1 High-energy techniques

The formation of large emulsion droplets is quite easy. However, the smaller size of dispersed phase the more surfactant and/or energy is required to produce emulsion. The dispersion of a drop into smaller droplets is achieved by a deformation [24]. The internal pressure of the droplet, called the Laplace pressure, can be expressed as follows:

$$\Delta p = \gamma \left(\frac{1}{R_1} + \frac{1}{R_2} \right) , \tag{1.24}$$

where R_1 and R_2 are the radii describing the curvature of the drop. For a spherical drop $R_1 = R_2 = R$, the Laplace equation can be simplified

$$\Delta p = \frac{\gamma}{2R} . \tag{1.25}$$

In order to break a droplet into smaller ones, a pressure gradient or shear force (stress) is needed. The energy needed to perform deformation is higher for smaller droplets. Addition of surfactant would decrease the interfacial tension, reduce the internal pressure of a droplet and stress required to tear it apart [44].

There are several procedures exploiting mechanical devices, which can be applied in the process of emulsion formation. High-pressure homogenization (HPH) is a fluid mechanical process divided in two stages. First, a coarse emulsion of oil and water is obtained using high-shear mixers. Later on, the raw emulsion is passed through a chamber under a high pressure in such a way that a homogeneous dispersion of smaller droplets is obtained. The control of parameters such as pressure, temperature and number of homogenization cycles allows to obtain a product with specific properties. Emulsions produced by HPH are characterized by more homogeneous droplet size distribution, usually within 500 nm–5 μm, and increased stability. Homogenization also limits the amount of required additives. This process is often used in the treatment of food and dairy products, improving their shelf life, digestion and taste [45–49].

Ultrasonication is another way of obtaining emulsions with a small droplet size. Its mechanism is not yet fully understood. The solution is treated with ultrasounds, which results in generation of cavitation bubbles. These bubbles tend to implode, which provides sufficient shear stress to create new interfacial area between two phases. Particle sizes are

controlled by the content of surfactant and limited to 500 nm. The disadvantage of the ultrasonication technique is the difficulty of implementation on the industrial scale [50–52].

Mechanical stirring involves use of devices such as rotor/stator, high speed mixers (Ultraturrax), or magnetic stirrers. They provide low to medium energy during the process. In comparison with two previous emulsification techniques, the droplet size of obtained emulsions is larger. A significant part of provided energy is dissipated in heat generation and viscous friction. However, mechanical stirring assisted by addition of a large amount of surfactants is often applied in industrial processes [38, 53].

3.4.2 Low-energy techniques

In some cases high-energy techniques cannot be used, e.g., for labile molecules, when excess of surfactants should be avoided, or just for economical reasons. Then, it is possible to choose between different low energy emulsification techniques. The most popular methods involve membrane emulsification, phase inversion and spontaneous emulsification process.

Membrane emulsification is a simple method of producing emulsions with narrow droplet size distribution. It has been extensively investigated over the last twenty years. In this process, which is schematically shown in Fig. 1.20, a microporous membrane with
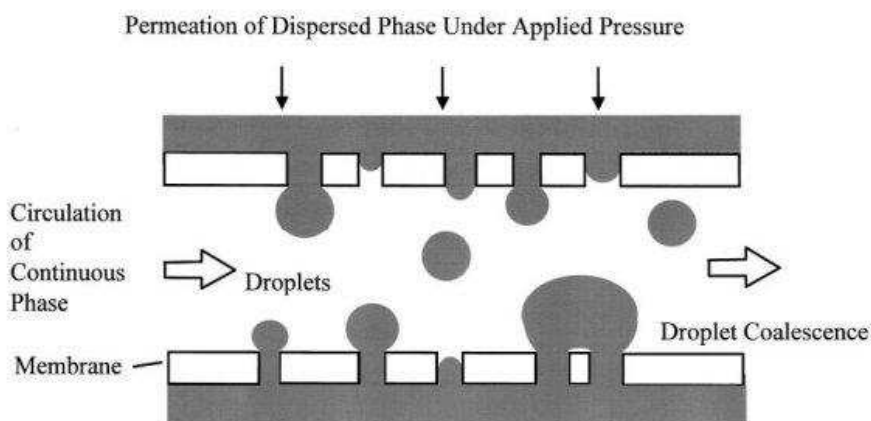
Figure 1.20: Schematic representation of membrane emulsification process [54].

well defined pore size serves as an emulsifying tool. The dispersed phase is pressed through the membrane into the continuous phase. The resulting droplets grow until they reach certain size. At this point detachment of droplets occurs, caused by the flow of the continuous phase. The size of resulting emulsion droplets is determined by many parameters, such as membrane properties (porosity, pore size and distribution, surface type), system

properties (emulsifier type and concentration, temperature, viscosity), and process parameters (velocity of continuous phase, emulsification pressure) [54–57]. The first membrane, used for emulsification by Nakashima, was made from glass, currently known as an SPG membrane (Shirazu porous glass) [58, 59]. The membranes can be made from another materials, such as ceramics, metals or polymers. The nominal pore sizes differ from about 0.05 to 14 μm. Usually the resulting droplet size ranges from 2 to 10 times the nominal pore diameter. The dispersed phase should not wet the pores of a membrane; therefore, hydrophilic membranes are appropriate for formation of O/W emulsions, while hydrophobic membranes are used for the W/O emulsions [60–62]. The porosity of a membrane is another g of the emulsion-important factor. If the pores in a membrane are too close, the resulting droplets are likely to coalesce before they detach from the surface. On the other hand, too low porosity can significantly decrease the effectiveness of emulsification. The pressure of a process must be carefully chosen as well. The minimum emulsification pressure, also referred to as critical or trans-membrane pressure, describes the conditions at which dispersed phase starts to permeate through the membrane pores. It can be calculated from the equation for the capillary pressure

$$P_{\mathrm{C}} = \frac{4\gamma \cos\theta}{d_{\mathrm{p}}} \, , \tag{1.26}$$

where d_{p} is the pore diameter and θ is the contact angle between the dispersed phase and the membrane surface.

For a membrane with small pore size, higher values of the pressure are required. Typically, formation of an O/W emulsion on a membrane with nominal pore size of 0.2 and 0.8 μm is between 20 and 500 kPa. Too low pressure unnecessarily prolongates the emulsification, while too high pressure causes formation of large droplets. A reasonable range of the emulsification pressure is 2 to 10 times greater than the critical pressure value [63, 64]. A careful choice of the above mentioned parameters allows to produce emulsions with desirable properties in a simple, low-energy, less surfactant-demanding process, that makes it highly attractive for a large-scale production.

Phase inversion is another low-energy technique, which allows to turn emulsion of one type into another, such as an O/W emulsion can be phase-inverted to the W/O emulsion [15, 50]. A typical example of this process in practice is inversion of milk (O/W

emulsion) into butter (W/O emulsion). The inversion can be evoked by changing some of the emulsification parameters, such as temperature, phase-to-volume ratio, electrolyte concentration, an order of phase addition, or the nature of an emulsifier (see Fig. 1.21). The most popular method is the so-called phase-inversion temperature (PIT), introduced
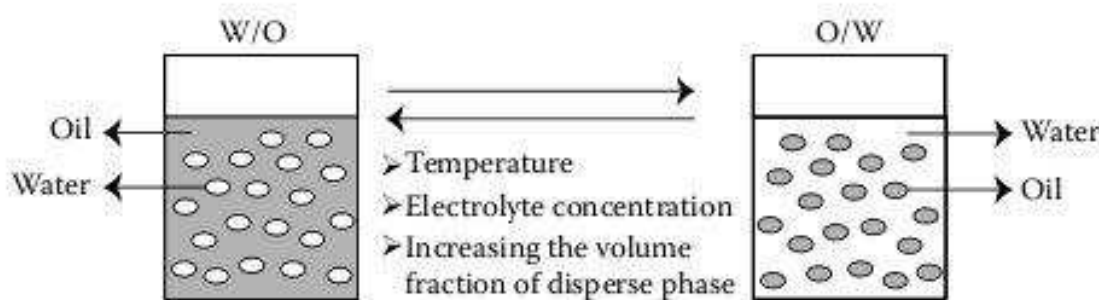
Figure 1.21: Schematic representation of phase-inversion method [3].

by Shinoda and Saito in 1968 [65, 66]. It is based on the ability of nonionic surfactants, namely polyoxyethylene-type, to change their solubility with temperature. As the temperature of a system increases, polar groups of polyoxyethylene surfactants become less hydrated and the molecules become more lipophilic. Therefore, a spontaneous curling of surfactant film between two phases will occur and a primary O/W emulsion will be replaced with W/O droplets [38]. Some emulsions stabilized by nonionic surfactants may invert to W/O upon cooling of a system. A disadvantage of the PIT method is that it is restricted to nonionic surfactants only. However, being the solvent-free and low-energy technique, it is widely used in pharmaceutical and cosmetics applications [67–69]. Another possibility is use of the emulsion inversion point method (EIP), where the inversion is obtained by changing the volume ratio between two phases. Initially, W/O emulsion is formed by addition of water into continuous oil phase. If the water concentration is permanently increasing, water droplets tend to merge together into bigger drops containing dispersed oil phase. At a given volume, the phase inversion is accomplished and O/W emulsion is formed [42]. The O/W emulsions stabilized by ionic surfactants can also undergo phase inversion upon electrolyte addition. The mechanism of this transition is related to neutralization of the charged film around dispersed droplets and decrease of hydrophilicity of surfactants. As a result, oil droplets tend to merge into a continuous phase and entrapped water is surrounded by uncharged, interfacial film, giving an inverted W/O emulsion.

Miller (1988), Vitale and Katz (2003) demonstrated a different spontaneous emulsification technique, also known as the "Ouzo effect" [70, 71]. Figure 1.22 shows a schematic
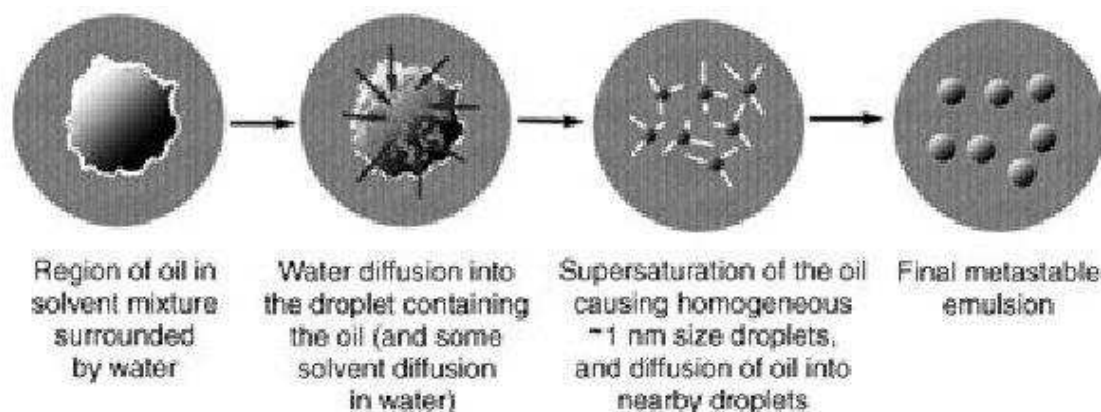
Figure 1.22: Schematic representation of the liquid-liquid nucleation process (Ouzo effect) [72].

representation of this process. In the first step, an organic phase consisting of oil in a water-miscible solvent is prepared. The resulting homogeneous solution is mixed with water under magnetic stirring. Rapid diffusion of the miscible solvent into the aqueous phase causes supersaturation of oil and homogeneous liquid-liquid nucleation. As a result, the O/W nanoemulsion with narrow droplet size distribution is formed instantaneously [72, 73]. During this process, solution becomes cloudy. This phenomenon can be observed upon dilution of aperitifs (Ouzo, Pastis) with water, due to the presence of water-insoluble anis seeds extract. The opposite effect, that is spontaneous formation of W/O emulsion is also possible, but the majority of research is focused on O/W formulations. The droplet size of a resulting emulsion can be easily controlled by changing parameters such as oil-to-solvent ratio, temperature and surfactant addition. Increasing the temperature during the process results in formation of smaller droplets [37–39]. The Ouzo emulsions remain stable during months without the presence of emulsifiers. The source of energy in the spontaneous emulsification is clearly related to interfacial turbulences and/or surface tension gradient, but its mechanism is not completely understood. There are several reviews discussing „diffusion and stranding", the Marangoni effect, or the zero interfacial tension as possible explanations for the Ouzo effect [74–79]. A major limitation in the use of Ouzo emulsification process is quite low content of oil in the emulsion (typically 1% v/v up to 5% v/v after solvent evaporation). A solvent used in the

process should be soluble in water in all proportions and possess low toxicity, especially if emulsion is intended for use in pharmaceutical formulations [80, 81].

3.5 Role of emulsifiers

The formation of emulsion with long-term stability requires the presence of emulsifying agent at the liquid-liquid interface [82]. There are four groups of materials, which can act
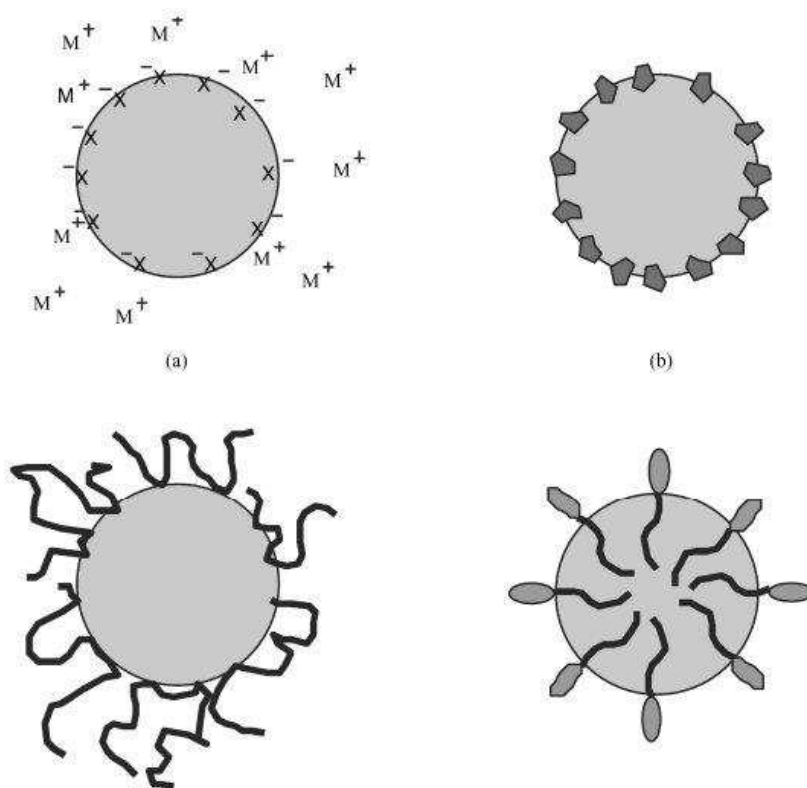
Figure 1.23: Different mechanisms of emulsion stabilization: (a) adsorbed ions – specific ions adsorption, (b) colloidal solid particles, (c) polymeric stabilizers, (d) adsorption of surfactants [17].

as emulsifiers: ionic (but not amphiphilic) materials, polymers, colloidal solid particles and surfactants (see Fig. 1.23). A role of surfactants will be described in details in the following chapters. There are considerable differences in the mechanism of action and effectiveness of particular emulsifiers. Specific ions adsorption results in stabilization by the electrostatic repulsion between the droplets, as well as by orienting solvent molecules in their neighborhood. Colloidal particles, e.g. clays, do not affect interfacial tension directly. They adsorb at the surface of droplets, thus forming a physical barrier around

the interface. Such a barrier can effectively prevent the droplets from collisions.

3.5.1 Steric stabilization

Polymeric macromolecules are another group of materials with great importance in emulsion formation. They favor the emulsification due to a combination of several factors. The presence of polymers at the oil-water interface leads to steric stabilization, also known as steric interactions. The commonly used steric stabilizers are both materials of natural origin, such as proteins or starches, as well as synthetic compounds like polyvinyl alcohol (PVA), polyacrylic acid (PAA), polyethylene glycol (PEG), alcohol ethoxylates and block copolymers. They strongly adsorb at the interface, forming a rigid, mechanical barrier between the droplets. Each molecule adsorbs at many sites of the interface, which makes desorption probability very low. When two emulsion droplets are approaching each other, the movement of polymeric chains is restrained, causing unfavorable decrease of the entropy. This effect is a source of repulsive interactions between the droplets. The presence of steric stabilizers can also lower the interfacial tension and increase viscosity of the continuous phase. As a result, many processes leading to breakdown of the emulsion can be significantly retarded. A serious limitation of the steric stabilization is related to the long time required for adsorption of polymers at the interface, compared to the emulsification itself.

3.5.2 Selection of a surfactant

Surfactants are the most important group of known emulsifiers. Their action in the emulsification process relies on several effects, such as lowering of the interfacial tension, increasing surface elasticity and viscosity, introducing repulsion between emulsion droplets and further stabilization of the obtained system [82]. The choice of surfactant for the specific application is determined by its solubility, the properties of liquid phases, the type of emulsion being formed (O/W or W/O), conditions of its use and so forth. There are several empirical approaches enabling a selection of proper surfactant for the emulsification process, i.e., Bancroft's rule, the hydrophile–lipophile balance (HLB), or hydrophilic-lipophilic deviation (HLD) [83–85].

The type of emulsion being formed depends mostly on the nature of surfactant; here, oil-in-water ratio of is not decisive factor. Surfactants have limited solubility in both

phases of the system. Some of them are better soluble in water, while the others are more soluble in oil. In 1913, Bancroft formulated the rule stating that the phase in which emulsifier is preferentially soluble tends to become the continuous phase of emulsion [86, 87]. Therefore, water-soluble surfactants will more likely produce O/W emulsions, while surfactants more soluble in oil will contribute to the formation of W/O emulsions. There are, of course, some limitations to Bancroft's rule. A comparison of two ratios describing phase behavior allows to determine the violations of the law. One is related to the bulk phases and it concerns the ratio of water — surfactant and oil — surfactant interactions. The other ratio stands for phenomena in the interfacial layer, namely compares interactions between hydrophilic heads of surfactant and water to those between hydrophobic chains of surfactant and oil. When both ratios are smaller or larger than unity, Bancroft's rule is obeyed [88].

The most useful approach, which correlates the type of emulsion being formed with a surfactant used in the process, was introduced in 1949 by Griffin [85]. The so-called hydrophile-lipophile balance (HLB) is a dimensionless scale describing the mutual effect of the hydrophilic and lipophilic groups of a surfactant in terms of some empirical formulas used to calculate HLB values for a specific molecule. The scale ranges from 0 to 20, with hydrophilic surfactants favoring formation of O/W emulsions at the high end of the scale (>11), and lipophilic surfactants stabilizing W/O emulsions corresponding to the low (<9) HLB values. Surfactants in the middle of HLB scale are very efficient in lowering interfacial tension, but do not perform well as emulsifiers due to their comparable solubility in both phases. There exist various methods for determining the HLB values of nonionic surfactants, such as follows:

$$\text{HLB} = 20\,\frac{M_\text{h}}{M}\,, \tag{1.27}$$

where M_h is the molecular weight of the hydrophilic moiety of a surfactant, while M is the molecular weight of the whole molecule.

The HLB values of nonionic surfactants with polyoxyethylene solubilizing groups can be calculated by the formula:

$$\text{HLB} = \frac{\text{mol\% hydrophilic groups}}{5}\,. \tag{1.28}$$

In 1957, Davies [89] introduced another concept of calculating HLB values, based on the chemical group contribution:

$$\text{HLB} = 7 + \sum (\text{hydrophilic group numbers}) - \sum (\text{hydrophobic group numbers}). \quad (1.29)$$

Typical HLB values for nonionic surfactants are presented in Table 1.1, while the group

Surfactant	HLB
Sorbitan trioleate	1.8
Sorbitan tristearate	2.1
Propylene glycol monostearate	3.4
Glycerol monostearate	3.8
Sorbitan monooleate	4.3
Sorbitan monostearate	4.7
Polyoxyethylene(2) cetyl ether	5.3
Diethylene glycol monolaurate	6.1
Sorbitan monolaurate	8.6
Polyexyethylene(10) cetyl ether	12.9
Polyexyethylene(20) cetyl ether	15.7
Polyexyethylene(6) tridecyl ether	11.4
Polyexyethylene(12) tridecyl ether	14.5
Polyexyethylene(15) tridecyl ether	15.4

Table 1.1: Typical group numbers for calculation of HLB numbers [17]. Numbers in parentheses indicate the average number of OE units in the hydrophilic chain.

numbers for calculation of HLB are gathered in Table 1.2. It is important to keep in mind, that the HLB characterizes the emulsifying properties of surfactant, but not its effectiveness, which is dependent on the balance between the surfactant HLB value and the oil phase. In general, mixtures of surfactants perform better than the pure compounds.

HLB of the mixture can be calculated as the weighted mean of the values of used surfactants. A major weakness of HLB scale is that changes in the emulsification conditions, such as temperature, presence of electrolytes or nature of oil phase, are not taken into account.

Group	HLB Number	Group	HLB Number
Hydrophilic		Hydrophobic	
$-SO_4Na$	38.7	$-CH-$	-0.475
$-COOK$	21.1	$-CH_2-$	-0.475
$-COONa$	19.1	$-CH_3$	-0.475
$-N$ (tertiary amine)	9.4	$-CH-$	-0.475
Ester (sorbitan)	6.8	$-CF_2-$	-0.87
Ester (free)	2.4	$-CF_3$	-0.87
$-COOH$	2.1	Miscellaneous	
$-OH$ (free)	1.9	$-(CH_2CH_2O)-$	0.33
$-O-$	1.3	$-(CH_2CH_2CH_2O)-$	-0.15
$-OH$ (sorbitan)	0.5		

Table 1.2: Calculated HLB values for typical nonionic surfactants according to Ref. [17].

Microemulsions are mostly formed in the presence of more than one surfactant. In 1979, Salager [90] suggested the equation determining the optimal formulation of microemulsions containing anionic surfactants

$$HLD = \ln S - k\,ACN - f(C_A) + \sigma - \alpha_T \Delta T\,, \tag{1.30}$$

Where S is the concentration of electrolyte (salinity), ACN is the carbon number of the alkane used, $f(C_A)$ is a function of the cosurfactant concentration, σ is a parameter increasing linearly with the hydrophobic chain length, ΔT stands for the temperature deviation from 25°C. The empirical constants are denoted here by k and α_T. The left side of Eq. (1.30) is described as the hydrophilic-lipophilic deviation (HLD). Various values of the HLD number indicate a type of the emulsion being formed: a microemulsion for HLD = 0, the W/O macroemulsion for HLD > 0, and the O/W macroemulsion for HLD < 0. A major disadvantage of the HLD concept lies in a necessity of determining numerous empirical constants [20].

3.6   Important aspects of emulsion stability

As previously mentioned, emulsions — or any other kind of colloidal dispersions — are not thermodynamically stable. Once prepared, the emulsions change their properties

with time. However, they can be stable enough to preserve their properties for days, months or even years (kinetic stability). Aging of emulsion can occur through different mechanisms, such as sedimentation and creaming, aggregation, coalescence or the Ostwald ripening [1, 20, 24]. Figure 1.24 presents the emulsion breakdown processes.
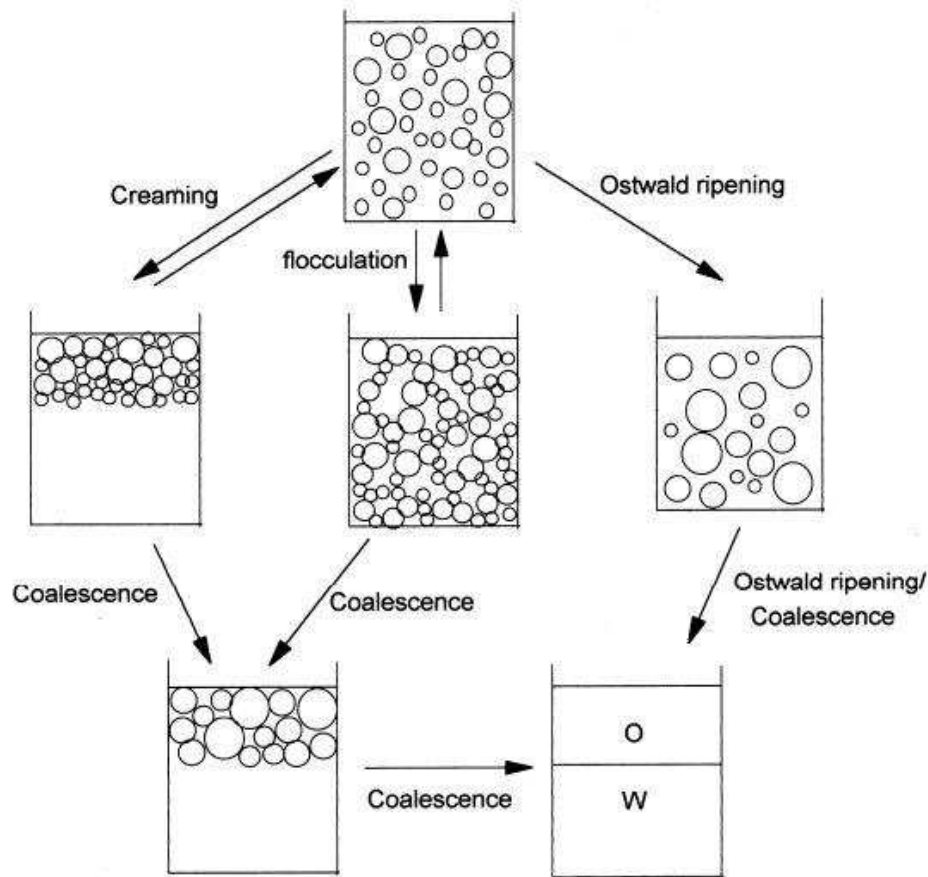
Figure 1.24: Schematic representation of the emulsion breakdown process [91].

Coalescence refers to the merging of two or more droplets, which results in the formation of a single unit characterized with greater volume and smaller surface area. Molecular contact of the neighboring emulsion droplets, followed by formation of a flat contact area and fusion of two surfactant films lead to the final coalescence step. Such process is energetically favorable due to decrease in the Gibbs free energy of the emulsion. That mechanism of breakdown leads to the significant changes in the average particle size and distribution of dispersed phase. Collision of droplets can occur at any time due to the presence of the Brownian motion, sedimentation or additional stirring of a dispersion. The collision rate between spherical droplets of radius R is limited by the diffusion and

can be described as [92]

$$\frac{\mathrm{d}c}{\mathrm{d}t} = -8\pi D R c^2 \,, \tag{1.31}$$

where c is the concentration of droplets and D is the diffusion coefficient, which is taken from the Stokes-Einstein equation

$$D = \frac{k_{\mathrm{B}}T}{6\pi\eta R} \,, \tag{1.32}$$

where k_{B} is Boltzmann's constant, T is temperature and η is the viscosity of the solution. The two last equations lead to the following expression for the rate of diffusion-limited coalescence

$$\frac{\mathrm{d}c}{\mathrm{d}t} = -\frac{4k_{\mathrm{B}}Tc^2}{3\eta} \,. \tag{1.33}$$

Aggregation occurs when two or more droplets clump together to contact at some points. However, integrity of the separating interfacial film and total surface area remain unaltered. Both flocculation and coagulation are considered as aggregation processes. Flocculation results in the formation of a loose network of the droplets, while coagulation refers to the formation of more compact aggregates. On the contrary to coalescence, aggregates consist from the species retaining their identity. Aggregation can be the first step leading to coalescence and phase separation of the emulsion.

Sedimentation or creaming occurs over the time in almost all emulsion systems. It results from the density difference between the continuous and dispersed phase. The emulsion droplets can migrate in the gravitational field and accumulate either at the bottom (sedimentation) or at the top (creaming) of a solution. As a result, two separate layers having different concentration of dispersed phase are being formed. The rate of creaming depends on the physicochemical properties of the system, such as density difference between the continuous and dispersed phase, or viscosity of the continuous phase. This effect can be often reversed with minimal energy input. On the other hand, once the emulsion droplets have been brought into vicinity, aggregation with following coalescence may be promoted. Therefore, the true stability of the emulsion is dependent on the delicate balance between aggregation and coalescence processes.

Ostwald's ripening of emulsion droplets is related to the solubility and the chemical potential difference of the dispersed phase in droplets of different size and solubility. Solubility increases with the decreasing radii of curvature of the droplets. As a consequence,

molecules of smaller droplets are dissolving into the bulk phase, diffusing and recondensing in the larger droplets [91]. It leads to an overall increase in the average particle size; larger emulsion droplets are growing at the expense of smaller ones. Since Ostwald ripening of the emulsions occurs by the transport of dissolved molecules through the bulk phase, it does not require the droplets to be in the vicinity. In most cases, the superior emulsion breakdown mechanism relies on the coalescence, but ripening of emulsions should also be taken into considerations for polydispersed systems.

Whether the emulsion will be thermodynamically or kinetically stable depends on the interactions between the droplets. The repulsive electrostatic forces between charged oil droplets tend to stabilize the system, while attractive van der Waals forces destabilize it. The following chapters are focused on the description of these interactions.

3.6.1 Van der Waals forces

There are four fundamental types of forces controlling the interactions between atoms and molecules [93]. The Coulomb interactions are acting only in systems containing at least one charged species, such as ions or polar molecules. They function over distances exceeding the covalent bonds and are the strongest of the physical interactions. Molecules, which do not carry a formal electrical charge can acquire one thanks to the presence of an unsymmetrical distribution of electron density (permanent dipoles) or can be polarized by external electric field (induced dipoles). The remaining forces are related to the fluctuations in the electron charge density distribution of molecules. All these interactions between uncharged molecules are referred to as van der Waals interactions [94]. They appear at short distances, comparable with the molecular dimensions and can be divided into three main categories:

- Keesom orientational forces (permanent dipole/permanent dipole)

- Debye inductive forces (permanent dipole/induced dipole)

- London dispersive forces (induced dipole/induced dipole)

The Keesom interactions occur between two polar molecules having a permanent dipole moment. A dipole results from the unsymmetrical distribution of electron density, caused by charge separation or differences in the electronegativities of the atoms involved

in a covalent bond. The dipole moment μ of the molecule can be defined as

$$\mu = ql \,, \tag{1.34}$$

where l is the distance between the two charges or the positive and negative ends of the electron cloud $(+q, -q)$. The free energy of interactions between permanent dipoles depends from their mutual orientation. Maximum interaction will occur when two polar molecules with dipole moments μ_1, μ_2 are aligned, such that their opposite charges face each other. The Boltzmann averaging of interaction energies of the dipoles over all possible orientations results in the expression for the energy of Keesom interactions:

$$G_{\mathrm{A}} = -\frac{\mu_1^2 \mu_2^2}{3k_{\mathrm{B}}T(4\pi\varepsilon)^2} \frac{1}{r^6} \,, \tag{1.35}$$

where ε is the dielectric constant and r is the distance separating two dipoles.

The Debye interactions are the second important component of intermolecular forces. The approach of a dipole to a non-polar molecule causes a charge shift and induces the dipole moment of this molecule. Thanks to the polarization effect, induced dipoles can also have an input to the intermolecular interactions. The dipole moment generated by the presence of electric field is given by the expression

$$\mu_{\mathrm{ind}} = \varepsilon\alpha E \,, \tag{1.36}$$

where α is the polarizability of a molecule, and E is the value of electric field generated around the permanent dipole. The energy of Debye interactions between a molecule with the permanent dipole moment μ and the induced dipole can be expressed as follows

$$G_{\mathrm{A}} = -\frac{\mu^2 \varepsilon\alpha}{(4\pi\varepsilon)^2} \frac{1}{r^6} \,. \tag{1.37}$$

The London dispersion force is considered to be the most important and fundamental contribution to the van der Waals interactions. It occurs both in nonpolar or slightly polar molecules (e.g., hydrocarbons) and dominates in nearly all cases of colloidal materials. The examples of phenomena caused by dispersion forces include the condensation of nonpolar molecules to the liquid/solid states, surface tension, adsorption, aggregation, flocculation and many others. Dispersion forces arise from the rapid fluc-

tuation of dipoles, being a result of the outer-valence-shell electrons movement. They are nonadditive forces and have a relatively long range of action (up to 1 nm or more). London forces may be attractive or repulsive; the interactions between similar molecules are always attractive, while the character of interactions between different molecules relies on the character of surrounding medium. The energy of London interactions can be approximated by the following equation:

$$G_A = -\frac{3}{2}\frac{\alpha_1\alpha_2}{(4\pi\varepsilon)^2}\frac{I_1 I_2}{I_1 + I_2}\frac{1}{r^6} = -\frac{c}{r^6}, \tag{1.38}$$

where I_1, I_2 are the first ionization potentials of the interacting molecules and c is the London dispersion constant.

The total van der Waals interaction between molecules is the sum of Keesom, Debye and London dispersion forces. Usually the London term is dominating. The exceptions are small and strongly polar molecules, such as water, where the Keesom term may contribute up to 80% of the total interaction [93]. In all of the cases, the energy of interactions is governed by the r^{-6} law.

The defined interaction energies between two molecules can be further used for calculation of the van der Waals force between various macrobodies. The microscopic approach, also referred to as the Hamaker theory, is based on the pairwise additivity principle. Implementation of Hamaker theory for calculating the attractive van der Waals interaction between two emulsion droplets with the radii R_1 and R_2 at a distance r results in

$$G_A = -\frac{A}{6r}\frac{R_1 R_2}{R_1 + R_2}. \tag{1.39}$$

If the emulsion is monodisperse ($R = R_1 = R_2$), the previous equation takes a simplified form

$$G_A = -\frac{AR}{12r}. \tag{1.40}$$

The parameter A known as the Hamaker constant depends on the number of molecules building the unit ρ_n and the London dispersion constant c:

$$A = \pi\rho_n{}^2 c. \tag{1.41}$$

For the interaction of similar particles (1) in a medium (2), the Hamaker constant is calculated using the following formula

$$A = \left(\sqrt{A_{11}} - \sqrt{A_{22}} \right)^2 , \tag{1.42}$$

where A_{11} and A_{22} refer to the Hamaker constants of the particles and medium material, respectively. Figure 1.25 shows the interaction energy between two droplets as a function
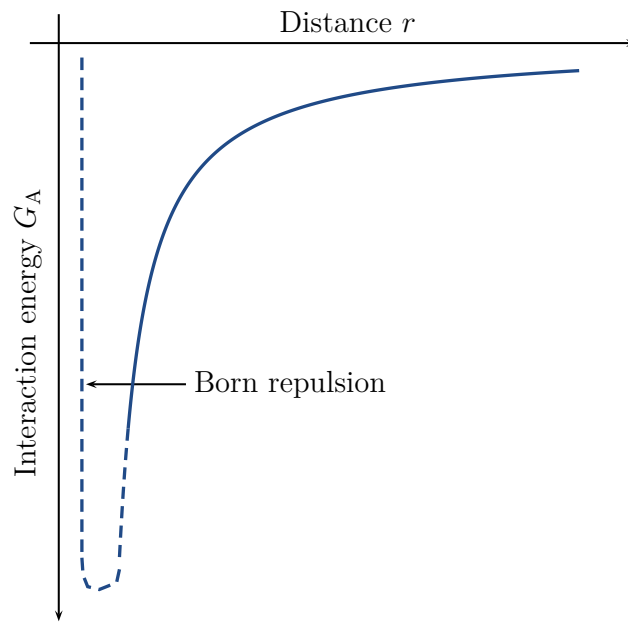
Figure 1.25: Interaction energy G_A between two droplets as a function of their distance r, according to Ref. [24].

of the distance between them. The energy increases instantaneously with decreasing distance. At a very short distance, the Born repulsion between nuclei dominates the attraction forces between molecules.

The attractive van der Waals forces present in the dispersions tend to destabilize the emulsion systems. In order to keep them stable, the presence of the repulsive forces is required. The electrostatic double-layer repulsion plays a major role in emulsions and therefore is discussed in detail in the next subsection.

3.6.2 Electrostatic forces

Due to its high dielectric constant, water is a great solvent for the ionic species. Therefore, most solid surfaces in contact with aqueous solutions carry an electrical charge. The

interactions between like charges are always repulsive. Repulsion between interfaces is a crucial mechanism in the stabilization of colloidal aqueous systems. A proper control of surface charges has a great importance in life and technological applications. There are several mechanisms leading to the surface charging, such as direct ionization of surface groups, specific ion adsorption, differential solution of surface ions, substitution of surface ions or charges originating from specific crystal structures [1, 2]. In general, colloidal systems are electrically neutral, which means that any surface charge on a particle is balanced by an equal amount of opposite charge (counterions) in the surrounding phase. A nonuniform distribution of ions in the vicinity of the surface evokes the formation of potential across the interface. The two layers of charge – surface charge together with counterions – are known as the electrical double layer. There are several models describing the nature of electrical double layer, as summarized below.

The earliest model of an electric double layer was proposed by **Helmholtz** in 1879 [15, 16]. He described an uniformly charged surface with directly bounded counterions, forming a layer adjacent to the surface. The electric field and related electrical potential

(a) Helmholtz model   **(b)** Gouy-Chapman model   **(c)** Stern-Graham model
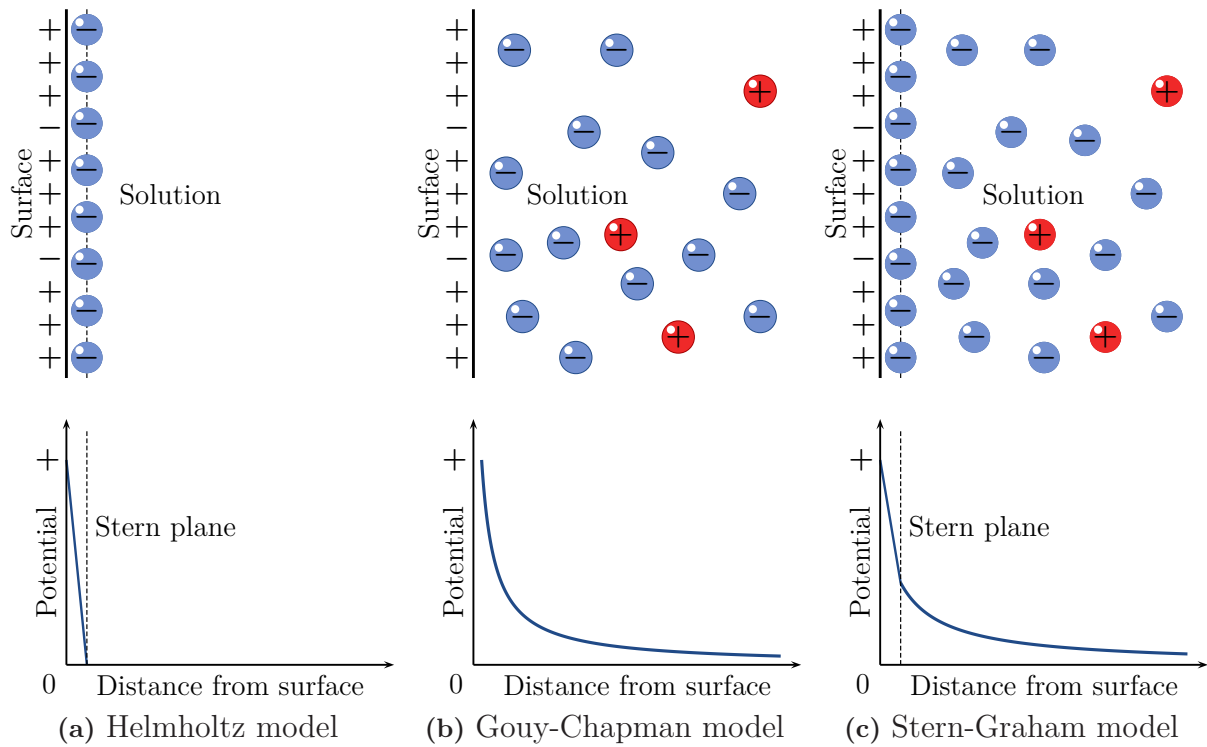
Figure 1.26: Schematic representation of the electrical double layer and changes in the potential according to the various models [16].

generated by the surface charge decreases rapidly to zero at a distance of the molecular layer thickness (see Fig. 1.26a). The counterions neutralize the surface charges on a similar basis as in a parallel-plate condenser. One of the model's simplifications was that Helmholtz treated the counterions as point charges, while they have a finite size and can interact with the surface. Secondly, the termal motion of counterions will oppose their concentration in the vicinity of the surface and cause them to diffuse. For that reason, the capacity of an electric double layer cannot be properly calculated in terms of the Helmholtz model.

The **Gouy-Chapman model** represented a step forward due to taking into account thermal fluctuations [95, 96]. Thermal motion of the ions drives them away from the surface. As a result, a diffuse layer of counterions, which is extended more than one molecular layer is being formed. Due to the screening effect, concentration of counterions decreases rapidly near the surface and gradually on a larger distance. The electrical potential declines approximately exponentially with the distance from the surface (see Fig. 1.26b). The Gouy-Chapman theory is the most accurate for simple planar surfaces characterized with a low charge density, and at distances far away from the surface. It fails in the case of a high surface charge density and at small distances from the surface due to negligence of molecular nature of the solvent and treatment of the ions as point charges.

The **Stern-Graham** model takes into account a finite volume occupied by the ions, having therefore certain steric requirements and not being able to approach the surface closer than their effective hydrated radius. Stern introduced a concept of dividing the electrical double layer into two parts, i.e., a fixed layer of strongly adsorbed ions followed by a diffuse layer of counterions, which are described by the Gouy-Chapman model [97]. A plane separating the diffuse double layer from the fixed wall of ions adjacent to the surface defines the Stern layer. The thickness of Stern layer reflects the finite size of ions associated with the surface and is of the order of few nanometers. The electrical potential drops rapidly and linearly in the Stern region. Within the diffuse layer, the potential decay is approximately exponential (see Fig. 1.26c). Graham divided the Stern layer into the two parts, which correspond to the presence of different ions [98]. Chemically adsorbed ions, which lost a fraction of their hydration shell, are related to the so-called inner Helmholtz plane. The physically adsorbed and hydrated counterions can approach

the surface as close as the outer Helmholtz plane location, equivalent to the Stern layer.

3.6.3 The Poisson-Boltzmann theory of diffuse double layer

The electric potential ψ near a flat uniformly charged surface depends on the distance x from that surface. Due to the planar geometry of the considered surface, the potential is constant in planes parallel to the surface. In a general case, the potential distribution $\psi(x, y, z)$ in the solution is given by the Poisson equation

$$\nabla^2 \psi(x, y, z) \equiv \frac{\partial^2 \psi}{\partial x^2} + \frac{\partial^2 \psi}{\partial y^2} + \frac{\partial^2 \psi}{\partial z^2} = -\frac{\rho_e}{\varepsilon_0 \varepsilon} \, , \tag{1.43}$$

where ∇^2 denotes the Laplace operator, ε_0 is the electric constant, and ρ_e stands for the local electric charge density [C/m^3], which is determined by the distribution of ions within the electrical double layer

$$\rho_e = z_+ e n_+ + z_- e n_- \, . \tag{1.44}$$

The valency of ions (cations or anions) is denoted here by z_+ and z_-, respectively, e is the elementary charge and n stands for the concentration of ions per unit volume.

Equation (1.43) is given in the Cartesian coordinates x, y and z. However, for a spherical particle, it is convenient to use the spherical coordinates in which the potential distribution is a function of the radial coordinate r only: $\psi = \psi(r)$. As a result, the partial derivatives of $\psi(r)$ with respect to the angular coordinates disappear and the Poisson equation takes a simpler form

$$\nabla^2 \psi(r) = \frac{1}{r^2} \frac{\mathrm{d}}{\mathrm{d}r} \left(r^2 \frac{\mathrm{d}\psi}{\mathrm{d}r} \right) = -\frac{\rho_e}{\varepsilon_0 \varepsilon} \, . \tag{1.45}$$

The Poisson equation (1.43) is the starting relationship for any issues related to the stability and electrostatic interactions of particle suspensions with the surfaces [94]. Since the ions are free to move, their local ion density can be estimated using the Boltzmann distribution

$$n_+ = n_{+,0} \exp \left(-\frac{E_+}{k_\mathrm{B} T} \right) \, ,$$
$$n_- = n_{-,0} \exp \left(-\frac{E_-}{k_\mathrm{B} T} \right) \, , \tag{1.46}$$

where $n_+(n_-)$ is the bulk concentration of the salt and $E_+(E_-)$ denotes the energy of a positive (negative) ion in the given position. In the Poisson-Boltzmann theory it is assumed that these energies are equal to work required to bring an ion from the infinite distance to the considered point.

$$E_+ = z_+e\psi\,, \qquad E_- = z_-e\psi\,. \tag{1.47}$$

Thus, Eq. (1.44) can be expressed as

$$\rho_e = z_+en_{+,0}\exp\left(-\frac{z_+e\psi}{k_BT}\right) + z_-en_{-,0}\exp\left(-\frac{z_-e\psi}{k_BT}\right). \tag{1.48}$$

On substitution of Eq. (1.48) into Eq. (1.45) for a spherical particle one obtains

$$\frac{1}{r^2}\frac{d}{dr}\left(r^2\frac{d\psi}{dr}\right) = -\frac{1}{\varepsilon_0\varepsilon}\left[z_+en_{+,0}\exp\left(-\frac{z_+e\psi}{k_BT}\right) + z_-en_{-,0}\exp\left(-\frac{z_-e\psi}{k_BT}\right)\right]. \tag{1.49}$$

The above equation is referred to as the Poisson-Boltzmann equation. It is the fundamental expression used in the chemistry of colloids for the description of the electric phenomena. This partial differential equation of the second order can be solved analytically only for the simple geometries, such as the planar surface [15].

Further simplifications of the Poisson-Boltzmann equation include the case of small potentials ($z_{+/-}e\psi/k_BT < 1$); for an univalent electrolyte the potential is smaller than 25 mV. Expanding the exponential function into series and taking into account only the first linear term leads to the formulation of the so-called linearized Poisson-Boltzmann equation

$$\frac{1}{r^2}\frac{d}{dr}\left(r^2\frac{d\psi}{dr}\right) = \left[(z_+^2n_{+,0} + z_-^2n_{-,0})\frac{e^2}{\varepsilon_0\varepsilon k_BT}\right] = \kappa^2\psi\,, \tag{1.50}$$

where κ is the inverse Debye length

$$\kappa = \sqrt{(z_+^2n_{+,0} + z_-^2n_{-,0})\frac{e^2}{\varepsilon_0\varepsilon k_BT}} \tag{1.51}$$

Taking into account the boundary conditions, i.e., the fact that at the surface the potential is equal to the surface potential $\psi(r = 0) = \psi_0$ and that the potential disappears at large distances $\psi(r \to \infty) = 0$, a solution of the linearized Poisson-Boltzmann equation takes

the following form:

$$\psi(r) = \psi_0 \exp(-\kappa r) \, . \tag{1.52}$$

One sees that in the linear case the potential decreases exponentially with increasing distance r. The Debye length $1/\kappa$ describes the range of electrostatic interactions and the thickness of the double electrical layer in the dispersed systems. The more ions are present in the solution the more effective is the screening of the surface charge, which is shown in Fig. 1.27. Therefore, the Debye length decreases when the salt concentration is
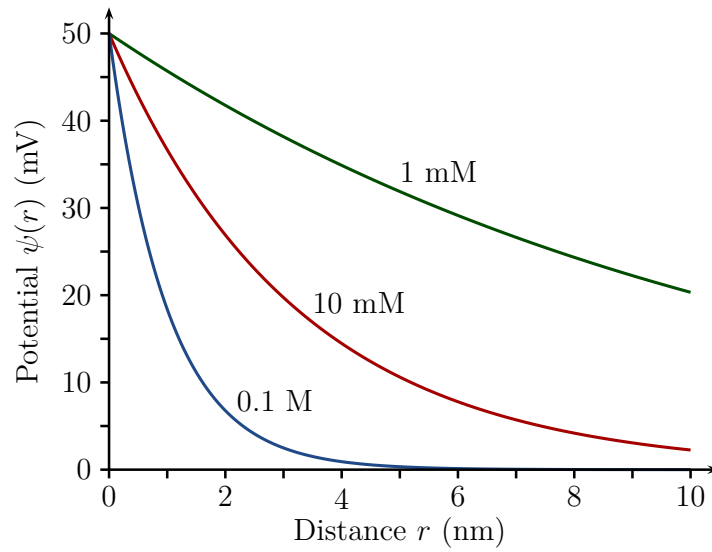
Figure 1.27: Potential ψ versus the distance r ($\psi_0 = 50$ mV) for different concentrations of the monovalent salt in water [1].

increasing. For example, the Debye length of 10^{-4} M NaCl solution is equal to 30.4 nm, while it decreases to 0.96 nm at 0.1 M and to 0.3 nm at 1 M solution [1]. Calculating the Debye length for multivalent ions requires taking into account the ionic strength I of a given solution

$$I = \frac{1}{2} \sum_{i=+,-} n_i z_i^2 \, . \tag{1.53}$$

Therefore, in a general case, the reverse Debye length is expressed as

$$\kappa = \sqrt{\frac{e^2}{\varepsilon_0 \varepsilon k_B T} \sum_{i=+,-} n_i z_i^2} \, . \tag{1.54}$$

Different expressions have to be employed for the potential distribution around the colloidal particles. In general, if the radius of a particle is much larger than Debye length,

the double electrical layer can be treated as planar. For another geometries, there exist only numerical solutions [16].

When two charged colloidal particles in a dispersion approach each other, they start to interact. Like charges repel each other; the repulsion in a vacuum is described by Coulomb's law, while in a polar liquid the interactions are screened by the ionic atmosphere. When particles are at distances smaller than twice the double layer extension, the double layers begin to overlap and a repulsion occurs. Figure 1.28 illustrates the case
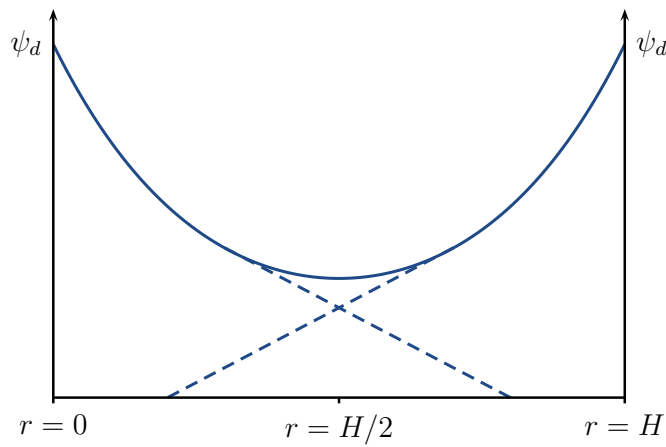
Figure 1.28: The total potential $\psi(r)$ in the case of double layer overlapping of the two flat plates separated by the fixed distance H [24]. The both plates have the same surface potential.

of two identical planar surfaces which have the equal surface potential ψ_d.

The Gibbs energy of electrical double layer repulsion occurring between two spherical particles of radius R and the surface potential ψ_0 ($\kappa R < 3$) is given by

$$G_{\text{el}} = \frac{4\pi\varepsilon_0\varepsilon R^2\psi_0^2 \exp(-\kappa h)}{2R + h},$$
$$(1.55)$$

where h is the shortest possible distance between two surfaces. As can be seen, the interaction energy decreases exponentially with the distance — the higher is the electrolyte concentration, the steeper is the decay.

3.6.4 Electrokinetic phenomena and the zeta potential

The most important parameter characterizing the electrical double layer is known as the zeta potential ζ. The zeta potential is directly relevant to the electrokinetic phenom-

ena, which results from a charge separation at the interface between two phases [99]. Electrokinetic effects rely on the movement between the liquid phase and the charged surfaces. They can be divided into the four categories: electrophoresis, electroosmosis, the streaming potential and the sedimentation potential. In the first two phenomena the electric field creates a hydrodynamic flow, while in the two latter the fluid flow creates the electric field. Electrophoresis is based on the movement of charged particles caused by the electric field applied to the suspension. In electroosmosis, a liquid flows due to the electrical potential parallel to the charged surface. The electric streaming potential is evoked by a fluid flow along the charged surface. When charged particles move relative to a stationary fluid under the influence of gravity, a sedimentation potential is being created [1, 15].
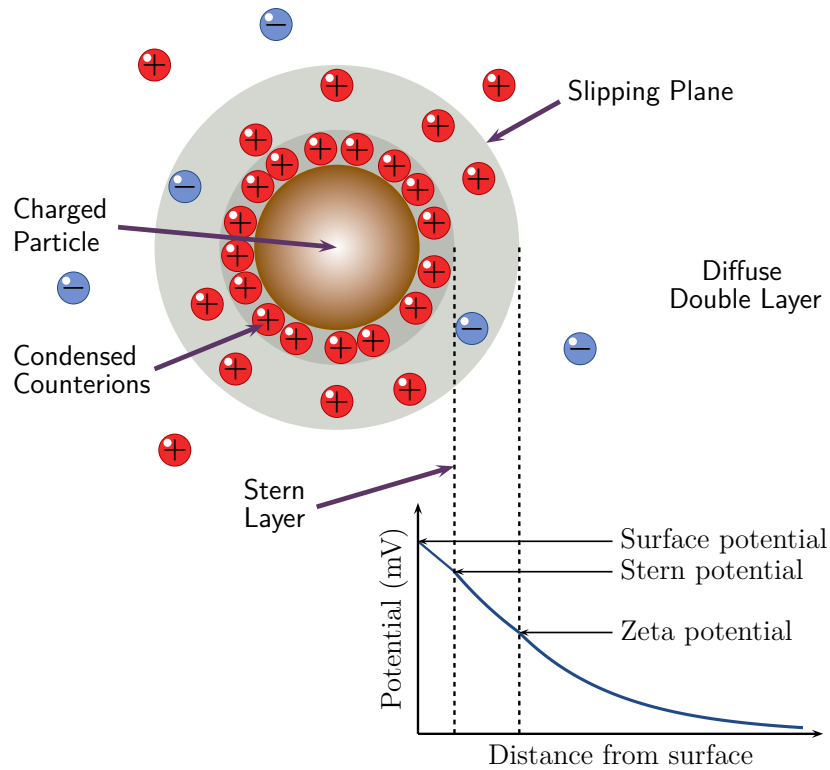
Figure 1.29: Ion distribution around a charged particle and the zeta potential location.

If we consider the motion of a charged particle in an electric field, the zeta potential is the potential measured at a distance δ from the particle surface. That surface is located in the plane, where the center of the first layer of moving liquid is located. This is termed the shear/slipping plane and the distance $R + \delta$ is the hydrodynamic radius of the particle. It is usually assumed that the slipping plane is located near a plane

where hydrated ions are one diameter away from the surface (Stern layer, see Fig. 1.29). However, it is not unambiguously defined distance. One can determine the zeta potential with a high accuracy, but the exact position of the slipping plane remains uncertain. The zeta potential is considered to be close in the value to the Stern potential. It can be calculated for spherical particle according to the Henry formulas

$$\mu_e = \frac{2\varepsilon_0 \varepsilon \zeta}{3\eta f(\kappa a)} \,, \tag{1.56}$$

where μ_e is the velocity of a particle in the unit electric field (electrophoretic mobility), η is the viscosity of the medium opposing the movement and $f(\kappa a)$ denotes the Henry function dependent on the ratio between the particle size and the electrical double-layer thickness. Henry's function changes between the two values: 1.5 or 1. The value of 1.5 is related to the moderate electrolyte concentrations and large microparticles. Under such conditions, Eq. (1.56) is reduced to the Smoluchowski equation. In the solutions characterized with a low electrolyte concentration and for small particles, $f(\kappa a) = 1$ (the Hückel approximation).

The value of zeta potential is not characteristic for a particular material and depends mostly on the surrounding conditions, such as the electrolyte concentration and possible adsorption of the ionic or non-ionic molecules. This is a main parameter used to estimate a stability of the colloidal systems. An emulsion can be stable over a long period of time, if the following conditions are fulfilled: a high value of the zeta potential (lower than -40 mV or higher than $+40$ mV), a low valency of the electrolyte, as well as its low concentration [24].

3.6.5 Total energy of interactions

Summation of the interaction energy coming from van der Waals attraction and electrical double layer repulsion leads to the expression

$$G_T = G_A + G_{el} \,. \tag{1.57}$$

The above equation is a foundation of the well-known theory of colloidal stability, which was developed by Derjaguin, Landau, Verwey and Overbeek and is now referred to as the DLVO theory [100, 101]. Figure 1.30 shows the dependence of interaction energy
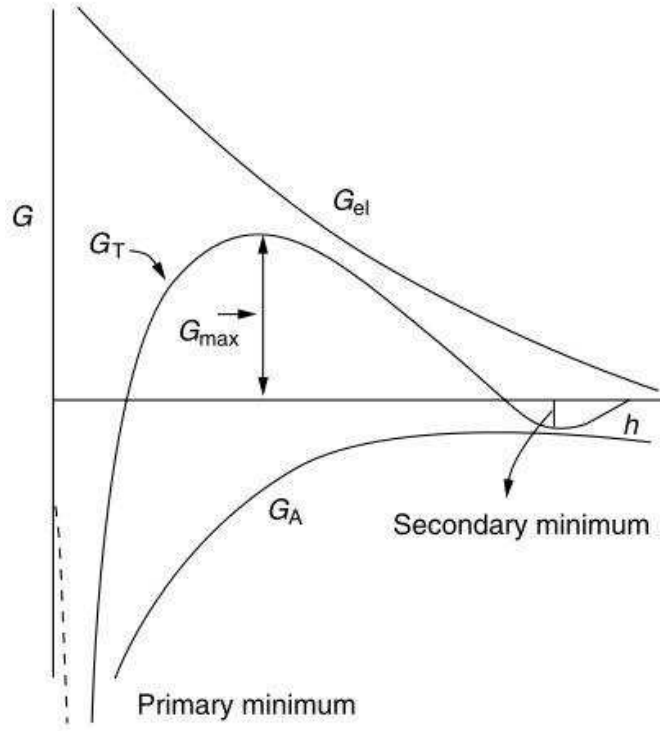
Figure 1.30: Changes in the interaction energy G_T with the distance h, according to the DLVO theory [24].

on the distance h between charged particles in the conditions of low electrolyte concentration (strong electrostatic repulsion). The interaction energy of the electrical double layer decays exponentially with the distance ($G_{el} \to 0$), while the van der Waals energy decreases with the the sixth power of the distance and does not disappear. At very short distances $G_A \gg G_{el}$, the total energy of interactions is negative, which results in a deep primary minimum of the energy. Particles on such a distance are subjects of the irreversible aggregation. In the case of a large particle separation, $G_A > G_{el}$, a shallow secondary minimum appears. This minimum corresponds to a weak and reversible flocculation of the particles. At intermediate distances, $G_{el} > G_A$, which gives rise to the energy maximum G_{max}. That is the electrostatic barrier, which prevents the particles from aggregation. The height of G_{max} depends on the value of ψ_0, as well as on the electrolyte concentration and the ion valency. In order to ensure satisfying colloidal stability, G_{max} has to be greater than $25 k_B T$. The higher is the valency and the electrolyte concentration, the lower is the energy maximum. A barrier of $25 k_B T$ is reached when the electrolyte concentration is smaller than 10^{-2} M (monovalent electrolyte) and the zeta potential is around ± 40 mV [24].

4 Polyelectrolytes

4.1 General properties

Polyelectrolytes are macromolecules carrying ionizable or ionic groups [102–104]. Due to their dual character of polymers and highly charged electrolytes, they exhibit unique properties. Most of polyelectrolytes are water-soluble. In polar medium under appropriate conditions, the ionizable groups dissociate into polyions and oppositely charged counterions. The electrostatic interactions between charged polymer backbone and counterions are determining the behavior of polyelectrolytes in solution. The conformation of these polymers — both in solution and at charged surfaces — depends on the fraction of dissociated ionic groups, ionic strength and dielectric constant of solution, pH, concentration, and polymer-substrate interactions [105, 106]. Similarly to acids or bases, polyelectrolytes
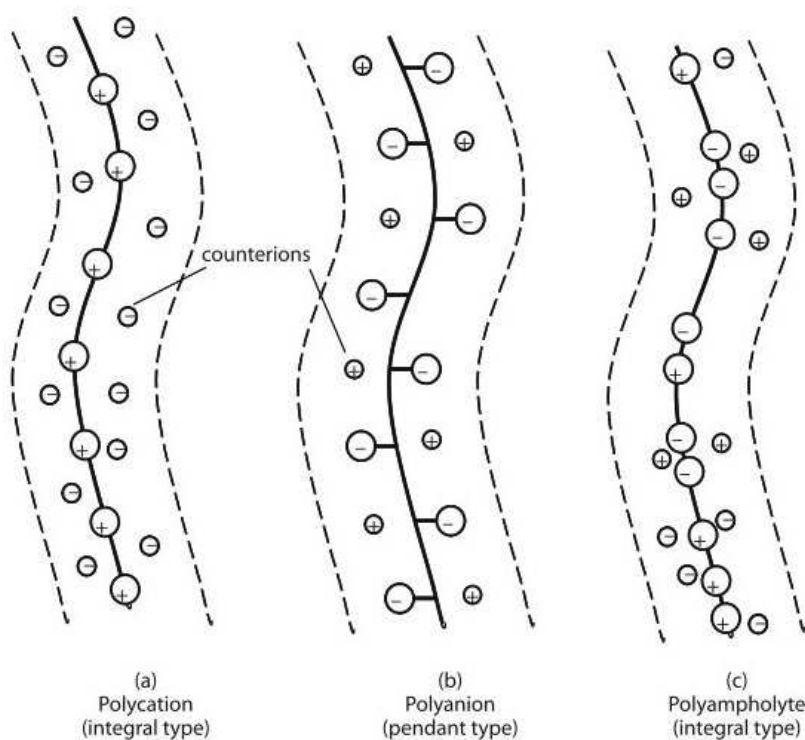
Figure 1.31: Classification of polyelectrolytes into polycations (a), polyanions (b) and polyampholytes (c) [108].

can be classified as weak or strong. Strong polyelectrolytes dissociate completely in the solution for almost entire range of pH. Weak polyelectrolytes are only partially dissociated and the degree of dissociation, i.e. their fractional charge can be changed substantially

by adjustment of the solution pH or ionic strength. The structure of the polyelectrolyte molecule can be therefore precisely tuned from an extended coil conformation, characteristic for high charge density and low ionic strength solution, to the globular conformation resulting from collapse of polyelectrolyte chains due to decreased charge density and attractive van der Waals interactions [107]. As shown in Fig. 1.31, polyelectrolytes can be divided into three categories, in respect of their ionic group character:

- Negatively charged polyanions, also known as polyacids, containing groups $-COOH$, $-SO_3H$, $-OP(O)(OH)_2$, $-PH(O)OH$.

- Positively charged polycations, also referred to as polybases, containing groups $-N^+H_3X$, $-NRH_2X$, $-N^+R_2HX$, N^+R_3X.

- Polyampholytes carrying both negative and positive groups along the polymer backbone. Their character depends on the pH value. In acidic conditions they become polycations, while in alkaline solution they are negatively charged. Polyampholytes contain groups such as $-NH_2$ (proton acceptor) or $-COOH$ (proton donor).

The most common examples of polyelectrolytes include proteins, nucleic acids (DNA, RNA), cellulose or chitin derivatives, carrageenans, polyacrylic acid and polystyrene sulfonate. Proteins and nucleic acids, being the very building blocks of life, have crucial importance in biological systems. Therefore, research in the area of polyelectrolytes allows for better understanding of the mechanisms of processes ongoing in biological systems, as well as of their impact on human life and health [109–111]. Apart from materials of natural origin, synthetic polyelectrolytes have been investigated for several decades and still are a very active area of the research.

4.2 Polyelectrolytes in solution

In dilute solution of polyelectrolyte the intrachain interactions dominate over the interchain ones [104]. Consider a polyelectrolyte chain comprising N monomers of size a, with fraction $\mathfrak{f}$ of charged groups in a solvent with the dielectric constant ε. If the fractional charge is very low, the electrostatic forces are negligible and the polyelectrolyte chain adopts to so called random coil conformation. When the charge density increases, the chain becomes stretched by the repulsive electrostatic interactions between monomers. In

the absence of added salt, the chain size R is determined by electrostatic repulsion and chain elasticity

$$R \sim Na \left(\frac{f^2}{a} \right)^{1/3} . \tag{1.58}$$

An addition of salt to the polyelectrolyte solution leads to the screening of electrostatic interactions and counterion condensation (see Fig. 1.32). As a result, the polyelectrolyte

Salt makes polyelectrolytes in solution collapse into random coils.
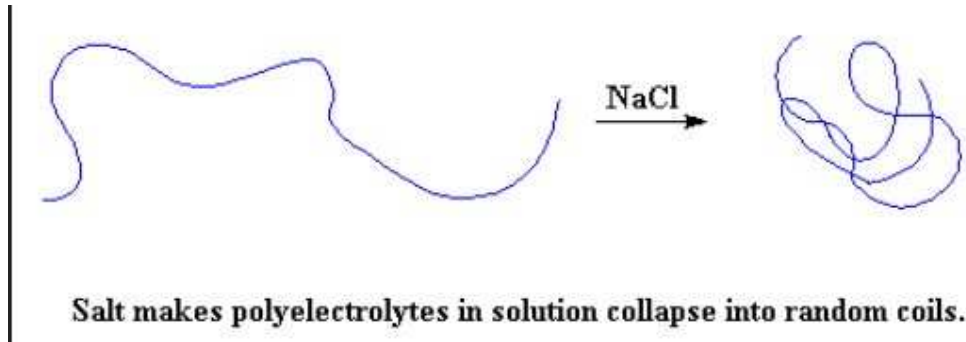
Figure 1.32: A change of polyelectrolyte conformation from the stretched chain to a random coil, induced by an addition of salt.

size is decreased due to the change in conformation from stretched chain to random coil. The interaction between two charges at a distance r is given by the Debye-Hückel potential

$$\psi(r) = k_{\mathrm{B}}T \, \frac{l_{\mathrm{B}}}{r} \exp(-\kappa r) , \tag{1.59}$$

where κ^{-1} is the Debye screening length and l_{B} is the Bjerrum length — a distance at which the electrostatic interactions between two elementary charges q are comparable to the thermal energy $k_{\mathrm{B}}T$

$$l_{\mathrm{B}} = \frac{q^2}{4\pi\varepsilon k_B T} . \tag{1.60}$$

On the length scales larger than the Debye screening length, the electrostatic interactions are exponentially screened. In the absence of salt, the concentration of counterions is very low ($\kappa^{-1} > R$) and the ionized groups on the polymer backbone interact with each other via the unscreened Coulomb potential [104, 105].

The potential energy $U(\{\mathbf{r}_i\})$ of the polyelectrolyte chain consisting of r_i monomers, which are located at positions $\mathbf{r}_1$, $\mathbf{r}_2$,..., $\mathbf{r}_N$ and carry corresponding charges eq_1, eq_2,..., eq_N,

is equal to

$$\frac{U(\{\mathbf{r}_i\})}{k_\mathrm{B}T} = \frac{3}{2b^2}\sum_{i=1}^{N-1}(\mathbf{r}_{i+1}-\mathbf{r}_i)^2 + \sum_{i=1}^{N}\sum_{j<i}\frac{l_\mathrm{B}q_iq_j}{|\mathbf{r}_i-\mathbf{r}_j|}\exp(-\kappa|\mathbf{r}_i-\mathbf{r}_j|) + \frac{U_\mathrm{sh}(|\mathbf{r}_i-\mathbf{r}_j|)}{k_\mathrm{B}T}, \quad (1.61)$$

where the first term on the right side of Eq. (1.61) expresses the entropic elasticity of harmonic bonds of the length b, connecting monomers into polymer chain. The second term is the screened Coulomb interaction between charged monomers, and the third term $U_\mathrm{sh}(r)$ represents the short-range interactions between monomers, typically described by the Lennard-Jones potential

$$U_\mathrm{LJ}(r) = 4\varepsilon_\mathrm{LJ}\left[\left(\frac{d}{r}\right)^{12} - \left(\frac{d}{r}\right)^{6}\right], \quad (1.62)$$

where ε_LJ is the interaction parameter and d is the monomer diameter.

4.3   Polyelectrolytes at interfaces

The adsorption of polyelectrolytes on solid/liquid interfaces is a remarkably important phenomena occurring in many natural and practical processes [112–114]. After implantation of the biomaterial in a living system, the proteins can be adsorbed on its surface in a time shorter than one second [115]. Adsorption of polyelectrolytes as the method to assemble thin films of novel materials will be discussed in detail in Section 4.5.

Assuming that solid surface carries an electrical charge with a sign opposite to the polyelectrolyte molecules, the electrostatic interactions between them will result in polyelectrolyte adsorption. The electric field near the surface can be expressed as

$$E = 4\pi\sigma l_\mathrm{B}\frac{k_\mathrm{B}T}{q}. \quad (1.63)$$

The field declines with the distance z from the surface due to the screening by the surface counterions

$$E \sim \frac{2}{z+\lambda}, \quad (1.64)$$

where λ is the Gouy-Chapman length

$$\lambda = \frac{1}{2\pi\sigma l_\mathrm{B}}. \quad (1.65)$$

In the presence of a salt (sufficient concentration, such that $\kappa^{-1} < \lambda$), screening is dominated by the salt and the expression for electric field E becomes

$$E \sim \frac{2\exp(-\kappa z)}{\lambda} \, . \tag{1.66}$$

A single polyelectrolyte chain is attracted by the electric field of the surface. In a very low ionic strength solution it gets confined within a distance δ from the surface. If the surface charge density is large enough ($\delta < \lambda$), the chain feels the surface field. The thickness of polyelectrolyte chain adsorbed on an oppositely charged surface can be expressed as

$$\delta \sim \left(\frac{a^2}{\mathfrak{f}\sigma l_{\mathrm{B}}} \right)^{1/3} \, . \tag{1.67}$$

In most cases, δ is in the range of few nanometers. The thickness is independent from the molecular weight of polyelectrolyte and decreases weakly with the surface charge. In a solution of higher ionic strength ($\kappa^{-1} > \lambda$), and in the absence of short range attraction between the chain and the surface, the polyelectrolyte desorbs. Adsorption can be induced by a sufficient short range non-electrostatic attraction of the molecule to the surface. The chain conformation of polyelectrolyte adsorbed at the interface varies depending on the parameters such as ionic strength of solution, polyelectrolyte concentration and surface charge density [116].

The adsorption kinetics of polyelectrolytes at solid interfaces has been investigated by optical and scattering methods, such as ellipsometry, surface plasmon resonance spectroscopy (SPR) or attenuated total reflectance (ATR). Another possibilities are X-ray reflectivity and quartz crystal microbalance (QCM) [117–120]. The studies showed that in the usual situation, i.e. concentration of polyelectrolyte higher than 100 ppm, the adsorption process is completed within 20–30 minutes. It occurs as the two-step process. In the first stage, polyelectrolyte chains are transported and deposited at the surface [104]. This step is governed by the diffusion and occurs during seconds to minutes. On the contrary to small molecules, polyelectrolyte chains adsorbed at the surface can rearrange their conformation. The adsorbed chain can be divided into three parts contacting the surface in a different way, as shown in Fig. 1.33. The segments of polyelectrolyte chain adsorbed completely at the surface are called trains. A loop is a loose part of chain between two trains, which do not stay in contact with the surface. Finally, the tail is the free end
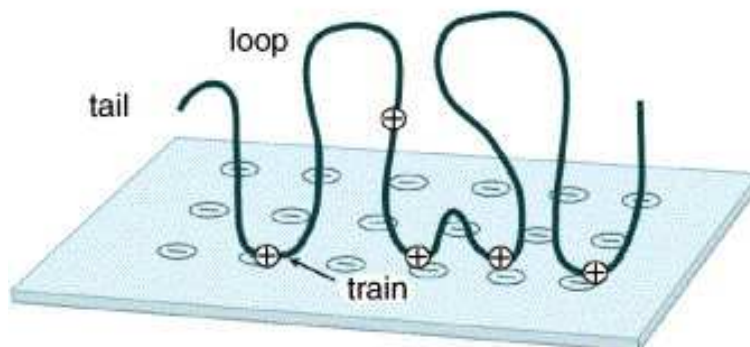
Figure 1.33: Possible conformations of polyelectrolyte at the surface.

of polyelectrolyte chain, directed towards the solution. The second stage of adsorption process relies on chains rearrangement at the surface until saturation is reached [121]. The salt concentration in the polyelectrolyte solution has a remarkable influence on the amount of chains adsorbed. In a salt-free solution polyelectrolyte chains are stretched and tend to form trains or long tails after adsorption. When the ionic strength of solution increases, the charges along the polyelectrolytes are screened (intrachain screening), such that coil conformation is obtained. The electrostatic repulsion between individual chains is also reduced (interchain screening). Adsorption of more flexible and coiled chains increase number of loops and, consequently, the thickness of obtained layer.

4.4 Multilayer formation

Adsorption of polyelectrolytes on the charged surfaces and interfaces has been extensively studied over the years [105, 113, 122]. The basic principle of so called layer-by-layer (LBL) assembly of polyelectrolytes was proposed by Decher [123, 124]. Polyelectrolyte multilayers are obtained via spontaneous sequential adsorption of oppositely charged polyions from aqueous solutions on charged surfaces. The principle of multilayer formation is presented in Fig. 1.34. Typically, a charged substrate (e.g., silicon, mica) is dipped in an oppositely charged polyion solution. Electrostatic attraction occurring between the surface and the polyelectrolyte chains leads to the adsorption of molecules until a complete charge reversal of the substrate is obtained. After adsorption of the first layer, the sample is rinsed with a washing solution in order to remove weakly bonded polyion molecules. In general, the pH and ionic strength of the washing solution should be the same as the one of dipping solution. The obtained monolayer film can be then immersed in the solution
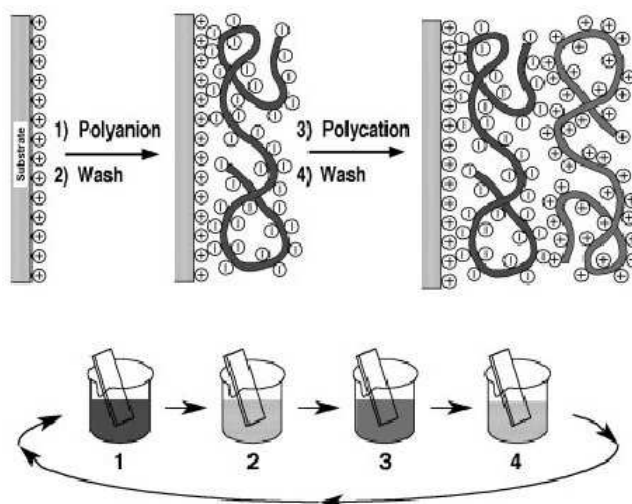
Figure 1.34: Schematic representation of the layer-by-layer assembly of polyelectrolytes [104].

of oppositely charged polyelectrolyte, which results in the formation of complete bilayer consisting of two monolayers. The procedure can be repeated until the desired number of bilayers is obtained. In some cases, hundreds of bilayers have been deposited. The films can be dried with a gentle flow of an inert gas (e.g., nitrogen) after each adsorption step or only at the end of the process. One has to keep in mind that drying can change the conformation of deposited polyelectrolyte chains. The layer-by-layer deposition technique is an efficient and versatile technique leading to the formation of a stable film assembly with desired thickness and properties. Polyelectrolyte adsorption in typical conditions is nearly irreversible [125]. The properties of obtained multilayer films are dependent on several parameters, such as type of the substrate, polyion charge and concentration, pH and ionic strength of the solution, deposition time. The structure and properties of obtained films are mainly determined by the choice of polycation/polyanion pairs and are most frequently controlled by adjusting the pH of solution [126–128]. It was observed in many cases that the first layers of polyelectrolytes, adsorbed directly on the surface, are thinner than the following layers [104]. The adsorbed amount per double layer increases and stabilizes to a constant value after approximately three bilayers. That can be explained by heterogeneity of the substrate and repulsive interactions between polyion molecules forming the first layer. Therefore, full coverage of the surface is not obtained after first deposition step. The first monolayer can be regarded as an anchor for subsequent layers, significantly affecting the stability of the whole film. It was found that use of branched polyethyleneimine (PEI) as first layer positively affects the thickness,

homogeneity and stability of subsequent multilayer films [129]. The thickness and surface properties of multilayers are also influenced by the pH of polyelectrolyte solution, even in the case of strong polyelectrolytes, which charge is not pH-dependent. That is explained by the dependence of surface charge density of the substrate on pH. Multilayers build from weak polyelectrolyte couples are thicker in the conditions of weakly charged chains, which lowers electrostatic repulsion between molecules [128]. Polyelectrolyte multilayers are widely used to modify the surface properties of different materials. Examples of particular applications will be discussed in Section 4.6.

4.5 Polyelectrolyte complexes

Another interesting feature of polyelectrolytes is the formation of complexes with oppositely charged nanoobjects, such as oppositely charged polyelectrolytes, surfactants or nanoparticles, which will be described in this section in more details.

4.5.1 Polyelectrolyte complex formation with oppositely charged polyelectrolytes

When two polyelectrolyte solutions of the opposite charge are mixed, a phase separation and the formation of coacervates takes place. The dense phase, referred to as polyelectrolyte complexes (PECs) or symplexes, is of high relevance since it combines physicochemical properties of two polyelectrolytes [108, 130, 131]. The process of complex formation is fast and entropy-driven. Strong Coulombic interactions between polyions lead to interpolymer ionic condensation and release of counterions, which are no longer restricted to the polymer backbone. Hydrogen bonding, Van der Waals forces and dipole interactions are also involved in the formation of PECs structures.

Studies on PECs have quite a long history. In 1896 Kossel precipitated egg albumin with protamine [132]. In the 1930s further studies upon mixing aqueous solutions of oppositely charged natural polyelectrolytes, such as gelatin and arabic gum, have been performed [133]. Complexes between synthetic polyelectrolytes, poly(4-vinylbenzyltrimethylammonium chloride) and poly(sodium styrene sulfonate), were initially studied in 1961 by Michaels [134].

The behavior of PECs varies significantly depending on the stoichiometry (the relative molecular weights and charge content of both polyelectrolytes), ionic strength of

solution, polyelectrolyte concentration, temperature and so on [135, 136]. The backbones of two different polyelectrolytes are not compatible and repel each other. For low charge fraction the backbone repulsion dominates and the solution consists of two phases containing mostly one of polyelectrolytes. When the charge fraction is high, the electrostatic attraction between polyelectrolytes dominates and a complex is formed. The examples of formed structures are schematically demonstrated in Fig. 1.35 [131]. When two strong

a)
"ladder" model

b)
"scrambled egg" model

c)
"sequential" model
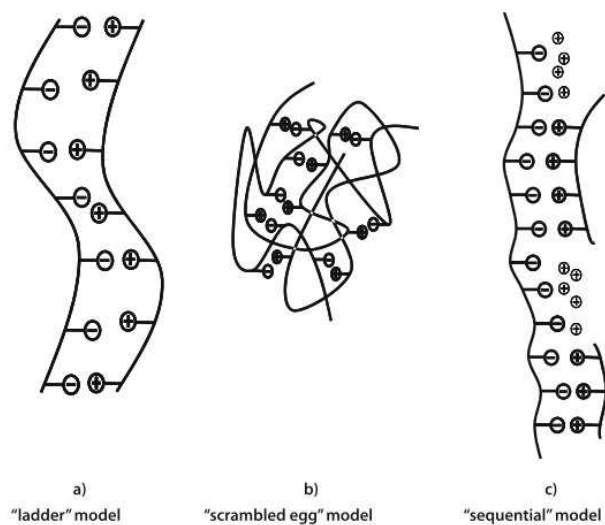
Figure 1.35: Polyelectrolytes complex models according to Michaels [108].

polyelectrolytes with similar molar masses are mixed together, the final structure of the complex aggregates can be either a "ladder structure" with fixed ionic cross-links (see Fig. 1.35a) or more chaotic "scrambled egg structure" with a statistical charge compensation (Fig. 1.35b). When polyelectrolytes with weak ionic groups and significantly different molar masses are mixed in a non-stoichiometric ratio of cationic and anionic functional groups, water-soluble complexes can be formed. Such a structure consist of a long host polymer backbone sequentially complexed with shorter guest polyions of opposite charge, as shown in Fig. 1.35c. Flexible water-soluble PECs are of special interest as potential drug carrier systems for parenteral administration [137].

4.5.2 Polyelectrolyte complex formation with oppositely charged surfactants

Polyelectrolytes can also be associated into complexes with surfactant molecules. Here, the ionic surfactants are of special interest with regard to Coulomb interactions. In the last two decades, most of research on polymer-surfactant interactions was focused on the

association of polyelectrolytes with oppositely charged surfactants, or the interactions between nonionic polymers and ionic surfactant micelles [138, 139]. Binding of polyelectrolytes to the oppositely charged ionic surfactants is more favorable than binding to a neutral polymer, due to the presence of well-defined binding sites on the polyelectrolyte backbone.

Polyelectrolyte-surfactant complex formation can be distinguished in two categories: polyelectrolyte-surfactant interactions in diluted systems below the critical micelle concentration, and as polyelectrolyte-micelle interactions. The presence of polyelectrolytes is known to induce aggregation of the oppositely charged surfactant [140]. Surfactant aggregates formed in polyelectrolyte solutions are similar to free micelles. The formation of polyelectrolyte-surfactant aggregates is schematically presented in Fig. 1.36. An in-
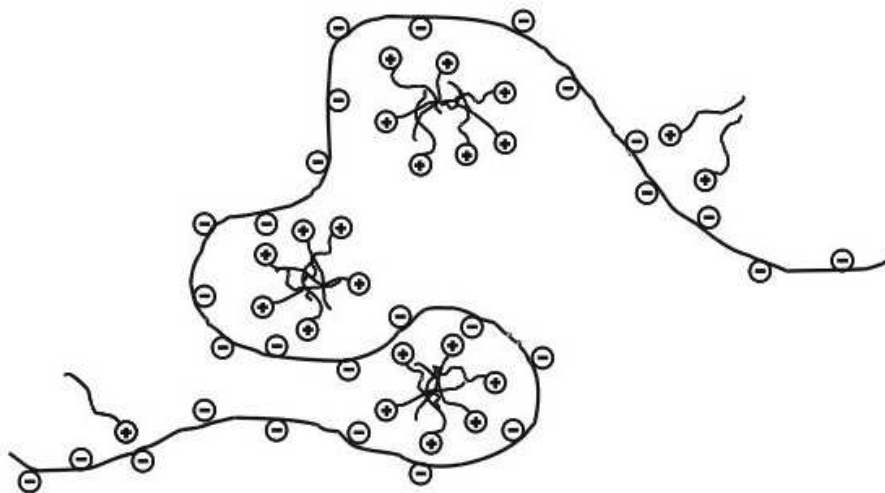
Figure 1.36: Model of the polyelectrolyte-surfactant aggregates [108].

crease in linear charge density of the polyelectrolyte, correlated to the distance between adjacent charges along the polymer backbone, gives rise to stronger interactions [141]. The detailed structure properties of the polyelectrolyte plays an important role in the binding process. Addition of salt reduces the binding affinity between polyelectrolyte and oppositely charged surfactant [142, 143]. Above the critical micelle concentration, the electrostatic interactions between polyelectrolytes and oppositely charged surfactant are so strong that irreversible macroscopic phase separation occurs. The interactions can be screened by "diluting" the charge of ionic surfactant micelles with nonionic surfactants, which leads to the formation of soluble polyelectrolyte-micelle aggregates [144].

Surfactants are well known for their ability to denaturize proteins [145]. The binding of charged surfactants to the specific site on the protein surface cause them to unfold from the secondary and tertiary structure, without the rupture of covalent links of the primary structure. A detailed review on the models of polymer-surfactant complexes is given by Shirahama [146].

4.5.3 Polyelectrolyte complex formation with nanoparticles

Nanoparticles made from metals (e.g., Ag, Au, Cd, Cu), metal oxides or semiconductors are of significant importance in many emerging applications [147, 148]. Size in the nanometer range gives rise to many unique physical features, such as high specific surface and reactivity, electrical, electrochemical, magnetic or optical properties. There exist many possible synthesis routes, including a classical sol-gel approach, where a colloidal suspension of nanoparticles is formed in the nucleation process [108]. The key limitation for practical use of nanoparticles is their restricted stability. They are sensitive to any changes of pH, ionic strength or temperature of the solution, which can lead to their irreversible aggregation and loss of size-related properties [149, 150]. Therefore, in order to stabilize individual nanoparticles, protective coatings have to be used. Polyelectrolytes are of special interest in controlling of colloidal stability of oppositely charged particles. They combine both steric and electrostatic stabilization effect, which results in an outstanding long-term stability of such prepared solutions [151].

The electrostatic complexation between polyelectrolytes and oppositely charged nanoparticles has numerous advantages. It is performed under normal atmospheric conditions of pressure and temperature. There are three main classes of the formulation processes:

- Direct mixing route: polyelectrolyte and nanoparticles dispersions are mixed together by pouring one liquid to another.

- Desalting transition pathway: electrostatic interactions are screened by addition of a large amount of salt, which is subsequently removed by dialysis.

- Layer-by-layer method: polyelectrolyte-stabilized colloidal nanoparticle can be further coated with oppositely charged polyelectrolyte or nanoparticles.

Coating procedures are based on the layer-by-layer assembly. In order to avoid flocculation, nanoparticles are directly mixed with polyelectrolyte solution with a large excess

of ionic charges. This technique was implemented on gold nanoparticles used as labels in DNA biomolecular detection [148, 152]. The main drawback of this method is a large excess of polyelectrolyte that has to be removed before generation of the next layer. The alternative technique, referred to as saturation method, will be discussed in Section 5.

4.6   Applications of polyelectrolytes

Polyelectrolytes have been and continue to be extremely important area of scientific research [106]. Being water-soluble, nontoxic and environmentally-friendly, they can be used for any applications where the presence of organic solvents is undesirable. The broad variety of polyelectrolytes makes them useful in different fields, such as medicine and biomedical engineering, cosmetics, pharmacy, paper-making processes, paint and food industries, water treatment, mineral separation [153–159]. They are often used as adsorbents, ion exchange resins, stabilizers, flocculants or adhesives. Polyelectrolytes are used as additives controlling the viscoelastic properties of colloidal solutions [160, 161]. Water treatment takes advantage in use of ion exchange resins as flocculants, reducing the turbidity of solution and improving parameters after filtration [162]. Polyelectrolytes can be also applied as separation membranes for gases or dissolved species [163, 164], in chemical and biochemical sensing [165, 166]. Assembly of thin films of novel materials is a very promising and emerging area of application. Layer-by-layer deposition of polyelectrolytes is a low-cost, simple and environmentally-friendly technique of producing one-dimensionally ordered nanocomposites. The broad range of parameters to be controlled during formation of polyelectrolyte multilayers allows to obtain films with specific, well-defined surface properties. Some of the applications are sensors, optical, optoelectronic or electroluminescent devices, corrosion protection, antireflective or antistatic coatings, litography and chromatography [167–172]. Polyelectrolyte multilayers are ubiquitous in all kind of biomedical applications, such as drug delivery, gene therapy, protein adsorption and entrapment [24, 111, 173–181]. They can be used as membranes, hydrophilic coating films for contact lenses, heart valves or implants possessing thromboresistant and antibacterial properties. The layer-by-layer coating of colloidal cores is a convenient method of obtaining capsules with potential application in drug delivery systems and microreactors [182–184].

5 Nanoparticles and nanocarriers for drug delivery

5.1 Drug delivery

Drug delivery can be defined as a process of administering pharmaceuticals in order to achieve a therapeutic effect in patients [24]. There are many possible ways of drug administration; the most popular one is known as the oral route. After being digested in the stomach, the drug is absorbed through the intestinal walls into the enterohepatic circulation and taken to the liver for detoxification. This process is referred to as the first pass effect [185]. Later on the drug is completely mixed with the bloodstream and distributed into the tissues. Other common routes of administration include the transdermal (skin), transmucosal (nasal, buccal, ocular) or inhalation routes [186]. However, these traditional delivery routes suffer from many weaknesses. For example, oral and nasal deliveries exhibit high drug levels in the bloodstream and have poor release profiles [187]. Many drugs, such as proteins, peptides, antibodies or vaccines are large, fragile and need a protection from hydrolysis or enzymatic degradation. Therefore, they can not be distributed using common routes and are often delivered intravenously (directly into a vein). Moreover, a considerable number of active compounds being potential drugs failed clinical trials due to their poor aqueous solubility [188]. Side effects of the treatment are another serious disadvantage of a therapy, being the result of drug affecting healthy organs and tissues. On average, 95% of new therapeutics are characterized with poor pharmacokinetics and biopharmaceutical properties [189].

An efficient approach to improve the bioavailability of therapeutics is targeted drug delivery, which aims to supply a medication strictly to the site of the treatment (e.g., cancerous tissue), avoiding over-dosage toxicity and host inflammatory response [190, 191]. Ideally, the drug is released over a period of time in a controlled manner and active only in the targeted area. Problems related with hydrophobicity and harsh biological environment can be solved by using different drug delivery vehicles, such as nanocapsules, liposomes, drug-polymer conjugates, microspheres, emulsions or nanoparticles.

5.2 Advantages of scaling down-nanosize

The nanoscale is of crucial importance to life, which justifies the common expression "nature's yardstick" [104]. Control on a cellular lever can be achieved only with structures of

size similar to biological components of interest, such as organelles, proteins or receptors. A significant drawback of macrosize results from the fact that most cells cannot effectively internalize microobjects with diameter bigger than 200 nm. Microvehicles cannot traverse through tumor cells with pore sizes as big as 380–780 nm [192, 193]. The conventional therapy suffers from inadequate targeting, inefficacy of delivery and side effects on healthy tissues [194, 195].

Most known anticancer drugs have no tumor selectivity and are randomly distributed in the body, which results in severe side effects and low therapeutic index. There are two possible ways of overcoming this problem, referred to as active and passive tumor targeting. Active tumor targeting takes advantage of increased cancer cells surface expression of proteins that are found only at low levels on normal cells (tumor-associated antigens), as well as proteins found only on cancer cells (tumor-specific antigens) [196–198]. Therefore, chemical attachment of tumor-specific antibodies to a targeting carrier will lead to preferential accumulation of the drug in the intended tissue. Another possible strategy of improving tumor selectivity without the conjugation of antibodies is passive tumor targeting [199]. It was proved that nano-sized carriers and nanoparticles show prolonged
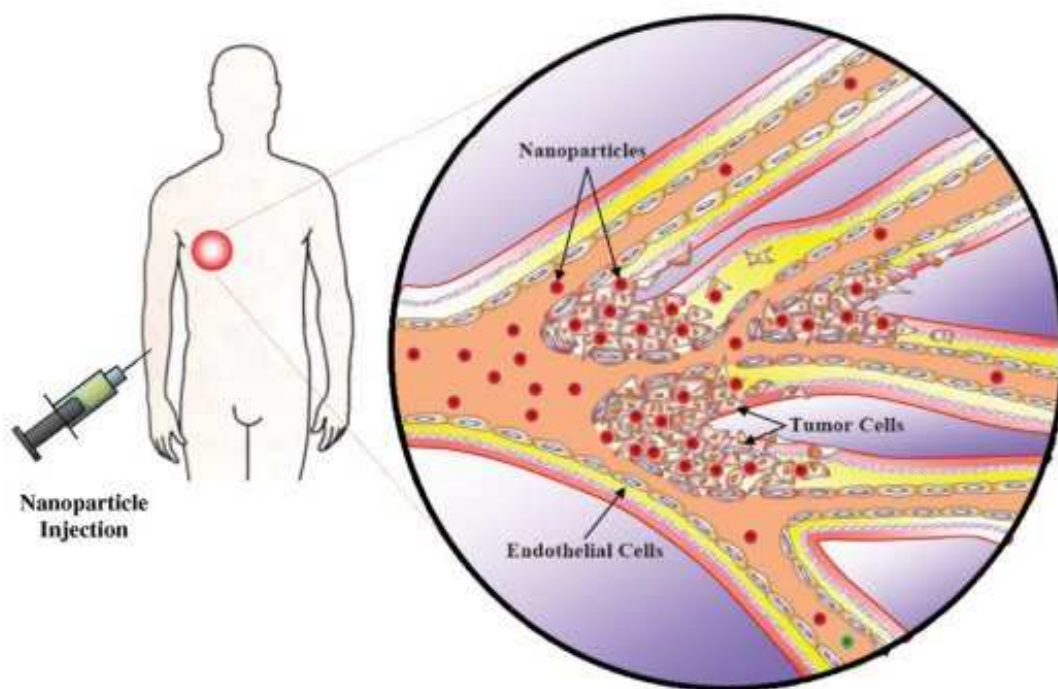
Figure 1.37: Enhanced permeability and retention effect in passive tumor targeting [195].

circulation in the blood and tend to accumulate passively in tumor interstitia more than

in surrounding tissues. That phenomena results from abnormalities of tumor cells which, in order to grow fast, have to stimulate the production of new blood vessels [200]. Rapid vascularization provides oxygen and nutrients for growing tumor. Nevertheless, the newly formed blood vessels usually have abnormal structure with high proportion of proliferating endothelial cells, lack of smooth muscle layer and increased tortuosity. This defective architecture results in decreased lymphatic drainage [201]. The blood vessels render permeable to nanoparticles, which once present in a tumor are not removed efficiently due to fluid transport disorder. This passive targeting phenomena is known as enhanced permeability and retention effect (EPR) and is presented in Fig. 1.37. Numerous studies shown that the EPR results in passive accumulation of nanocarriers in tumor tissues, increasing therapeutic effect and reducing side effects of the treatment [202–205].

5.3 Application of colloidal properties in drug delivery

Colloidal drug delivery has been and continues to be a foundation for problematic formulations of active drug ingredients. Colloidal systems have come a long way from use in the enhancement of solubility and protection of labile compounds to reduction in the drug toxicity. Colloidal carriers are usually required for the following reasons:

- Poor aqueous solubility of many therapeutically effective drugs.

- Protection of labile substances from hydrolysis, enzymatic degradation and absorption through the membranes.

- Increase of drug efficacy by reducing its size to nanoparticles.

- Decrease of drug toxicity.

- Avoidance of recognition by mononuclear phagocyte system and host inflammatory response.

- Possibility of conjugating a specific vector to the carrier — active targeted delivery.

- Easy to administer intravenously due to their small size.

The morphological, physicochemical, optical, kinetic, charge and magnetic properties of colloids are decisive for their use in drug delivery. The morphological properties of

colloidal particles (size, shape, surface area) greatly influence delivery systems. Any alteration in the morphological properties may modify the stability, biocompatibility and distribution of drug carriers [206]. Particle size reflects the surface area for adsorption and its settling in the suspensions. Therefore, particle size distribution is one of the most important parameters determining the selection of the route for drug delivery [207]. The charge properties of colloids are another critical factor as they determine interactions of drug carrier with the biological components. Blood can be a harsh environment for intravenously injected drugs since it acts as barrier against infections. For example, the polyanionic DNA molecule can be condensed with polycationic carrier in order to reduce its size and to protect it against nucleases; an excess of positive charge enables sufficient compaction of DNA [208]. The resulting net positive surface-charge is advantageous for binding to a negatively charged cell surface when used in cell culture. On the other hand, positive surface charge can cause adverse situation when injected into the bloodstream. Cellular components of blood (i.e., thrombocytes, erythrocytes), as well as plasma proteins (albumins, immunoglobulins) are negatively charged. Injected positively charged particles can bind to plasma proteins and negatively charged erythrocyte membranes, which leads to activation of host defense mechanism and rapid clearance from the blood. Therefore, use of negatively charged colloidal carriers is advantageous for prolonged circulation time in the bloodstream [209–211]. Nanoparticles with hydrophobic surface are rapidly taken up by the liver, spleen and lungs, while hydrophilic ones repel plasma proteins and remain in the bloodstream for longer. Surface modification of colloidal carriers with poly(ethylene glycol) (PEG) can prolong circulating half-live up to 45 hours, as opposed to few hours or minutes for conventional systems [212]. The optical properties (Tyndall effect, turbidity, dynamic light scattering) are widely used to observe the size and structure of colloidal particles and can be used as tools to access rational criteria for new drug formulations. The kinetic properties (Brownian motion, diffusion, osmosis, viscosity, sedimentation) deal with the movement of particles against body fluids and provide transportation criteria of colloidal particles across cell membranes. The physicochemical properties (lyophilicity, lyophobicity, interfacial properties) are helpful in the selection of drug carrier for particular type of active compound [213, 214]. Osmosis and osmotic pressure are of vital importance in biology and drug delivery. An osmotic pressure results from the tendency of a solvent to move through a semi-permeable membrane (e.g., cell

membrane) into a solution containing ions or molecules, which cannot traverse through the membrane. Osmosis happens spontaneously and the molecules of a solvent move from a lower solute concentration to a higher solute concentration in order to reduce the pressure difference (osmotic pressure) between two compartments. The osmotic pressure provides a selection criteria for the absorption of colloidal solution in transdermal applications [215]. Understanding of all the above properties allows predicting the behavior of colloidal carriers in the living system, such as mechanism of transport, absorption, drug distribution and interactions with the cells membrane.

5.4 Nanoparticles for imaging applications

Development of noninvasive imaging techniques is of great importance in biomedical applications [216, 217]. Detection and tracking of abnormalities, such as cancer or inflammation, would be difficult without using a proper contrast agent. Clinical diagnosis, cellular biology and drug discovery have evolved tremendously thanks to the use of nanoparticles in place of conventional biomarkers. Among the others, quantum dots and magnetic nanoparticles should be named as most promising and versatile nanolabels. This chapter covers the properties and applications of these materials.

5.4.1 Quantum dots

Quantum dots are nearly spherical, luminescent nanocrystals made of semiconductor materials [218]. They comprise of a few hundreds atoms from groups II–VI or III–V of the periodic table. The physical dimensions of quantum dots are smaller than the excitation Bohr radius, which results in their unique optical and electronic properties [220]. In a bulk semiconductor an energy bandgap, which is the minimum energy required to excite an electron from the valence to the conductance band, is fixed and only composition-dependent. Relaxation of the exciton to the ground state may be accompanied by the fluorescent emission of a photon. Sizing down the semiconductor to a nanocrystal is a reason for quantum confinement effect, which means that excitons of quantum dots are confined in all the spatial dimensions [221]. The electronic excitation states respond to the particle boundaries by adjusting their energy states. As a consequence, decreasing or increasing size of quantum dots results in respectively increase or decrease of their bandgap energy. The absorption spectra and emission wavelength are shifted to the blue
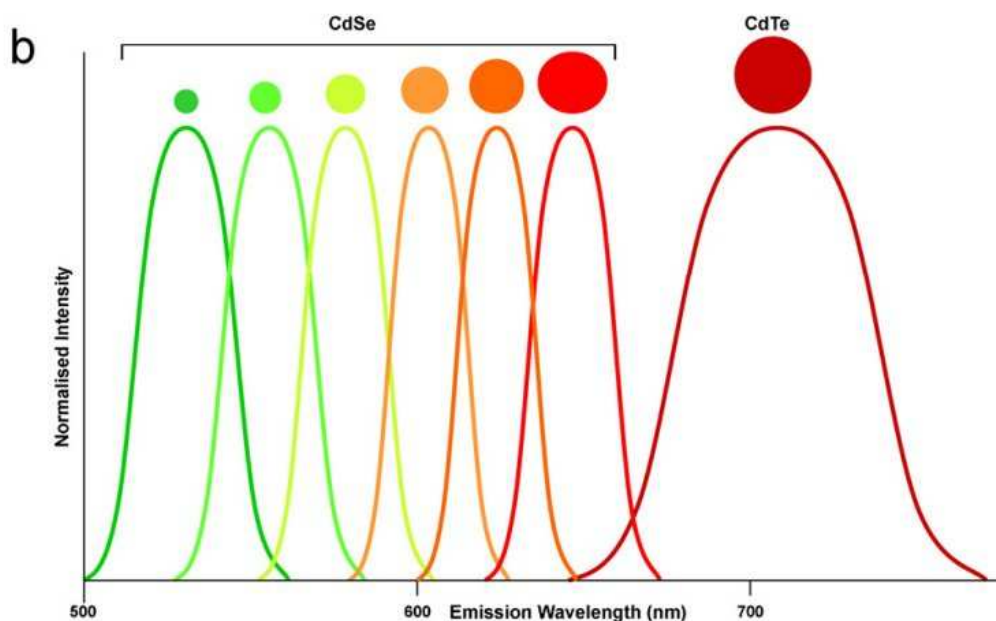
Figure 1.38: Size-dependent optical properties of CdSe quantum dots [219].

or red spectral region [222]. Owing to that phenomena, quantum dots are character-ized with wide excitation spectra and intensive, narrow emission tunable by varying both their size or composition. Figure 1.38 presents the optical properties of CdSe quantum dots as a function of their size. In comparison with traditional fluorescent markers (e.g., organic dyes or proteins), quantum dots are about 10–100 times brighter, more stable and resistant to photobleaching [223–225]. A single light source can excite quantum dots with different emission wavelengths — from the ultraviolet throughout the visible and near-infrared spectra [226–228]. Quantum dots can be used as photosensitizers for cancer therapy. Photodynamic therapy (PDT) is an approved treatment for some types of cancer and skin disorders [229]. In PDT tumor cells are selectively killed by chemically targeting them with a photosensitizing agent. The tissue is then exposed to visible light, which stimulates photosensitizer for generation of highly toxic singlet oxygen. Photosensitized oxidation induces cell damage and death [230]. Several groups demonstrated cytotoxicity of quantum dots under exposure to the UV radiation [231, 232]. PDT therapy is highly selective; only the cells in close vicinity to the photosensitizer are affected.

Quantum dots synthesis was first described by Efros and Ekimov in 1982 [233, 234]. They grew nanocrystals and microcrystals of semiconductors in glass matrices. Since then, a wide variety of methods have been developed, including the preparation of quantum dots

in aqueous solution, high-temperature organic solvents and on solid substrates [235–237]. The colloidal semiconductor nanocrystals are commonly synthesized through the introduction of semiconductor precursor into a solvent under conditions favoring crystal growth. The semiconductor core determines the emission wavelength of resulting nanocrystals as characteristic for chosen material. Quantum dots are often coated with an outer shell of a different material characterized with a wider bandgap than the core, which provides higher electronic insulation and photoluminescence efficiency, as well as enhanced protection against oxidation or degradation. A presence of ZnS coating around core made of CdSe, CdS or CdTe increases the quantum yield (brightness) up to 80% [219].

Most quantum dots are synthesized in nonpolar solvents, while an important prerequisite for use of nanoparticles in medicine is their aqueous dispersability. Therefore, the third step of synthesis should involve replacement of hydrophobic surface ligands with amphiphilic ones. There are two general approaches to render quantum dots water-soluble: ligand exchange or encapsulation within an amphiphilic polymer [222, 226]. In the ligand exchange approach, a suspension of quantum dots in high-temperature solvent (e.g., TOPO-trioctylphosphine oxide) is mixed with a solution containing heterobifunctional ligand, which has one functional group binding to TOPO-coated nanocrystals and another functional group that is hydrophilic [186, 219, 238]. The transition of quantum dots from nonpolar solvent to aqueous solution was first reported by Bruchez et al. and Chan and Nie in 1998 [239, 240]. CdSe/ZnS have been coated with mercaptoacetic acid and (3-mercaptopropyl) trimethoxysilane, in which basic thiol groups bind to the surface atoms of quantum dots, providing carboxylic acid or silane monomers rendering them water-soluble. The other ligands used for surface modification are mercaptopropionic acid and arabic gum [241]. However, it needs to be emphasized that ligand exchange is often associated with decreased fluorescence efficiency and a tendency to aggregate in biological buffers. Encapsulation of quantum dots with amphiphilic polymers is another option for rendering them water-soluble [226, 242, 243].

The last phase in preparation of quantum dots for biological applications involves their functionalization with diverse biological labels, such as proteins, peptides, antibodies, nucleic acids or small organic molecules [244]. The carboxylic groups, normally present at the surface of quantum dots after aqueous stabilization, enable the formation of a covalent bond with the amine groups of biomolecules. Quantum dots – biomolecules

bonding can also occur through electrostatic interactions (most quantum dots are negatively charged and can interact with positively charged molecules), or receptor-ligand binding (e.g., streptavidin-biotin). Bioconjugation determines the role and targeting of quantum dots in cellular and tissue application. Functionalized quantum dots are widely used as fluorescent probes in biological staining and diagnostics, e.g., in nucleic acid/antibodies/antigens assays, cancer imaging and diagnosis or in single quantum dot studies of membrane dynamics and organization [245–247]. A schematic representation of functionalized quantum dot is shown in Fig. 1.39.
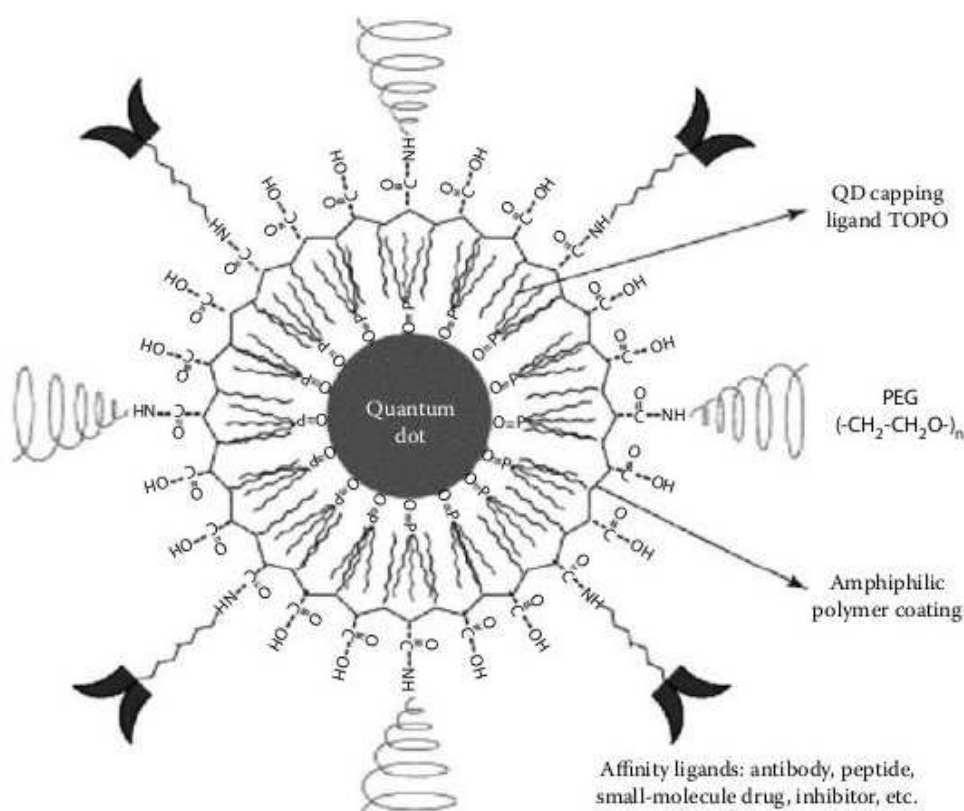
Figure 1.39: A schematic representation of the functionalized quantum dots [3].

A major weakness of most frequently used quantum dots lies in their in vitro and in vivo toxicity [248, 249]. Toxicity of cadmium-based quantum dots is caused by release of cadmium ions with subsequent generation of radicals, malfunction of organelles and cell damage. Beside heavy metal related toxicity, the tendency of nanoparticles to aggregate, precipitate on cells in the culture or nonspecifically adsorb to biomolecules may be just as important contribution to overall toxicity [226, 249]. The toxicity issue might be eliminated by use of quantum dots from non-hazardous materials, such as water-soluble ZnS

nanoparticles or carbon-based quantum dots [250, 251]. Another approach to eliminate quantum dots related toxicity relies on encapsulation of nanoparticles in a stable polymer coating, which should hinder their corrosion, prevent dissociation and, therefore, avoid the cytotoxicity of such prepared carriers [241, 249, 252, 253]. Embedding of quantum dots in phospholipid micelles for bioimaging applications has also been reported [254]. Encapsulation of hydrophobic or hydrophilic quantum dots by layer-by-layer assembly of polyelectrolytes will be discussed in more details in following chapters.

5.4.2 Magnetic nanoparticles

Use of magnetic nanoparticles is gradually gaining importance in biomedical applications. They are used in the enhanced magnetic-resonance imaging (MRI), enabling early disease detection, accurate prognosis and the medical treatment [255, 256]. Magnetic contrast agents are dominated by various forms of iron oxides, such as magnetite (Fe_3O_4) or maghemite (γ-Fe_2O_3) [257]. The two most common methods to produce magnetic nanoparticles are coprecipitation and microemulsification; another methods use ultrasound irradiation, thermal decomposition of precursor, laser process and are described in the literature [255]. The magnetic nanoparticles can be classified according to their size:

- Superparamagnetic iron oxides (SPIOs) with sizes bigger than 50 nm (including the coating).

- Ultrasmall superparamagnetic iron oxides (USPIOs) with sizes smaller than 50 nm.

The size of SPIOS determines their plasma half-life and biodistribution. Magnetic nanoparticles are often coated with polymers such as dextran, PEG, polyvinyl alcohol (PVA), starches, poly(lactic-*co*-glycolic acid) (PLGA). Paramagnetic materials are usually categorized according to ability of aligning their magnetic domains with external magnetic field. The magnetic domains are randomly oriented in the absence of an external field, and become aligned in its presence. This property is extremely important as it enables to guide magnetic nanoparticles to the site of interest [24]. Passive targeting of SPIOs leads to accumulation of particles in lymph nodes, liver, spleen and tumor site, improving contrast during imaging. Active targeting of SPIOs with biomolecules, such as nucleotides, peptides or antibodies, renders them highly specific and enables to target the desirable site of interest.

Another possible application of magnetic nanoparticles in medicine is to use them as heat sources to generate magnetic hyperthermia [258]. Hyperthermia occurs when body produces or absorbs more heat than it dissipates. It leads to locally elevated body temperature, cell damage and apoptosis. Hyperthermia can be deliberately induced as a part of medical treatment. When magnetic nanoparticles are in the presence of an alternating high-frequency magnetic field, they generate heat through Néel and Brown relaxation processes [259–262]. Endocytosis of magnetic nanoheaters localize them in the cell interior. The resulting temperature increase is high enough to selectively kill tumor cells.

Magnetic nanoparticles can be also incorporated together with bioactive substances and drugs into liposomes or polymeric carriers. Such prepared colloidal vesicles posses magnetic properties and enable targeted delivery of drugs directed by external magnetic field. Beside the possibility to be navigated, the magnetic nanocarriers can be remotely triggered to release their load in a site of interest [262].

5.5 Nanocapsules prepared by layer-by-layer adsorption of polyelectrolytes

5.5.1 Introduction

The list of colloidal carriers used for drug delivery and imaging purposes includes simple emulsions, liposomes, different nanoparticles and nanocapsules. Polymeric nanocapsules are colloidal systems, in which active compound is confined to a reservoir or is within a cavity surrounded by a polymer membrane or coating [263, 264]. The core of the capsule can be either solid (e.g., charged colloidal particles, hydrophilic nanoobjects) or liquid (emulsion droplets). These systems are commonly used in the encapsulation and delivery of hydrophobic and hydrophilic drugs. Encapsulation of active agent within the capsule's shell aims for protection of the load from harsh biological environment, increase of solubility and compatibility of a drug, control of drug release profile and targeted delivery improving efficiency of the treatment [104]. A convenient procedure of fabricating nanocapsules with promising therapeutic benefits is the previously mentioned layer-by-layer assembly of polyelectrolytes. Adsorption of polyelectrolytes on the charged surfaces and interfaces has been extensively studied over the years [105, 113, 114, 122]. Initially applied on flat mi-

croscopic surfaces, layer-by-layer adsorption technique on colloidal templates has become a versatile tool for the formation of polyelectrolyte nanocapsules [265–268]. The shell can be further functionalized by including a host of inorganic nanoparticles, biomolecules, clays or dyes in polyelectrolyte multilayer assemblies [269–271].

Layer-by-layer assembly of polyelectrolytes around charged colloidal cores is based on sequential adsorption of polyanions and polycations [272–274]. The process is schematically shown in Fig. 1.40. The electrostatic attraction between charged template and
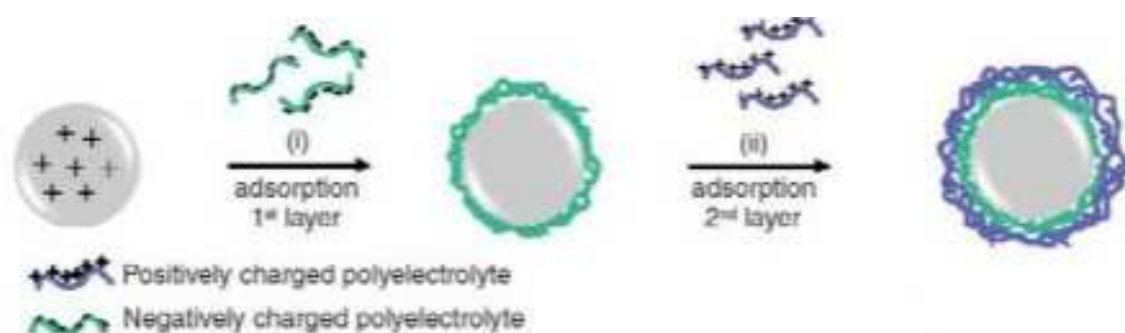
Figure 1.40: Polyelectrolyte multilayer formation process on a charged colloidal core [217].

oppositely charged polyion molecules leads to the formation of first layer and surface charge reversal. Adsorption of each layer of polyelectrolyte results in an overcompensation of charge, which enables the alternate deposition of subsequent layers. The presence of polyelectrolyte multilayers improves the stability of colloidal templates. A proper choice of experimental parameters, such as polyelectrolyte type, length, molecular weight, ionic strength and concentration of dipping solution, size and concentration of colloidal core, allows to create multifunctional and uniformly coated particles.

The greatest challenge in the layer-by-layer coating procedure of colloidal templates is the effective separation of the remaining unadsorbed polyions from colloidal solution prior to the next deposition step. There are two possible ways to eliminate this problem: saturation method or removal of excessive polyelectrolyte molecules from the solution [275]. In the saturation approach, during each step of adsorption the amount of added polyelectrolyte is limited to form the saturated layer, such that the presence of free polyelectrolyte in solution will be constrained. Figure 1.41 illustrates changes in the zeta potential of the negatively charged polystyrene particles as a function of the polyelectrolyte concentration. With increasing bulk concentration of the adsorbing polyelectrolyte, a surface charge re-
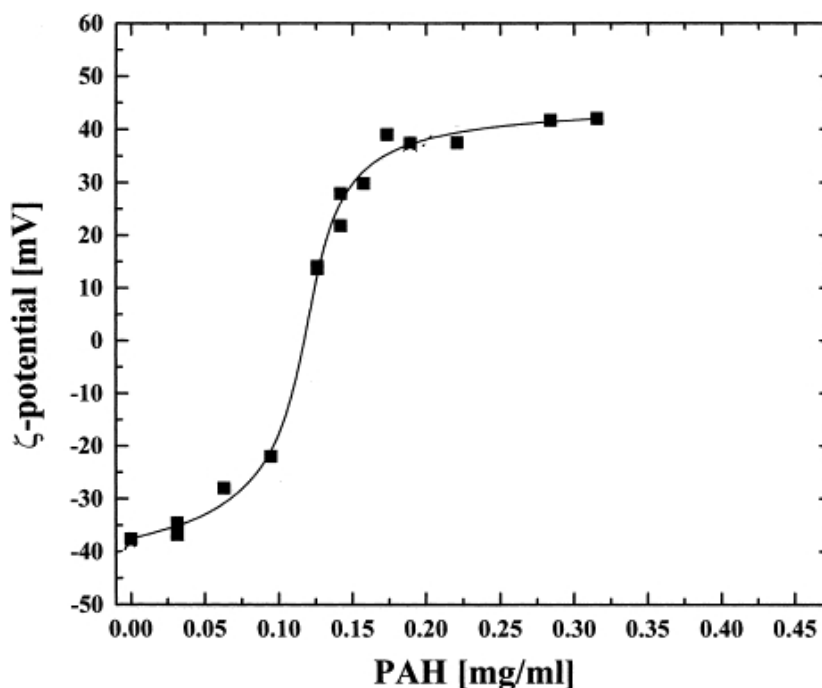
Figure 1.41: The zeta potential of negatively charged polystyrene particles as a function of the polycation concentration [104].

versal of colloidal particles occurs. At a certain concentration, the zeta potential reaches a saturation plateau, corresponding to the coating of total available particle surface area. Below that concentration most polyelectrolyte is adsorbed on the particles, depleting the solution from the majority of free polyelectrolyte. Further increasing of polyelectrolyte bulk concentration does not influence the zeta potential value of particles. Therefore, the volume of polyelectrolyte added to form a saturated layer is considered as optimal when the zeta potential of coated template reach the value close to the zeta potential of polyelectrolyte used to form the shell. The consecutive layers are formed in a similar manner, using volume of polyelectrolyte optimized to a certain particle concentration. The major drawback of saturation technique is the probability of forming unwanted polyelectrolyte complexes and particle aggregates in the multilayer assembly process [266]. This problem can be overcome by using a dilute particle suspension. However, the concentration of all components need to be carefully determined and controlled during the entire coating procedure.

In the second method, coating of colloidal cores is performed at excess concentration of polyelectrolyte. The non-adsorbed polyelectrolyte remaining in the solution is removed prior to the deposition of next, oppositely charged layer in order to avoid formation of

aggregates. Usually the removal of free polyelectrolyte is performed by centrifugation, filtration or dialysis [184, 272, 273]. The main drawbacks of centrifugation process are the difficulties in centrifuging smaller particles (e.g., < 50 nm) and the significant loss of particles during preparation. Use of filtration set-up, where the colloid particles are retained on the filter and small free polyelectrolytes pass through the pores, seems to be milder procedure. Nevertheless, the centrifugation is still widely used for layer-by-layer coating of colloids.

5.5.2 Polyelectrolyte capsules with solid core

Once the polyelectrolyte carrier is fabricated by layer-by-layer adsorption process, the solid core can be either kept as it is (e.g., complexes of nanoparticles with the oppositely charged polyelectrolyte can be used as cores for further encapsulation) or removed in the dissolution step in order to obtain hollow and stable capsules. This process is schematically shown in Fig. 1.42. The inner cavity of the capsule and polymer wall can be loaded
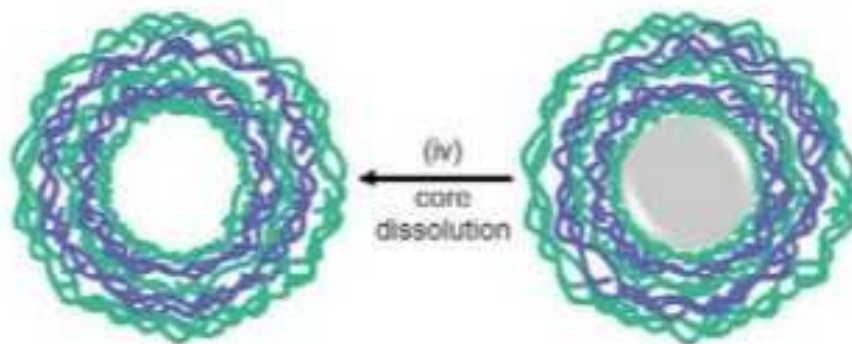
Figure 1.42: Schematic representation of core dissolution [217].

and functionalized with a variety of active substances, such as drugs, nanoparticles, dyes and biomolecules [217, 276]. The resulting hollow capsules can have a wall thickness in the range between tens to several hundreds of nanometers [277, 278]. The size of capsule can be up to several micrometers, depending on the size of original template.

The colloidal template should be characterized by a narrow size distribution. It has to be stable during layer-by-layer deposition process and completely removable from the inside of the capsules. The core removal conditions should be mild and should not affect the morphology and stability of the resulting hollow capsule [279]. The template may

consist of inorganic, organic or biological materials, polymers or cells. Polystyrene latex, melamine formaldehyde, carbonate particles ($MnCO_3$, $CaCO_3$) and silica are among most often used colloidal cores [280–284]. Due to the diversity of core materials, the removal chemistry is also highly varied. Solvents like tetrahydrofuran, hydrochloric acid, hydrogen fluoride, EDTA and saline solution are being used. Polymeric cores can also be destroyed by use of light, heat or enzymes. The major drawback of the process is that core dissolution step often has a negative influence on the integrity of the shell [217]. Some core material tends to remain inside the shells. After core destruction the driving force for release disappears and the pores will close. Consequently, some core material is captured inside; degradation products of positively charged melamine formaldehyde core will interact with the polycation in the multilayer. This may significantly alter the properties of obtained shell. Inorganic cores are less problematic when it comes to product removal after core destruction; on the other hand, it is difficult to obtain particles of uniform size in the micrometer range. Another promising alternative is low-cost, sufficiently monodisperse silica core. It can be easily coated in layer-by-layer assembly of polyelectrolytes and removed afterwards by hydrofluoric acid treatment. The procedure is quite dangerous due to removal chemistry, but polyelectrolyte shell remains rather stable in the end of process. Organic particles of low molecular weight compounds are used as well, but they are often soluble in solvents different from those for polyelectrolytes. That problem can be overcome by coating their surface with surfactants or polymeric amphiphiles in order to render cores water-soluble [104].

5.5.3 Polyelectrolyte capsules with liquid core

As an alternative for capsules with solid cores, hydrophobic components can be solubilized in a form of emulsion droplets and directly encapsulated within polyelectrolyte shell [285–287]. Liquid cores are more difficult to handle then the solid ones due to their higher flexibility and mobility. However, it is possible to "freeze" the oil droplets by coating them with polyelectrolytes [104].

Oil-in-water emulsions have been widely used as drug carriers since they have the ability to solubilize lipophilic drugs [288–291]. A necessary prerequisite for application of emulsions in pharmaceutical formulations is their lack of in vitro/in vivo cytotoxicity [292]. In order to fulfill that requirement, all the compounds used to form an emulsion

should be non-toxic. Vegetable oils, composed predominantly of medium-chain or long-chain triglycerides, are lipid materials derived from plants [293]. They are commonly used in industry, including food industry, paints, personal care and cosmetic products. Many natural oils such as soybean oil, olive oil, jojoba bean oil, linseed oil, castor oil, coconut oil and sunflower oil, have already been used to form emulsions. A major limiting factor to use vegetable oils is their instability. The relatively high content of unsaturated esters in linseed oil makes it susceptible to polymerization reaction when exposed to air [294]. Soybean oil hydrolyses causing harmful side effects in patients [295]. Emulsion formulations applied as drug delivery systems involve use of another oils, such as octyldodecanol, decane, or isopropyl myristate [296–298].

Surfactants are often known to have toxic or irritant effect on living organisms. Therefore, it is important to consider the use of harmless compounds to stabilize emulsion droplets. Cationic surfactants can be toxic and their use in pharmaceutical applications is limited [24]. Non-ionic surfactants, such as fatty acids ethoxylates, are biocompatible and widely accepted in cosmetics and pharmaceuticals. However, emulsion droplets used as liquid cores for layer-by-layer (LbL) encapsulation by formation of polyelectrolyte shell must have stable surface charge ensured by use of ionic surfactants in the emulsification process. It is preferred that surfactants used are scarcely soluble or insoluble in water for two reasons: firstly, because it constrains their presence in the water phase and by that limits their toxicity and secondly, because water-soluble surfactants tend to form polyelectrolyte-surfactant complexes, which decrease surfactant concentration at emulsion droplets, causing their instability [299, 300]. Docusate sodium salt (AOT) is oil-soluble, anionic surfactant approved by FDA, which makes it a good emulsifier for liquid core encapsulation. Another surfactant proposed by several authors, didodecyldimethylammonium bromide (diDDAB), was used to stabilize emulsion droplets of MCT (medium chain triglycerides) and dodecane, coated with anionic starch or by poly(styrene sulfonate) (PSS)/poly(dimethyldiallylammonium chloride) (PDDA), respectively [301]. Furthermore, a number of biological origin compounds posses surface-active properties. Lecithin is a zwitterionic surfactant made of a mixture of phospholipids with phosphatidylcholine as main component [302]. It acts by modifying the interface between oil droplets and the aqueous phase; the excess of lecithin would form liposomes in water [303]. Cholesterol, being an important constituent of liposomes, is another compound with amphiphilic

structure responsible for the emulsifying capability [24].

5.5.4 Shell materials

Several polyelectrolytes can be utilized to form multilayers around charged cores using the layer-by-layer assembly technique. The capsule wall composition has a significant importance as their permeability/porosity strongly depends on the molecular weight and chemical structure of the employed polyelectrolytes. Standard synthetic polyelectrolytes described in the literature are polycations – poly(dimethyldiallylammonium chloride) (PDDA), poly(N-isopropyl acrylamide (PNIPAM), poly(ethylenimine) (PEI), poly(allyamine hydrochloride) (PAH), and polyanions – poly(styrene sulfonate) (PSS), poly(acrylic acid) (PAA), poly(methacrylic acid) (PMA), poly(vinyl sulfate) (PVS) [117]. Among this polyelectrolytes, multilayers composed from a pair of PAH/PSS are particularly well described and known for numerous advantages [276]. However, it is favorable to use more biocompatible and potentially biodegradable materials for medical applications. Example of synthetic biocompatible pair of polyelectrolytes is positively charged poly-L-lysine (PLL) and negatively charged polyglutamic acid (PGA). Natural polyelectrolytes include nucleic acids, proteins and polysaccharides of which chitosan, alginate, hyaluronan, DNA, heparin and cellulose sulfate are the most common [304–307]. Charge of the proteins can be tuned by varying the pH value below or above their isoelectric point in order to obtain either polycation or polyanion layers.

Due to the great diversity of materials used to form multilayer shells it is possible to control permeation and release properties by changing pH, ionic strength, temperature or light. PAH/PSS capsules can be an example of carriers with pH-switchable permeability. As reported by authors, capsules prepared and kept at pH ~ 8 were not permeable for fluorescently labeled proteins [308]. By lowering the pH value to below 6 the shell became permeable such that fluorescence inside the capsules could be seen. After returning to initial pH value and removal of external proteins by centrifugation the remaining emission was coming exclusively from capsule's interior, proving that the fluorophores have been entrapped. That effect is caused by the structure of multilayer consisting of the weak polycation PAH and strong polyanion PSS. At the initial conditions only some side groups of PAH are charged, compensating the PSS negatively charged side groups. Therefore the shell interior contains additional uncharged side groups from PAH. Lower-

ing the pH causes uncharged groups to protonate, the shell interior becomes altogether charged, and Coulombic repulsion destabilize the film. This is partly compensated by counterions penetrating the film, but the resulting osmotic pressure destabilize the shell anyway. Light-induced destabilization of drug-loaded polymeric micelles and liposomes with consequent drug release has been demonstrated elsewhere [309]. Upon illumination, the temperature of nanoparticles embedded within the walls rises as light energy is converted into heat. The heat transiently melts the surrounding polymeric network, which locally increases the membrane permeability and causes drug release [310].

Electrophoretic mobility and light scattering measurements are typically used to follow the layer-to-layer growth of polyelectrolytes around charged cores [266]. Atomic force microscopy, as well as scanning electron microscopy are often employed for their structural characterization [285]. Confocal laser scanning microscopy is widely used for real-time observation of core dissolution in vitro, characterization of permeability and cellular uptake of the capsules [311, 312].

5.6 Nanoparticles: health and environmental risks

Medicine and health care industry take tremendous advantages from use of nanoparticles. Bionanotechnology is a new field of rapid growth and development [186]. The key features of nanoparticles qualifying them for biomedical applications are, among others, their high surface area to volume ratio, small size, special optical, electric or magnetic properties, as well as possibility of surface coating and functionalization. However, it should be stressed that the very same properties, which make them so unique, raise many questions regarding the possible long-term toxicity and impact on the human health [313–315]. If nanoparticles are able to permeate tissue, cell membranes, or even hardly accessible bloodbrain barrier, is there a limit of safe exposure? Do the nanoparticles clear the body after a certain time without adverse effects? What happens, when the nanoparticles intrude and defeat host immune defense? These and many other questions introduce the need for long-term studies concerning the possible toxic impact of nanoparticles on humans and the environment, not only during therapy but also manufacturing and disposal. There are several groups working on better understanding of the mechanisms which govern the cellular uptake, transportation, metabolization and secretion of nanoparticles both *in vitro* and *in vivo* [316–320].

Chapter 2

EXPERIMENTAL PART

6   The aim of the work

Assemblies of surfactants, polyelectrolytes and nanoparticles have become a versatile tool for the formation of soft nanostructures, which can find application in targeted delivery systems. Oil-in-water emulsions stabilized by surfactants and/or nanoparticles are widely used as drug carriers since they have ability to solubilize hydrophobic active ingredients. Nanocapsules are the specific type of containers composed of a core surrounded by a shell formed from various materials with the size in the range of 100 nm and below, which enables them crossing the biological barriers. Encapsulation of active agents within the capsule's cavity protects the load from the external environment, regulates the release rate and can reduce the toxicity effect of the drug by targeted delivery i.e. by selective accumulation in the area of interest. The aim of my thesis was to develop the methods of formation and to characterize various nanocarriers, aimed for biomedical applications, using the combination of surfactants, polyelectrolytes and nanoparticles as the building blocks. As the model cargo for the nanocarriers I selected model drugs (Naproxen and Vitamin D), as well as fluorescent markers Cumarine 6 and hydrophilic CdTe and hydrophobic CdSe/ZnS quantum dots. The main aim of the encapsulation of quantum dots was to obtain coatings, which significantly reduced their toxic effect on the cells, i.e. formation of the QD containing nanocapsules, which can be used as fluorescent probes, as well as in the photodynamic therapy. I proposed combination of experimental techniques to follow the process of nanocarriers formation and to determine their properties,

such as the dynamic light scattering, microelectrophoresis, AFM, fluorescence and UV-vis spectroscopy. For the analysis of cytotoxicity proliferation assays, flow cytometry and MTT test were used. Combination of such methods allows full characterization of the nanostructures obtained by assembly of surfactants, polyelectrolytes and nanoparticles..

7 Experimental methods

7.1 Dynamic Light Scattering

Dynamic Light Scattering (DLS), also known as Photon Correlation Spectroscopy (PCS), is of the special importance for characterization of nanoparticles and macromolecules in their solution. It can provide information on the molecular weight, size and polydispersity of the particles. The particles in a suspension undergo the Brownian motion. Because of that constant movement, the intensity of light scattered by the particles undergoes time-dependent fluctuations. The intensity of scattered light is a function of the particle size and its ability to scatter the light. Analysis of intensity fluctuations enables to determine the diffusion coefficient D. Once the diffusion coefficient is established, the hydrodynamic radius of the particles can be derived via the Stokes-Einstein equation:

$$R_{\mathrm{H}} = \frac{k_{\mathrm{B}}T}{6\pi\eta_0 D} \,, \tag{2.1}$$

where R_{H} is the hydrodynamic radius, i.e., the radius of the sphere that diffuses at the same speed as the given particle, k_{B} is the Boltzmann constant, T is the absolute temperature, and η_0 is the suspension viscosity.

The measured particle size is related to the correlation function, which defines the degree of similarity between two signals over a period of time [321]. The autocorrelation function $C(\tau)$ can be defined as follows:

$$C(\tau) = < I(t)I(t + \tau) > \tag{2.2}$$

Where I(t) is the signal intensity measured at a given time and $I(t + \tau)$ is the signal intensity measured after a time delay τ.

The correlation between intensity signals separated by a short period of time is very

high, because the particles did not move too far from their initial position. A perfect correlation coming from comparison of signal intensity at (t) with itself is reported as 1. If the original signal is compared with the intensity at a much later time, these two signals will have no relation at all as the particles are moving in random directions. That situation corresponds to lack of correlation between the two signals and reported as zero. In the case of a monodisperse suspension of spheres, the autocorrelation function can be treated as exponential decay

$$C(\tau) = \exp(-T\tau),\tag{2.3}$$

where T is the decay rate related to the diffusion coefficient by the formula

$$T = Q^2 D,\tag{2.4}$$

in which Q is the length of the scattering vector defined as

$$Q = \frac{4\pi n}{\lambda} \sin\frac{\theta}{2}.\tag{2.5}$$

Here, the refractive index is denoted by n and θ is the angle between the sample and the detector.

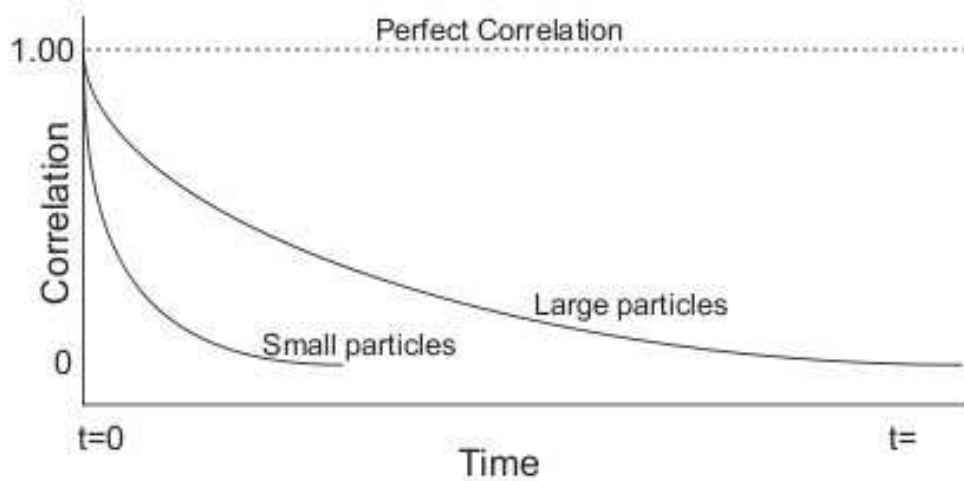As shown in Fig. 2.1, the rate of decay for the correlation function is related to the

Figure 2.1: The correlation function for small and large particles [322].

particle size. Since large particles move slowly, the intensity of scattering also fluctuates slowly and the rate of decay is much slower than for quickly moving, smaller particles.

2. EXPERIMENTAL PART

Once the correlation function has been measured, the decay rates can be extracted for a number of size classes to calculate the size distribution of a sample. Figure 2.2 presents a typical size distribution graph. The x axis shows a distribution of size classes,
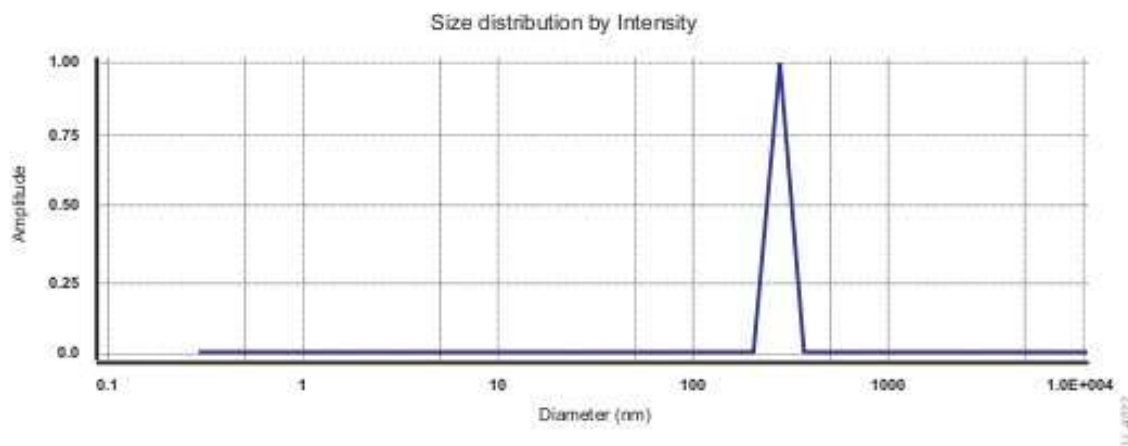

Figure 2.2: Typical size distribution by intensity graph [322].

while the y axis shows the relative intensity of scattered light. The intensity distribution graph can be then converted to a volume or number distribution using Mie theory of light scattering [322].

A typical DLS measuring system is shown in Fig. 2.3. A laser, being a source of monochromatic and coherent light, illuminates the sample within the cell. Most of the laser beam passes straight through the solution, while some light is scattered by the particle suspension. A detector measures the intensity of the scattered light. The detector can be placed in different positions to detect the scattering. The intensity of scattered light must be within a range specific for the detector. Therefore, in order to optimize the amount of detected light, an attenuator is used to reduce or increase the intensity of the laser. The scattering light is passed to a correlator, which compares its intensity at time intervals to derive the rate at which the intensity is changing. The resulting information is passed to a computer, ready for analysis [321].

The size distribution (hydrodynamic diameter) of the samples prepared in the present work was determined by DLS using Zetasizer NanoSeries from Malvern Instruments, UK. The angle of detection was equal to 173° (backscatter detection), which prevents multiple scattering and light scattering on large contaminants, such as dust particles. All the measurements were performed at 25°C. The presented size values are an average from at
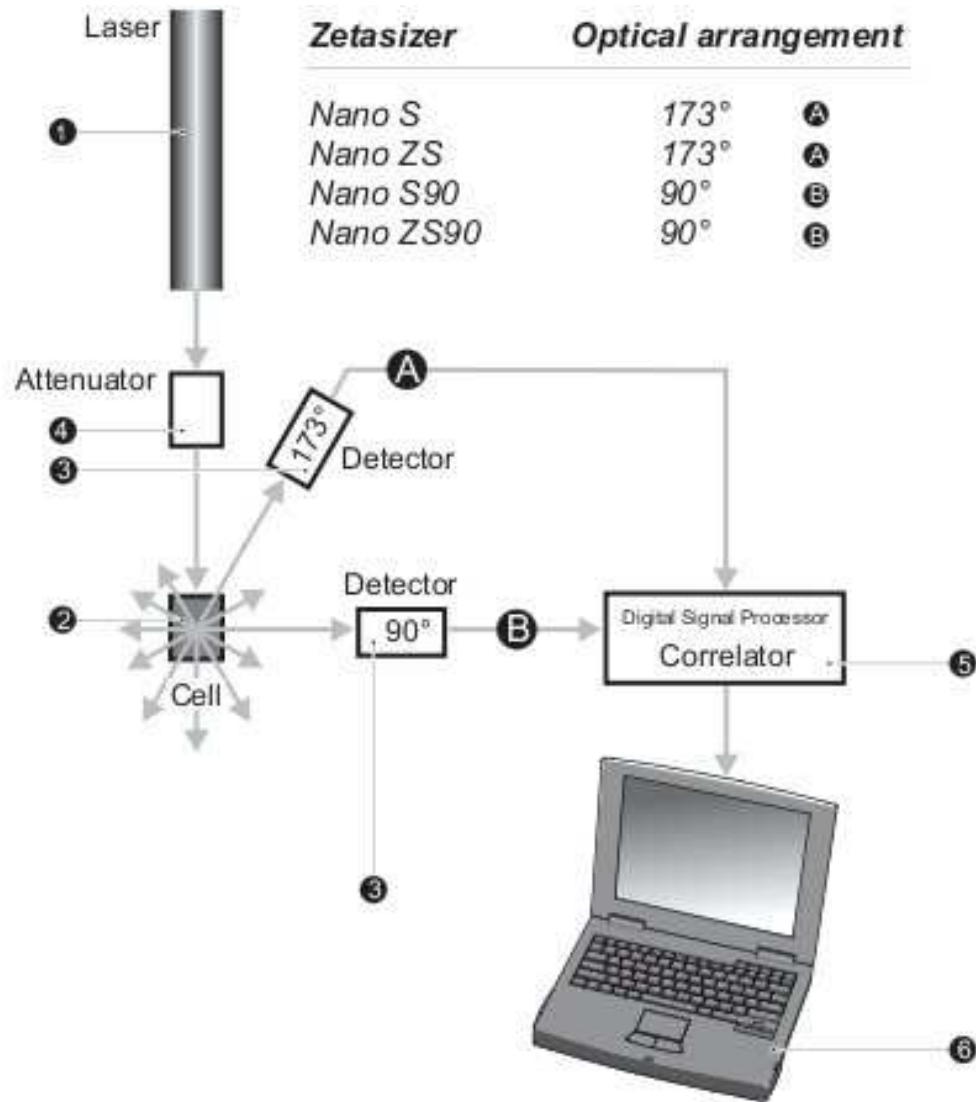
Figure 2.3: A typical DLS measuring system [322].

least three subsequent runs with ten measurements.

7.2 Electrophoretic mobility measurements

The zeta potential value of particles can be determined by electrophoretic mobility measurements. Figure 2.4 schematically shows the principle of the microelectrophoresis. When an electric field is applied across a cell filled with electrolyte, the charged particles suspended in the medium start to move towards the electrode of the opposite charge [322]. The viscosity of a medium tends to oppose this movement. The particles in an electric field move with constant velocity when the equilibrium between electric and viscous forces

is reached. The electrophoretic mobility (velocity per unit electric field) of the particle depends on the dielectric constant, viscosity of the medium and the zeta potential, which is related to the electrophoretic mobility by the Henry and Smoluchowski equations discussed in details in Section 3.6.4.
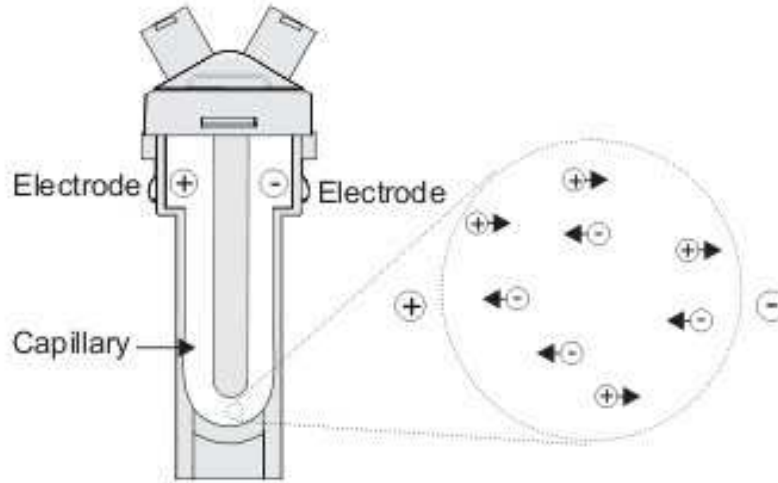

Figure 2.4: The principle of electrophoretic mobility measurement [322].

One of the convenient techniques used to measure the velocity of the particles in electrophoresis is so-called Laser Doppler Velocimetry (LDV). It utilizes the Doppler shift in a laser beam scattered by particles moving in the electric field. The laser light is splitted into two beams, ensuring the coherence between them. The receiving optics collects the light scattered by the particles and combines it with the reference beam. By measuring the Doppler frequency-shift of the scattered light, it is possible to calculate the electrophoretic mobility μ_e of the particles

$$\Delta v = -\frac{\mu_e}{\lambda}, \tag{2.6}$$

where Δv is the Doppler shift in a frequency of the scattered light and λ is the wavelength of a beam.

A typical zeta-potential measurement system is presented in Fig. 2.5. It comprises of six main components. A laser provides the light source illuminating particles suspended within the medium. The sample is placed in the cell with electrodes attached on both sides and to which a potential is applied. The laser light is split into incident and reference beam. The incident beam passes through the sample, while the reference beam is modulated to measure the Doppler-frequency shift of the analyzing beam.
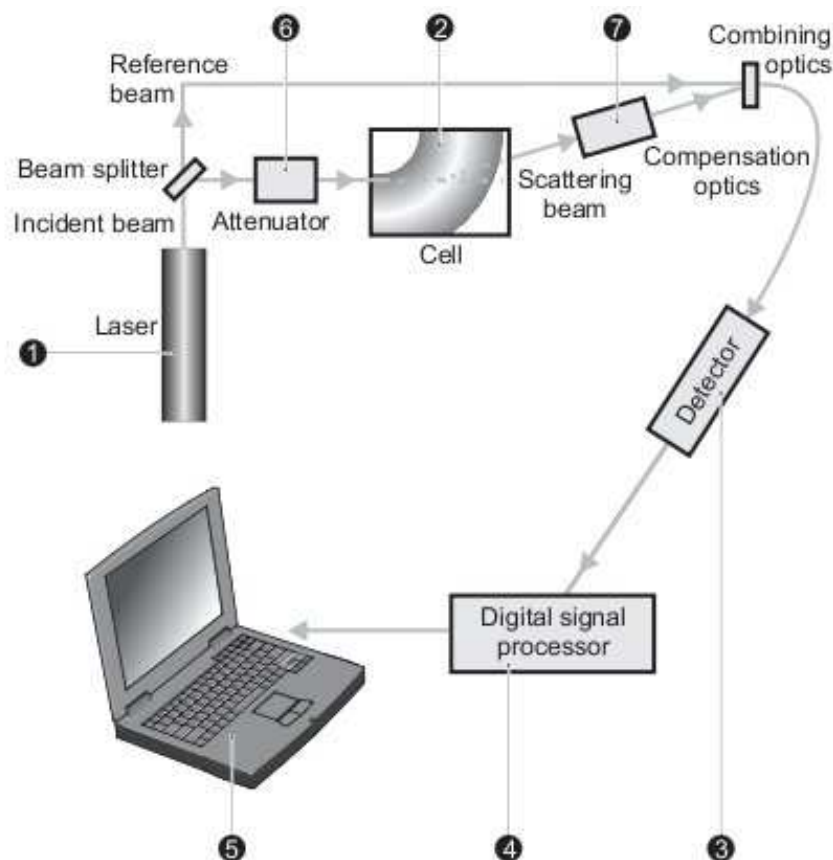
Figure 2.5: A scheme of zeta potential measurement system [322].

The scattered light is detected at an angle of 17°. The detector passes the information to the digital signal processor and later to the computer. The software enables to obtain electrophoretic mobility and zeta potential values from the frequency spectrum [322]. Similarly to the DLS measurements, the attenuator is used to adjust the intensity of the scattered light to a range specific for a detector.

The electrophoretic mobility (zeta potential) of the samples prepared in the present work was determined by microelectrophoresis using Zetasizer NanoSeries from Malvern Instruments, UK. All the measurements were performed at 25°C. The presented zeta potential values are the average from at least three subsequent runs with twenty measurements.

7.3   Atomic Force Microscopy

The atomic force microscope (AFM) was invented in 1986 in Zurich [323]. AFM is commonly used for characterization of surface topography of many materials, including ce-

ramics, glasses, composites, metals, polymers, film coatings and many others. It is particularly useful for studies of soft, non-conductive biological samples, such as cells or proteins. Moreover, phenomena of practical importance, such as friction, adhesion, and local magnetism can also be studied on a microscopic scale [324].

The AFM, like all other scanning microscopes, utilizes a sharp probe situated at the end of a flexible cantilever. The cantilever is illuminated by the laser beam. When the tip is scanning the sample surface, the cantilever is deflected in a z-direction due to the interaction forces between the tip and the sample. The laser light, which illuminates the cantilever is reflected from its surface to a photodiode, which converts the cantilever's deflection into the drift signal [325]. This information is transferred into a topographic image of the sample surface. The scheme of the method is presented in Figure 2.6.
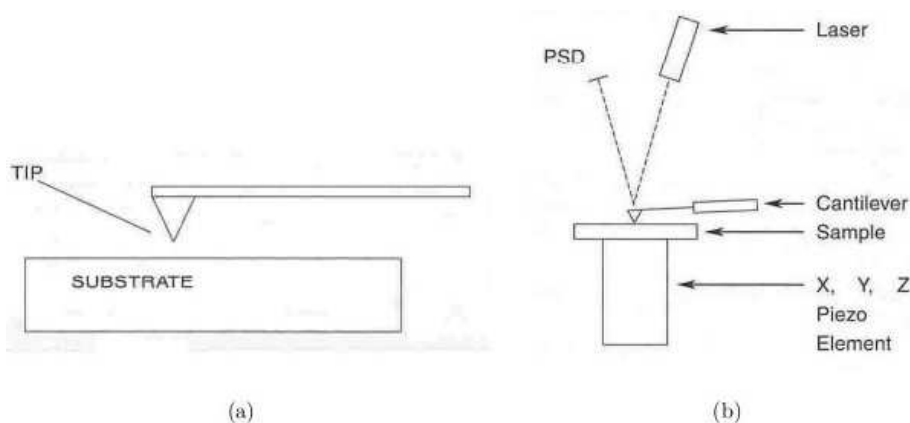
Figure 2.6: AFM cantilever movement over the sample surface — the beam deflection principle (a) and working principle of AFM (b) [325].

The AFM can be used in high-resolution imaging of both conductive and insulating surfaces. The investigations can be performed in gases, liquids or vacuum. A number of AFM imaging modes (contact, non-contact, tapping) are available [325, 326]. In the contact mode, tip and the sample remain in a close contact (< 1 Å). It is possible to obtain very detailed pictures of a surface. However, in the case of soft materials it is necessary to limit the interaction force in order to avoid destruction of the sample. In the non-contact mode, the distance between the tip and the sample is bigger (1–10 nm), so the tip is never in contact with the substrate. This mode is dedicated for studies of very fragile or deformable materials. In semi-contact (tapping) mode the cantilever is oscillating with a high amplitude, contacting the tapping surface once every period. It

allows to obtain very high resolution images of the surface.

The microscopic observations of nanocarriers prepared in the present work were performed using NTegra Vita atomic force microscope (NT-MDT, Russia). In order to obtain the topographical images of the samples, i.e., nanoparticles, nanocapsules and nanoemulsions were deposited on the mica surface. Natural mica is often used as a substrate for colloid particle adsorption processes due to its ultra-flat surface. In the aqueous solutions it exhibits a reproducible, negative charge and can be easily covered by adsorption of positively charged species. In the case of negatively charged samples, mica surface was covered with the positively charged poly(ethylenoimine) PEI (0.02 g/l in 0.015 M NaCl, t_{ads} = 15 min) prior to the particle deposition. The tapping-mode topographic images were recorded in the air using high resolution silicon tips with a force constant of 4.4 N/m and with a nominal curvature radius of 10 nm (NT-MDT ETALON probes, HA NC series). The images were recorded within different scan areas, mostly 20 μm×20 μm, 10 μm×10 μm and 5 μm×5 μm, for the three randomly chosen places, and with the scan rate of 1.1 lines/s. All the images were flattened using an algorithm provided with the instrument.

7.4 Fluorescence spectroscopy

Luminescence can be defined as the emission of light by substances occurring from the radiative relaxation of their electronically excited states. There are different stimuli that
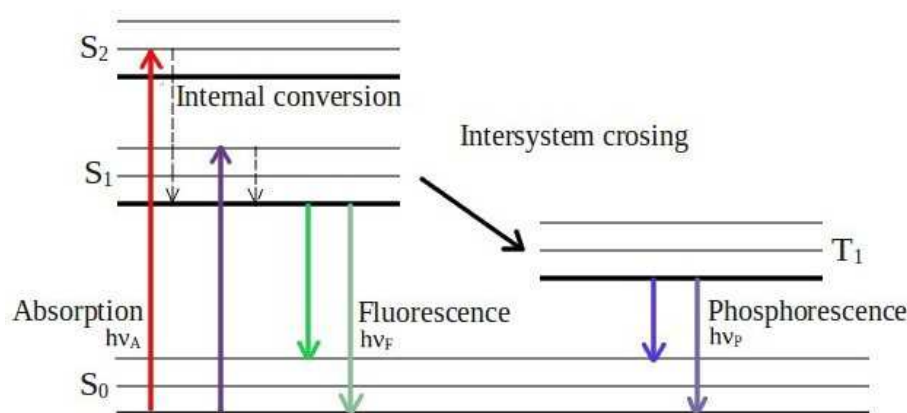

Figure 2.7: The Jabłoński diagram.

can transfer the substance from its ground state to the excited state, such as chemical reac-

tion (chemiluminescence), electric field (electroluminescence), light (photoluminescence), ionizing radiation (radioluminescence), friction and deformation (triboluminescence), or even sound (sonoluminescence). Once excited, a molecule can relax by various competing pathways [327]. The electronic states of a molecule and the possible transitions between them are illustrated by Jabłoński diagram, presented in Figure 2.7. The state S_0 represents the ground state of the fluorescent molecule, while S_1 and S_2 are the first and second singlet excited states, respectively. The state T_1 is so called triplet excited state. The absorption of energy causes the transition of electron from its ground state to a higher quantum state S_1. Then, there are many possible mechanisms of molecule relaxation:

- **Fluorescence.** The return to the ground state from the singlet excited state occurs rapidly and spontaneously by emitting a photon of light. Fluorescence lifetime is very short, typically ca 10^{-8} s.

- **Phosphorescence.** Unlike fluorescence, time between the absorption and emission processes is longer. The slower time scale is associated with the forbidden energy state transitions. The absorbed photon energy undergoes intersystem crossing into a metastable triplet state before the final transition to the ground state. The photon energy $h\nu_P$ is emitted at a lower intensity for up to several hours after the excitation.

- **Heat dissipation.** Heat dissipation. The excited molecule can undergo non-radiative relaxation, in which the excitation energy is dissipated as heat (vibrations) in the surrounding medium.

- **Collisional quenching.** Part of the energy from excited molecules can be transferred to the solvent molecules located in their vicinity.

In the fluorescence process emission occurs from the excited state S_1, which is not dependent on the excitation wavelength. In other words, the fluorescence emission spectrum of a substance will remain the same for different excitation wavelength. There are two main types of fluorescence measurements, i.e., steady-state and time-resolved measurements. In the steady-state experiment a sample is exposed to a continuous beam of light while the emission spectrum is being recorded. In the time-resolved fluorescence the sample is exposed to a pulse of light and the decay of fluorescence intensity is recorded [327].

A typical spectrofluorimeter is schematically presented in Fig. 2.8. A source of radiation produces photons. There are different types of excitation sources, such as lasers, light-emitting diodes or lamps, e.g., high-pressure xenon arc lamp. A xenon arc lamp
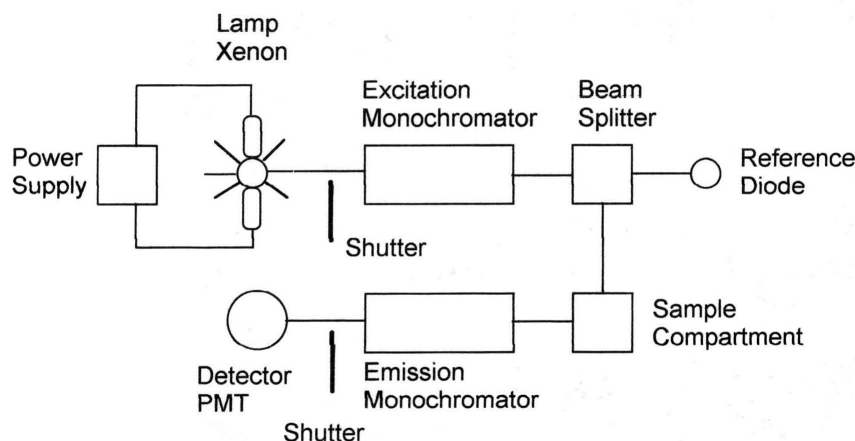

Figure 2.8: Schematic diagram of spectrofluorimeter.

exhibits the continuous emission in the range of 250–800 nm. The monochromators select both the excitation and emission wavelengths. In the sample compartment, the sample responds to the incoming radiation. The resulting fluorescence is emitted in all directions. Some of this fluorescent light is filtered by an emission monochromator and reaches a detector, which is usually placed at 90° relative to the excitation light in order to avoid interference of the transmitted excitation light. The spectrum is produced by recording the variations in fluorescence intensity as a function of the wavelength.

In the presented work, the luminescent properties of prepared samples were determined using Spectrofluorimeter Fluorolog-3 from Jobin Yvon Inc. The fluorescent emission spectra have been recorded over a range of 450–800 nm.

7.5 UV-vis spectroscopy

Ultraviolet-visible spectroscopy (UV-vis) is an absorption spectroscopy using light in the visible and ultraviolet ranges. It is a technique complementary to fluorescence spectroscopy since it measures absorption of light upon transitions from the ground state to the excited state. UV-vis is an important technique used for the qualitative and quantitative determination of different substances, such as transition metal ions, biological macromolecules or highly conjugated organic compounds [328]. Each substance has a unique

ultraviolet-visible spectra, which also allows for the identification of unknown sample.

The basic equation used to determine the concentration of absorber in the solution is so called Beer-Lambert law. It states that the measured absorbance A of a substance in the solution is directly proportional to its concentration c and the path length L

$$A = -\log T = -\log(I_0/I) = \epsilon \, cL \, , \tag{2.7}$$

where T is the transmittance — fraction of incident light that passes through a sample, I_0 and I are the intensity of the incident and transmitted light, respectively, and ϵ is the extinction coefficient.

The basic parts of a spectrophotometer are a light source (hydrogen/deuterium lamp for the UV region and tungsten/halogen lamp for the visible one), a holder for the sample (liquid samples are placed in a quartz cell), diffraction grating in a monochromator or a prism separating the different wavelengths of light, and a detector. After the light has passed through the sample, the spectrometer records the absorption spectrum by scanning the wavelength of transmitted light.

In the present work, the absorption spectra of substances were recorded using the UV-vis Shimadzu Spectrophotometer.

7.6   Interfacial tension measurements

The interfacial tension between oil and aqueous phase was measured by the pendant drop shape analysis method (DSA100 Contact Angle Measuring System, Kruss). In this optical technique a drop of liquid hanging from a syringe needle will assume a characteristic shape, from which the surface tension can be determined. The theoretical drop profile is determined on the basis of the solution of the Young-Laplace equation of capillarity and fitted to experimental drop shapes of aqueous phase suspended in oil at equilibrium.

Young-Laplace equation relates the capillary pressure difference sustained across the interface between two fluids to the shape of that surface

$$\Delta p = \gamma \left(\frac{1}{R_1} + \frac{1}{R_2} \right) , \tag{2.8}$$

where R_1 and R_2 are the principal radii of curvature of the interface. In the conditions

of equilibrium the capillary pressure corresponds to the force of gravity acting on the drop. The duration of the interfacial tension experiments needs to be adjusted to assure enough time to reach the equilibrium values. The most important components of a typical pendant drop analysis system are illumination system, CCD cameras, temperature control system, microsyringe, microinjector and computer with installed software.

7.7 Cytotoxicity tests

7.7.1 Proliferation assay and test of unspecific binding

In order to estimate the cytotoxicity of chosen nanoparticles and capsules, their influence on B-lymphoblastoid cell line (B-LCL) proliferation was tested. B-LCL cells are B cells infected with Epstein-Barr virus, resulting in lymphoblastoid cell lines (LCL) that are capable of indefinite growth. Tritium (^{3}H) is a radioactive isotope of hydrogen that emits β-rays. Thymidine labeled with tritium will, when added to cells, incorporate into the DNA of the dividing cells, and the radiation emitted from the tritium can be measured in a microplate scintillation counter (as CPM, counts per minute).

The proliferation assay was performed as follows: different concentrations of the nanoparticles were incubated with B-LCL cells. The cells were resuspended in RPMI 1640 (cell culture medium, PAA Laboratories GmBH, Pasching, Austria) and in Garamycin (Schering-Plough Labo, Heist-op-den-Berg, Belgium). They were counted using a counting chamber and diluted to 0.5×10^6 cells/ml. The volume of 100 µl of cell suspension and 3.7×104 Bq ^{3}H-thymidine (American Radiolabeled Chemicals, Inc., St. Louis, MO) were then added to triplicate wells of a round-bottom 96-well plate (Costar, Corning Inc., Corning, NY). To the negative controls, only 100 µl of RPMI medium with garamycin was added. The plate was incubated at 37°C over night. After approximately 20 h, the plates were harvested onto the filter plates (UniFilter, PerkinElmer Inc., Waltham, MA) and dried for 1.5 h at 45°C. Later, 25 µl of Microscint O (PerkinElmer Inc.) was added to each well. Thymidine labeled with tritium was incorporated into the DNA of dividing cells, and the radiation emitted from the tritium was measured in a microplate scintillation counter (PerkinElmer Inc.). The results were calculated from a mean of triplicates and expressed as a percent of the ^{3}H-thymidine incorporation related to the negative control.

2. EXPERIMENTAL PART

The test of unspecific binding of nanoparticles to the P-blood mononuclear cells (PBMC) was performed using flow cytometry. It is a laser based technique often employed in cell counting, biomarker detection, clinical trials and diagnosis. It allows simultaneous
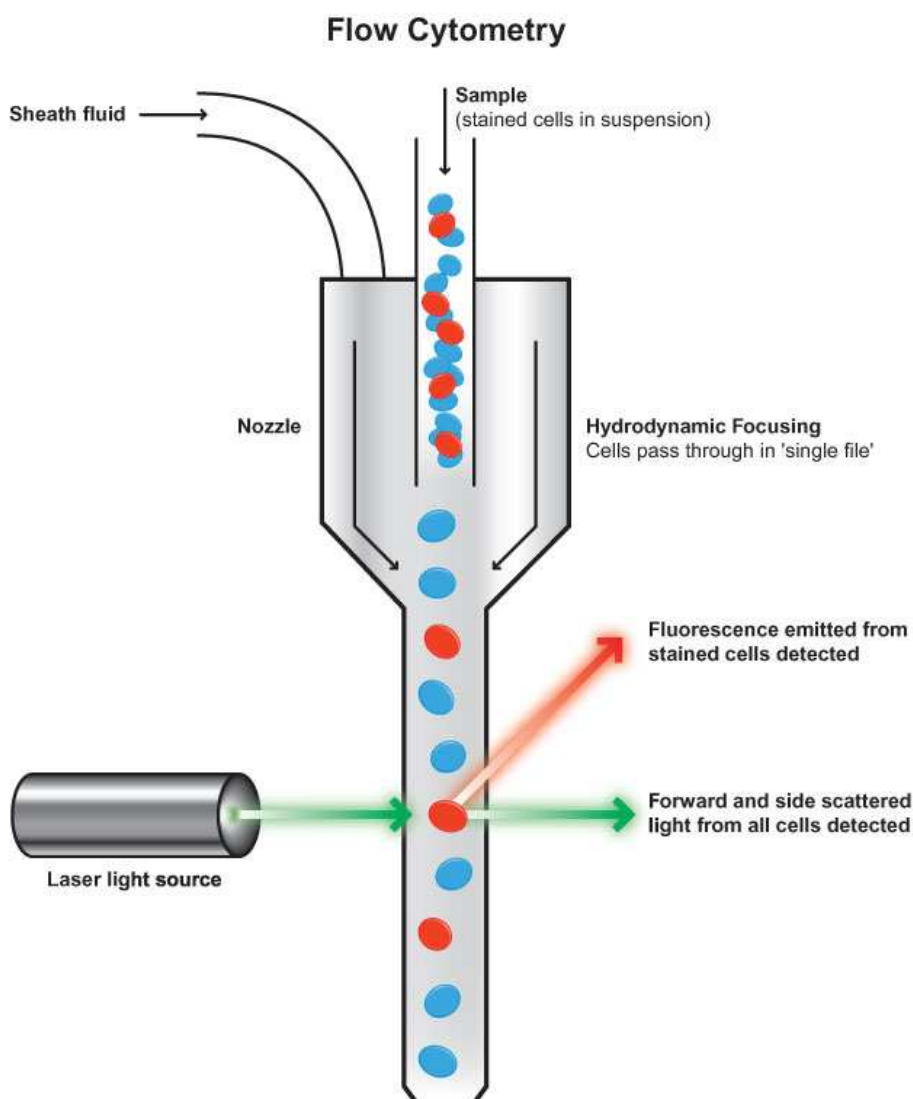
Figure 2.9: Scheme of the flow cytometer.

analysis of the physical and chemical characteristics of up to thousands of particles per second. A beam of light of a single wavelength coming from the laser or mercury/xenon lamp is directed onto a flow cell. Cells are suspended in a stream of fluid and passing through the light beam for sensing. A number of detectors can be used: forward scatter detector, side scatter detector and one or more fluorescence detectors. The fluorescent chemicals present in the cells may be excited into emitting light, and the internal com-

ponents of the cell scatter the light. This combination of fluorescent and scattered light is picked up by the detectors. Analysis of fluctuations in brightness at each detector enables to obtain different informations about the cells. A flow cytometer is similar to a microscope, only that instead of producing an image of the cell it offers high-throughput automated quantification of set parameters. Figure 2.9 presents a scheme of typical flow cytometer.

The test of unspecific binding was performed as follows: PBMC were thawed in the DC CellGro medium (CellGenix, Freiburg, Germany) with Garamycin (Schering-Plough Labo, Heist-op-den-Berg, Belgium), spun down, resuspended in the same medium and counted using a counting chamber. The concentration of the cell suspension was adjusted to 1×10^6 cells/ml, and 500 µl (0.5×10^6 cells/ml) of the suspension were added to the wells of a 48-well plate (Costar, Corning Inc., Corning, NY). Different concentrations of nanoparticles were incubated in the cells at 37°C for 3 h, before they were washed twice in the medium and resuspended in 0.2 ml of the phosphate buffer saline (PBS) for analysis of fluorescence by a flow cytometer (BD LSR II). The results were analyzed using the FlowJo Software (Tree Star, Inc., Ashland, OR).

7.7.2 Cell-viability test MTT

The cell-viability assay test (MTT) measures the biological activity of energetical alterations in a cell. It utilizes the capability of the mitochondrial dehydrogenase enzymes to reduct the tetrazolium salts [329]. The yellow water-soluble tetrazolium MTT is converted to the purple formazan, which is not soluble in water. Only alive and metabolically active cells have an ability to reduct the MTT salts. Therefore, the MTT test determines their viability (the number of alive cells with a recognizable level of the mitochondrial activity). The resulting intracellular purple formazan can be solubilized in dimethylsulfoxide and quantified by spectrophotometric methods [330].

Cytotoxicity of chosen capsules was tested on NIH 3T3 mouse embryonic fibroblast cell line. The experiment was performed in a following way: 3T3 fibroblasts were cultured on tissue culture polystyrene (TCPS, 48-well plates, Nunclon, Denmark) at the initial density of 2.5×10^4 cells per well in 1 ml of DMEM culture medium, supplemented with 10% fetal bovine serum and antibiotics (1% penicillin/streptomycin). The cells were incubated at 37°C under 5% CO_2 atmosphere. After 24 hours the nanoparticles were added to

each well and incubated for the next day. MTT solution (5 mg/ml) was incubated with cells for 3 hours. After this time, the resulting intracellular formazan was solubilized in dimethylsulfoxide (DMSO) and quantified by spectrophotometric methods. The optical density of the blue dye was determined at 540 nm on Multiscan FC Microplate Photometer (Thermo Scientific, USA). The results were expressed as mean and standard error of the mean from three independent samples.

7.7.3 Cell morphology observations

Cell viability assay was followed by observation of the morphology of 3T3 fibroblasts seeded on TCPS. After incubation with the samples, cells were observed under optical microscope (Axiovert, Carl Zeiss, Germany). The cultured fibroblasts were fixed in 4% paraformaldehyde for 1 hour, washed in PBS and stained with hematoxylin and eosin (H&E, Sigma Aldrich, Poland). The order of staining was as follows: first, the samples were incubated in 0.5 ml hematoxylin for 5 minutes. After that step, they were washed with tap water several times, until the liquid became transparent. Eosin (0.5 ml) was added during 2 minutes, followed by repeating of washing procedure. Such prepared samples were dried and observed under the microscope.

8 Materials

8.1 Surfactants

In the present work, the following surface active agents were used:

- AOT ($C_{20}H_{37}NaO_7S$ — docusate sodium salt, $\geq 99\%$; $M_W = 444,56$ g/mol) — oil-soluble, anionic surfactant approved by FDA, which makes a good emulsifier for liquid core encapsulation

- Lecithin (L-α-phosphatidylcholine from egg yolk, $\sim 60\%$ and type VI-E $\geq 99\%$) — biocompatible, zwitterionic surfactant being a mixture of phospholipids with phosphatidylcholine as main component; integral part of cell membranes

- Cholesterol ($C_{27}H_{46}O$, 94%, $M_W = 386,65$ g/mol) — major component of all biological membranes; approximately 25% of total brain lipid is cholesterol.

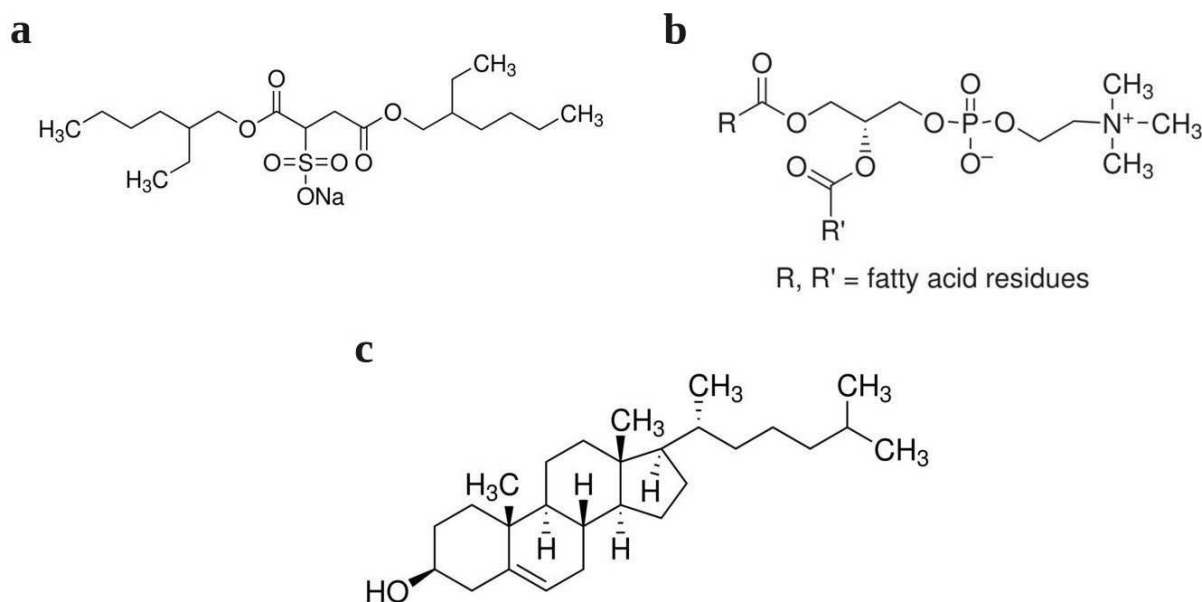All the surfactants were purchased from Sigma-Aldrich. Their chemical structures are presented in Fig. 2.10.

Figure 2.10: Chemical structures of studied surfactants: (a) AOT, (b) lecithin and (c) cholesterol.

8.2 Polyelectrolytes

The polyelectrolytes used in the studies were as follows:

a) **Polycations**

- Poly(allyamine hydrochloride) (PAH) ($M_W = 70$ kDa)
- Poly(ethylenoimine) (PEI) ($M_W = 75$ Da)
- Poly-L-lysine hydrobromide (PLL) ($M_W \sim 15$–30 kDa)

b) **Polyanions**

- Poly(sodium styrene sulfonate) (PSS) ($M_W = 70$ kDa)
- Poly-D-glutamic acid sodium salt (PGA) ($M_W \sim 15$–50 kDa)

The polyelectrolytes used in the study are synthetic materials. Synthetic, biocompatible pair of poly-L-lysine and poly-D-glutamic acid sodium salt is frequently used in

biomedical applications. All the polyelectrolytes used were obtained from Sigma-Aldrich. The chemical structures of polyelectrolytes used for layer-by-layer formation of capsules shell are presented in Fig. 2.11.
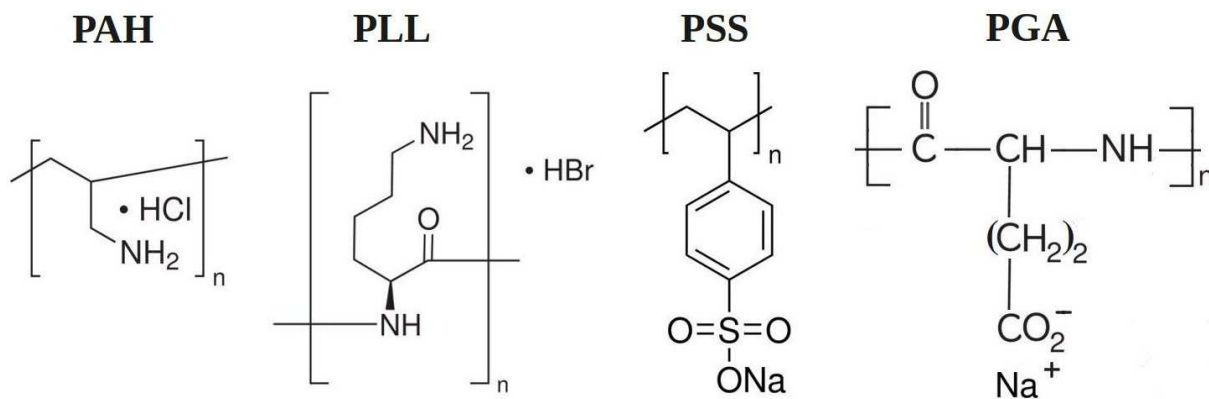

Figure 2.11: The chemical structures of studied polyelectrolytes.

8.3   Oils

In the present work, the following oils were used in the emulsification process:

- Linseed oil ($d = 0.93$ g/ml at 25°C)

- Soybean oil ($d = 0.91$ g/ml at 25°C)

- Jojoba bean oil ($d = 0.87$ g/ml at 25°C)

- Squalene ($d = 0.85$ g/ml at 25°C)

Linseed oil, soybean oil and jojoba bean oil are composed predominantly of medium-chain or long-chain triglycerides and derived from plants. Use of natural oils in the emulsification process is advantageous due to their lack of cytotoxicity. Squalene is a natural hydrocarbon obtained from shark liver oil or plant sources, such as wheat germ or amaranth seed. It is natural part of the synthesis of cholesterol and vitamin D in the human body. It is often used as an immunologic adjuvant in the vaccines. All the oils were purchased from Sigma-Aldrich. Figure 2.12 presents the chemical structures of chosen compounds.
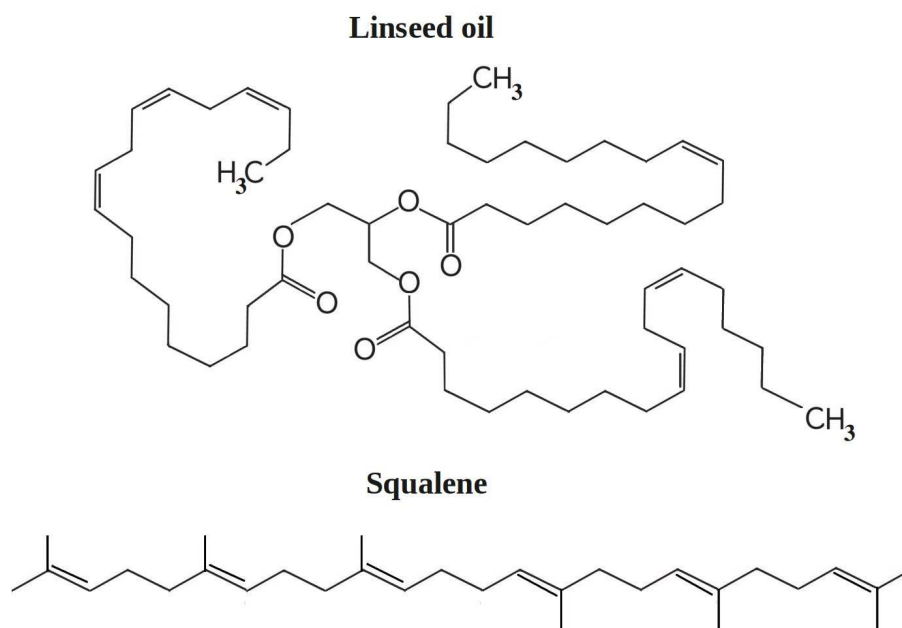
Linseed oil

Squalene

Figure 2.12: The chemical structures of linseed oil and squalene.

8.4 Active agents for encapsulation

Various compounds were chosen as model active agents for the encapsulation:

a) **Nanoparticles**

- CdTe quantum dots, coated with $-$COOH groups and water-soluble. The emission maximum $\lambda_{max} = 720$ nm.

- CdSe/ZnS quantum dots, hydrophobic, soluble in most non-polar organic solvents, e.g., hexane, toluene, chloroform. Not soluble in water, alcohols or ethers. The emission maxima $\lambda_{max} = 650$ nm.

b) **Organic dyes**

- Coumarin 6 [3-(2-benzothiazolyl)-7-(diethylamino) coumarin], $\geq 99\%$; $M_W = 146.14$ g/mol. Hydrophobic dye, $\lambda_{max} = 500$ nm.

c) **Drugs**

- Naproxen (6-methoxy-α-methyl-2-naphtaleneacetic acid), $M_W = 230.26$ g/mol. Often used as non-steroidal anti-inflammatory drug, for the reduction of pain

and fever. Poorly soluble in water, its delivery can be improved by use of appropriate vehicles, e.g., emulsions.

- Vitamin D_3 (cholecalciferol), $M_W = 384.64$ g/mol. Fat-soluble, responsible for intestinal absorption of calcium and phosphate.

Coumarin, naproxen and vitamin D_3 were purchased from Sigma-Aldrich. Quantum dots were ordered from PlasmaChem GmBH (Berlin). The chemical structures of coumarin and naproxen are presented in Fig. 2.13.

Coumarin 6 **Naproxen** **Cholecalciferol**
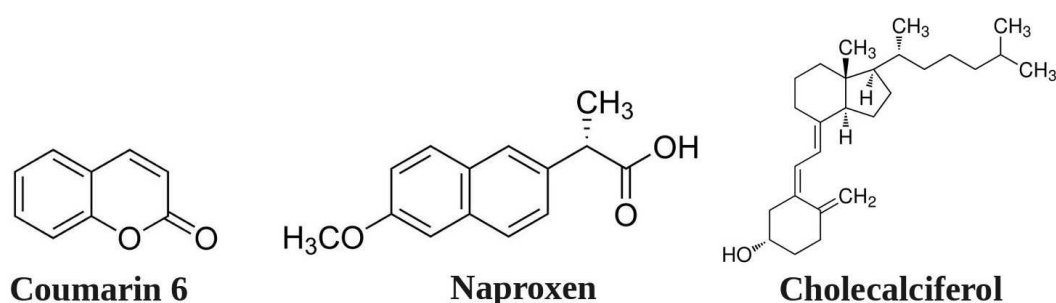
Figure 2.13: The chemical structures of coumarin and naproxen.

8.5 Others

Ethanol (99.8% pure), sodium chloride, sodium hydroxide, hydrochloric acid and chloroform were obtained from POCH Gliwice. All materials were used without further purification. The water used in all experiments was prepared in a three-stage Millipore Direct-Q 3UV purification system.

9 Experimental results and discussion

9.1 Polyelectrolyte multilayer capsules with hydrophilic quantum dots

9.1.1 Outline

In the following chapter I described the encapsulation of CdTe (cadmium telluride) quantum dots within the nanocapsules, which shells were prepared by the layer-by-layer adsorption of polyelectrolytes. Two different polyelectrolyte pairs were used as the compo-

nents of the shell: synthetic polycation poly(allyamine hydrochloride) (PAH), together with anionic poly(sodium styrene sulfonate) (PSS), and biocompatible cationic poly-L-lysine hydrobromide in the pair with biocompatible anionic poly-D-glutamic acid sodium salt (PGA). The saturation method was used for formation of the consecutive polyelectrolyte layers on the initial CdTe-polyelectrolyte complex. The preparation process of nanocapsules is schematically shown in Fig. 2.14. A growth of the polyelectrolyte shell
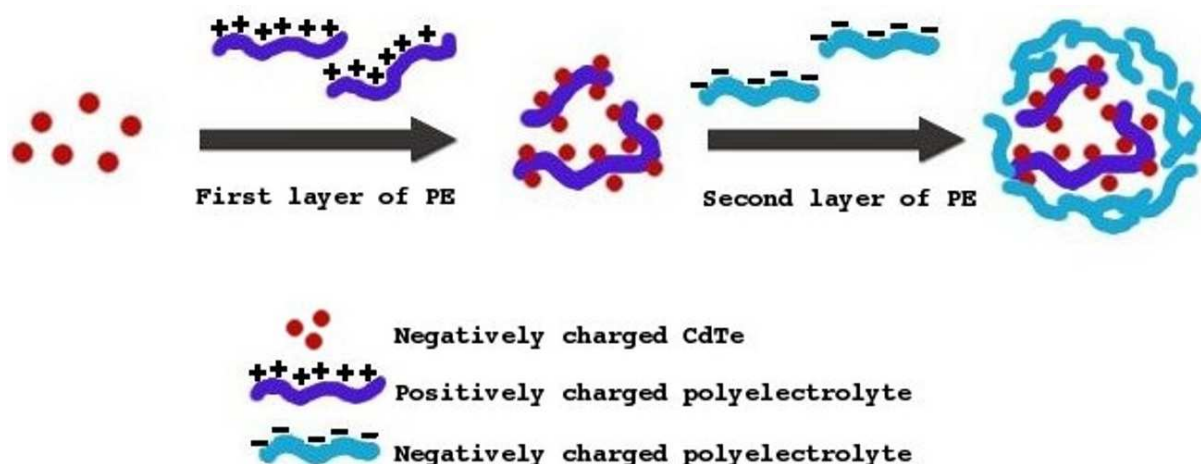

Figure 2.14: Scheme of nanocapsules formation using the layer-by-layer adsorption of poly-electrolytes on the hydrophilic quantum dots.

was followed with the electrophoretic mobility and light scattering measurements, in order to determine the zeta potential and the size of capsules, respectively. The fluorescent spectra of the quantum dots, which were embedded within the capsules, were characterized by spectrofluorimetry. Later on, the capsules were deposited on a negatively charged mica surface and studied by the means of atomic force microscopy. In order to estimate the cytotoxicity of capsules, their influence on the B-lymphoblastoid cell line proliferation and the unspecific binding to the P-blood mononuclear cells was examined using the proliferation assay and flow cytometry, respectively.

9.1.2 Preparation of the complexes of quantum dots with polycations and formation of capsules by LbL adsorption

A quantity of 0.2 mg/ml of CdTe was dissolved in deionized water. The average size of CdTe quantum dots, which was measured by DLS, was around 10 nm. Coating of the nanoparticles with $-$COOH groups has brought a strong negative charge onto their surface, as the

value of the measured zeta potential was equal to -45 ± 3 mV. The size distribution and the zeta potential distribution of the quantum dots are presented in Figs. 2.15 and 2.16, respectively.
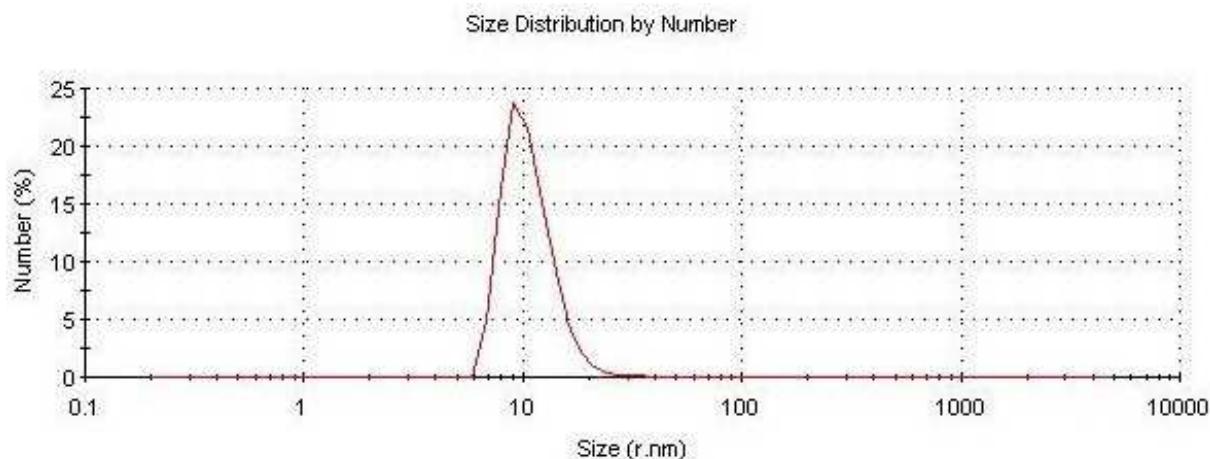
Figure 2.15: The size distribution of CdTe quantum dots.
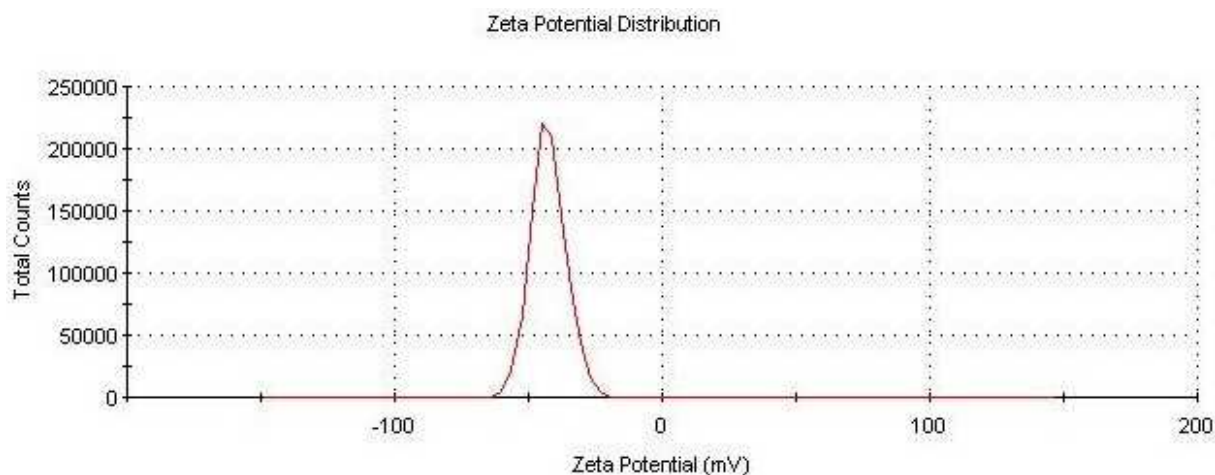
Figure 2.16: The zeta potential distribution of CdTe quantum dots.

In order to obtain the polyelectrolyte solutions of concentration 1 g/l, PLL, PGA, PAH and PSS were dissolved in the NaCl solution of the ionic strength 0.015 M. No additional pH adjustment or dialysis was involved. First, the complexes of quantum dots with polycations were formed. It was performed in the way that the loading capacity of the capsules with nanoparticles was maximized, whereas the zeta potential of complexes was still high enough to ensure their stability. Figure 2.17 presents in detail changes

(a) first layer
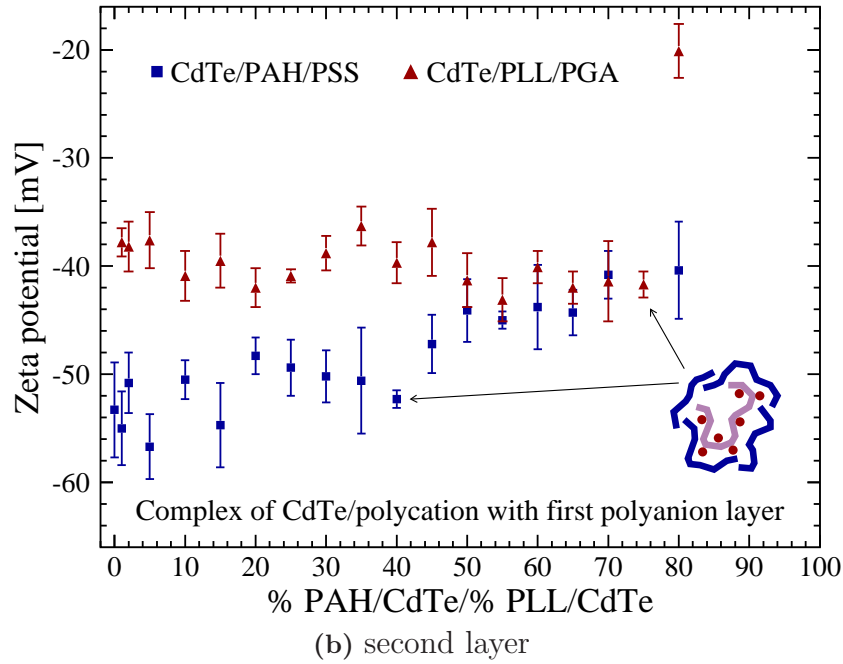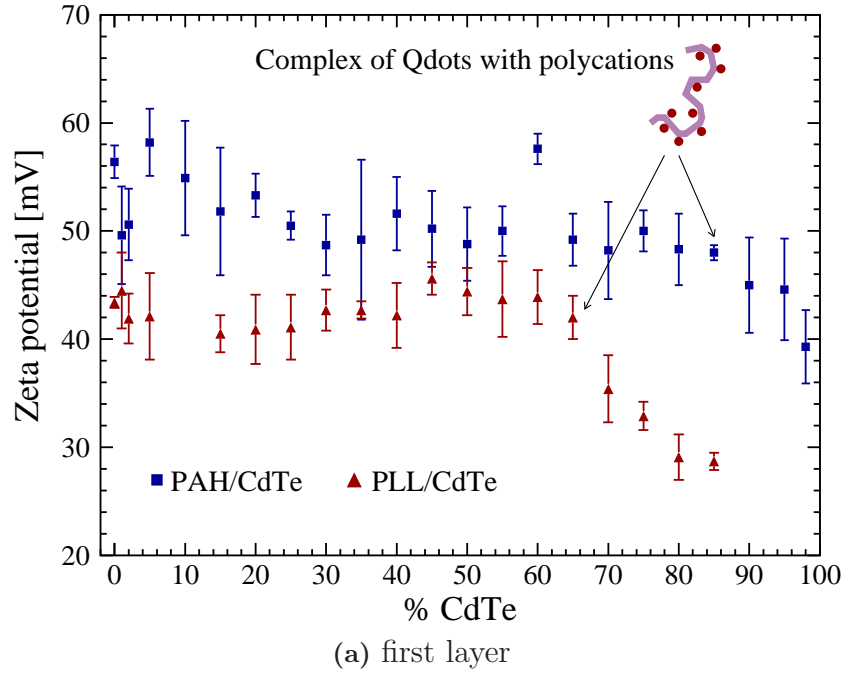
(b) second layer

Figure 2.17: Changes in the potential during formation of the first (a) and the second (b) layer as a function of the CdTe or complexes concentrations [331].

in the zeta potential during formation of the first and the second layer of complexes as functions of the CdTe concentration. Starting from pure solution of polyelectrolyte, different amount of quantum dots was added to reach the point of the highest possible loading of nanoparticles (Fig. 2.17a). It corresponded to the onset of the drop of zeta

2. EXPERIMENTAL PART

potential of complexes due to their neutralization by the excess of quantum dots, which is marked by arrows in Fig. 2.17a.

The optimal conditions for the preparation of the PLL/CdTe complex were obtained when 6.5 ml of aqueous CdTe solution of concentration of 0.2 mg/ml was added to 3.5 ml of aqueous PLL solution ($c = 1mg/ml$), during continuous mixing. On the other hand, stable complexes of PAH/CdTe were fabricated when 8.5 ml of the CdTe solution was added to 1.5 ml of aqueous PAH solution in the concentration of 1mg/ml. The size of PLL/CdTe complex was around 18 nm with the polydispersity index (PDI) < 0.3, while its zeta potential was equal to 42 mV. For the PAH/CdTe complex, the measured size was ca. 16 nm and the zeta potential approximately amounted to 48 mV. A further increase of the CdTe content in both PAH and PLL led to a decrease of the zeta potential, which resulted in lower stability of the complexes.

Once the quantum dots were embedded in the complexes with polycations, the consecutive multilayers were formed by the layer-by-layer technique using the saturation method, i.e., the complexes of quantum dots with polycations were added to the solution of polyanion and again the optimal conditions for the CdTe/polycation/polyanion complexes were determined (cf. Fig. 2.17b). During each step of the sequential adsorption of the oppositely charged PAH/PSS or PLL/PGA, the amount of added polyelectrolyte was limited so as to form the saturated layer. During addition of the capsules to the polyelectrolyte solution, which was performed to create a consecutive layer, the solution was stirred with an approximate speed of 300 - 400 rpm. The shell formation was followed with the zeta potential measurements. The volume of polyelectrolyte added to form a layer was considered as optimal when the zeta potential of the capsule reached the value close to the zeta potential of polyelectrolyte used to form the external layer of the shell. The procedure was repeated until the desired number of polyelectrolyte layers was obtained. Consequently, the polymer shells of the resulting nanocapsules were composed of 1–7 alternating polycation/polyanion layers, either of the synthetic pair PAH/PSS or biocompatible PLL/PGA.

Unlike the second main method of sequential adsorption of polyelectrolytes at colloidal cores, which is performed at an excess concentration of PE, the saturation technique used in this work does not require subsequent removal of free polyelectrolyte by dialysis or centrifugation. Strong electrostatic interactions between the polycations and polyanions,

which are the driving force for the deposition of subsequent shell layers, cause an over-charge of the external layer and also a characteristic layer-to-layer oscillatory behavior of the capsule zeta potential. Figure 2.18 illustrates the dependence of the zeta potential of
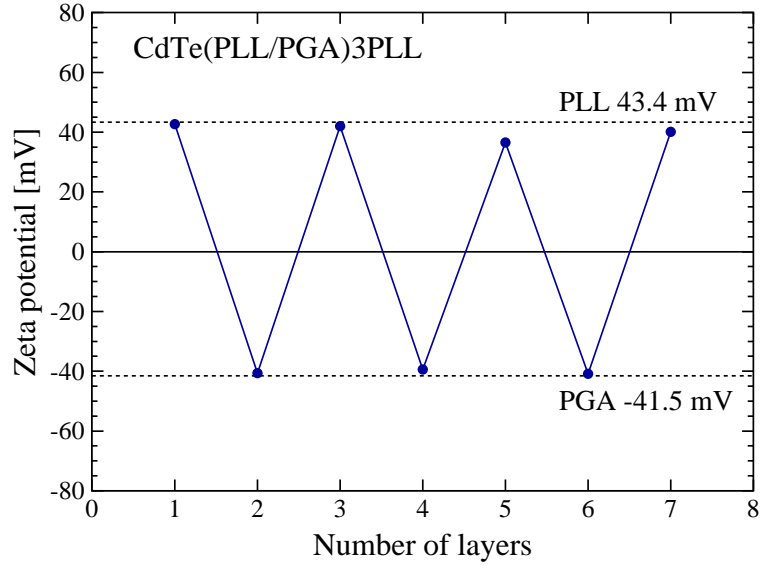
(a) PLL/PGA
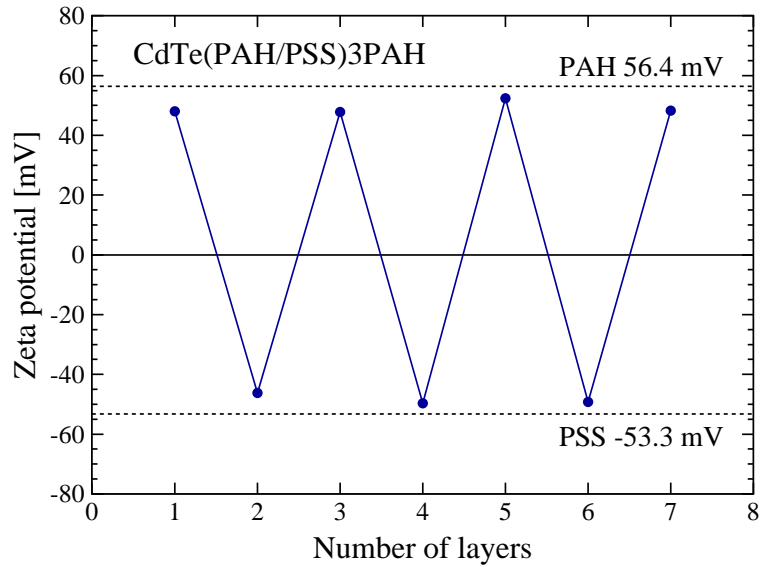
(b) PAH/PSS

Figure 2.18: Zeta potential of complexes of quantum dots with biocompatible or synthetic polyelectrolytes as a function of number of polyelectrolyte layers: (a) CdTe encapsulated within PLL/PGA multilayers, (b) CdTe encapsulated within PAH/PSS multilayers [331].

107

capsules on the number of layers in the capsule shell, for PLL/PGA (a) and PAH/PSS (b). One can see that the adsorption of a single layer of polyanions on the positively charged cores, which are built of quantum dots/polycation complexes, caused the reversal of the zeta potential to negative values. The following deposition of polycations results in the

(a) PLL/PGA

(b) PAH/PSS

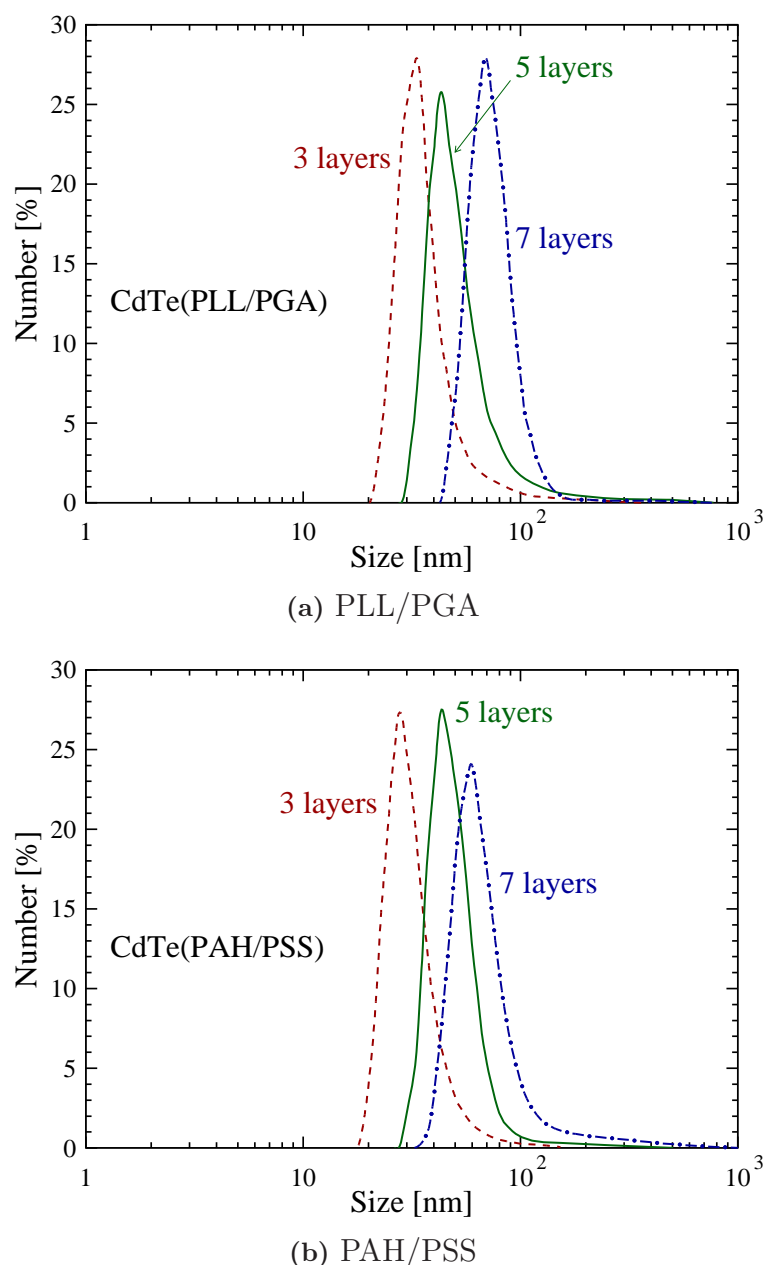**Figure 2.19:** Typical size distribution of nanocapsules with 3, 5 and 7 layers of polyelectrolytes measured by DLS: (a) capsules of CdTe with PLL/PGA multilayers, (b) capsules of CdTe with PAH/PSS multilayers. Dashed line represents the size distribution of complexes with 3 layers, while solid and dot–dashed lines represent size distribution of complexes with 5 and 7 layers, respectively [331].

overcharging of the film and return to positive values of the potential. The changes of zeta potential ranged from 42 mV to -40 mV for the PLL/PGA pair, while for PAH/PSS the variations of zeta potential approximately were in between 52 mV to -49 mV. A layer-to-layer zigzag shape of the zeta potential dependence is a typical one, which confirms the multilayer growth of the capsule shell. This type of behavior was demonstrated before for different pairs of polyelectrolytes [104, 305].

The average size of CdTe-polyelectrolyte capsules with seven PLL/PGA layers or seven PAH/PSS layers was equal to 84 nm and 75 nm, respectively. Figure 2.19 presents an increase of the size of complexes after the depositions of 3, 5 and 7 layers of polyelectrolytes,

Number of layers	Composition	Volume of added polyelectrolyte [ml]	Volume of the dispersion [ml]	CdTe concentration [μg/ml]
0	100% CdTe		1	200
1	35% PLL 65% CdTe	0.538	1.538	130
2	25% PGA 75% K1	0.513	2.051	97.5
3	20% PLL 80% K2	0.513	2.564	78
4	20% PGA 80% K3	0.641	3.205	62.4
5	20% PLL 80% K4	0.801	4.006	49.9
6	20% PGA 80% K5	1.002	5.008	39.9
7	20% PLL 80% K6	1.252	6.26	31.9

Table 2.1: Summary of the capsules composition, added polyelectrolyte volumes and corresponding CdTe concentrations. The labels "K1–K6" stand for the capsules with 1–6 layers, respectively.

as another evidence for LbL encapsulation of the quantum dots. The composition of ob-

2. EXPERIMENTAL PART

tained capsules, as well as volumes of polyelectrolyte solutions used for the formation of consecutive layers and corresponding CdTe concentrations are summarized in Tables 2.1 (PLL/PGA pair) and 2.2 (PAH/PSS pair), respectively.   These data showed that the

Number of layers	Composition	Volume of added polyelectrolyte [ml]	Volume of the dispersion [ml]	CdTe concentration [μg/ml]
0	100% CdTe			200
1	15% PAH 85% CdTe	0.176	1.176	170
2	60% PSS 40% S1	1.764	2.94	68
3	30% PAH 70% S2	1.26	4.2	47.6
4	40% PSS 60% S3	2.8	7	28.6
5	30% PAH 70% S4	3	10	20
6	50% PSS 50% S5	10	20	10
7	20% PAH 80% S6	5	25	8

Table 2.2: Summary of the capsules composition, added polyelectrolyte volumes and corresponding CdTe concentrations. The labels "S1–S6" stand for the capsules with 1–6 layers, respectively.

amount of polyelectrolyte used for the formation of consecutive layers is increasing with the number of layers. That growth is correlated with the increasing volume of overall solution, as well as with the increase of the capsule size. In the case of PLL/PGA capsules, the volume increase was rather monotonous, while in the case of PAH/PSS capsules the volume of PSS required for the formation of 6th layer was considerably higher (50% PSS/50% S5).

9.1.3 AFM topographical images of quantum dots and nanocapsules

The representative AFM images of the bare quantum dots and CdTe-labeled nanocapsules deposited on the mica surface are presented in Fig. 2.20.
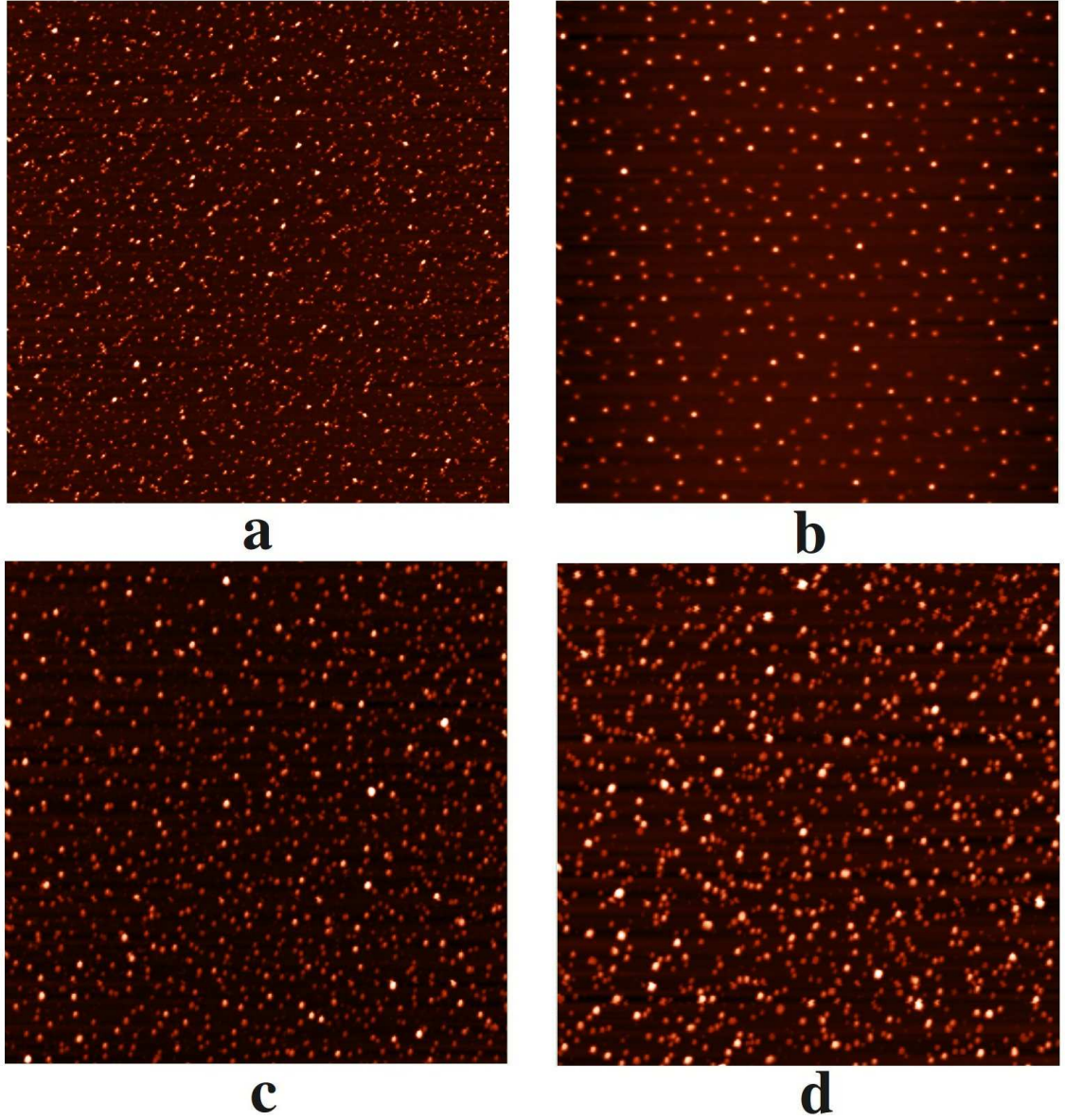
Figure 2.20: AFM images (10 μm×10 μm) of (a) CdTe quantum dots, (b) PLL/CdTe complex, (c) PAH/CdTe complex, and (d) PSS/PAH/CdTe nanocapsules. The topographical scale $z = 20$, 30, 40, and 60 nm is used, respectively. The samples (a) and (d) were deposited on the PEI-covered mica, while the samples (b) and (c) were deposited on pure mica. These pictures were obtained in the tapping mode.

The obtained topographical images shows that both quantum dots and the capsules

are mostly spherical and do not show any signs of aggregation. The results concerning the size distribution of QD/polyelectrolyte capsules obtained by the DLS technique were in a good agreement with the sizes measured by the atomic force microscope. Size of the most observed particles is below 60 nm.

9.1.4 Fluorescence spectra of encapsulated quantum dots

For the biological applications, it is recommended to use quantum dots with an emission wavelength within the red region (ca. 630–740 nm) as the measurements performed in the spectral region of 500–600 nm could result in a significant background signal coming from the cellular autofluorescence [225]. In order to confirm fluorescent properties of the CdTe-labeled multilayer capsules, the fluorescent emission spectra have been recorded in the range of 600–800 nm (see Fig. 2.21).
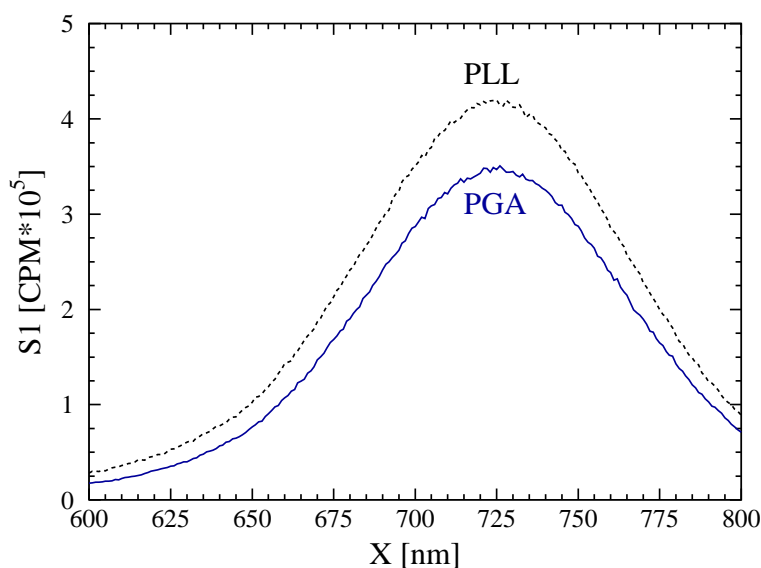
Figure 2.21: Fluorescence emission spectra of the capsules terminated with PLL (CdTe/PLL, dashed line) and the PGA-terminated capsules (CdTe/PLL/PGA, solid line) [331].

A characteristic peak for CdTe at 720 nm could observed. It was found that the encapsulation of quantum dots in PLL/PGA did not affect the fluorescence intensity of their spectra, as long as the capsule shells were terminated with a PLL layer. For the PGA-terminated capsules, a slight decrease of the fluorescence intensity was observed, due to the presence of carboxylic groups (electron withdrawing groups). There were no significant differences between the fluorescence of PLL/PGA and PAH/PSS capsules

labeled with CdTe, except of the small peak shift occurring in (PSS/PAH)3-CdTe.

9.1.5 Cytotoxicity test of encapsulated quantum dots

The cytotoxicity of CdTe-labeled capsules, plain capsules (PLL/PGA, PAH/PSS), and CdTe nanoparticles was tested in a proliferation assay performed with a flow cytometer. The obtained results indicate that the quantum dots were toxic in a wide range of tested concentrations, as shown in Fig. 2.22. The quantity of 0.5 µg/ml of the CdTe aqueous
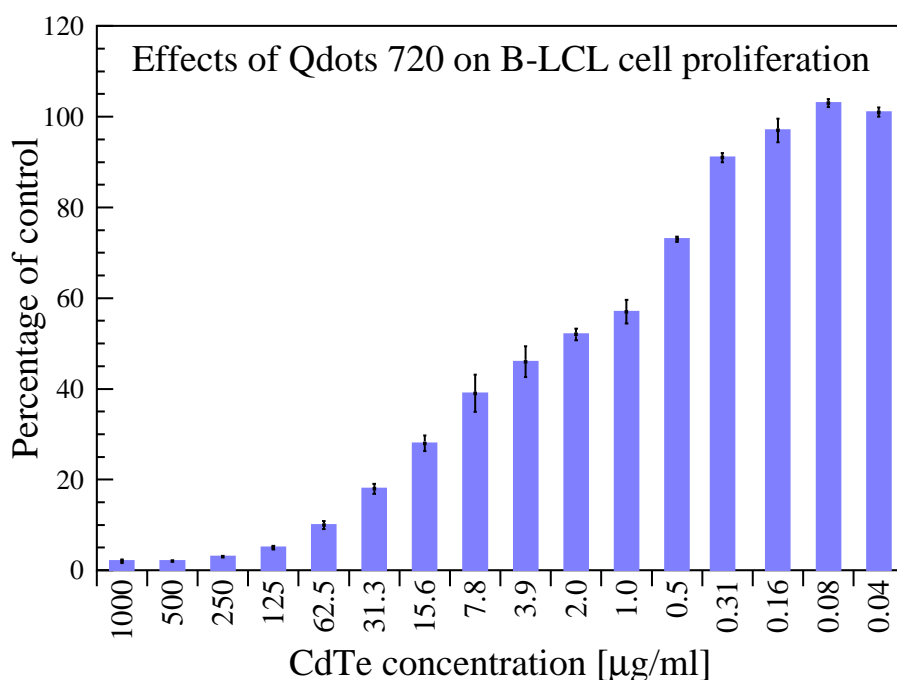
Figure 2.22: Cytotoxicity test — the effect of quantum dots (Qdots) on B-LCL cell proliferation. The obtained data are expressed as the mean ±SD of the experiments carried out in a triplicate [331].

solution reduced the proliferation of the B-LCL cell line to 73% of the control. The quantum dots ceased affecting cell proliferation at the concentration of 0.08 µg/ml. On the contrary, the B-LCL cells proliferation was unaffected by the complex of PLL/PGA at any concentrations, indicating that it was biocompatible, as expected for this polyelectrolyte pair. The plain capsules of PAH/PSS stopped affecting cells proliferation below the concentration 2.5 µg/ml.

Figure 2.23 presents the results of cytotoxicity test for the CdTe-labeled capsules with 1, 3 and 7 layers of polyelectrolytes. The sample of CdTe/PLL stopped inhibiting proliferation of the cells when diluted 1:20 times, which corresponded to the quantum

dot concentration of 1.5 µg/ml. This means that the encapsulation of quantum dots

(a)

(b)
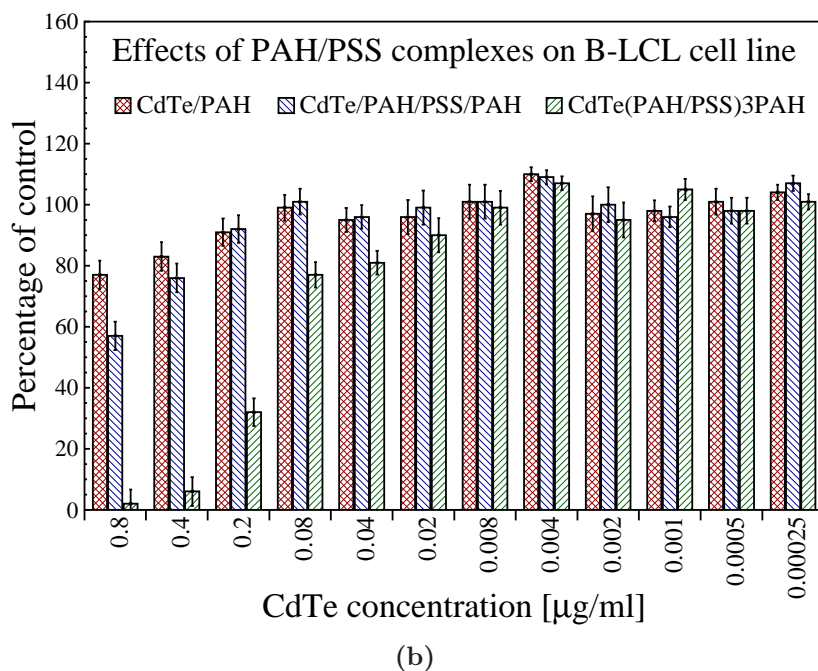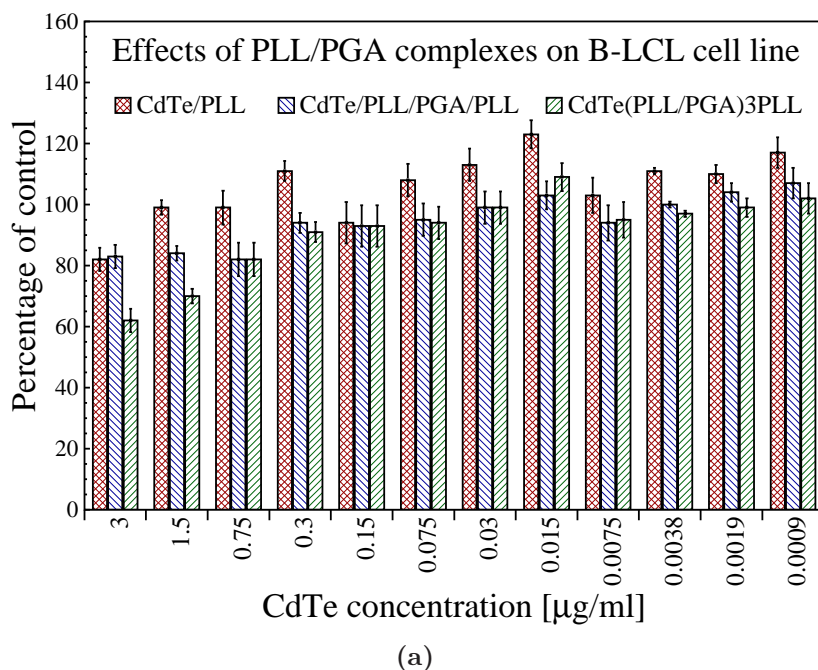
Figure 2.23: Results of cytotoxicity test for CdTe-labeled capsules with 1, 3 and 7 layers of polyelectrolytes: (a) capsules of CdTe with PLL/PGA multilayers, (b) capsules of CdTe with PAH/PSS multilayers. The obtained data are expressed as the mean ±SD of the experiments carried out in triplicate [331].

within polylysine caused nearly 20-time increase in biocompatibility. Surprisingly, the

cytotoxicity of PLL/PGA capsules labeled with quantum dots did not decrease with an

increase of the number of polyelectrolyte multilayers. The samples of CdTe/PLL/PGA and CdTe/PLL/PGA/PLL (2 and 3 PE multilayers, respectively) stopped inhibiting the proliferation of cell line, when they were diluted 1:100 times and the concentration of embedded quantum dots was 0.3 μg/ml.

The capsules with 5–7 layers are biocompatible at even lower concentration of CdTe (0.03 μg/ml). The encapsulation of quantum dots within complexes of synthetic polyelectrolytes (PAH/PSS couple) does not seem to have a significant effect on cell viability as compared to bare CdTe. Regardless of the number of PE multilayers, all the capsules with 1–6 layers do not affect cell proliferation when diluted 100 times (cCdTe= 0.08 μg/ml). The amount of quantum dots encapsulated within such diluted capsules is equal to the concentration at which the bare CdTe samples are not toxic. An inexplicable decrease of biocompatibility for the CdTe-labeled capsules with 7 layers of PAH/PSS (lack of influence on the cell line, when cCdTe = 0.008 μg/ml) is most probably related to aggregation of the polyelectrolytes.

9.1.6 Test of unspecific binding

The nanoparticles were also tested for unspecific binding to PBMC (human peripheral blood mononuclear cells). As an important part of immune system, these blood cells fight infections and adapt to intruders. For applications in drug delivery systems, it is required that the capsules should not bind to the cells or proteins present in the human blood. In these studies, two different PBMC populations were used. Lymphocytes can indicate whether particles can easily stick to the cells, while monocytes are white blood cells which digest pathogens and foreign materials, such as injected capsules.

Lymphocytes incubated with the most of CdTe-labeled PLL/PGA capsules did not show any fluorescence (see Fig. 2.24). This indicates that these samples do not bind to and are not taken up by the lymphocytes. Only the cells with capsules with 5 and 7 layers of polyelectrolytes were fluorescent. In the monocyte samples, however, all the cells were more or less fluorescent; the capsules with 5 and 7 layers had the highest MFI, while the CdTe/PLL and CdTe/PLL/PGA/PLL samples only yield a slight increase of fluorescence. Among the CdTe-labeled PAH/PSS samples (shown in Fig. 2.25), there was only a slight fluorescence in the lymphocytes incubated with CdTe/PAH/PSS/PAH and CdTe(PAH/PSS)2PAH, which indicates that they hardly bind the cells or that they have

Figure 2.24: Test of unspecific binding to lymphocytes and monocytes for empty (unstained) and CdTe-labeled capsules with PLL/PGA multilayers. The 1–7 layers of polyelectrolytes are marked as K1–K7, respectively.

a low fluorescence. However, the monocyte samples incubated with all the CdTe-labeled PAH/PSS samples were more or less fluorescent. The results of unspecific binding test suggest that nanocapsules with up to three monolayers of PLL and PGA are most suitable for biological applications.
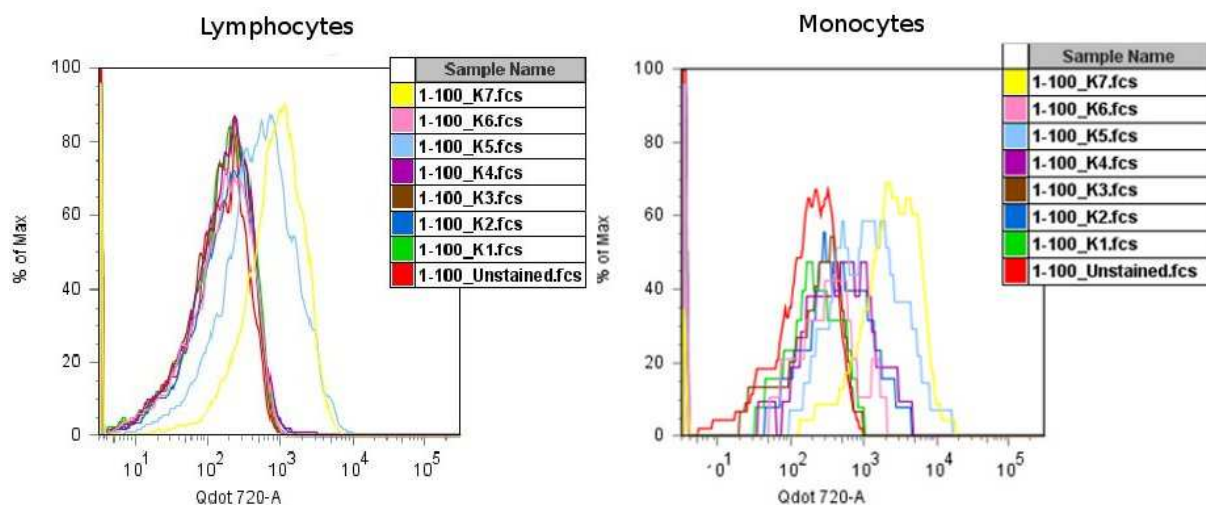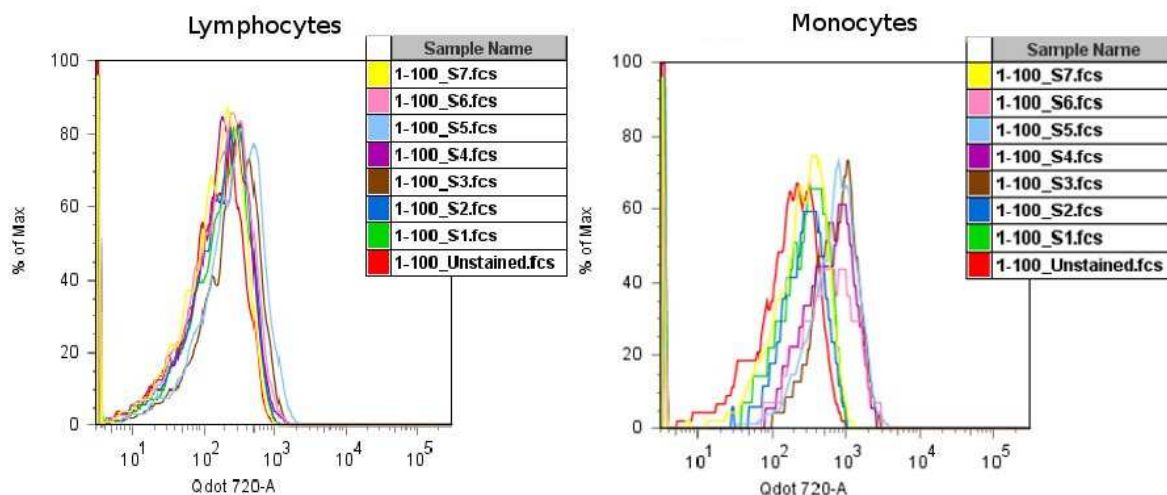

Figure 2.25: Test of unspecific binding to lymphocytes and monocytes for empty (unstained) and CdTe-labeled capsules with PAH/PSS multilayers. The 1–7 layers of polyelectrolytes are marked as S1–S7, respectively.

9.2 Natural oil cores prepared by spontaneous emulsification technique

9.2.1 Outline

The emulsions of three different natural oils (linseed oil, soybean oil and jojoba bean oil) were prepared using spontaneous emulsification technique. The effect of three emulsifiers: AOT, lecithin and cholesterol on emulsion properties was studied. Their influence on the interfacial tension at oil/water interface was evaluated by the pendant drop shape analysis method. Then, the mean droplet size, zeta potential and stability of emulsions were investigated in relation with the type of oil, surfactant, oil-to-ethanol ratio and surfactant concentration. We found that in the case of linseed oil, fine emulsion droplets are formed even without any surfactant due to its low oil/water interfacial tension. A hydrophobic dye (Coumarin 6) was encapsulated within oil cores and its presence was confirmed by fluorescence spectroscopy and microscopy. The obtained emulsions can be used alone or as the cores for layer-by-layer encapsulation, which was demonstrated by enclosing droplets within the first layer of synthetic polycation poly(allyamine hydrochloride).

9.2.2 Interfacial tension measurements at vegetable oils/water interface

Figure 2.26 presents results of the dynamic interfacial tension measurements carried out at oil/water interface for linseed oil, soybean oil and jojoba bean oil with or without addition of AOT or cholesterol. It was found that linseed oil had the lowest interfacial tension among the studied oils (4 mN/m), followed by much higher value for soybean oil equal to 22 mN/m. The jojoba bean oil showed the highest value of 25 mN/m. Interfacial tension of oils decreased in the presence of anionic surfactant AOT. For linseed oil, addition of 2×10^{-3} M AOT caused the reduction of the interfacial tension to approximately 1.5 mN/m, while the same concentration decreased the interfacial tension of jojoba bean oil to 19 mN/m. Saturation of soybean oil with AOT resulted in the decrease of interfacial tension to 13 mN/m. Compared to the results with AOT, the addition of cholesterol to the oil phase did not show any significant influence on the interfacial tension of solutions. The interfacial tension for soybean and jojoba bean oil did not seem to be affected (data not shown), while the interfacial tension of linseed oil was decreased to 2.8 mN/m with
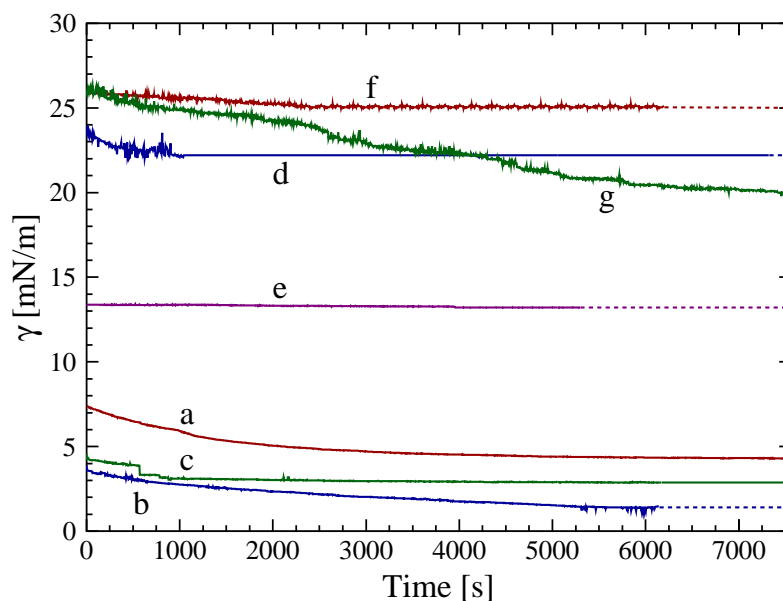
Figure 2.26: Dynamic interfacial tension at the oil-water interface with or without addition of AOT/cholesterol: (a) linseed oil, (b) linseed oil with 2×10^{-3} M AOT, (c) linseed oil with 1.6×10^{-3} M cholesterol, (d) soybean oil, (e) soybean oil saturated with AOT, (f) jojoba oil, (g) jojoba oil with 2×10^{-3} M AOT. The dashed lines represent extrapolated values of interfacial tension [332].

1.6×10^{-3} M cholesterol. The results of the interfacial tension experiments clearly indicate that the linseed oil can spontaneously form nanoemulsion even without any surfactant, while addition of surfactant is required for the other oils.

The evaluation of the influence of lecithin at oil/water interfacial tension required more complicated procedure of measurements, since its solubility in natural oils was rather limited. Therefore, emulsions containing lecithin were prepared by dissolving lecithin in ethanol prior to addition of oils. Interfacial tension measurements were performed first to determine the optimum ethanol-to-water ratio on the water/soybean oil interface. Soybean oil was chosen for the measurements because of its intermediate interfacial tension properties, which would allow checking the ability of lecithin to decrease the interfacial tension. For the ethanol-to-water ratio equal to 2:1, the interfacial tension was decreased to 14 mN/m. In these conditions, high content of ethanol in water caused fast dissolution of aqueous phase in soybean oil. At the 1:100 ethanol-to-water ratio, the interfacial tension was just slightly decreased to 21.7 mN/m. Therefore, the isotherm measurements were performed at 1:10 ethanol-to-water ratio (IFT = 17 mN/m) to keep concentration of lecithin in aqueous phase relatively high. Figure 2.27 illustrates the obtained isotherm.
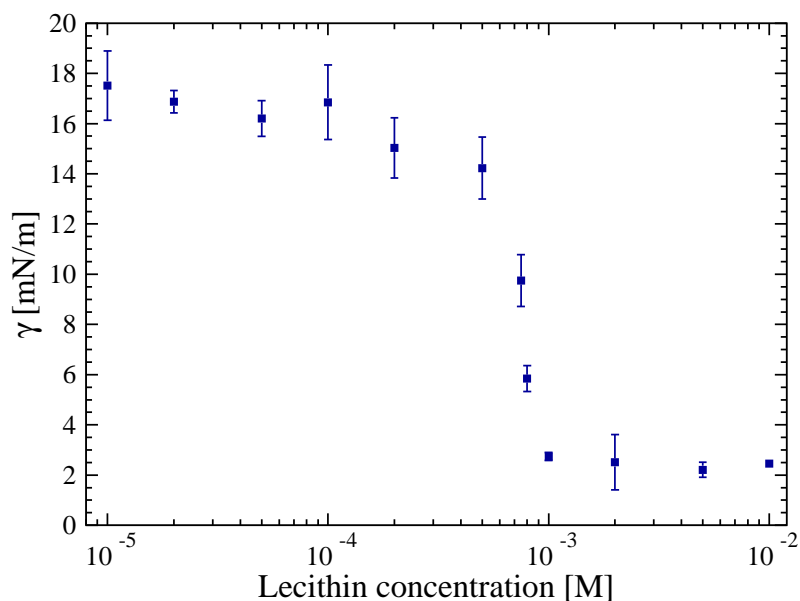
Figure 2.27: The interfacial tension isotherm of lecithin at the ethanol/water - soybean oil interface [332]. The lecithin concentration is expressed as a concentration in the ethanol/water mixture.

One can see that addition of lecithin leads to a significant decrease of the interfacial tension. In the range of low lecithin concentration, the surface tension of solution decreases with the increase in concentration up to the formation of micelles. For instance, at concentration 1×10^{-3} M of lecithin in ethanol, the interfacial tension is lowered by ca. 14 mN/m, i.e., the conditions favoring emulsification are reached. Starting from the critical micelle concentration (about 2×10^{-3} M), the surface tension reaches a constant value of 2 mN/m.

9.2.3 The dependence of emulsion drop size and zeta potential on type of oil, oil-to-ethanol ratio and preparation technique

The oil-in-water emulsions of linseed, soybean and jojoba bean oil were prepared by spontaneous emulsification technique in the two-step process. First, a certain amount of linseed, soybean or jojoba bean oil was added to ethanol to form a homogeneous solution of the desired oil-to-solvent ratio (0.1, 1, or 10% v/v). The oil-ethanol mixture was stirred for a few hours until it formed a clear, single-phase solution. Then, the organic phase was mixed with water (1:100) by injection of oil-in-ethanol phase to the aqueous phase under magnetic stirring. Depending on the process conditions, emulsions with different properties were obtained. Table 2.3 summarizes the measured emulsion droplet

2. EXPERIMENTAL PART

Oil	Internal tension	Oil-in-ethanol concentration	Size	Polydispersity	Zeta potential
	[mN/m]	[% v/v]	[nm]		[mV]
Linseed oil	4	0.1	77.7	0.11	−36
		1	158.7	0.07	−73
		10	206.9	0.26	−87
Soybean oil	22	0.1	96.6	0.14	−40
		1	162.2	0.16	−66
		10	210.4	0.21	−82
Jojoba bean oil	25	0.1	99.8	0.27	−27
		1	171.7	0.22	−72
		10	227.5	0.31	−96

Table 2.3: The dependence of average particle size, polydispersity and zeta potential of natural oil emulsions from type of oil and oil-to-ethanol ratio. Emulsions were prepared by injection of organic phase to water under magnetic stirring.

size and the zeta potential as a function of the type of oil and oil-to-ethanol ratio. The average droplet sizes were in the range of 80–230 nm. The DLS results show that the smallest and monodisperse (PDI < 0.3) emulsions were formed when the oil-to-ethanol ratio was equal to 1:1000. In these conditions, linseed oil gave the smallest emulsion with an average size around 78 nm and a polydispersity index as low as 0.11. Emulsions of soybean and jojoba bean oil were of very similar size — approximately 100 nm — but the soybean oil emulsions were more monodispersed compared to jojoba oil (polydispersity of 0.14 and 0.27, respectively). An increase of the oil-to-ethanol concentration to 1% v/v resulted in an increase of emulsions size. Similarly as for low oil content, the emulsion droplet size increased in the following order: linseed oil < soybean oil < jojoba oil. This tendency was also revealed for 10% v/v of oil-in-ethanol. For these ratios, all the oils formed droplets with a size exceeding 200 nm and a polydispersity index higher than 0.2, with the largest polydispersity (0.3) for jojoba oil. The obtained results are consistent with the interfacial tension measurements. As thermodynamically unstable systems, emulsions tend to reduce the surface free energy, therefore, the oil with the lowest interfacial tension produces more stable emulsion with small droplet size [48]. The linseed oil had the lowest

interfacial tension among the studied oils, whereas interfacial tension of jojoba oil was the highest. Consequently, the linseed oil produced emulsion with the smallest droplet size, while the jojoba oil droplets were the biggest ones. The measured zeta potential of the obtained emulsions was within the range from -27 to -96 mV. It is worth noticing that value of zeta potential is increasing with the concentrations of oil-in-ethanol phase for the preparation of emulsion. That increase of zeta potential is probably caused by adsorption of saturated fatty acids (e.g., palmitic acid), which can dissociate proton at the oil/water interface (pKa of palmitic acid is equal to 4.8). Nevertheless, the zeta potential values obtained for 1% v/v of oil-in-ethanol concentration (corresponding to 0.01% of the total oil concentration in the emulsion) are high enough to ensure emulsions kinetic stability over a long period of time even without addition of surfactants.

In some studies dealing with the spontaneous emulsification technique, it is recommended to prepare emulsions in the way that the organic phase is injected to the water phase under stirring [41], while others suggest reverse order without additional mixing [73]. It was also reported that the emulsion droplet size is strongly affected by the temperature

Oil	No stirring, water-to-organic phase		Stirring at 50°C, organic phase-to-water	
	Size [nm]	Polydispersity	Size [nm]	Polydispersity
Linseed oil	176.6	0.22	143.9	0.11
Soybean oil	174.9	0.27	152.6	0.11
Jojoba bean oil	189.1	0.34	162.2	0.28

Table 2.4: The dependence of the average particle size and polydispersity of natural oil emulsions from method of preparation. The results are presented for oil-in-ethanol ratio equal to 1% v/v.

during the process [295]. Therefore, we decided to study the influence of the method of preparation on the properties of natural oil emulsions. The organic phase was mixed with water (1:100) by pouring it rapidly in to the glass beaker containing the oil-in-ethanol phase, without additional stirring. In order to investigate the influence of temperature on the droplet size distribution, emulsions containing 1% of oil-in-ethanol were prepared by mixing components at 50°C, followed by cooling down to the room temperature. The re-

sults obtained for 1% v/v of oil-in-ethanol are summarized in Table 2.4. It was found that the emulsions obtained by pouring water to the organic phase without mixing have bigger droplet sizes and a higher polydispersity compared to emulsions prepared by injection of organic phase to water under magnetic stirring. It means that supplying mechanical energy to the system helps to obtain smaller and more uniform drops. Increasing temperature during the process has an additional influence on size distribution. For instance, the emulsion of linseed oil prepared without stirring gave droplets of size equal to 177 nm (PDI 0.22). Emulsions of the same composition, but prepared by injection of oil-in-ethanol to water under stirring with approx. speed of 300 rpm, had a mean droplet size of 159 nm (PDI 0.07). When the components were stirred at 50°C, the emulsion size was brought down to 144 nm (PDI 0.11), most probably due to faster diffusion of ethanol to the aqueous phase.

9.2.4 The dependence of the emulsion particle size and zeta potential on the type of surfactant and its concentration

In further preparation of the o/w emulsions, AOT, cholesterol or lecithin were added to oil phase in the concentration range from 5×10^{-3} M to 2×10^{-2} M. In the case of emulsions containing AOT or cholesterol, emulsifiers were dissolved in oil prior to addition of ethanol. Emulsions with lecithin, however, were prepared by dissolving lecithin in ethanol followed by addition of oil to ethanol-surfactant phase. Figure 2.28 presents a comparison of a typical size distribution of emulsion droplets with and without surfactants. As can be seen in the picture, the addition of AOT to oil phase caused a significant decrease of the emulsion size compared to bare emulsion without surfactant. For instance, the droplet size of primary emulsions of jojoba bean oil in water has been reduced from 172 nm to 106 nm, when 5×10^{-3} M AOT was dissolved in oil prior to ethanol addition. Size reduction was followed by a decrease of polydispersity index (from 0.22 to 0.13, respectively). An increase of AOT concentration to 1×10^{-2} and 2×10^{-2} M did not cause further significant changes in size distribution (97 nm for 2×10^{-2} M AOT in jojoba oil). Soybean oil behavior was very similar to that of jojoba bean oil emulsion. For 2×10^{-2} M AOT in soybean oil, the size of emulsion was equal to 76 nm (PDI = 0.13). In the case of linseed oil emulsions, an addition of AOT to bare emulsion with droplet size of 159 nm decreased its size to 104 and 68 nm (for 5×10^{-3} and 2×10^{-3} M AOT, respectively). The linseed oil emulsion
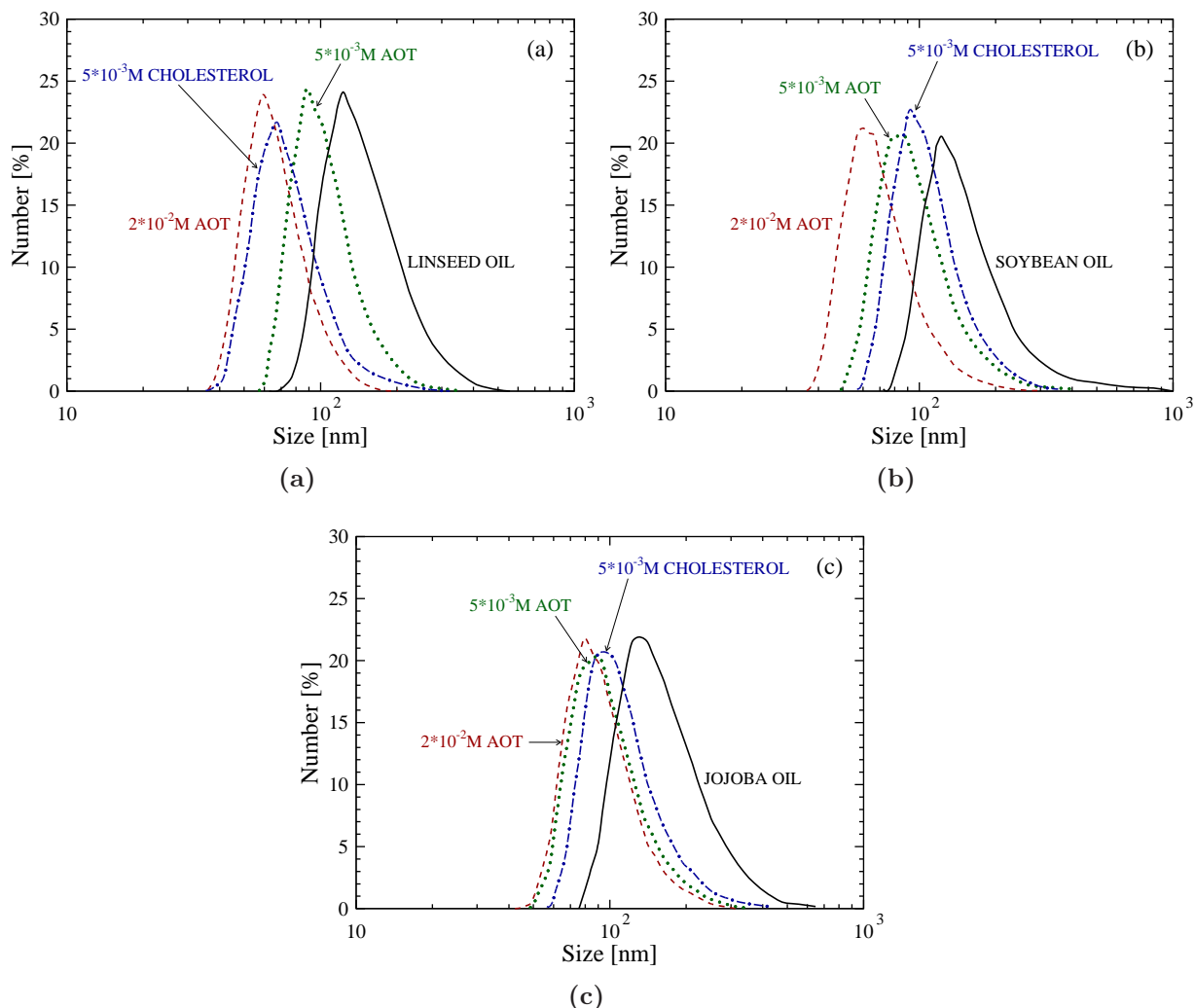
(a)

(b)

(c)

Figure 2.28: The dependence of mean droplet diameter on surfactant concentration for (a) linseed oil, (b) soybean oil and (c) jojoba bean oil. The solid lines represent the size distribution of bare emulsions, while the dotted and dashed lines describe the size distribution of emulsions containing 5×10^{-3} M and 2×10^{-3} M AOT in oil phase, respectively. The dot-dashed lines show the size distribution of emulsions containing 5x10-3 M cholesterol [332].

containing 5×10^{-3} M AOT in oil phase had extremely low polydispersity index equal to 0.05. On the other hand, the zeta potential of emulsions did not seem to be affected by addition of AOT (data not shown) in the studied range of concentrations.

An addition of cholesterol to the emulsions also decreased the droplet size distribution. However, the dimension of emulsions of linseed, soybean and jojoba bean oil seemed to be most affected for the lowest concentration of cholesterol (5×10^{-3} in the oil phase) and its further increase did not cause significant changes. The emulsions of linseed oil with

different cholesterol concentration were within size range of 82–88 nm with polydispersity index between 0.07–0.1, while the emulsions of soybean oil were between 107–115 nm (PDI < 0.1). The jojoba oil emulsions had the droplet size between 100 and 119 nm with PDI within 0.09–0.18. Similarly to AOT, an addition of cholesterol to the emulsions did not influence the zeta potential of the emulsions.

The size distribution of emulsions containing lecithin showed a very similar behavior to that of the emulsions containing cholesterol. An addition of lecithin largely decreased the droplet size compared to the bare emulsions (down to 62 nm for linseed/soybean oil and 77 nm for jojoba oil containing $5 \times 10-2$ M lecithin), but there were no significant changes depending on the concentration of emulsifier (the data not shown). However, the zeta potential of these emulsions showed a strong dependence on the concentration of lecithin, which is presented in Fig. 2.29. When the concentration of lecithin was increased, the
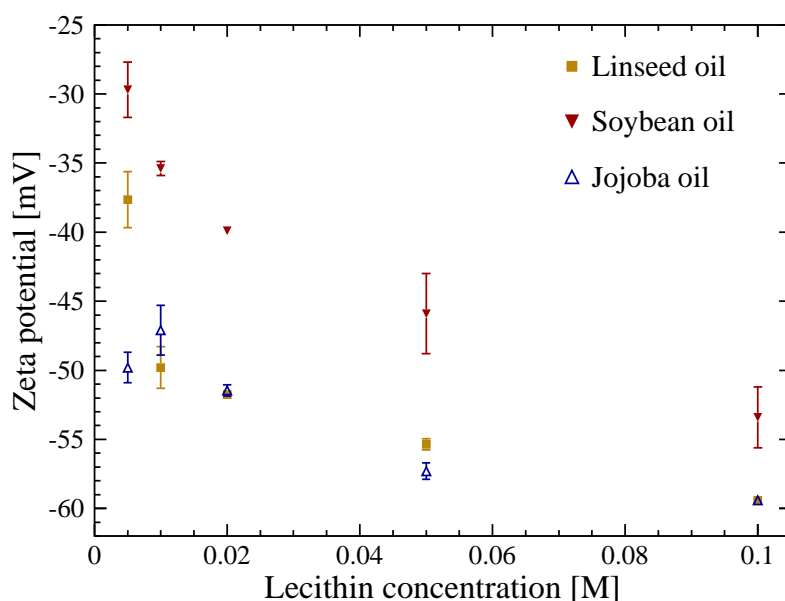
Figure 2.29: The dependence of the emulsion zeta potential on the concentration of lecithin [332].

zeta potential of emulsions was shifted to more negative values. Nevertheless, the zeta

potential of emulsion droplets containing lecithin was always less negative than those without, as it is demonstrated in Fig. 2.30 on the example of linseed oil. This figure illustrates the dependence of droplets zeta potential on pH of the emulsion without and with 5×10^{-2} M lecithin. It can be seen that although the isoelectric point of the emulsion seems not to be influenced by presence of lecithin, for the pH values above 5, the pure

Figure 2.30: The dependence of the zeta potential of emulsions on pH for the linseed oil emulsions with and without 5×10^{-2} M lecithin, $I = 10^{-3}$ M NaCl, $T = 20°C$ [332].

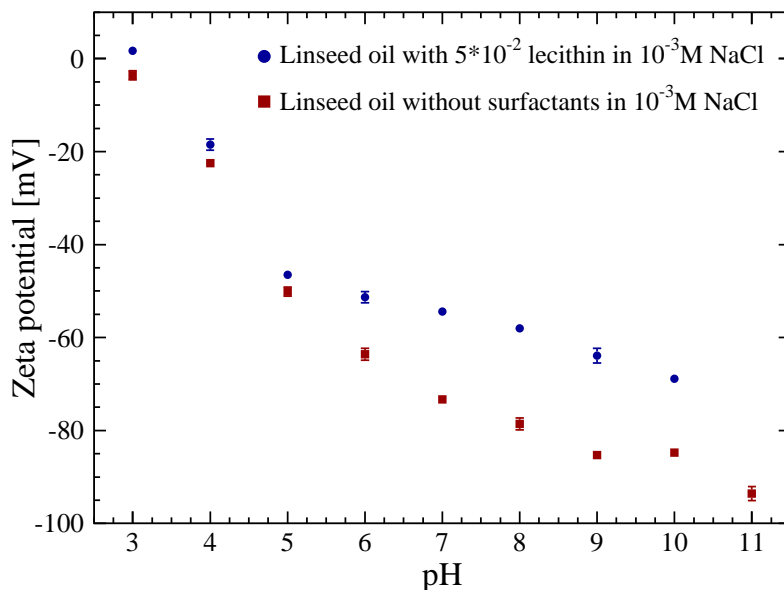linseed oil droplets are significantly more negative. That can be explained by the fact that zwitterionic lecithin, which is preferentially adsorbed at oil/water interface, brings less negative surface charge than fatty acids. The value of zeta potential of the micellar solution of 2×10^{-2} M lecithin in the ethanol-to-water =1:10 (pH = 6.2) was equal to -38 mV. No shift of isoelectric point upon addition of lecithin indicates coadsorption of fatty acids and lecithin.

9.2.5 Stability of the emulsions

The size distribution and the zeta potential of the selected emulsions were monitored during three months in order to investigate their stability. The bare emulsions and emulsions containing AOT and cholesterol were stored at the room temperature, while the emulsions containing lecithin were kept in a refrigerator. The size distribution and the zeta potential of emulsions were measured 1, 5, 10, 15, 20, 30, 60, and 90 days after the preparation. The results for the bare emulsion of linseed oil and for the emulsion containing 5×10^{-3} M AOT (1% v/v oil-in-ethanol) are exemplified in Fig. 2.31. It was found that the size and the zeta potential of the emulsions containing 0.1% and 1% v/v of oil in organic phase, both the with and without surfactants, did not change with time beyond the statistical error range. In the case of emulsions containing 10% v/v of the

(a)

(b)
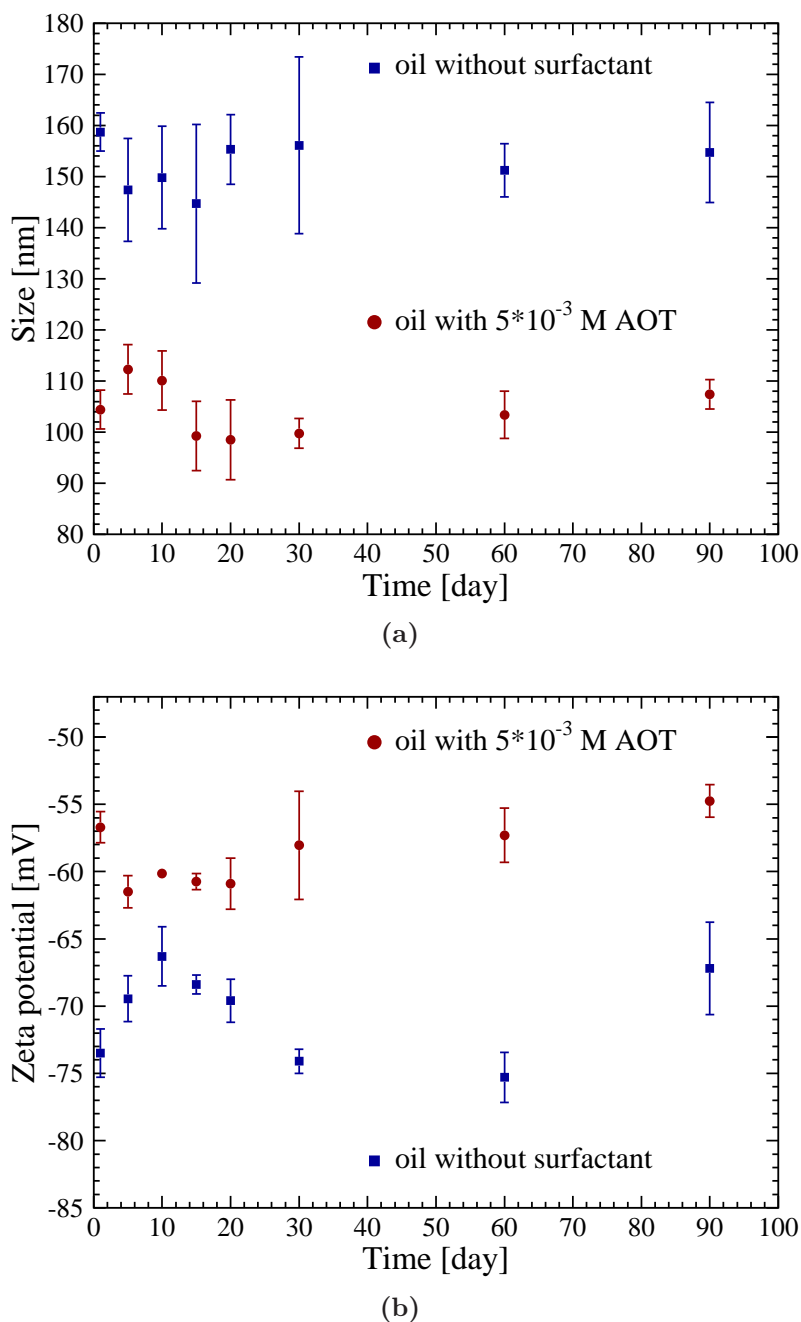
Figure 2.31: Time-dependent changes in the average particle size (a) and in the zeta potential (b) for the bare emulsion of linseed oil and for the emulsion containing 5×10^{-3} M AOT [332].

oil in ethanol, phase separation was observed quite fast. This confirms that one of the limitations in use of the spontaneous emulsification process is a low concentration of oil in the final emulsion [295]. A higher stability of remaining emulsions results from both the small droplet size and their low polydispersity. Small droplet sizes with higher resulting diffusion rates provide stability against sedimentation and creaming, while the

homogeneous size retards significantly the Ostwald ripening, being the main mechanism for nanoemulsion destabilization [299]. Additionally, stability of the emulsions containing 5×10^{-2} M of lecithin was tested in a wide pH range. It was found that the emulsions were stable within a pH range of 4–12. These findings correlate well with the results of the zeta-potential measurements on oil droplets containing 5×10^{-2} M lecithin. They are collected in Fig. 2.32. As it can be noticed, the zeta potential of all the emulsions decreases monotonically with pH having a value below ˘30 mV (which is usually assumed as the stability threshold for an electrostatically stabilized system) at pH 4. Around pH $= 3$ (i.e., close to the isoelectric point), the size and polydispersity of the emulsions increased significantly.
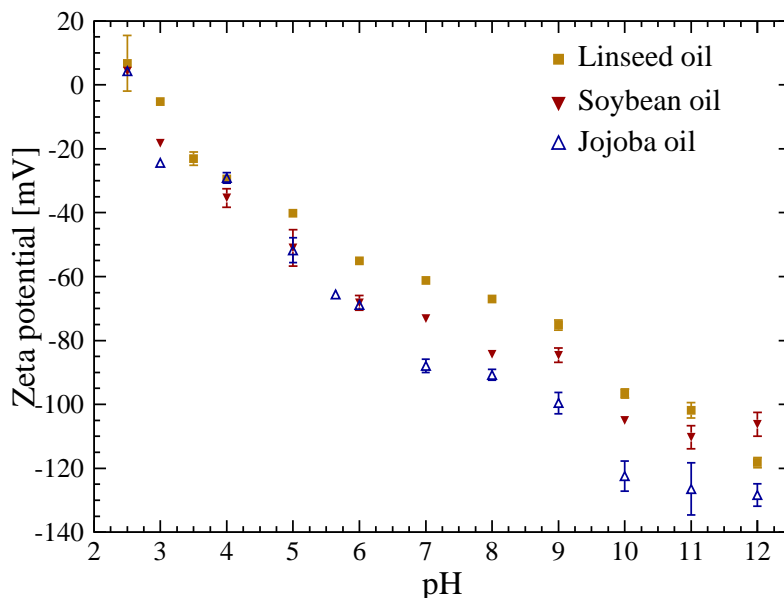
Figure 2.32: The dependence of the zeta potential of emulsions on pH for the linseed oil, soybean oil and jojoba bean oil emulsions containing 5×10^{-2} M lecithin [332].

9.2.6   Encapsulation of emulsions within a first layer of polyelectrolyte

The nanocapsules were formed by the addition of 0.1 ml of AOT in oil-ethanol solution to 100 ml of the aqueous PAH solution, during continuous stirring. As shown in Fig. 2.33, the size of obtained emulsion droplets, which were stabilized with the AOT/PAH complex, varied depending on the concentration of polyelectrolyte and the type of oil used to form the liquid core. For example, an average droplet size of the capsule with the linseed oil core stabilized with PAH ($c = 0.1$ g/dm^3) was equal to 120 nm with PDI < 0.1. Increasing

the concentration of PAH to 0.5 and 1 g/dm^3 resulted in the increased size of capsules as well (138 and 171 nm, respectively). Similarly, a dependence was observed for the
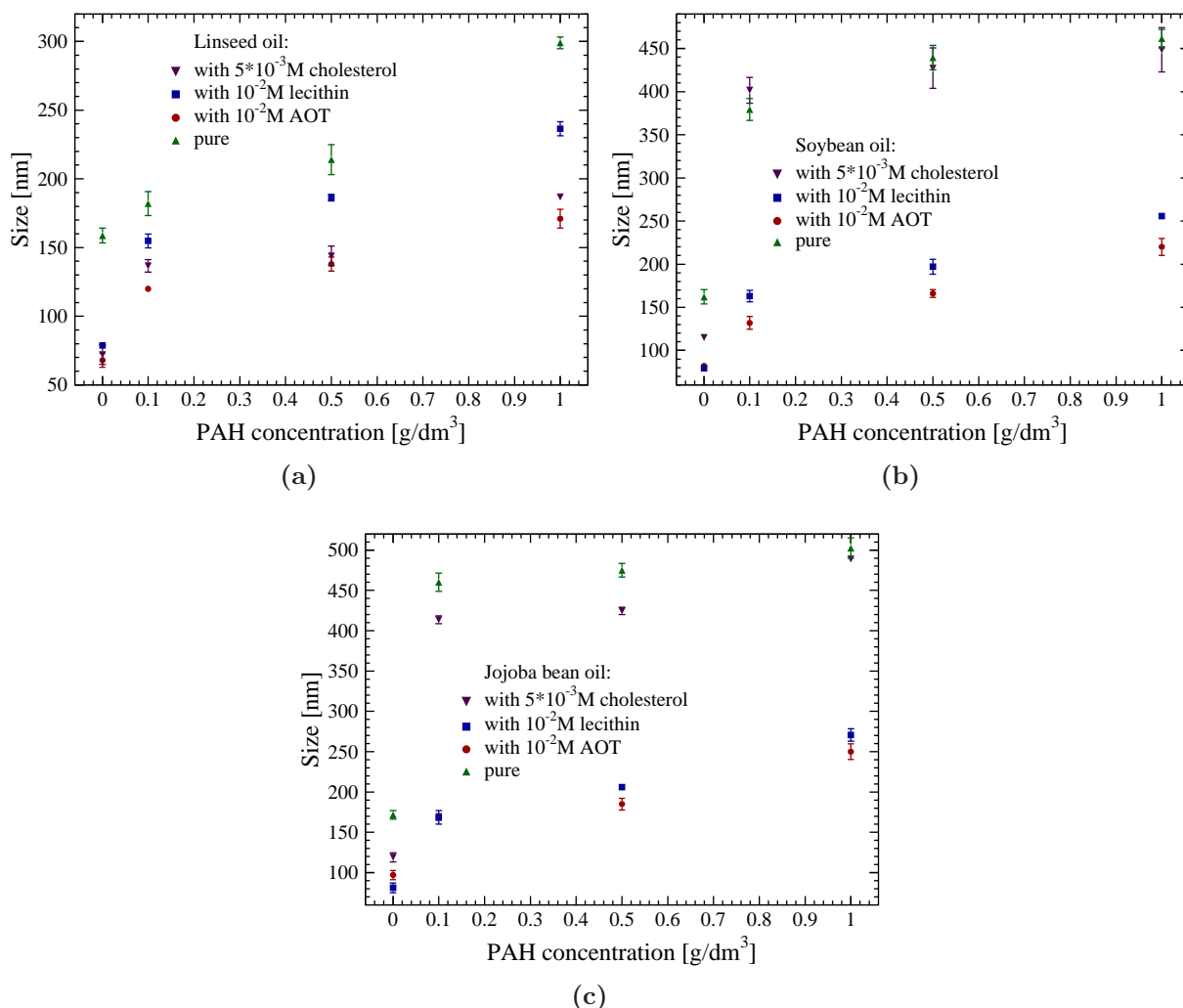
Figure 2.33: A dependence of the size of emulsion droplets encapsulated within the first layer of polyelectrolyte on poly(allyamine hydrochloride) concentration, in the case of using: (a) linseed oil, (b) soybean oil, and (c) jojoba bean oil. The points for 0 g/dm^3 PAH denote the emulsion cores without an addition of the polyelectrolyte [332].

capsules with the soybean and jojoba bean cores. It is worth noticing that the correlation between the type of oil and the size of obtained droplets, which was before revealed for emulsions, was also preserved for the capsules. The capsules with the linseed oil core were the smallest ones, while the capsules with the soybean oil core were of the intermediate size (132–220 nm, depending on the PAH concentration). The capsules with the jojoba

core were the biggest ones (169–250 nm). The zeta potential of the obtained capsules was within the range 53–76 mV, thus providing a sufficient stability of the droplets and qualifying them for a further layer-by-layer encapsulation.

9.2.7 Fluorescence of encapsulated hydrophobic dye

Dissolution of the hydrophobic fluorescent dye, Coumarin 6, in the oil phase gives a direct evidence for the success of encapsulation in the emulsion droplets. Therefore, the dye was dissolved in oil prior to addition of ethanol. After that, the organic phase was dispersed in water in the proportion 1:100. In order to confirm the fluorescent properties of emulsions, the fluorescence emission spectra were recorded in the range 450–700 nm. It is important to keep in mind that the final emulsions contained 1% of ethanol and therefore, part of the hydrophobic dye could be present in the aqueous phase as well. In order to distinguish the signal coming from Coumarin present in the oil droplets and the one in the surrounding phase, additional measurements of the background of emulsion were performed. Coumarin was dissolved in ethanol and water, in the same amount and proportions as in the case of O/W emulsion, but the linseed oil was not added. Such prepared solution was treated as the background phase for determining the amount of hydrophobic dye eventually present in the aqueous phase. Figure 2.34 shows the rep-
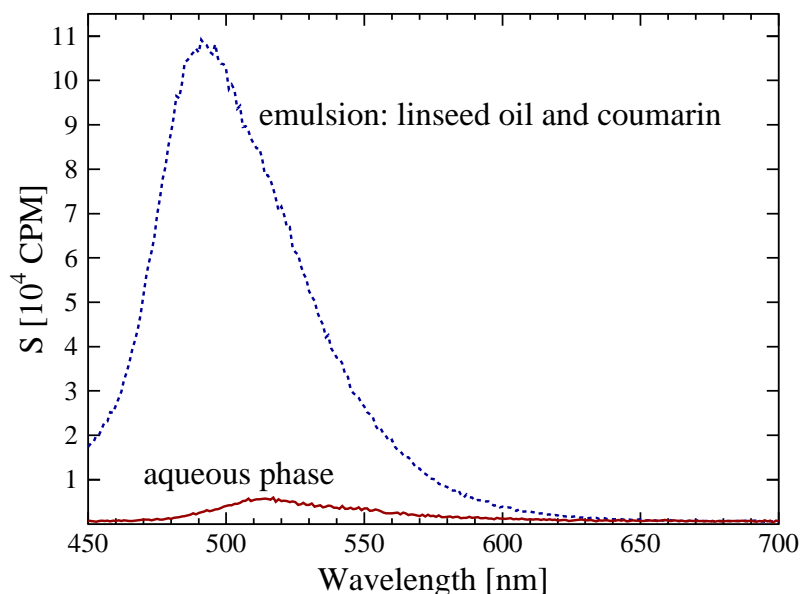

Figure 2.34: The fluorescence emission spectrum of the emulsion of linseed oil with Coumarin (dashed line) and the aqueous phase of emulsion (continuous line) [332].

resentative fluorescence emission spectrum obtained for the emulsion of linseed oil with Coumarin. Coumarin possesses a characteristic emission wavelength at 491 nm. Therefore, the dashed-line spectrum gives an evidence of enclosure of Coumarin within the oil core. The solid line represents a signal coming from the surrounding phase. The characteristic peak was shifted to 514 nm and its intensity was significantly lower than 1×10^4 CPM for the emulsion containing oil phase. The obtained results confirm that most of Coumarin was encapsulated within the oil phase of the emulsion. Figure 2.35
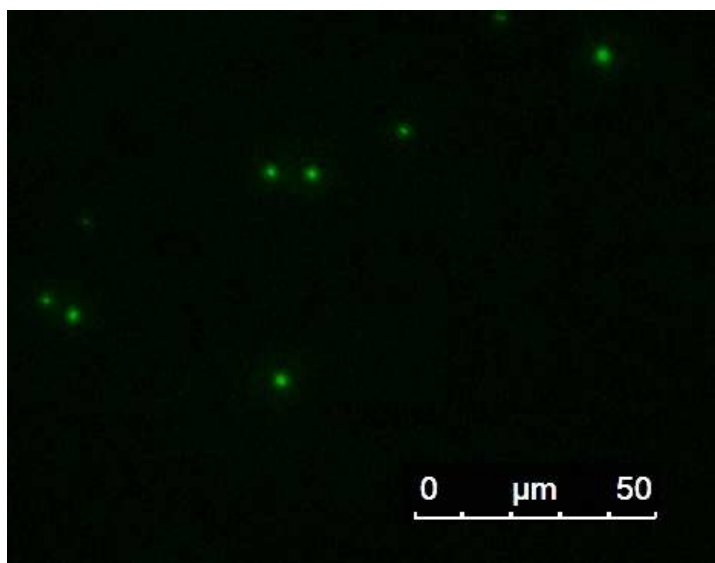
Figure 2.35: The fluorescence micrograph of the Coumarin-labelled linseed oil emulsion encapsulated in the one layer of PAH [332].

illustrates fluorescence of the linseed oil droplets covered by a single layer of PAH, which was deposited on a mica surface. It is evident that the fluorescence comes only from the encapsulated dye. The emulsion drops covered with single PAH layer preserve their integrity upon adsorption on the mica surface and the fluorescence from background is negligible.

9.3 Linseed oil based nanocapsules as delivery system for hydrophobic quantum dots

9.3.1 Outline

The CdSe/ZnS hydrophobic quantum dots were embedded within the polyelectrolyte nanocapsules. The core of the capsules, which consists of a mixture of the linseed oil with

chloroform, was prepared using the spontaneous emulsification technique described in the previous section. The obtained emulsions were stabilized with lecithin and encapsulated within the two (PLL/PGA) bilayers using the saturation method. The process of direct encapsulation of oil cores within polyelectrolyte shell is schematically shown in Figure 2.36. The shell growth was evidenced by the capsule size and the electrophoretic mobility
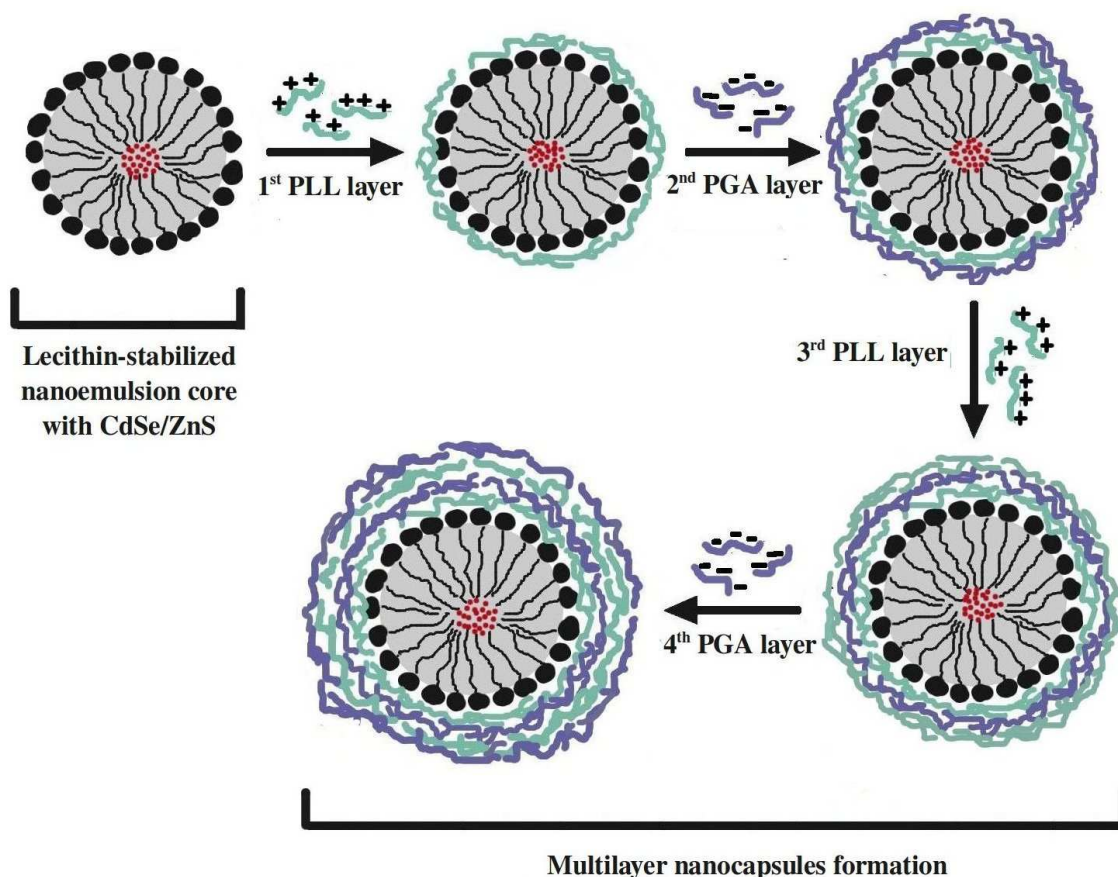
Figure 2.36: A scheme of the multilayer-nanocapsule formation via the layer-by-layer adsorption of polyelectrolytes on the liquid emulsion core.

measurements. The emulsion and the capsules were deposited on a mica surface and the deposit topology was examined by means of the atomic force microscopy. The presence of quantum dots within the oil cores was confirmed by recording the fluorescent spectra of samples containing CdSe/ZnS. In order to evaluate cytotoxicity of the capsules, their influence on the viability of the mouse embryonic fibroblasts was examined using the MTT test, followed by observation of the morphology of cells, after the hematoxylin-eosin staining under the optical microscope.

9.3.2   Encapsulation of CdSe/ZnS quantum dots

The emulsions were prepared using the spontaneous emulsification technique, as reported in Sec. 9.2. Here, in order to increase the solubility of the hydrophobic quantum dots in the emulsion core, a part of the linseed oil was replaced with chloroform containing 1–5 mg/ml of CdSe/ZnS. The volume ratio between the linseed oil and chloroform was equal to 1:1. Later on, 0.1 ml of the oil phase was injected to 2 ml of ethanol, containing 5×10^{-2} M lecithin. A solution of the oil with ethanol was mixed with a magnetic stirrer at 350 rpm for a few hours until clear, single-phase solution was obtained. In the second step of the process, 0.1 ml of the previously prepared organic phase was added to 10 ml of water, during continuous stirring. Due to the rapid diffusion of ethanol into the aqueous phase, an O/W emulsion containing 0.05 vol % of the oil phase was formed instantaneously. The average droplet size of the nanoemulsion prepared according to the procedure described above, measured by DLS was around 100 nm with the polydispersity index (PDI) < 0.25, as shown in Fig. 2.37). The zeta potential of emulsion was
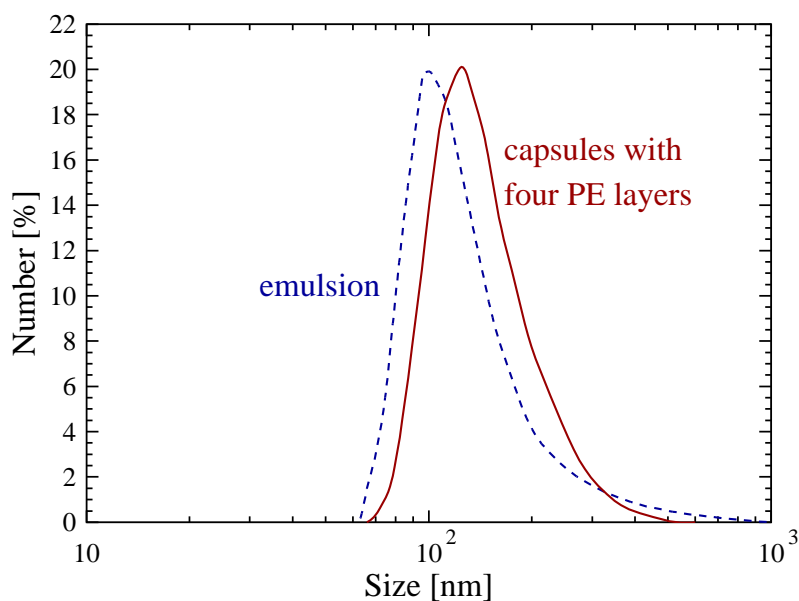
Figure 2.37: A typical size distribution of the emulsion core (dashed line) and the capsules terminated with the two (PLL/PGA) bilayers (solid line) [333].

equal to -47.6 mV, which is high enough to ensure electrostatic stability of the system. Encapsulation of the nanoemulsion template within the first layer of polyelectrolyte (positively charged poly-L-lysine hydrobromide) was accomplished by addition of 0.1 ml of emulsion phase to 10 ml of the aqueous PLL solution ($c = 1$ g/l, 0.015 M NaCl). The

organic phase was added to the beaker containing polycation solution and stirred with an approximate speed of 350 rpm. The replacement of water phase with polycation solution resulted in the reversal of zeta potential of the emulsion drops to the positive value of 41.3 mV. The size of these drops, stabilized now by the lecithin-PLL complex, was equal to 106 nm. The consecutive layers of polyelectrolytes were formed in a similar manner, i.e., the nanoemulsion with first layer of PLL was added to the solution of polyanion PGA in order to form the second layer, and so forth. The procedure was repeated to receive the shell of nanocapsules composed of 1–4 consecutive polyelectrolyte layers. The average size of nanocapsules with the linseed oil core and the two (PLL/PGA) bilayers was around 127 nm with PDI equal to 0.12 (c.f. Fig. 2.37).

A growth of the polyelectrolyte shell was monitored with the zeta-potential measurements. Figure 2.38 presents the dependence of the zeta potential of the shell as a function of the number of polymer layers. As mentioned before, deposition of a single PLL layer on
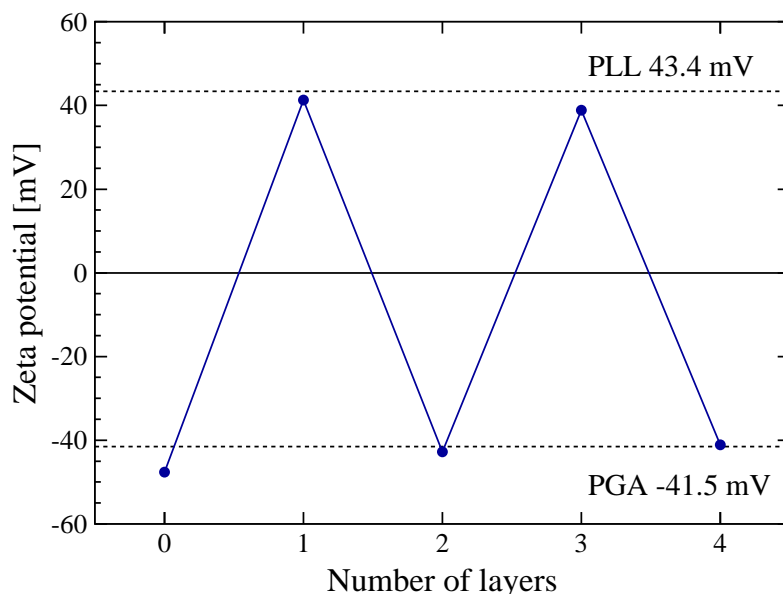
Figure 2.38: Changes of the zeta potential as a function of the number of polyelectrolyte layers: for the bare emulsion ($n = 0$) and for the following 1–4 consecutive layers of PLL/PGA [333].

the negatively charged nanoemulsion template caused the reversal of the surface charge to the positive values. The following deposition of PGA reversed it back to the negative values. Therefore, layer-to-layer zigzag dependence of the zeta potential accounts for a credible evidence of multilayer shell formation.

9.3.3 AFM measurements of nanocapsules morphology

The morphology of prepared samples was studied by means of the atomic force microscopy. The representative AFM images of emulsion and capsules are shown in Fig. 2.39. One can see that after a short adsorption time ($t_{ads} = 15$ s) of the bare emulsion at the PEI modified (positively) charged mica surface, the deposited drops preserved a spherical shape (see Fig. 2.39a). However, when the adsorption was progressing and the surface concentration
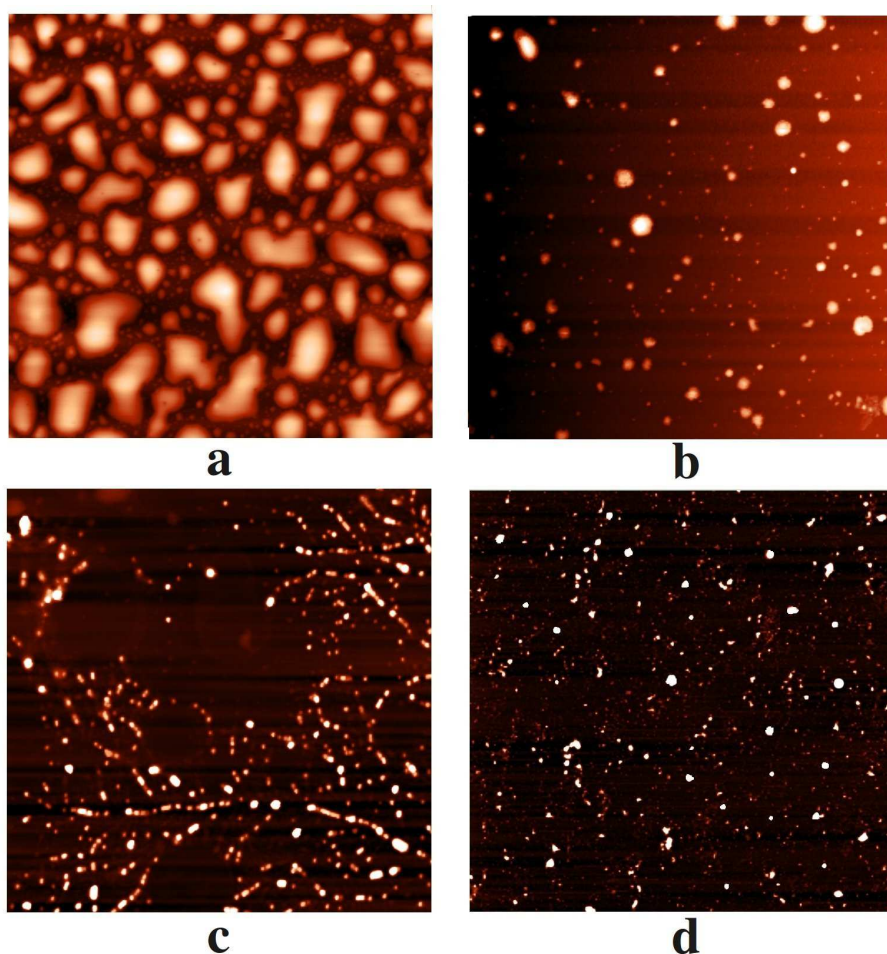
Figure 2.39: The AFM images (10 μm × 10 μm) of emulsion deposited on the PEI-covered mica for: (a) $t_{ads} = 15$ s or (b) 15 min, (c) the PLL-terminated capsules ($t_{ads} = 15$ s), and (d) the PLL/PGA/PLL-terminated capsules ($t_{ads} = 15$ s). The topographical scale is $z = 70$, 90, 180, and 200 nm, respectively. The pictures were obtained in the tapping mode [333].

of drops increased, they started to coalesce. That is evidently seen in Fig. 2.39b, where the image of the PEI modified mica plate after 15 minutes of the emulsion deposition is shown. Stabilization of the emulsion core with the polyelectrolyte layers resulted in a significant

change of the emulsion stability and resulting structure of the deposited drops. The PLL and (PLL/PGA)PLL-covered nanocapsules at the mica plates were mostly spherical and well defined, as shown in Figs. 2.39c and d, respectively. No signs of aggregation were visible as well. The size of capsules measured by DLS was in a good agreement with the results obtained by the atomic force microscopy (up to 100 nm). It is important to keep in mind that sometimes a comparison of the results obtained in wet (DLS) and dry conditions (AFM in the air, SEM) leads to an underestimation of the capsule size, due to their possible shrinking caused by the drying step.

9.3.4   Fluorescence of encapsulated quantum dots

Encapsulation of the hydrophobic quantum dots within the emulsion cores was confirmed by recording the fluorescence emission spectra in the range of 600–700 nm. The CdSe/ZnS quantum dots used in our study possess a characteristic emission wavelength at 650 nm. That is advantageous in the biomedical applications due to the elimination of the background cellular fluorescence, which appears between 500–600 nm. Figure 2.40 presents the
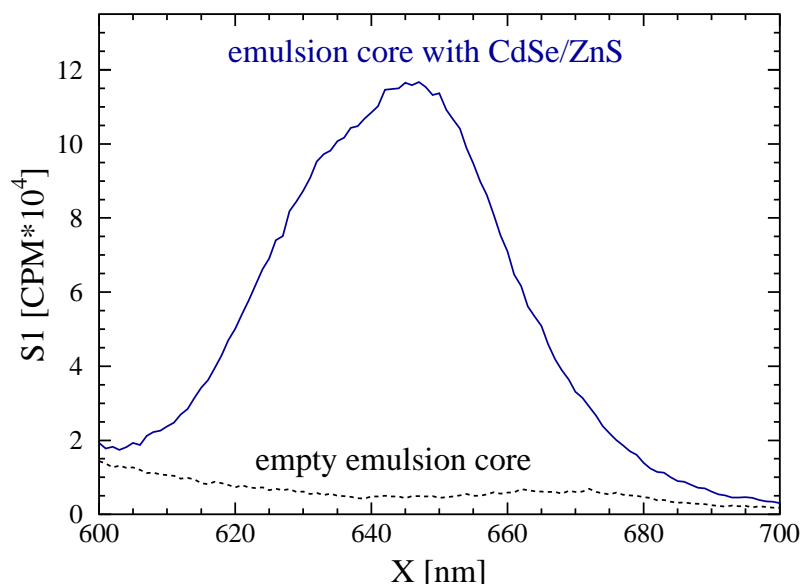

Figure 2.40: The fluorescence emission spectra of the empty emulsion core and the CdSe/ZnS-labeled emulsion [333].

intensive CdSe/ZnS emission peak, thus confirming the fluorescent properties of encapsulated quantum dots. A comparison of the fluorescent emission spectra of the emulsions with and without quantum dots is a clear evidence for encapsulation. Despite of the

presence of ethanol in the final emulsion (1 vol %), there is no need to distinguish the signal coming from the quantum dots, which is present in the oil domain, and the signal possibly present in the aqueous phase, because the CdSe/ZnS quantum dots are neither soluble in water nor in ethanol.

9.3.5 MTT viability test

Cytotoxicity of the CdSe/ZnS labeled emulsions and capsules terminated with 1, 2, and 4 layers of polyelectrolytes was tested in the MTT assay and by estimating the cell growth and morphology of the mouse embryonic fibroblasts. A formation of the polyelectrolyte multilayer shell on the emulsion core leads to the dilution of nanocapsule suspension. Therefore, the concentration of quantum dots in the studied samples was within the range 0.06–0.5 µg/ml. In order to compare the effect of capsules with a different number of layers, the samples were diluted with PBS, such that the final concentration of CdSe/ZnS would be the same for all of them and equal to 0.06 µg/ml. The emulsion and capsules containing the initial (referred to as higher) amount of quantum dots without dilution were tested in the MTT assay, as well. That initial concentration was equal to 5 µg/ml for the emulsion (the lower concentration tested was equal to 0.5 µg/ml), or 0.5 µg/ml, 0.22 µg/ml, and 0.06 µg/ml for the capsules with 1, 2 or 4 layers, respectively. The capsules terminated with 4 layers were also tested at the CdSe/ZnS concentration accounting for 0.03 µg/ml. The detailed values of the quantum-dot concentration in the tested samples are given in Table 2.5.

Layers in the shell	Quantum-dot concentration [µg/ml]	
	Lower	Higher
0 (emulsion)	0.50	5.0
PLL	0.06	0.50
PLL/PGA	0.06	0.22
(PLL/PGA)$_2$	0.03	0.06

Table 2.5: The concentration of CdSe/ZnS quantum dots in the samples tested in the MTT assay and for morphology of fibroblasts.

The results of MTT test for all the samples described in Table 2.5 are presented

in Fig. 2.41. One can see that incubation of the cells with the bare emulsion led to a significant decrease in the cell viability when compared to the negative control (cells seeded on TCPS without addition of nanoparticles), regardless to the quantum-dot concentration. Encapsulation of the emulsion template within the first layer of PLL did not seem
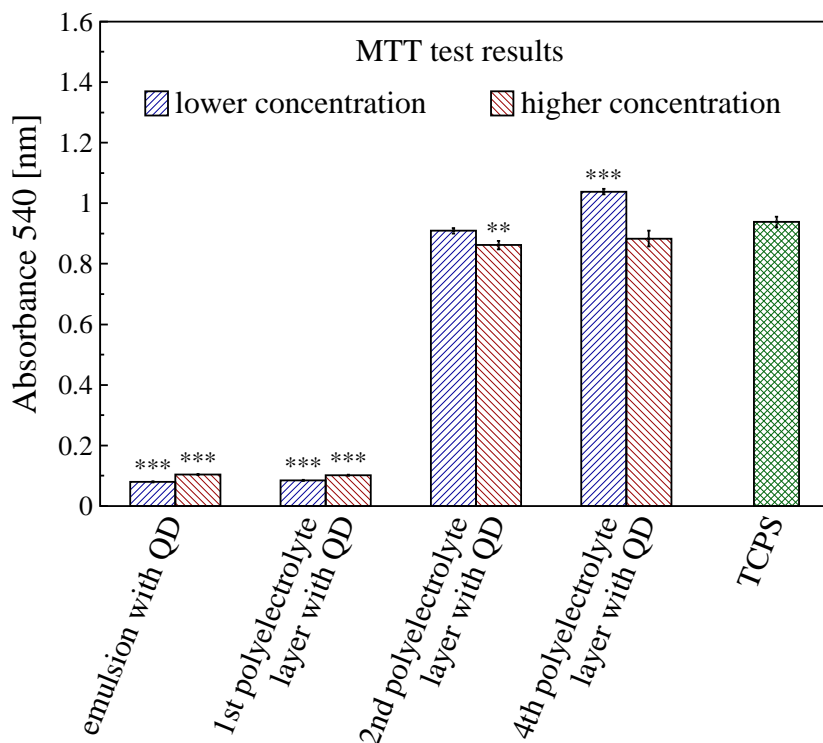
Figure 2.41: The results of MTT viability test of the NIH 3T3 mouse embryonic fibroblasts. The cells were cultured for 24 hours and incubated with nanoparticles for the next 24 hours. The data are expressed as the mean $\pm$SEM of the three similar experiments carried out in a triplicate. The asterisks indicate a statistical significance from the control TCPS group: $^{**}p < 0.01$ and $^{***}p < 0.001$ [333].

to improve the cell viability. A low absorbance value indicates that after 24 hours of incubation most of the cells were dead. Besides the toxic effect of CdSe/ZnS nanoparticles, it can be related to the fact that positively-charged polyelectrolyte shell is known to be less biocompatible than negatively-charged polyelectrolytes. Deposition of the subsequent layer of PGA caused a substantial improvement in cell viability, which was comparable with the negative control sample. A similar situation was observed for the capsules terminated with the two (PLL/PGA) bilayers. In the case of lower concentration tested, the cell growth was slightly higher than for negative control. A comparison made between the capsules terminated with 1, 2 or 4 layers clearly showed that encapsulation of the

emulsion core within the one and two bilayers of (PLL/PGA) has practically eliminated their cytotoxicity.

9.3.6 Cell morphology observations

The microscopic observations of the morphology of fibroblasts, examined under optical microscope (see Fig. 2.42), confirmed the results of MTT assay. The fibroblasts cultured with the bare emulsion with quantum dots were sparse and mostly rounded, proving its negative influence on cell morphology and proliferation. Similarly, very few cells were present after incubation with PLL-terminated capsules. The stained structures visible in the pictures are probably complexes of positively charged PLL-capsules with negatively charged dye (eosin).

In the case of capsules terminated with (PLL/PGA) or (PLL/PGA)$_2$, the cultured fibroblasts were numerous and well-flattened. Their polygonal shape resembled the cells from the control sample of TCPS. Most of the surface was covered by a uniform layer of fibroblasts. These results of microscopic observations on the morphology of fibroblasts evidently indicated that nanocapsules terminated with one or two (PLL/PGA) bilayers had no effect on the fibroblast proliferation. According to many studies, non-coated quantum dots can severely impair cell structure and functions [246, 321]. Presence of surface coatings, such as inorganic ZnS, poly(ethylene glycol), or mercaptoacetic acid is known to have positive influence on the cell viability [238, 254]. In this study I found that encapsulation of CdSe/ZnS quantum dots in the natural oil emulsion cores coated with biocompatible polyelectrolyte layers is another effective approach of decreasing their cytotoxic effect. The quantum dots carriers prepared in such a way can be considered for further use in biomedical applications.

9.4 Preparation of the squalene-based nanocapsules on membrane emulsification unit

9.4.1 Outline

The emulsions of squalene stabilized with the AOT/PAH complex were prepared with the membrane emulsification unit. The influence of AOT and PAH concentration on the
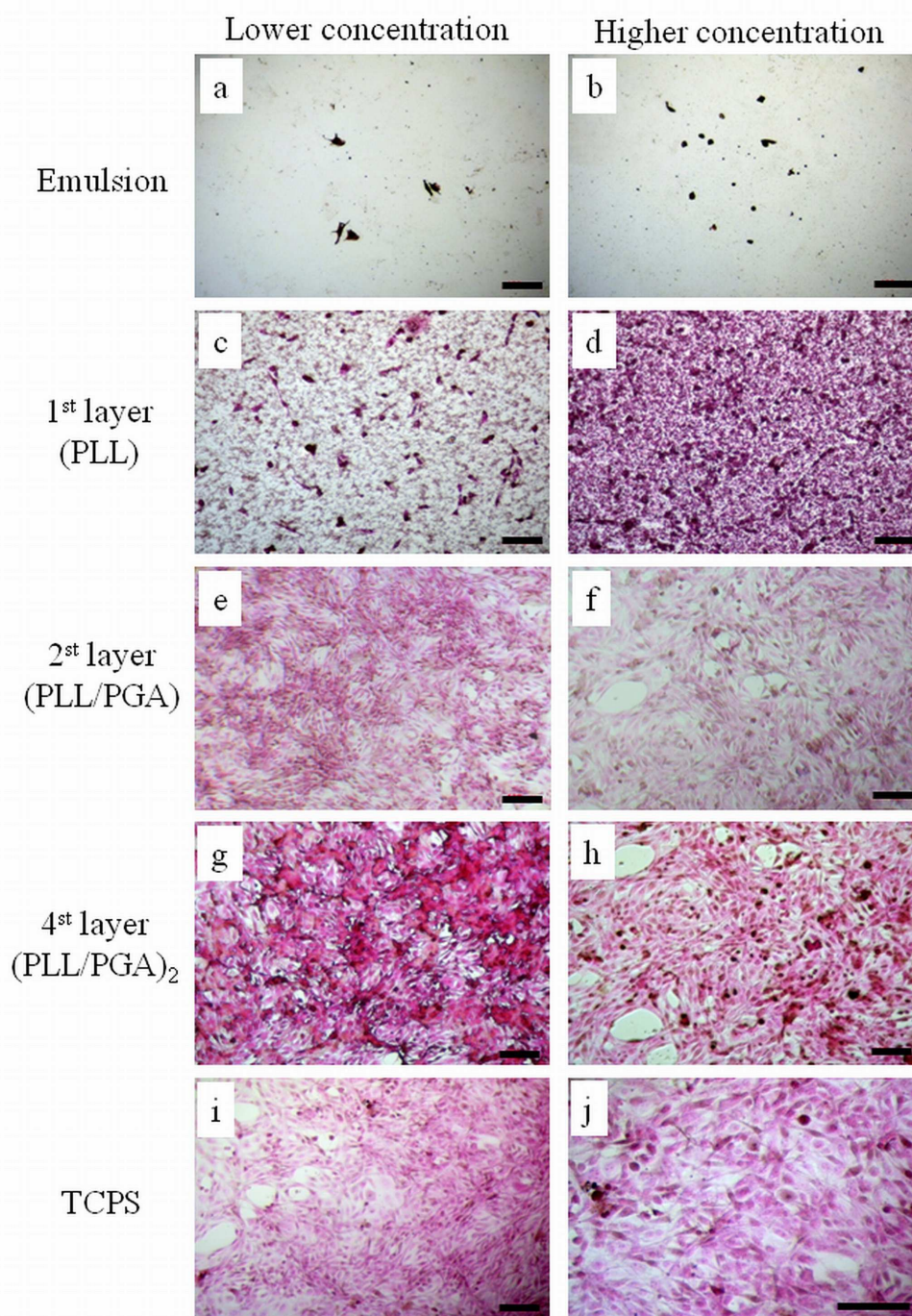
Figure 2.42: The morphology of NIH 3T3 fibroblasts incubated with the bare emulsion (a, b) and the CdSe/ZnS-labeled capsules terminated with 1 (c, d), 2 (e, f) or 4 (g, h) layers of polyelectrolytes and on the control sample $-$TCPS(i,j). The images (a, c, e, g) are for a lower concentration and the images (b, d, f, h) for a higher concentration of quantum dots. The morphology of cells was examined after hematoxylin-eosin staining under the optical microscope with obj. 10× (cells incubated with nanoparticles) or 10× and 20× (cells on TCPS). The scale bars correspond to 100 μm [333].

size and zeta potential of the obtained emulsions was investigated. The emulsion droplets were used as cores for further layer-by-layer encapsulation with PAH/PSS pair of polyelectrolytes (up to ten layers). To this point, the saturation technique has been used. A growth of the polyelectrolyte shell was followed using the electrophoretic mobility and DLS measurements. Mechanical properties of capsules were investigated by the AFM force-distance measurements. The hydrophobic drug (Naproxen) and the oil-soluble vitamin D were encapsulated within the cores and their presence was confirmed by the UV-vis measurements.
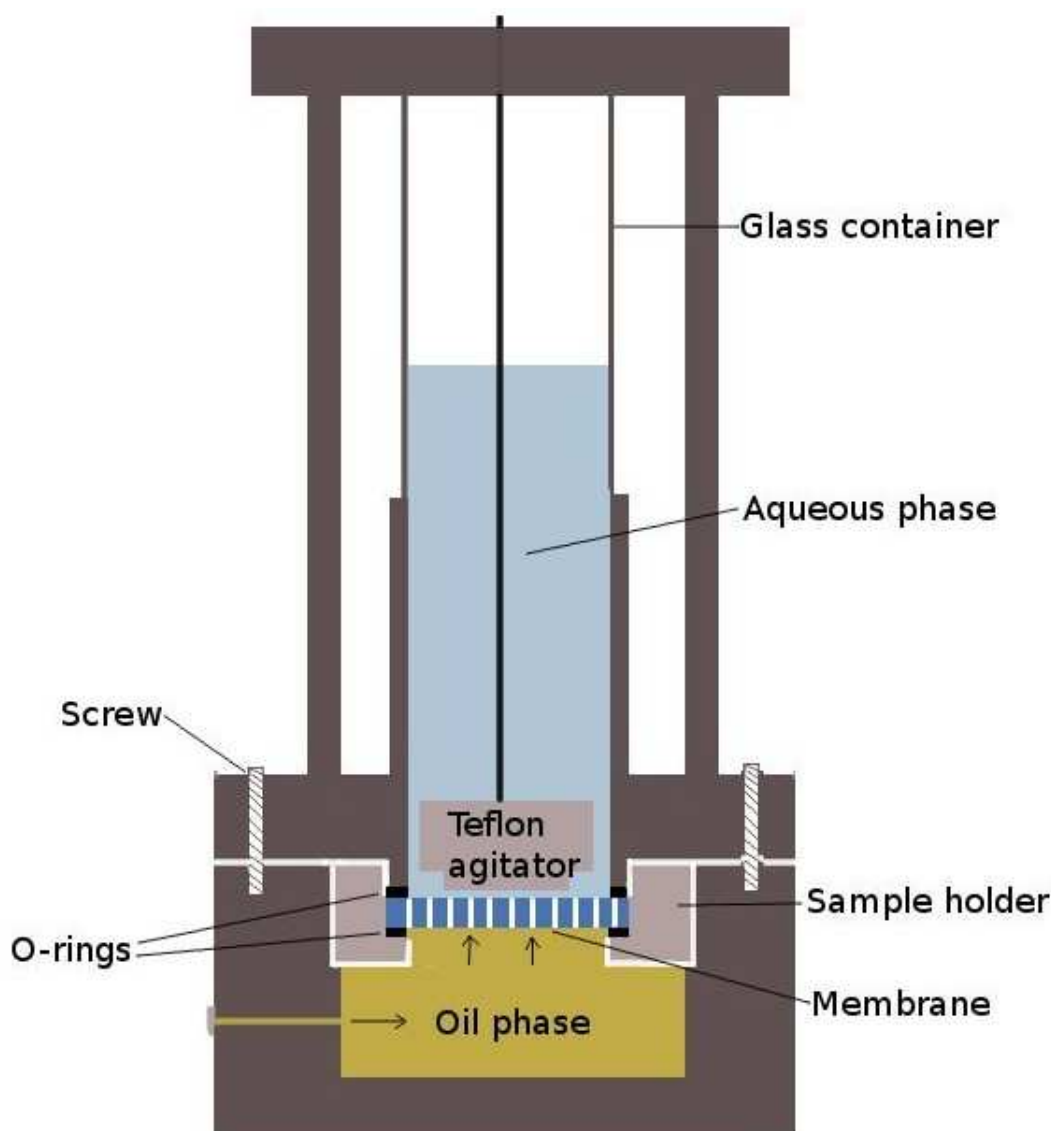
Figure 2.43: A scheme of the membrane emulsification unit.

9.4.2 Formation of the squalene-based nanocapsules

To prepare the primary emulsion and emulsion based nanocapsules, 4.44–1000 g/l of AOT was dissolved in squalene. Such prepared oil phase was pumped (Gilson 305 piston pump, USA) through the hydrophilic ceramic membrane (KeraNor, Norway) into the aqueous solution of PAH, which was being stirred with a teflon agitator.

The final concentration of obtained emulsion was equal to 0.1% v/v. The concentration of aqueous PAH solution in 0.015 M NaCl varied from 100 ppm up to 2000 ppm. Figure 2.43 presents the scheme of the membrane emulsification unit used in the process. The unit is shown in more details in Fig. 2.44a and b.

Figure 2.44: The membrane emulsification unit in the lab (a) and the lower part of unit with the mounted ceramic membrane and o-rings (b).

2. EXPERIMENTAL PART

The average pore size of the membrane used was equal to 200 nm. The established optimal flow rate and stirring speed used during the emulsification process were equal to 0.1ml/min and 400 rpm, respectively.

In order to establish an optimal concentration of surfactant in the solution, the primary emulsions of squalene stabilized with AOT/PAH complex were prepared at a constant PAH concentration (100 ppm) and at variable AOT concentrations. Figure 2.45 presents

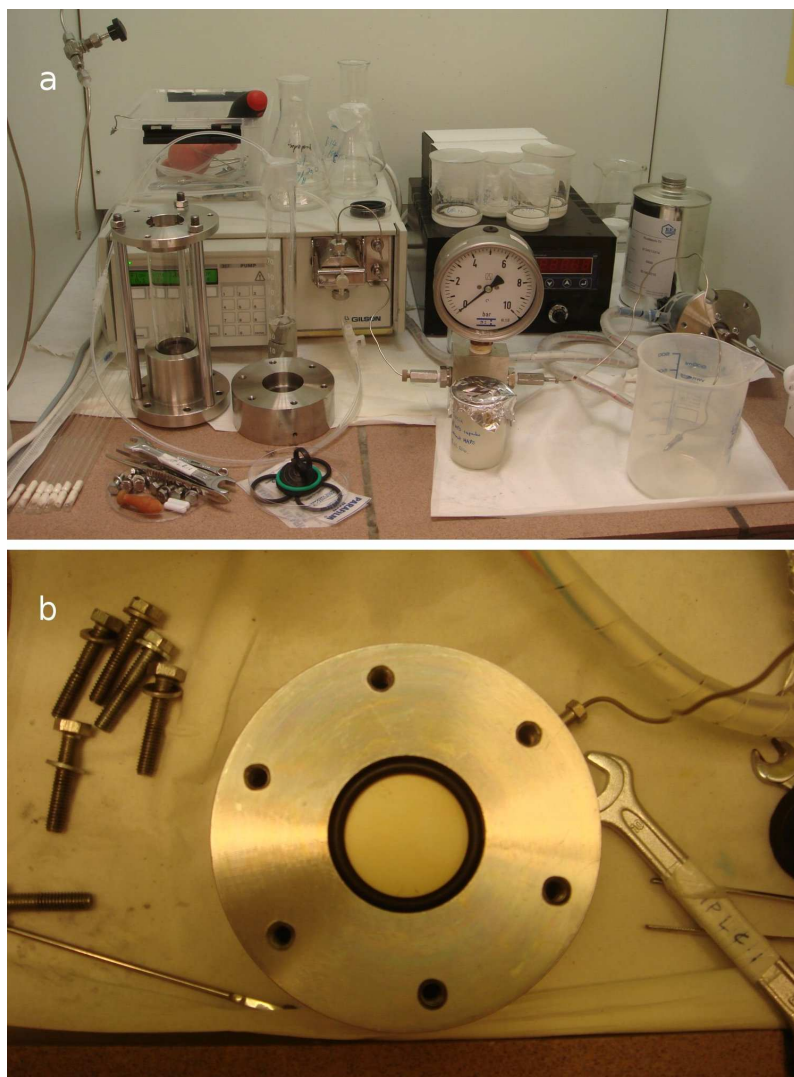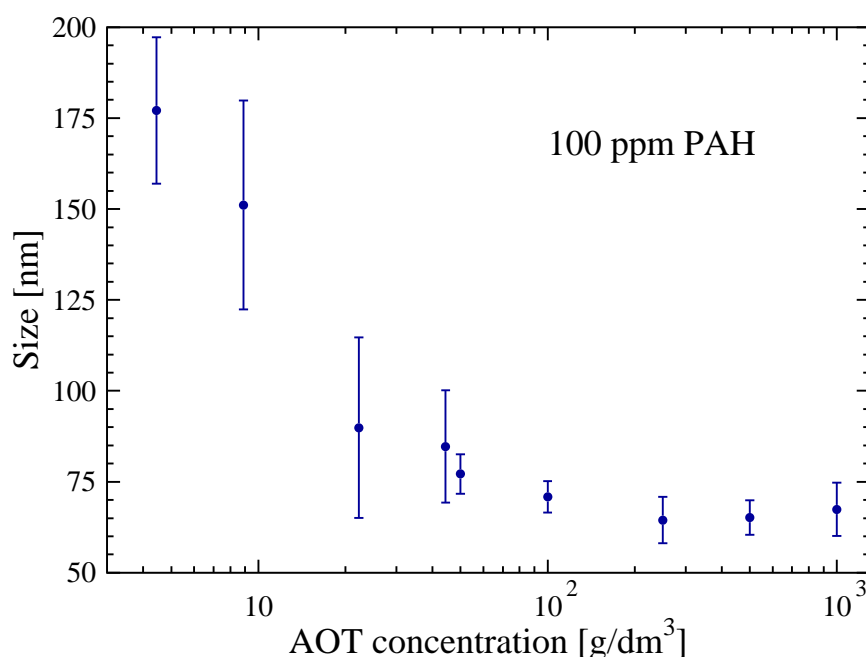**Figure 2.45:** A dependence of the emulsion size on the concentration of AOT for a fixed PAH concentration of 100 ppm.

the dependence of emulsion size on the concentration of AOT. One can see that the size of emulsion decreases with increasing AOT concentration. The minimum concentration of AOT necessary for the formation of stable emulsion was equal to 50 g/l. The samples containing lower concentration of AOT tended to destabilize after 1–2 days of storage at the room temperature. Above that threshold concentration, the obtained emulsions were stable over a long period of time. The increasing AOT concentration stopped to influence size of the emulsions at 250 g/l. That concentration of AOT in squalene was used for the further encapsulation of primary emulsion within the polyelectrolytes. The zeta potential of the emulsions did not seem to be affected by addition of AOT in the studied range of concentrations. Its value was rather constant at the level of about 90 mV, which is shown in Fig. 2.46.
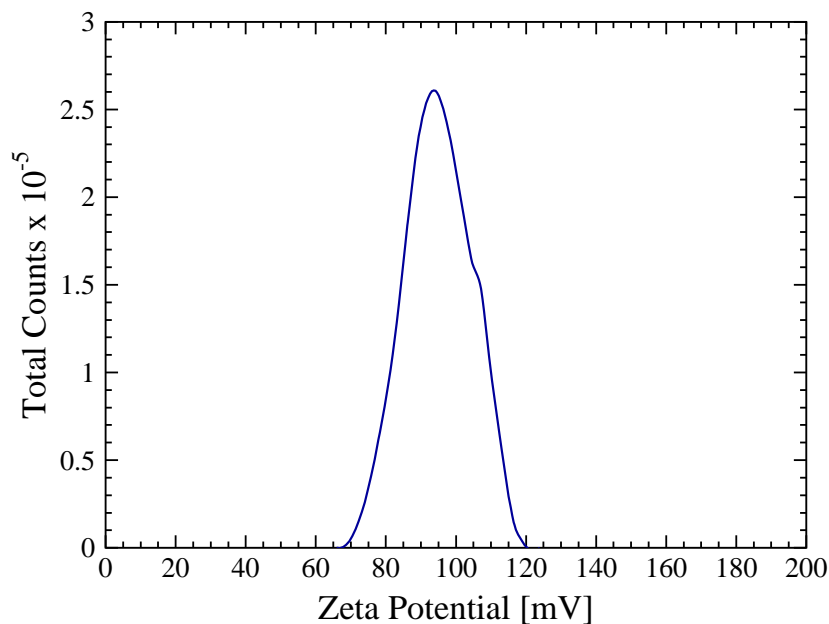
Figure 2.46: The distribution of zeta potential of the emulsions with AOT.

The size of the obtained emulsion droplets stabilized with AOT/PAH interfacial complex also depended on the concentration of polyelectrolyte. Figure 2.47 and Table 2.6
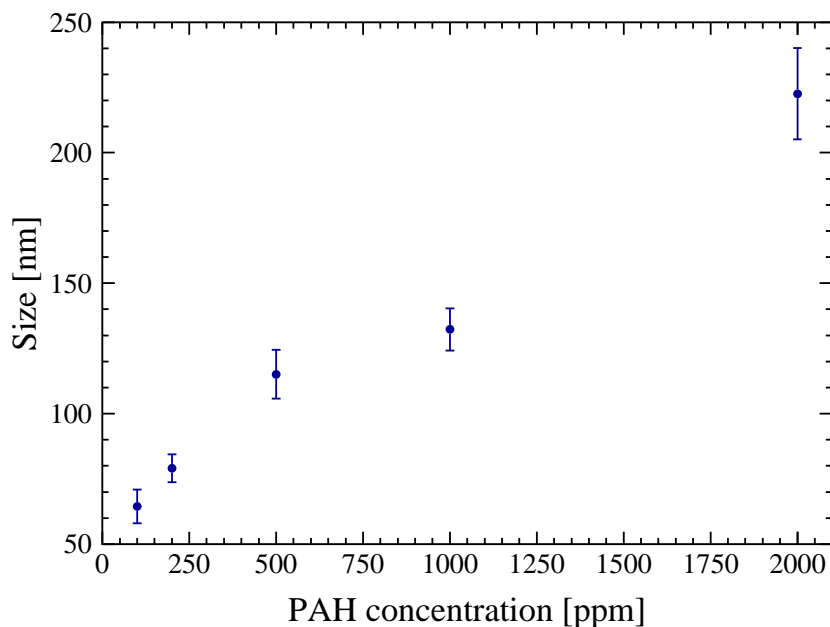
Figure 2.47: A dependence of the emulsion size on the PAH concentration.

present the results of these measurements. The higher was the concentration of polyelectrolyte, the bigger was the size of emulsion droplet. Changing PAH concentration from

PAH concentration [ppm]	Size [nm]	PDI
100	64.5	0.2
200	79	0.1
500	115	0.2
1000	132	0.2
2000	223	0.3

Table 2.6: A dependence of the emulsion size on the PAH concentration.

100 ppm to 2000 ppm resulted in variation of the droplet size from 65 nm up to 220 nm. The polydispersity index of all dispersions was lower than 0.3. The corresponding size distributions of the emulsions prepared at 100, 500, and 2000 ppm PAH are presented in Fig. 2.48. The emulsions formed at PAH concentration equal to 200 ppm were character-
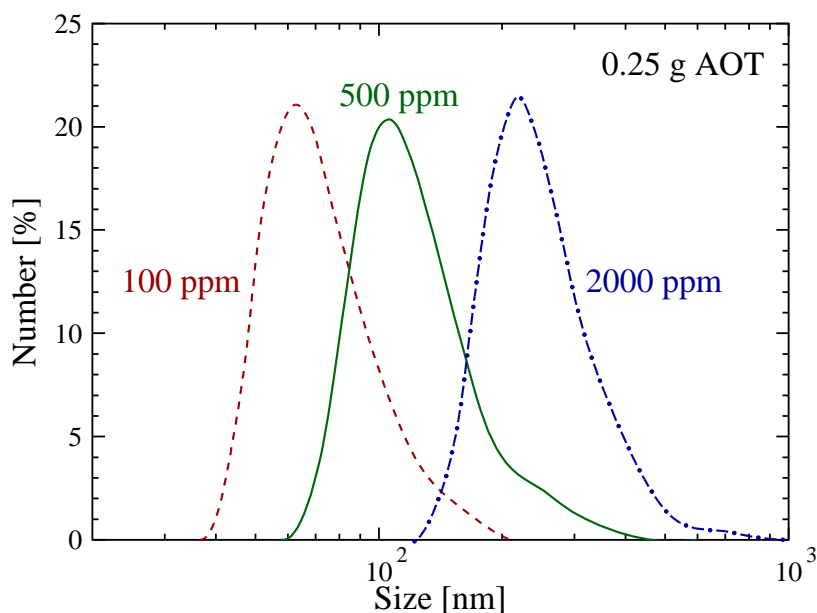
Figure 2.48: The size distributions for the 100 ppm, 500 ppm, and 2000 ppm PAH.

ized with low PDI (<0.2), while the average droplet size was around 80 nm. Later on, they were used for a further preparation of the multilayer capsules.

After the formation of the primary emulsion, the consecutive layers were formed using PAH/PSS in the concentration of 2000 ppm in the similar manner as described in the previous chapters. The nanoemulsion containing 250 g/l AOT and stabilized with 200 ppm PAH was added to the solution of negatively charged PSS in order to form the second

layer, and so forth. As presented in Fig. 2.49, deposition of polyelectrolytes on the oil
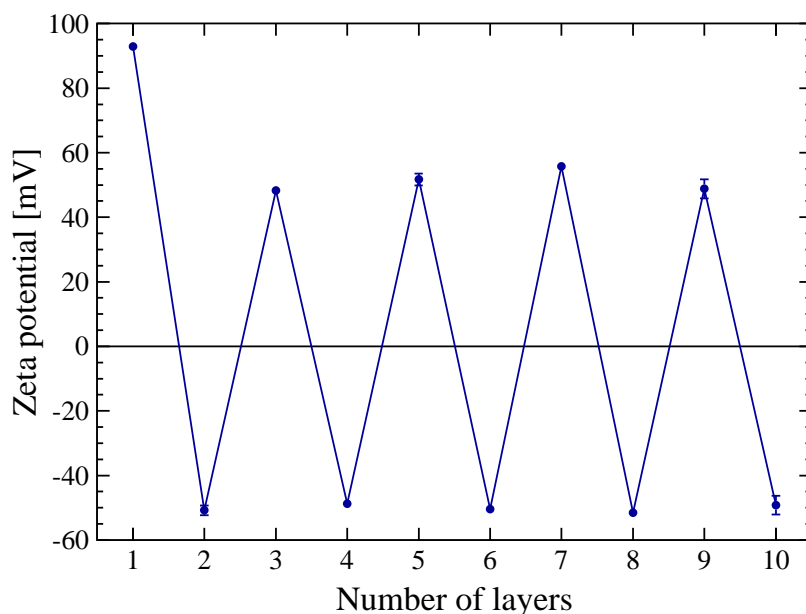
Figure 2.49: Changes of the zeta potential as a function of the number of polyelectrolyte layers.

core resulted in a characteristic layer-to-layer zigzag dependence of the zeta potential. The average size of nanocapsules with 5 layers was around 100 nm, while the size of ultimate capsules terminated with 10 layers was equal to 120 nm. Fig. 2.50 shows a typical size
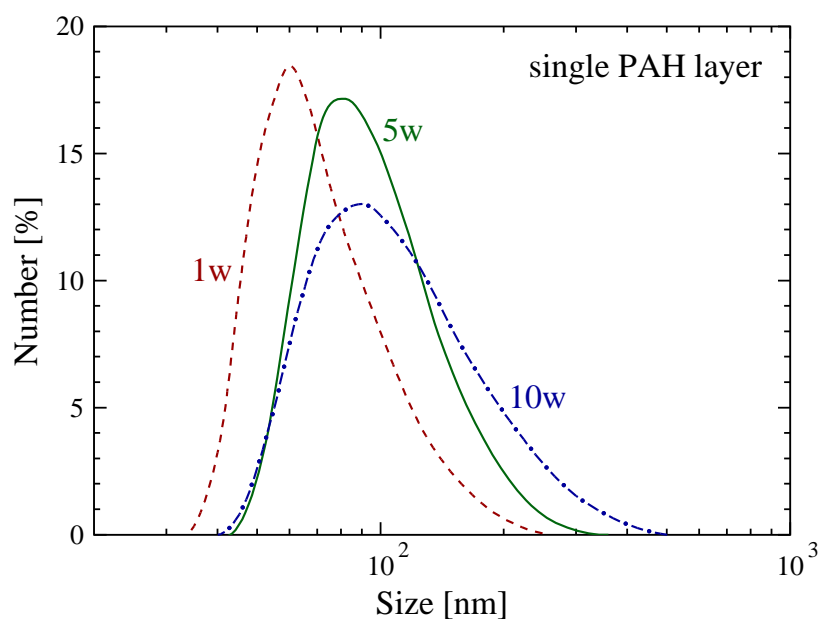
Figure 2.50: The size distributions of the capsules (1w, 5w, 10w).

distribution of the emulsion covered with a single PAH layer and the capsules with 5 and

10 layers of polyelectrolytes.

9.4.3 Elastic properties of the squalene-based capsules

The encapsulation of oil core within consecutive polyelectrolyte multilayers should be able to modify the mechanic rigidity of the capsules. Therefore, AFM force measurements were performed as the further evidence of multilayer shell formation. To this end, positively charged PAH-terminated capsules were deposited on mica surface and the cantilever deflection (DFL) was measured as a function of the scanner z-piezotube extension (height) for the chosen places in the sample. After the probe has touched the surface, any changes in the voltage applied to the scanner z-piezotube extension (height) causes a proportional change in the DFL signal. Before the force measurements, a preliminary scan (10 μm × 10 μm) of the positively charged PAH-terminated capsules deposited on mica was performed. The measurements were performed in a three randomly chosen places. A high resolution noncontact silicon cantilever (NSG01 series, spring constant $k = 3.21$ N/m, NT-MDT, Russia) was used in the experiments.
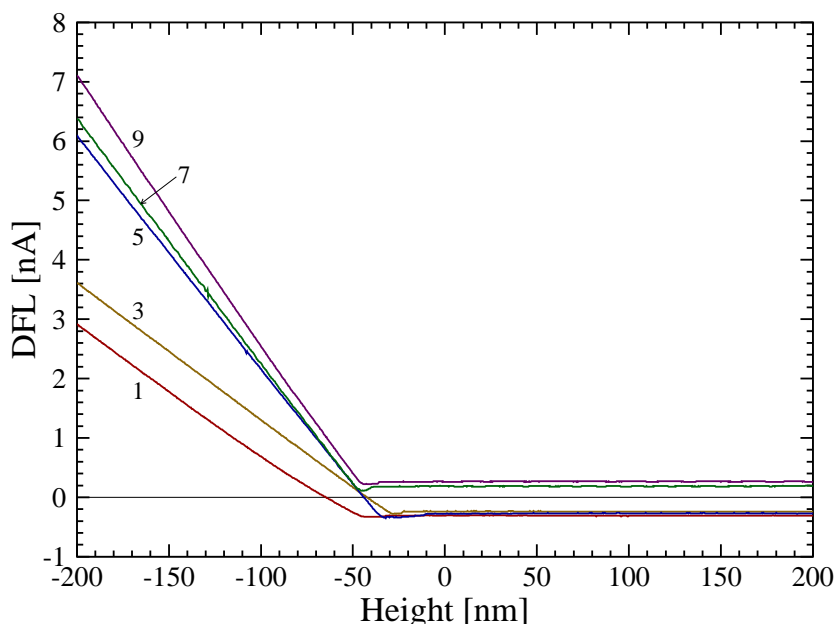
Figure 2.51: A comparison of the force-distance curves for the capsules terminated with 1, 3, 5, 7 and 9 layers of polyelectrolytes.

The slope of the force-distance curve in the contact region is a measure of samples' stiffness. In order to compare properties of all the measured samples, the average (from the three measurements) force-distance curves are summarized in Fig. 2.51. One can

see that the thicker is the shell of the capsule (more layers) the larger is the cantilever deflection. The steeper slope of the force curve indicates that the stiffness of examined sample has increased. A soft emulsion consisting from the oil core surrounded with only one layer of PAH showed a much smaller slope than the capsules terminated with 9 layers. The absolute values of the slope for all samples are gathered in Fig. 2.52. The slope and,
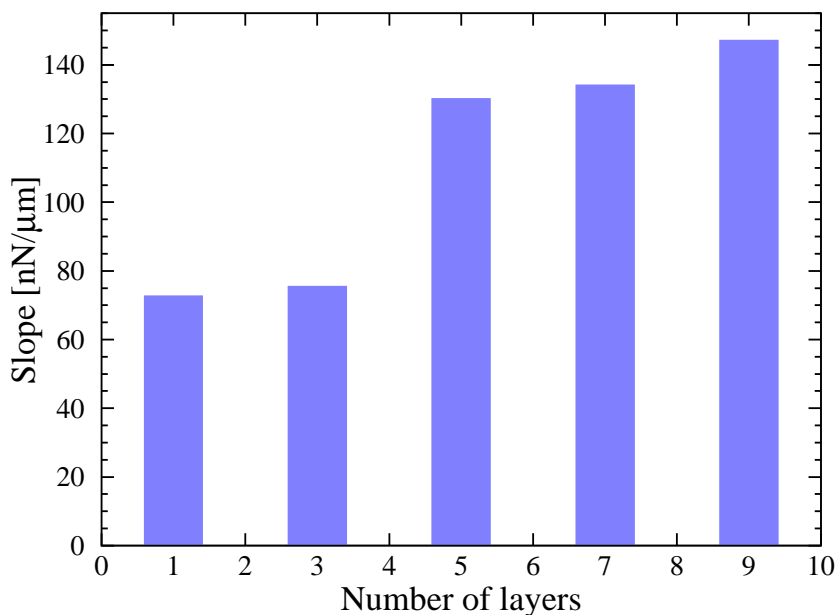
Figure 2.52: A comparison of the absolute slope of AFM approach DFL (height) curves for different samples.

therefore, the shell stiffness are raising with the increasing number of layers surrounding an oil core.

9.4.4 Encapsulation of model drugs in squalene based nanocapsules

Two different compounds — Naproxen and vitamin D — were selected as model hydrophobic drugs for encapsulation within the squalene core of the capsules. The drugs were dissolved in the oil phase prior to emulsification ($c = 0.5$ mg/ml). Then the oil core was encapsulated within polyelectrolytes according to the previously described saturation method. After encapsulation the UV-vis absorption spectra of suspensions were recorded. As the example, the spectra of squalene-based capsules with coating of five (PAH/PSS) bilayers are presented in Figs. 2.53 and 2.54. The characteristic absorption peak at 230 nm

was observed for Naproxen-containing capsules, while in the spectra obtained for empty
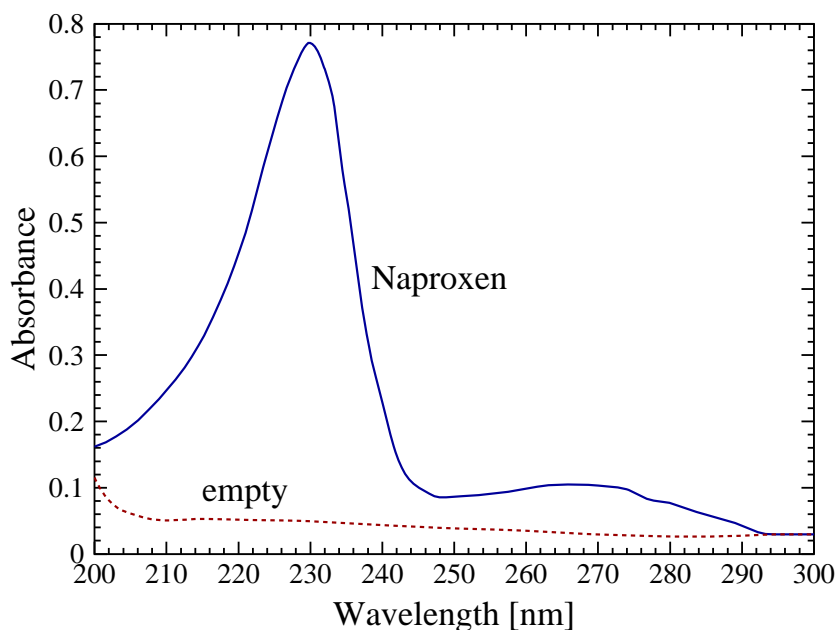
Figure 2.53: The UV-vis absorption spectra for the empty and Naproxen-loaded capsules that were terminated with five (PAH/PSS) bilayers.

capsules that peak was absent (see Fig. 2.53). Similarly, the capsules containing vitamin D exhibited a characteristic peak adsorption at 268 nm (c.f. Fig. 2.54). These results
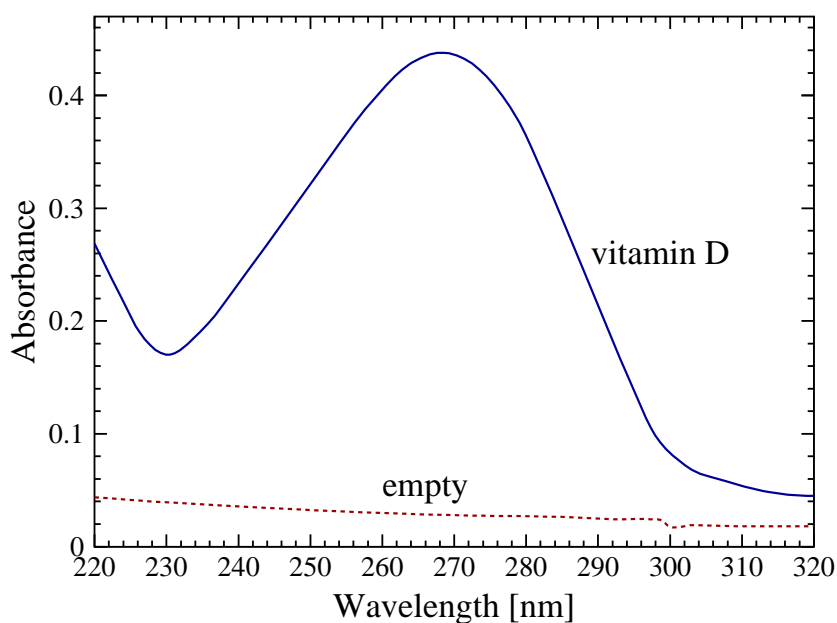
Figure 2.54: The UV-vis absorption spectra for the empty and vitamin D-loaded capsules that were terminated with five (PAH/PSS) bilayers.

proved the successful encapsulation of hydrophobic model drugs in the squalene core of nanocapsules.

10   Conclusions

Nanocarriers are of significant importance in drug delivery and imaging applications. In this work, different components (surfactants, polyelectrolytes, oils and nanoparticles) were used as a versatile tool for the formation of nanocapsules. Nanocapsules are a particular type of nanosized containers composed of a core surrounded by a polymeric shell. The core can be either solid (e.g., colloidal microspheres, nanoparticles) or liquid (emulsion droplets). A convenient method of a shell formation around a charged core is the layer-by-layer adsorption of polyelectrolytes. Encapsulation of active agents within the capsule's cavity aims for the protection of the load from the biological environment, reduction of its toxicity and interactions with the immune system, or regulation of release ratio of the encapsulated active component.

Nanocapsules based on both solid and liquid core were produced. Solid core nanocapsules were produced via direct encapsulation of hydrophilic quantum dots within the polyelectrolyte multilayer shell. In that case, a complex of quantum dots with oppositely charged polyelectrolyte was used as a core for further encapsulation. Liquid core nanocapsules were obtained by direct LbL encapsulation of emulsion droplets. Two methodologies of emulsification were proposed: spontaneous emulsification technique, also known as the "Ouzo effect", and membrane supported emulsification technique. The first method is based on the instantaneous formation of oil droplets dispersed in water after an organic phase consisting of oil in a water-miscible solvent is mixed with an aqueous phase. In the second technique, the phase to be dispersed is pressed through a microporous membrane into the continuous phase. The detachment of droplets from the membrane occurs due to the flow of the continuous phase. A necessary prerequisite for application of emulsions in pharmaceutical formulations is lack of their cytotoxicity; therefore, it is necessary that all compounds used in the formulation are non-toxic. Use of vegetable oils, such as linseed, soybean or jojoba bean oil, as well as surfactants of biological origin (cholesterol, lecithin) helps to meet that requirement.

The proposed methods of obtaining nanostructures using as the building blocks combination of various surfactants, polyelectrolytes and nanoparticles are not restricted to the materials used in this work. Any type of hydrophobic nanoparticles can be incorporated in the hydrophobic cores of emulsion based nanocapsules. On the other hand hydrophilic nanoparticles, as for example, iron oxide used for the purpose of magnetic imaging can

be either enclosed in the nanoparticles/polyelectrolyte core or directly embedded in the polymer shell formed by the LbL technique. The results of this work also demonstrate that microemulsification (Ouzo effect) or membrane emulsification are very convenient methods to obtain nano-or microsize emulsion droplets formed from natural oils with the perspective application as a drug carriers. Biocompatible or natural surfactants can be used for that purpose. The results of performed cytotoxicity tests demonstrated that such prepared nanostructures proved to be suitable for further testing and use in biomedical applications. The detailed conclusions concerning the methodologies of the nanostructures formation used in my work are as follows.

10.1 Encapsulation of hydrophilic quantum dots within polyelectrolyte multilayers

A simple and effective way of preparing the CdTe-labeled polyelectrolyte multilayer capsules using the layer-by-layer technique was proposed. The polymer nanocapsules were composed of 1–7 consecutive layers, either of the pair of synthetic polyelectrolytes PAH/PSS or of the biocompatible ones PLL/PGA. The size of obtained complexes was below 100 nm. The encapsulation of CdTe quantum dots within the first three layers of biocompatible polyelectrolytes (PLL, PGA) reduced their cytotoxicity. A further increase of the number of PE layers did not bring improvement in biocompatibility of the capsules. On the other hand, the capsules prepared with synthetic PAH and PSS regardless of the shell thickness were toxic to cells. The CdTe-labeled capsules of PLL/PGA with up to three layers did not bind to the blood cells, which allows considering their application for medical purposes.

10.2 Natural oil cores prepared by spontaneous emulsification technique

A spontaneous emulsification technique was used to produce nanoemulsions from natural oils such as linseed, soybean and jojoba bean oil. Depending on the parameters of the process, type of oil and oil-to-ethanol ratio, emulsions with various size and stability were obtained. The average droplet size of emulsions was in the range of 60–230 nm. The formation of fine emulsion droplets has been achieved even without the presence of sur-

factants. Addition of AOT, cholesterol and lecithin in various concentrations was found to have a positive influence on the size and polydispersity of the emulsions. Enclosing of the oil-soluble dye, Coumarin 6, in the emulsion droplets has confirmed the possibility of encapsulation of hydrophobic species. Due to the small size of the droplets and their low polydispersity, the emulsions were stable within the long period of time. The obtained emulsions had a stable surface charge, making them good candidates for further encapsulation of oil cores within polyelectrolytes. Formation of the first polyelectrolyte layer was demonstrated.

10.3 Linseed oil based nanocapsules as delivery system for hydrophobic quantum dots

Linseed oil based nanocapsules labeled with CdSe/ZnS quantum dots were produced using simple and effective, two steps procedure: preparation of emulsion core by the spontaneous emulsification technique and subsequent formation of the shell by layer-by-layer adsorption of polyelectrolytes. Fine emulsion droplets stabilized with lecithin had an average size of 100 nm, whereas the nanocontainers formed by a direct encapsulation of the linseed oil core within 1–4 consecutive layers of the biocompatible polyelectrolytes, poly-L-lysine hydrobromide and poly-d-glutamic acid sodium salt, had the size around 130 nm. Bare emulsion containing quantum dots and capsules with single poly-L-lysine layer proved to be toxic for NIH 3T3 mouse embryonic fibroblasts. On the other hand, linseed oil capsules with CdSe/ZnS enclosed in one or two (PLL/PGA) bilayers were non-toxic and did not affect the cell growth. Therefore, the produced nanocapsules can be useful as biocompatible drug delivery system for poorly water-soluble compounds, allowing to eliminate their potential toxic effects.

10.4 Preparation of squalene-based nanocapsules on membrane emulsification unit

The emulsions of squalene stabilized with AOT/PAH complex were produced using membrane emulsification technique. The emulsions were used for further preparation of PAH/PSS multilayer capsules using the layer-by-layer technique. The average size of nanocapsules with five layers was around 100 nm, while the size of ultimate capsules ter-

minated with five (PAH/PSS) bilayers was equal to 120 nm. Increase of the shell thickness enhanced the stiffness of the capsules, as confirmed by AFM force measurements. In order to demonstrate the possibility of encapsulating a hydrophobic active agent within the capsule's cavity, the antiflammatory drug Naproxen and the oil-soluble vitamin D were dissolved in squalene core prior to emulsification and their presence was confirmed with the UV-vis measurements.

Bibliography

[1] H. J. Butt, K. Graf, and M. Kappl, *Physics and Chemistry Interfaces* (Wiley-VCH Verlag & Co., 2003).

[2] D. Myers, *Surfaces, Interfaces, and Colloids: Principles and Applications* (John Wiley & Sons, 1999).

[3] M. Fanun, *Colloids in Drug Delivery* (CRC Press, 2010).

[4] E. Kissa, *Fluorinated Surfactants and Repellents* (CRC Press, 2001).

[5] R. Zana, *Gemini Surfactants: Synthesis, Interfacial and Solution-Phase Behavior* (CRC Press, 2003).

[6] I. Piirma, *Polymeric surfactants* (CRC Press, 1992).

[7] N. Kosaric, W. L. Cairns, and N. C. C. Gray, *Biosurfactants and Biotechnology* (Marcel Dekker, 1987).

[8] P. Krüger, J. E. Baatz, R. A. Dluhy, and M. Lösche, Biophys. Chem. **99**, 209 (2002).

[9] M. Fanun, *Colloids in Biotechnology* (CRC Press, 2011).

[10] C. Stubenrauch, Curr. Opin. Colloid Interface Sci. **6**, 160 (2001).

[11] M. J. Rosen and S. B. Sulthana, J. Colloid Interface Sci. **239**, 528 (2001).

[12] R. D. Swisher, *Surfactant Biodegradation* (CRC Press, 1986).

[13] M. J. Rosen, *Surfactants in Emerging Technologies* (Marcel Dekker, 1987).

[14] M. M. Rieger, *Surfactants in Cosmetics* (Marcel Dekker, 1985).

[15] J. W. Goodwin, *Colloids and Interfaces with Surfactants and Polymers* (John Wiley & Sons, 2004).

[16] K. Holmberg, *Handbook of Applied Surface and Colloid Chemistry* (John Wiley & Sons, 2002).

[17] D. Myers, *Surfactant Science and Technology* (John Wiley & Sons, 2006).

[18] S. Dukhin, G. Kretzschmar, and R. Miller, *Dynamics of Adsorption at Liquid Interfaces* (Elsevier, 1995).

BIBLIOGRAPHY

[19] P. C. Hiemenz and R. Rajagopalan, *Biosurfactants and Biotechnology* (Marcel Dekker, 1997).

[20] M. J. Rosen, *Surfactants and Interfacial Phenomena* (John Wiley & Sons, 2004).

[21] G. Para, E. Jarek, and P. Warszyński, Adv. Colloid Interface Sci. **122**, 39 (2006).

[22] W. C. Preston, J. Phys. Colloid Chem. **52**, 84 (1948).

[23] K. Hess, W. Philipoff, and H. Kiessig, Kolloid Z. **88**, 49 (1939).

[24] T. F. Tadros, *Applied Surfactants: Principles and Applications* (Wiley-VCH Verlag & Co., 2005).

[25] G. M. Cooper, *The Cell: a Molecular Approach* (ASM Press, 2000).

[26] S. D. Christian and J. F. Scamehorn, *Solubilization in Surfactant Aggregates* (CRC Press, 1995).

[27] R. M. Pashley and M. E. Karaman, *Applied Colloid and Surface Chemistry* (John Wiley & Sons, 2004).

[28] P. Becher, *Encyclopedia of Emulsion Technology* (Marcel Dekker, 1983).

[29] G. Gompper and M. Schick, *Self-assembling Amphiphilic Systems* (Academic Press, 1994).

[30] S. Matsumoto, Y. Kita, and D. Yonezawa, J. Colloid Interface Sci. **57**, 353 (1976).

[31] N. Garti, Colloids Surf. A **123-124**, 233 (1997).

[32] T. P. Hoar and J. H. Schulman, Colloids Surf. A **152**, 102 (1943).

[33] J. H. Schulman, W. Stoeckenius, and L. M. Prince, J. Phys. Chem. **63**, 1677 (1959).

[34] I. Danielsson and B. Lindman, Colloids Surf. B **3**, 391 (1943).

[35] J. Sjoblom, R. Linbergh, and S. E. Friberg, Adv. Colloid Interface Sci. **95**, 125 (1996).

[36] R. Strey, Prog. Colloid Polym. Sci. **272**, 1005 (1996).

[37] K. Bouchemal, S. Briancon, E. Perrier, and H. Fessi, Int. J. Pharm. **280**, 241 (2004).

[38] T. F. Tadros, P. Izquierdo, J. Esquena, and C. Solans, Adv. Colloid Interface Sci. **108-109**, 303 (2004).

[39] C. Solans, P. Izquierdo, J. Nolla, N. Azemar, and M. J. Garcia-Celma, Curr. Opin. Colloid Interface Sci. **10**, 102 (2005).

[40] G. Guglielmini, J. Clin. Dermatol. **26**, 341 (2008).

[41] S. Amselem and D. Friedman, in *Submicron emulsions in drug targeting and delivery*, edited by S. Benita (Harwood Academic Publishers, London, 1998), pp. 153–173.

[42] P. Fernandez, V. André, J. Rieger, and A. Kühnle, Colloids Surf. A **251**, 53 (2004).

[43] P. Walstra, in *Encyclopedia of Emulsion Technology*, edited by P. Becher (Marcel Dekker, New York, 1983), vol. II, pp. 57–77.

[44] P. Walstra and P. E. A. Smoulders, in *Modern Aspects of Emulsion Science*, edited by B. P. Binks (Royal Society of Chemistry, Cambridge, 1983), p. 56.

[45] M. Y. Levy and S. Benita, Int. J. Pharm. **54**, 103 (1989).

[46] M. Sznitowska, M. Gajewska, S. Janicki, A. Radwańska, and G. Lukowski, Eur. J. Pharm. Biopharm. **52**, 159 (2001).

[47] T. Hagigiy, T. Nassar, F. Behar-Cohen, G. Lambert, and S. Benita, Eur. J. Pharm. Biopharm. **70**, 248 (2008).

[48] S. Tamilvanan, S. Schmidt, R. H. Müller, and S. Benita, Eur. J. Pharm. Biopharm. **59**, 1 (2005).

[49] S. Mohan and G. Narsimhan, J. Colloid Interface Sci. **192**, 1 (1997).

[50] N. Anton et al., J. Control. Release **128**, 185 (2008).

[51] C. Bondy and K. Söllner, Trans. Faraday Soc. **31**, 835 (1935).

[52] T. S. H. Leong, T. J. Wooster, S. E. Kentish, and M. Ashokkumar, Ultrason. Sonochem. **16**, 721 (2009).

[53] S. E. Friberg and S. Jones, *Othmer Encyclopedia of Chemical Technology* (Kroschwith, J.I., 1994).

[54] S. M. Joscelyne and G. Trägårdh, J. Membr. Sci. **169**, 107 (2000).

[55] K. Kandori, in *Food Processing: Recent Developments*, edited by A. G. Goankar (Elsevier Science, Amsterdam, 1995), pp. 113–142.

[56] V. Schröder, O. Behrend, and H. Schubert, J. Colloid Interface Sci. **202**, 334 (1998).

[57] S. J. Peng and R. A. Williams, Chem. Eng. Res. Des. **76**, 894 (1998).

[58] T. Nakashima, M. Shimizu, and M. Kukizaki, *Membrane emulsification: Operation manual, 1st edition*, Industrial Research Institute of Miyazaki Prefecture, Miyazaki, Japan (1991).

[59] T. Nakashima, M. Shimizu, and M. Kukizaki, Key Eng. Mat. **61/62**, 513 (1991).

[60] Y. Mine, M. Shimizu, and T. Nakashima, Colloids Surf. B **6**, 261 (1996).

BIBLIOGRAPHY

[61] K. Kandori, K. Kishi, and T. Ishikawa, Colloid Surface **61**, 269 (1991).

[62] R. Katoh, Y. Asano, A. Furuya, K. Sotoyama, and M. Tomita, J. Membr. Sci. **113**, 131 (1996).

[63] R. A. Williams, S. J. Peng, D. A. Wheeler, N. C. Morley, D. Taylor, M. Whalley, and D. W. Houldsworth, Chem. Eng. Res. Des. **76**, 902 (1998).

[64] E. Dickinson, in *Controlled Particle, Droplet and Bubble Formation*, edited by D. J. Wedlock (Butterworth–Heinemann, Oxford, 1994), chap. 7, pp. 189–216.

[65] K. Shinoda and H. Saito, J. Colloid Interface Sci. **26**, 70 (1968).

[66] T. Föster and H. Tesmann, Cosmet. Toiletries **106**, 49 (1991).

[67] I. Solè, A. Maestro, C. González, C. Solans, and J. M. Gutiérrez, Langmuir **22**, 8326 (2006).

[68] T. Föster, W. Von Rybinski, H. Tesmann, and A. Wadle, Int. J. Cosmetic Sci. **16**, 84 (1994).

[69] D. J. Miller, T. Henning, and W. Grünbein, Colloids Surf. A **183-185**, 681 (2001).

[70] C. A. Miller, Colloid Surface **29**, 89 (1988).

[71] S. A. Vitale and J. L. Katz, Langmuir **19**, 4105 (2003).

[72] F. Ganachaud and J. L. Katz, Chem. Phys. Chem. **6**, 209 (2005).

[73] R. G. Kelmann, G. Kuminek, H. F. Teixeira, and L. S. Koester, Int. J. Pharm. **342**, 231 (2007).

[74] K. J. Ruschak and C. A. Miller, Ind. Eng. Chem. Fund. **11**, 534 (1972).

[75] J. C. Lopez-Montilla, P. E. Herrera-Morales, S. Pandey, and D. O. Shah, J. Dispersion Sci. Technol. **23**, 219 (2002).

[76] E. Rubin and C. J. Radke, Chem. Eng. Sci. **35**, 1129 (1980).

[77] M. El-Aasser, C. D. Lack, J. W. Vanderhoff, and F. M. Fowkes, Colloid Surface **29**, 103 (1986).

[78] M. Trotta, M. Gallarate, F. Pattarino, and S. Morel, J. Control. Release **76**, 119 (2001).

[79] M. Ostrovsky and R. Good, J. Colloid Interface Sci. **102**, 206 (1984).

[80] N. S. S. Magalh aes, A. Pontes, V. M. V. Pereira, and N. P. Caetano, Int. J. Pharm. **208**, 71 (2000).

[81] D. Fasolo, L. Schwingel, M. Holzschuh, V. Bassani, and H. Teixeira, J. Pharm. Biomed. Anal. **44**, 1174 (2007).

[82] L. L. Schramm, *Emulsions, Foams and Suspensions: Fundamentals and Applications* (Wiley-VCH, 2005).

[83] S. Ross and I. D. Morrison, *Colloidal Systems and Interfaces* (Wiley, New York, 1988).

[84] P. Becher, *Emulsions: Theory and Practice* (American Chemical Society, Washington, 2001), 3rd ed.

[85] W. C. Griffin, J. Soc. Cosmet. Chem. **1**, 311 (1949).

[86] W. D. Bancroft, J. Phys. Chem. **17**, 501 (1913).

[87] W. D. Bancroft, J. Phys. Chem. **19**, 275 (1915).

[88] E. Ruckenstein, Langmuir **12**, 6351 (1996).

[89] J. T. Davies, in *Proceedings of the International Congress of Surface Activity* (1957), pp. 426–438.

[90] J. L. Salager, L. Morgan, R. S. Schechter, W. H. Wade, and E. Vasquez, Soc. Petrol. Eng. J. **19**, 107 (1979).

[91] P. Taylor, Adv. Colloid Interface Sci. **75**, 107 (1998).

[92] M. von Smoluchowski, Phys. Z **17**, 557 (1916).

[93] J. N. Israelachvili, *Intermolecular and surface forces* (Academic Press, London, 1992).

[94] Z. Adamczyk, *Particles at interfaces. Interactions, deposition, structure* (Academic Press Elsevier, 2006).

[95] G. Gouy, J. Phys.-Paris **9**, 457 (1910).

[96] D. L. Chapman, Philos. Mag. **25**, 475 (1913).

[97] J. Lyklema, *Fundamentals of Interface and Colloid Science*, vol. 1 (Academic Press, London, 1991).

[98] D. C. Graham, Chem. Rev. **41**, 441 (1947).

[99] R. J. Hunter, *Zeta potential in colloid science: principles and applications* (Academic Press, London, 1981).

[100] E. J. W. Verwey and J. T. G. Overbeek, *Stability of Lyophobic Colloids* (Elsevier, Amsterdam, 1948).

[101] B. V. Derjaguin and L. D. Landau, Acta Physicochimica URSS **14**, 633 (1941).

[102] S. Forster and M. Schmidt, Adv. Polym. Sci. **120**, 51 (1995).

BIBLIOGRAPHY

[103] T. Radeva, *Physical chemistry of polyelectrolytes* (Marcel Dekker, New York, 2001).

[104] G. Decher and J. B. Schlenoff, *Multilayer thin films* (Wiley-VCH, Weinheim, 2003).

[105] A. V. Dobrynin and M. Rubinstein, Prog. Polym. Sci. **30**, 1049 (2005).

[106] S. K. Tripathy, J. Kumar, and H. S. Nalwa, *Handbook of polyelectrolytes and their applications* (American Scientific Publishers, 2002).

[107] B. Jachimska, T. Jasiński, P. Warszyński, and Z. Adamczyk, Colloids Surf. A **355**, 7 (2010).

[108] J. Koetz and S. Kosmella, *Polyelectrolytes and Nanoparticles* (Springer-Verlag, Heidelberg, 2001).

[109] Y. Lvov, K. Ariga, I. Ichinose, and T. Kunitake, J. Am. Chem. Soc. **117**, 6117 (1995).

[110] G. Decher and J. Schmitt, Prog. Polym. Sci. **89**, 160 (1992).

[111] S. Anandhakumar, V. Nagraja, and A. M. Raichur, Colloids Surf. B **78**, 266 (2010).

[112] J. Lyklema, *Fundamentals of interface and colloid science: solid-liquid interfaces* (Academic Press, London, 1995).

[113] M. Kawaguchi and A. Takahashi, Adv. Colloid Interface Sci. **37**, 219 (1992).

[114] R. R. .Netz and D. Andelman, Phys. Rep. Rev. Sect. Phys. Lett. **380**, 1 (2003).

[115] J. L. Brash and T. A. Horbett, *Proteins at interfaces II: fundamentals and applications* (American Chemical Society, Washington, 1995).

[116] A. V. Dobrynin, A. Deshkovski, and M. Rubinstein, Macromolecules **34**, 3421 (2001).

[117] R. Advincula, E. Aust, W. Meyer, and W. Knoll, Langmuir **12**, 3536 (1996).

[118] P. Bertrand, A. Jonas, A. Laschewsky, and R. Legras, Macromol. Rapid Commun. **21**, 319 (2000).

[119] F. Caruso, E. Rodda, D. Furlong, K. Niikura, and Y. Okahata, Anal. Chem. **69**, 2043 (1997).

[120] T. Plech, C. Salditt, C. Münster, and J. Peisl, J. Colloid Interface Sci. **74**, 223 (2000).

[121] S. T. Dubas and J. B. Schlenoff, Macromolecules **32**, 8153 (1999).

[122] G. Decher, Science **277**, 1232 (1997).

[123] G. Decher, J. D. Hong, and J. Schmitt, Thin Solid Films **210**, 831 (1992).

[124] Y. Lvov, H. Haas, G. Decher, and H. Möhwald, J. Phys. Chem. **97**, 12835 (1993).

[125] N. G. Hoogeveen, M. A. C. Stuart, G. J. Fleer, and M. R. Böhmer, Langmuir **12**, 3675 (1996).

[126] M. Kolasińska and P. Warszyński, Appl. Surf. Sci. **252**, 759 (2005).

[127] M. Kolasińska and P. Warszyński, Bioelectrochemistry **66**, 65 (2005).

[128] M. Elżbieciak, M. Kolasińska, and P. Warszyński, Colloids Surf. A **321**, 258 (2008).

[129] M. Kolasińska, R. Krastev, and P. Warszyński, J. Colloid Interface Sci. **305**, 46 (2007).

[130] V. A. Kabanov, Macromol. Chem. **8**, 121 (1973).

[131] V. A. Kabanov and A. B. Zezin, Macromol. Chem. **6**, 259 (1984).

[132] A.Kossel, J. Phys. Chem. **22**, 178 (1896).

[133] H. G. B. de Jong, Trans. Faraday Soc. **28**, 27 (1932).

[134] A. S. Michaels and R. G. Miekka, J. Phys. Chem. **65**, 1765 (1961).

[135] E. Bekturov and A. Bakauova, *Synthetic water soluble polymers in solution* (Hütig and Wopf Verlag, Berlin, 1986).

[136] B. Philipp, H. Dautzenberg, K. Linow, J. Kötz, and W. Dawydoff, Prog. Polym. Sci. **14**, 823 (1998).

[137] C. Davison, K. E. Smith, L. E. F. Hutchinson, J. E. O'Mullane, K. Petrak, and S. E. Harding, J. Bioact. Compat. Polym. **5**, 267 (1990).

[138] E. D. Goddard, J. Am. Oil Chem. Soc. **71**, 1 (1994).

[139] P. M. Holland and D. N. Rubingh, *Cationic surfactants: physical chemistry* (Marcel Dekker, New York, 1991).

[140] E. D. Goddard, Colloid Surface **19**, 301 (1986).

[141] P. Hansson and M. Almgren, Langmuir **10**, 2115 (1994).

[142] J. Liu, N. Takisawa, and K. Shirahama, J. Phys. Chem. **101**, 7520 (1997).

[143] A. Malovikova and K. Hayakawa, J. Phys. Chem. **88**, 1930 (1984).

[144] P. L. Dubin and R. Oteri, J. Colloid Interface Sci. **95**, 453 (1983).

[145] J. Liu, N. Takisawa, H. Kodami, and K. Shirahama, Langmuir **14**, 4489 (1998).

[146] K. Shirahama, *Polymer-surfactant systems* (Marcel Dekker, New York, 1998).

[147] J. P. Chapel and J. F. Berret, Curr. Opin. Colloid Interface Sci. **17**, 97 (2012).

[148] N. C. Tansil and Z. Gao, Nano Today **1**, 28 (2006).

[149] H. C. Huang, S. Barua, D. B. Kay, and K. Rege, ACS Nano **3**, 2941 (2009).

[150] G. Schneider and G. Decher, Langmuir **24**, 1778 (2008).

[151] J. Hierrezuelo, A. Sadeghpour, I. Szilagyi, A. Vaccaro, and M. Borkovec, Langmuir **26**, 15109 (2010).

[152] A. Dorris, S. Rucareanu, L. Reven, C. J. Barrett, and R. B. Lennox, Langmuir **24**, 2532 (2008).

[153] S. R. Gray and C. B. Ritchie, Colloids Surf. A **273**, 184 (2006).

[154] S. R. Gray, N. S. C. Becker, N. A. Booker, and A. Davey, Colloids Surf. A **298**, 262 (2007).

[155] H. Saveyn, S. Meersseman, O. Thas, and P. V. der Meeren, Colloids Surf. A **262**, 40 (2005).

[156] Z. S. Wang, M. T. Hung, and J. C. Liu, Water Sci. Technol. **56**, 125 (2007).

[157] R. Greenwood and K. Kendall, Powder Technol. **113**, 148 (2000).

[158] J. Porubská, B. Alince, and T. G. M. van de Ven, Colloids Surf. A **210**, 223 (2002).

[159] O. J. Rojas and R. D. Neuma, Colloids Surf. A **155**, 419 (1999).

[160] J. L. Ortega-Vinuesa, A. Martin-Rodriguez, and R. Hidalgo-Álvarez, J. Colloid Interface Sci. **184**, 259 (1996).

[161] A. Hess, M. Pretzl, L. Heymann, A. Fery, and N. Aksel, Phys. Rev. E: Stat. Nonlin. Soft Matter Phys. **84(3Pt1)**, 031407 (2011).

[162] B. A. Bolton, D. R. Dixon, S. R. Gray, C. Ha, P. J. Harbour, N. Le, and A. J. Ware, Water Sci. Technol. **34**, 117 (1996).

[163] Q. Zhao, Q. F. An, Y. Li, J. Quian, and C. Gao, J. Membr. Sci. **379**, 19 (2011).

[164] X. Li, W. Goyens, P. Ahmadiannamini, W. Vanderlinden, S. D. Feyter, and I. Vankelecom, J. Membr. Sci. **358**, 150 (2010).

[165] M. Yamada and S. Shiratori, Sens. Actuators B **64**, 124 (2000).

[166] C. W. Lee, Y. Kim, S. W. Joo, and M. S. Gong, Sens. Actuators B **88**, 21 (2003).

[167] A. H. Jafari, S. M. A. Hosseini, and E. Jamalizadeh, Electrochim. Acta **55**, 9004 (2010).

[168] L. Zhang, Y. Li, J. Sun, and J. Shen, J. Colloid Interface Sci. **319**, 302 (2008).

[169] P. V. Pavoor, B. P. Gearing, A. Bellare, and R. E. Cohen, Wear **256**, 1196 (2004).

[170] G. Decher, M. Eckle, J. Schmitt, and B. Struth, Curr. Opin. Colloid Interface Sci. **3**, 32 (1998).

[171] D. J. Liaw, K. L. Wang, Y. C. Huang, K. R. Lee, J. Y. Lai, and C. S. Ha, Prog. Polym. Sci. **37**, 907 (2012).

[172] S. Hrapovic, Y. Liu, G. Enright, F. Bensebaa, and J. H. T. Luong, Langmuir **19**, 3958 (2003).

[173] G. Decher, B. Lehr, K. Lowack, Y. Lvov, and J. Schmitt, Biosens. Bioelectron. **9**, 677 (1994).

[174] M. J. Tapia, M. Montserin, A. J. M. Valente, H. D. Burrows, and R. Mallavia, Adv. Colloid Interface Sci. **158**, 94 (2010).

[175] Y. Li, L. Lu, H. Zhang, and J. Wang, Colloids Surf. B **93**, 121 (2012).

[176] E. M. Saurer, D. Yamanouchi, B. Liu, and D. M. Lynn, Biomaterials **32**, 610 (2011).

[177] C. M. Jewell, J. Zhang, N. J. Fredin, and D. M. Lynn, J. Control. Release **106**, 214 (2005).

[178] Q. Tan, J. Ji, M. A. Barbosa, C. Fonseca, and J. Shen, Biomaterials **24**, 4699 (2003).

[179] M. Cécius and C. Jérôme, Prog. Org. Coat. **70**, 220 (2011).

[180] M. Oćwieja, Z. Adamczyk, M. Morga, and A. Michna, J. Colloid Interface Sci. **364**, 39 (2011).

[181] N. A. Samoilova, M. A. Krayukhina, S. P. Novikova, T. A. Babushkina, I. O. Volkov, L. I. Komarova, L. I. Moukhametova, R. B. Aisina, E. A. Obraztsova, I. V. Yaminsky, et al., J. Biomed. Mater. Res. **82**, 589 (2007).

[182] T. Mauser, C. Déjugnat, H. Möhwald, and G. B. Sukhorukov, Langmuir **20**, 5888 (2006).

[183] D. G. Shchukin and T. Shutava, Chem. Mater. **16**, 3446 (2004).

[184] A. Voigt, H. Lichtenfeld, G. B. Sukhorukov, H. Zastrow, E. Donath, H. Baumler, and H. Möhwald, Ind. Eng. Chem. Res. **38**, 4037 (1999).

[185] L. S. A. B. C. Yu, *Dekker Pharmaceutical Technology: Biopharmaceutics. Dekker Encyclopedias* (Taylor and Francis Books, New York, 2002).

[186] E. S. Papazoglou and A. Parthasarathy, *Bionanotechnology* (Morgan & Claypool, 2007).

[187] A. Lee and L. Lee, *Onco-Imaging, Medicine-Hematology/Oncology* (Springer, Berlin, 2006).

[188] O. M. Koo, I. Rubinstein, and H. Onyuksel, Nanomed. Nanotechnol. **1**, 193 (2005).

BIBLIOGRAPHY

[189] D. J. Brayden, Drug Discovery Today **8**, 976 (2003).

[190] F. Chellat, Y. Merhi, A. Moreau, and L. H. Yahia, Biomaterials **26**, 7260 (2005).

[191] A. Nagayasu, K. Uchiyama, and H. Kiwada, Adv. Drug Deliv. Rev. **40**, 75 (1999).

[192] J. Rejman, M. Conese, and D. Hoekstra, J. Liposome Res. **16**, 237 (2006).

[193] L. Brannon-Peppas and J. O. Blanchette, **56**, 1649 (2004).

[194] S. Ma, J. Zhou, Y. C. Kang, J. E. Reddic, and D. A. Chen, Langmuir **20**, 9686 (2004).

[195] J. H. Park, S. Lee, J. H. Kim, K. Park, K. Kim, and I. C. Kwon, Prog. Polym. Sci. **33**, 113 (2008).

[196] J. Khandare and T. Minko, Prog. Polym. Sci. **31**, 359 (2006).

[197] E. Ruoslahti, Nat. Rev. Cancer **2**, 83 (2002).

[198] S. Sengupta, D. Eavarone, I. Capila, G. Zhao, N. Watson, and T. Kiziltepe, Nature **436**, 568 (2005).

[199] R. Duncan, Nat. Rev. Drug Discov. **2**, 347 (2003).

[200] B. E. Oeffinger and M. A. Wheatley, Ultrasonics **42**, 343 (2004).

[201] J. Holash, P. C. Maisonpierre, D. Compton, P. Boland, C. R. Alexander, and D. Zagzag, Science **284**, 1994 (1999).

[202] Y. Matsumura and H. Maeda, Cancer Res. **46**, 6387 (1986).

[203] H. Maeda, Adv. Enzyme Regul. **41**, 189 (2001).

[204] M. V. Lozano, D. Torrecilla, D. Torres, A. Vidal, F. Dominguez, and M. J. Alonso, Biomacromolecules **9**, 2186 (2008).

[205] S. Maillard, T. Ameller, J. Gauduchon, A. Gougelet, F. Gouilleux, P. Legrand, V. Marsaud, E. Fattal, B. Sola, and J. M. Renoir, J. Steroid Biochem. **94**, 111 (2005).

[206] L. Yang and P. Alexandridis, Curr. Opin. Colloid Interface Sci. **5**, 132 (2000).

[207] D. J. Burgess, *Encyclopedia of Pharmaceutical Technology* (Informa Healthcare, London, 2007).

[208] M. D. Brown, Int. J. Pharm. **229**, 1 (2001).

[209] M. Ogris, S. Brunner, S. Schuller, R. Kirchejs, and E. Wagner, Gene Ther. **6**, 595 (1999).

[210] C. Plank, K. Mechtler, F. C. S. Jr, and E. Wagner, Hum. Gene Ther. **7**, 1437 (1996).

[211] M. Ogris and E. Wagner, Drug Discov. Today **7**, 479 (2002).

[212] G. M. Barratt, Pharm. Sci. Technol. Today **3**, 163 (2000).

[213] J. Swarbrick and A. Martin, *Colloids in Physical Pharmacy* (PA: Lea & Febiger, Philadelphia, 1991).

[214] J. Wong, A. Brugger, A. Khare, and M. Chaubal, Adv. Drug Deliv. Rev. **60**, 939 (2008).

[215] J. B. Diane, *Encyclopedia of Pharmaceutical Technology* (Informa Healthcare, 2007).

[216] V. Patravale and M. Joshi, in *Colloids in Drug Delivery*, edited by M. Fanun (Boca Raton: CRC Press, 2010), pp. 563–611.

[217] P. Rivera-Gil, L. L. D. Mercato, P. del Pino, A. Munoz-Javier, and W. J. Parak, Nano Today **3-4**, 12 (2008).

[218] H. E. Schaefer, *Nanoscience: The Science of the Small in Physics, Engineering, Chemistry, Biology and Medicine* (Springer-Verlag, Berlin Heidelberg, 2010).

[219] R. J. Byers and E. R. Hitchman, Prog. Histochem. Cyto. **45**, 201 (2011).

[220] S. K. Sahoo and V. Labhaserwar, Drug Discov. Today **8**, 1112 (2003).

[221] J. D. Carter, N. N. Cheng, Y. Qu, G. D. Suarez, and T. Guo, J. Phys. Chem. B **111**, 11622 (2007).

[222] P. Juzenas, W. Chen, Y. P. Sun, M. A. N. Coelho, R. Generalov, N. Generalova, and I. L. Christensen, Adv. Drug Deliv. Rev. **60**, 1600 (2008).

[223] W. C. Chan, D. J. Maxwell, X. Gao, R. E. Bailey, M. Han, and S. Nie, Curr. Opin. Biotechnol. **13**, 40 (2002).

[224] F. Pinaud, S. Clarke, A. Sittner, and M. Dahan, Nat. Methods **7**, 275 (2010).

[225] B. O. Daboussi, J. Rodriguez-Viejo, F. V. Mikulec, J. R. Heine, H. Matoussi, R. Ober, K. F. Jensen, and M. G. Bawendi, J. Phys. Chem. B **101**, 9463 (1997).

[226] A. M. Smith, H. Duan, A. M. Mohs, and S. Nie, Adv. Drug Deliv. Rev. **60**, 1226 (2008).

[227] X. H. Zhong, Y. Y. Feng, W. Knoll, and M. Y. Han, J. Am. Chem. Soc. **125**, 13559 (2003).

[228] J. Pietryga, R. Schaller, D. Werder, M. Stewart, V. Klimov, and J. Hollingsworth, J. Am. Chem. Soc. **126**, 11752 (2004).

[229] A. Juarranz, P. Jaen, F. Sanz-Rodriguez, J. Cuevas, and S. Gonzalez, Clin. Trans. Oncol. **10**, 148 (2008).

BIBLIOGRAPHY

[230] M. Niedre, M. S. Patterson, and B. C. Wilson, Photochem. Photobiol. **75**, 382 (2002).

[231] S. J. Clarke, C. A. Hollmann, Z. Zhang, D. Suffern, S. E. Bradforth, N. M. Dimitrijevic, W. G. Minarik, and J. L. Nadeau, Nat. Mater. **5**, 409 (2006).

[232] A. C. Samia, X. Chen, and C. Burda, J. Am. Chem. Soc. **125**, 15736 (2003).

[233] A. L. Efros, Sov. Phys. Semicond. **16**, 772 (1982).

[234] A. I. Ekimov, A. L. Efros, and A. A. Onushchenko, Solid State Commun. **56**, 921 (1985).

[235] A. P. Alivisatos, Science **271**, 933 (1996).

[236] D. Crouch, S. Norager, P. O'Brien, J. H. Park, and N. Pickett, Philos. Trans. R. Soc. London **361**, 297 (2003).

[237] P. Bhattacharya, S. Ghosh, and A. D. Stiff-Roberts, Annu. Rev. Mater. Res. **34**, 1 (2004).

[238] M. G. Bawendi, NATO Asi Ser. **340**, 339 (1995).

[239] M. Bruchez, M. Moronne, P. Gin, S. Weiss, and A. P. Alivisatos, Science **281**, 2013 (1998).

[240] W. C. W. Chan and S. M. Nie, Science **281**, 2016 (1998).

[241] S. K. Mahto, C. Park, T. H. Yoon, and S. W. Rhee, Toxicol. in Vitro **24**, 1070 (2010).

[242] X. H. Gao, Y. Y. Cui, R. M. Levenson, L. W. K. Chung, and S. M. Nie, Nat. Biotechnol. **22**, 969 (2004).

[243] B. Dubertret, P. Skourides, D. J. Norris, V. Noireaux, A. H. Brivanlou, and A. Libchaber, Science **298**, 1759 (2002).

[244] F. Pinaud, D. King, H. P. Moore, and S. Weiss, J. Am. Chem. Soc. **126**, 6115 (2004).

[245] Y. Liang, Y. Yu, Y. Cao, X. Hu, J. Wu, W. Wang, and D. E. Finlow, Spectrochim. Acta A **75**, 1617 (2010).

[246] A. Sukhanova and I. Nabiev, Crit. Rev. Oncol. Hematol. **68**, 39 (2008).

[247] K. M. S. O'Connell, A. S. Rolig, J. D. Whitesell, and M. M. Tamkun, J. Neurosci. **26**, 9609 (2006).

[248] C. Kirchner, T. Liedl, S. Kudera, T. Pellegrino, A. Munoz-Javier, H. E. Gaub, S. Stölzle, N. Fertig, and W. J. Parak, Nano Lett. **5**, 331 (2005).

164

[249] C. Kirchner, A. Munoz-Javier, A. S. Susha, A. L. Rogach, O. Kreft, G. B. Sukhorukov, and W. J. Parak, Talanta **67**, 486 (2005).

[250] J. W. Lee, K. Cho, H. Kim, J. H. Kim, B. Park, T. Noh, S. H. Kim, and S. Kim, J. Appl. Phys. **44**, 7694 (2005).

[251] Y. P. Sun, B. Zhou, Y. Lin, W. Wang, K. A. Fernando, P. Pathak, M. J. Meziani, B. A. Harruff, X. Wang, H. Wang, et al., J. Am. Chem. Soc. **128**, 7756 (2006).

[252] R. Hardman, Environ. Health Perspect. **114**, 165 (2006).

[253] A. M. Derfus, W. C. Chan, and S. Bhatia, Nano Lett. **4**, 11 (2004).

[254] O. Carion, B. Mahler, T. Pons, and B. Dubertret, Nano Protoc. **2**, 2383 (2007).

[255] D. Thorek, Ann. Biomed. Eng. **34**, 23 (2006).

[256] W. J. Rogers and P. Basu, Atherosclerosis **178**, 67 (2005).

[257] Z. G. Forbes, in *School of Biomedical Engineering, Science and Health System* (Drexel University, Philadelphia, 2005), p. 139.

[258] C. Wilhelm and F. Gazeau, J. Magn. Magn. Mater. **321**, 671 (2009).

[259] A. Jordan, P. Wust, H. Fahling, W. John, A. Hinz, and R. Felix, Int. J. Hyperthermia **9**, 51 (1993).

[260] J. P. Fortin, C. Wilhelm, J. Servais, C. Menager, J. C. Bacri, and F. Gazeau, JACS **129**, 2628 (2007).

[261] H. Grüll and S. Langereis, J. Control. Release **161**, 317 (2012).

[262] M. N. Antipina and G. B. Sukhorukov, Adv. Drug Deliv. Rev. **63**, 716 (2011).

[263] I. Brigger, C. Dubernet, and P. Couvreur, Adv. Drug Deliv. Rev. **54**, 631 (2002).

[264] K. S. Soppimath, T. M. Aminabhavi, and A. R. Kulkarni, J. Control. Release **70**, 1 (2001).

[265] N. Gaponik, I. L. Radtchenko, M. R. Gerstenberger, Y. A. Fedutik, G. B. Sukhorukov, and A. L. Rogach, Nano Lett. **3**, 369 (2003).

[266] G. B. Sukhorukov, E. Donath, H. Lichtenfeld, H. Knippel, M. Knippel, A. Budde, and H. Möhwald, Colloids Surf. A **137**, 253 (1998).

[267] A. S. Susha, F. Caruso, and A. L. Rogach, Colloids Surf. A **163**, 39 (2000).

[268] S. D. Koker, L. J. D. Cock, P. Rivera-Gil, W. J. Parak, R. A. Velty, C. Vervaet, J. P. Remon, J. Grooten, and B. G. D. Geest, Adv. Drug Deliv. Rev. **63**, 748 (2011).

[269] K. Ariga, Y. Lvov, K. Kawakami, Q. Ji, and J. Hill, Adv. Drug Deliv. Rev. **63**, 762 (2011).

[270] N. Habibi, L. Pastorino, F. C. Soumetz, F. Sbrana, R. Raiteri, and C. Ruggiero, Colloids Surf. B **88**, 366 (2011).

[271] S. W. Keller, S. A. Johnson, E. S. Brigham, E. H. Yonemoto, and T. E. Mallouk, J. Am. Chem. Soc. **117**, 12879 (1995).

[272] E. Donath, G. B. Sukhorukov, F. Caruso, S. A. Davis, and H. Möhwald, Angew. Chem. Int. Ed. **37**, 2201 (1998).

[273] F. Caruso, E. Donath, and H. Möhwald, J. Phys. Chem. B **102**, 2011 (1998).

[274] F. Caruso, R. A. Caruso, and H. Möhwald, Science **282**, 1111 (1998).

[275] G. B. Sukhorukov, E. Donath, S. Davis, H. Lichtenfeld, F. Caruso, V. I. Popov, and H. Möhwald, Polym. Adv. Technol. **9**, 759 (1998).

[276] C. S. Peyratout and L. Dähne, Angew. Chem. Int. Ed. **43**, 3762 (2004).

[277] A. G. Skirtach, J. Mat. Chem. **17**, 1050 (2007).

[278] S. D. Koker, Adv. Funct. Mater. **17**, 3735 (2007).

[279] F. Caruso, R. A. Caruso, and H. Möhwald, Chem. Mater. **11**, 3309 (1999).

[280] I. Pastoriza-Santos, B. Schöler, and F. Caruso, Adv. Funct. Mater **11**, 122 (2001).

[281] C. Dejugnat, D. Halozan, and G. B. Sukhorukov, Macromol. Rapid Commun. **26**, 961 (2005).

[282] G. B. Sukhorukov, D. V. Volodkin, and A. M. Günther, J. Mater. Chem. **14**, 2073 (2004).

[283] D. V. Volodkin, N. I. Larionova, and G. B. Sukhorukov, Biomacromolecules **5**, 1962 (2004).

[284] S. E. Moya, Med. Biol. Eng. Comp. **41**, 504 (2003).

[285] C. Preetz, A. Rübe, I. Reiche, G. Hause, and K. Mäder, Nanomedicine **4**, 106 (2008).

[286] A. Voigt, N. Buske, G. B. Sukhorukov, A. A. Antipov, S. Leporatti, H. Lichtenfeld, H. B´aumler, E. Donath, and H. Möhwald, J. Magn. Magn. Mater. **225**, 59 (2001).

[287] K. Szczepanowicz, D. Dronka-Góra, G. Para, and P. Warszyński, J. Microencapsulation **27**, 198 (2010).

[288] P. Kan, Z. B. Chen, R. Y. Kung, C. J. Lee, and I. M. Chu, Colloids Surf. B **15**, 117 (1999).

[289] K. Kawakami, T. Yoshikawa, Y. Moroto, E. Kanaoka, K. Takahashi, Y. Nishihara, and K. Masuda, J. Control. Release **81**, 65 (2002).

[290] R. N. Gursoy and S. Benita, Biomed. Pharmacoter. **58**, 173 (2004).

[291] B. Subramanian, F. Kuo, E. Ada, T. Kotyla, T. Wilson, S. Yoganathan, and R. Nicolosi, Int. Immunopharmacol. **8**, 1533 (2008).

[292] A. G. Floyd, J. Pharm. Sci. Tech. Today **2**, 134 (1999).

[293] H. Chung, T. W. Kim, M. Kwon, I. C. Kwon, and S. Y. Jeong, J. Control. Release **71**, 339 (2001).

[294] D. Bera, D. Lahiri, and A. Nag, J. Food Eng. **74**, 542 (2006).

[295] M. J. Francis and R. M. Pashley, Colloids Surf. A **260**, 7 (2005).

[296] N. Uson, M. J. Garcia, and C. Solans, Colloids Surf. A **250**, 415 (2004).

[297] D. Fasolo, L. Schwingel, M. Holzchuh, V. Bassani, and H. Teixeira, J. Pharm. Biomed. Anal. **44**, 1174 (2007).

[298] M. Porras, C. Solans, C. Gonzalez, A. Martinez, A. Guinart, and J. M. Gutierrez, Colloids Surf. A **249**, 115 (2004).

[299] D. J. F. Taylor, R. K. Thomas, and J. Penfold, Adv. Colloid Interface Sci. **132**, 69 (2007).

[300] K. Szczepanowicz, H. J. Hoel, L. Szyk-Warszyńska, E. Bielańska, A. M. Bouzga, G. Gaudernack, and P. Warszyński, Langmuir **26**, 12592 (2010b).

[301] D. O. Grigoriev, T. Bukreeva, H. Möhwald, and D. G. Shchukin, Langmuir **24**, 999 (2008).

[302] M. Kanamaru and Y. Einaga, Polymer **43**, 3925 (2002).

[303] D. P. Krickau, R. H. Mueller, and J. Thomsen, Int. J. Pharm. **342**, 62 (2007).

[304] A. L. Becker, A. P. R. Johnston, and F. Caruso, Macromol. Biosci. **10**, 488 (2010).

[305] A. P. R. Johnston, E. S. Read, and F. Caruso, Nano Lett. **5**, 953 (2005).

[306] K. Cai, A. Rechtenbach, J. Hao, J. Bossert, and K. D. Jandt, Biomaterials **26**, 5960 (2005).

[307] R. Dhamodharan and T. J. McCarthy, Macromolecules **32**, 4106 (1999).

[308] G. B. Sukhorukov, A. A. Antipov, A. Voigt, E. Donath, and H. Möhwald, Macromol. Rapid Commun. **22**, 44 (2001).

[309] A. Hogset, L. Prasmickaite, P. Selbo, M. Hellum, B. Engesæter, A. Bondted, and K. Berg, Adv. Drug Deliv. Rev. **56**, 95 (2004).

[310] A. G. Skirtach, A. A. Antipov, D. G. Shchukin, and G. B. Sukhorukov, Langmuir **20(17)**, 6988 (2004).

[311] D. I. Gittins and F. Caruso, J. Phys. Chem. B **105**, 6846 (2001).

BIBLIOGRAPHY

[312] C. Cortez, E. Tomaskovic-Crook, A. P. R. Johnston, B. Radt, S. H. Cody, and A. M. Scott, Adv. Mater. **18**, 1998 (2006).

[313] R. F. Service, Science **300**, 243 (2003).

[314] P. Hoet, I. Bruske-Hohfeld, and O. Salata, J. Nanobiotechnol. **2**, 12 (2004).

[315] E. Bermudez, Toxicol. Sci. **77**, 347 (2004).

[316] T. G. Iversen, T. Skotland, and K. Sandvig, Nano Today **6**, 176 (2011).

[317] D. Maysinger, J. Lovric, A. Eisenberg, and R. Savic, Eur. J. Pharm. Biopharm. **65**, 270 (2007).

[318] V. Vailander and K. Landfester, Biomacromolecules **10**, 2379 (2009).

[319] H. Hillaireau and P. Couvreur, Cell. Mol. Life Sci. **66**, 2873 (2009).

[320] G. Sahay, D. Y. Alakhova, and A. V. Kabanov, J. Control. Release **145**, 182 (2010).

[321] W. Sch'artl, *Light Scattering from Polymer Solutions and Nanoparticle Dispersions* (Springer-Verlag, 2007).

[322] *Zetasizer NanoSeries User Manual*, Malvern Instruments Ltd., Worcestershire, UK (2003).

[323] G. Binning, C. F. Quate, and C. Gerber, Phys. Rev. Lett. **56**, 930 (1986).

[324] P. von Blanckenhagen, *Atomic Force Microscopy/Scanning Tunneling Microscopy* (Kluwer Academic, 1999).

[325] K. S. Birdi, *Scanning probe microscopes. Applications in Science and Technology* (CRC Press, 2003).

[326] J. Drelich and K. L. Mittal, *Atomic Force Microscopy in Adhesion Studies* (Springer, 2005).

[327] J. R. Lakowicz, *Principles of Fluorescence Spectroscopy* (Springer, 2006).

[328] H. H. Perkampus, *UV-VIS Spectroscopy and Its Applications* (Springer-Verlag, 1992).

[329] M. Theiszova and S. Jantova, Biomed. Pap. **149**, 393 (2005).

[330] *American Type Culture Collection, MTT Cell Proliferation Assay Instructions*, Manassas, USA (2007).

[331] M. Adamczak, H. J. Hoel, G. Gaudernack, J. Barbasz, K. Szczepanowicz, and P. Warszyński, Colloids Surf. B **90**, 211 (2012).

[332] M. Adamczak, G. Para, C. Simon, and P. Warszyński, J. Microencapsulation **doi:10.3109/02652048.2012.752536** (2012).

[333] M. Adamczak, M. Krok, E. Pamuła, U. Posadowska, K. Szczepanowicz, J. Barbasz, and P. Warszyński, Colloids Surf. B **110**, 1 (2013).

List of Symbols

G the Gibbs free energy

k_B the Boltzmann constant

S entropy

AFM   atomic force microscope

AOT   docusate sodium salt

CMC   critical micelle concentration

CTABr   cetyl trimethylammonium bromide $C_{16}H_{33}N(CH_3)_3Br$

diDDAB   didodecyldimethylammonium bromide

DLS   Dynamic Light Scattering

DMSO   dimethylsulfoxide

DNA   deoxyribonucleic acid

DTABRr   dodecyl trimethylammonium bromide $C_{12}H_{25}N(CH_3)_3Br$

EIP   emulsion inversion point method

HLB   hydrophile-lipophile balance

HLD   hydrophilic-lipophilic deviation

HPH   high-pressure homogenization

LbL   layer-by-layer

LDV   Laser Doppler Velocimetry

MCT   medium chain triglycerides

MRI   magnetic-resonance imaging

NMR	nuclear magnetic resonance
O/O	oil-in-oil emulsion
O/W	oil-in-water emulsion
O/W/O	oil-in-water-in-oil emulsion
PAH	poly(allyamine hydrochloride)
PCS	Photon Correlation Spectroscopy
PDDA	poly(dimethyldiallylammonium chloride)
PDT	photodynamic therapy
PEG	poly(ethylene glycol)
PEI	poly(ethylenoimine)
PEI	polyethyleneimine
PGA	polyglutamic acid
PIT	phase-inversion temperature
PLGA	poly(lactic-*co*-glycolic acid)
PLL	poly-L-lysine
PMA	poly(methacrylic acid)
PNIPAM	poly(N-isopropyl acrylamide
PSS	poly(styrene sulfonate)
PVA	polyvinyl alcohol
PVS	poly(vinyl sulfate)
SAXS	small-angle X-ray scattering
SDS	sodium dodecyl sulfate
SPG	Shirazu porous glass
SPIO	superparamagnetic iron oxide
USPIO	ultrasmall superparamagnetic iron oxide
W/O	water-in-oil emulsion